Optimising the Blending of Biosurfactants with Conventional Home and Personal Care Components: A Surface and Solution Study

A thesis submitted in partial fulfilment of the requirements for the degree of
Doctor of Philosophy
at the University of Oxford

by Jessica R. Liley

University College

Hilary Term 2014

Declaration of authorship

The work presented in this thesis was carried out at the Physical and Theoretical Chemistry Laboratory at the University of Oxford, under the supervision of Professor Jeff Penfold and Dr Bob Thomas. All the work presented is entirely my own, except where otherwise stated, and has not been submitted for any other degree at this University or any other institution.

Jessica R. Liley

April 2014

Abstract

Optimising the Blending of Biosurfactants with Conventional Home and Personal Care Components: A Surface and Solution Study

Jessica R. Liley
University College
Submitted for the degree of Doctor of Philosophy in Physical Chemistry
Hilary Term 2014

The surface adsorption behaviour of a model ternary anionic/nonionic surfactant mixture, representative of many current detergent formulations; the nonionic surfactant $C_{12}E_8$ with the anionic surfactants LAS and SLES, and its mixing behaviour with the biosurfactant rhamnolipid R1 and R2, has been studied at the air/water interface, using surface tension (ST) and neutron reflectivity (NR). The self-assembly behaviour of these mixtures has been studied using small angle neutron scattering (SANS).

In the $C_{12}E_8$/LAS/SLES system, NR reveals unexpectedly high non-ideal surface behaviour in the form of highly dominant adsorption of $C_{12}E_8$ and LAS, with surprisingly low relative adsorption of SLES. All mixtures are in the form of small interacting globular micelles up to a concentration of 50 mM, with the variation in aggregation number of the mixed micelles indicating ideal mixing. For the replacement of SLES with sodium dodecyl sulphate (SDS), there is also a similar depletion of SDS at the surface with a dominance of $C_{12}E_8$ and LAS. The addition of Na^+ and Ca^{2+} counterions drives the surface compositions of the mixtures closer to their solution compositions, and results in a large synergy in total adsorption. The divalent Ca^{2+} counterion is more effective at driving these effects.

The addition of rhamnolipids to form a complex biosurfactant mixture causes a pronounced synergy in total adsorption which is not observed in the ternary conventional mixture alone. The surface composition is closer to its solution composition. Increasingly complex solution behaviour exists for the biosurfactant mixtures, which is not observed in the ternary mixtures or any individual component

at these concentrations or compositions. There is a transition from micellar to mixed micellar/lamellar phase behaviour, an effect associated with the rhamnolipids promoting packing which favours planar structures. More planar structures are favoured at higher solution concentrations, and solutions richer in LAS, rhamnolipids and R1.

The impact of lower temperatures on the surface behaviour of $C_{12}E_8$/LAS/SLES and R1/R2/$C_{12}E_8$/LAS/SLES reveals some striking initial results. At lower temperature, significant variations in surface adsorption behaviour exist for $C_{12}E_8$, SLES and the ternary mixture, but almost no change is observed for R1, R2, LAS and the mixtures containing rhamnolipids. These important results suggest that the incorporation of rhamnolipids, especially R1, provide a degree of tolerance to lower temperatures, suggesting a viable route to efficient low temperature detergency.

Acknowledgements

First and foremost, I would like to thank Bob and Jeff for accepting me into the Thomas-Penfold group, for their supervision and for being genuine inspirations to me as scientists over the last four years. I feel very privileged to have had the opportunity to work with you.

I am indebted to my industrial supervisors Ian Tucker, Paul Stevenson and Jordan Petkov at Unilever Port Sunlight, for the CASE award and for the opportunity to work on such a fulfilling project. I am grateful for the ever-available scientific discussions, project direction and the generous assistance during neutron experiments. I am very grateful to EPSRC for their funding for the project.

I am very thankful to all the instrument scientist at ISIS and the ILL, especially John Webster (INTER, ISIS), Max Skoda (SURF, ISIS), Richard Campbell (FIGARO, ILL), Isabelle Grillo (D33, ILL) and Ann Terry and Sarah Rogers (LOQ, SANS2D, ISIS) for their generous assistance with my neutron experiments. Working at ISIS and the ILL was always a highlight for me. I am also thankful for the help of James Wickens at the CRL mass spec facility at Oxford.

I have been lucky enough to spend four months of my DPhil at the University of Ulster, Coleraine, and I am indebted to Ibrahim Banat and Roger Marchant for allowing me to produce the deuterated rhamnolipids in their research group, and to Thomas Smyth for all his advice, assistance with HPLC-MS and allowing me to work at Teagasc.

Many thanks go to my colleagues in the RKT group; Chu Chuan, Pei Xun, Hui, Kun Ma and Sylvia, for being great colleagues and for the much-appreciated help with columning, fitting reflectivity data, and for their company during beam time. To my colleagues in Team Micro at UUC, especially Michelle, Sid, Debbie, Balkis and Shaez, thank you for accepting me as one of your own and teaching me everything I know about microbiology. To Top 12 – you are friends for life, thank you for giving me a home from home during my long periods away from Oxford, fantastic memories, introducing me to the Anchor and making my time in NI better than I ever could've imagined. Will we go for wan?!

Thank you to every single one of the BGD group, past and present, for your friendship, lunchtimes, tea-times and countless pot-luck dinners.

Smita and Becky: I'm so happy we ended up in the same place for another 4 years, being here with you has made it all the better for me! I'm really thankful for the friendship and support of both old and new friends I've made here. Laura, Charley, Cat, Kylie, Ruby, Chris, Bex and Smita: thanks for the great times outside the lab, the many girlie dinners, nights in the Uni Club and the PT! To all my friends at Univ, thank you for all the fun we've had inside and outside college, the BOPs and dinner parties in the nest, and T-Dog, Lucy and Claudia for being the best housemates I could wish for. Katie and Bex - I am so glad I have you both, and that I've been able to have my best friends there all the way to the finish. We all got there in the end!

Last but not least, to Mum, Dad and Harriet, thank you for your endless help, humour, advice and love. This thesis is for you and I hope it makes you proud. You are my rocks and I could not have done it without you!

Finally, I would very much like to thank Professor Jian Lu and Professor Dirk Aarts for a stimulating, thought-provoking and thoroughly enjoyable Viva.

Table of Contents

Chapter 1

Introduction to surfactants, biosurfactants and surfactant mixing

Surfactants (surface-active agents) are one of the most important classes of chemicals, with a large variety of uses ranging from detergents and cosmetics in the home and personal care industry, to agrochemicals, adhesives and paint emulsions. In many of these practical applications, surfactants are present as mixtures, partly because they may be a combination of polydisperse surfactants with different chain lengths or headgroup sizes, and partly because of the synergistic effects and enhanced performance of mixtures over that of single surfactant systems. The environmental impact of conventional synthetic surfactants, which are usually petroleum-derived, is of growing concern.[1,2] Biosurfactants, microbial compounds synthesised by living cells, are becoming increasingly appealing in addition to or as a replacement for conventional surfactants. They have uses mainly reported in bioremediation and enhanced oil recovery processes, but also in products ranging from cosmetics and household detergents to coating emulsions. Biosurfactants have particularly high surface activity and emulsification abilities when compared to their synthetic equivalents. However, disadvantages such as the high cost of large-scale production and difficulties in separating and purifying components in the natural biosurfactant mixtures are an ongoing problem and have so far hindered their replacement of conventional surfactants. Nevertheless, biosurfactants' superior surface-activity, environmental compatibility, biodegradability[3] and lower toxicity means they are becoming a more plausible alternative to the current chemical surfactants.[4]

Although there is extensive literature on biosurfactants, their uses and commercial potential,[5,6] very little is reported on their surface adsorption and solution self-assembly behaviour. Characterising the behaviour of the individual components in mixtures is imperative for understanding and optimising the performance and formulation of detergents, where mixtures of at least three surfactants are usually used. This thesis aims to target this deficiency in understanding, and focuses firstly on the surface adsorption and solution self-assembly behaviour of a model conventional surfactant mixture, and

secondly on the incorporation of one of the most well-known biosurfactants, rhamnolipid, into this surfactant mixture to form one of the most complex multicomponent biosurfactant/conventional surfactant mixtures studied to date.

1.1 Conventional surfactants

Surfactants are amphiphilic molecules formed of a hydrophobic hydrocarbon "tail" which has an attraction to non-polar media and a hydrophilic polar "head" with an attraction to polar media. The alkyl chain can be single, branched or even a ring structure whilst the headgroup defines the form of the surfactant depending on its charge: anionic, containing a negatively-charged headgroup, cationic, where the headgroup is positively-charged, zwitterionic (or amphoteric), containing positive and negative parts on the headgroup and which can be of either charge depending on the pH, and nonionic, with no such charges. In terms of the work presented here, the anionic and nonionic surfactants are the most important.

Anionic surfactants are the most widely used surfactants in detergents which require good foaming properties, such as shampoos and laundry detergents. The most widely used surfactant types are the linear alkylbenzene sulfonates (LAS), alkyl sulfates such as sodium dodecyl sulfate (SDS) and alkyl ether sulfates such as sodium lauryl ether sulfate (SLES). They have an average carbon chain length of C_{12}, but this can range from C_8 to C_{16}. The C_{12} chain is usually the best for detergency, with the C_{10} and below possessing superior wetting abilities, and C_{14} and above possessing better emulsifying characteristics.

Nonionic surfactants are found in almost all detergent formulations. They are very often used as co-surfactants with anionic or cationic surfactants because of their absence of charge, allowing surfactants to aggregate in closer proximity and micelles to form at lower concentrations, hence reducing the mixed critical micelle concentration (CMC). One very common class of nonionic surfactant used in current detergent formulations is the polyoxyethylene alkyl ethers, for example octaethylene glycol monododecyl ether ($C_{12}E_8$) as well as ethoxylated alkylphenols and fatty acid esters.

Cationic surfactants are also important surfactants but with lower detergency, and they tend to be stronger and harsher. Due to the intrinsic anionic nature of many surfaces, they are able to adsorb to these surfaces and give antistatic effects, hence their common use in fabric and hair conditioners. Examples include the quaternary ammonium surfactants and alkyltrimethylammonium salts, for example, dodecyltrimethylammonium bromide (C_{12}TAB).[7]

Zwitterionic (amphoteric) surfactants are also often used as co-surfactants as they can be effectively neutral depending on the solution pH. At low pH they have properties consistent with those of a cationic surfactant, whereas at high pH they make good detergents like the anionic surfactants. Zwitterionic surfactants often have an amine or a quaternary ammonium salt as the cationic part and a sulfonate or carboxylate group as the anionic part. Examples include betaines such as *n*-dodecyl-*N*,*N*-dimethylaminoacetate (C_{12}Betaine or C_{12}B)[8] and phosphatidylcholine surfactants such as lecithin.

1.1.1 Octaethylene glycol monododecyl ether, $C_{12}E_8$

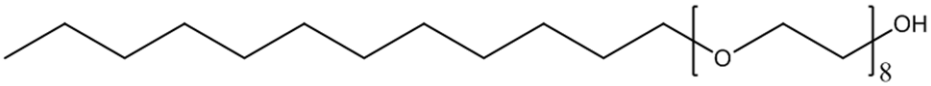

Figure 1.1: Molecular structure of $C_{12}E_8$

Octaethylene glycol monododecyl ether, $C_{12}E_8$, is a common polyoxyethylene nonionic surfactant used in many detergent formulations. Its structure consists of eight ethylene oxide (EO) groups and a terminal hydroxide as the hydrophilic portion and a C_{12} hydrocarbon chain as the hydrophobic portion. It has a relatively low CMC quoted in the range from 7.1×10^{-5} M,[9] 8.1×10^{-5} M[10] to 1.09×10^{-4} M.[11] For nonionic surfactants the Krafft point, the temperature below which micellisation of surfactants cannot occur, is usually very low and is below 0°C for $C_{12}E_8$. With increasing temperature, nonionic surfactants become more dehydrated up to their "cloud point" or upper solubility temperature. For $C_{12}E_8$ this is around 65°C,[12] depending on the concentration. The temperature conditions used in this work (25°C, unless otherwise stated) are far from either the Krafft point or cloud point of $C_{12}E_8$.

Penfold et al[13] found the area per molecule of $C_{12}E_8$ to be approximately 62 Å^2, which is consistent with other literature.[11] The CMC and area per molecule both increase with increasing hydrophilic EO chain length, as the molecule becomes less hydrophobic and larger in size.[14,15,16,17] The length of the

alkyl chain length affects the hydrophobicity of the molecule and also the packing constraints and structural conformation at the interface, as was observed by Penfold et al in mixtures between $C_{10}E_6$ and $C_{14}E_6$.[18] Ueno et al[9] observed a linear decrease in CMC with increasing alkyl chain carbon number for a series of octaethylene glycol *n*-alkyl ethers. The area per molecule and surface tension at CMC decreased as the molecule became more hydrophobic, but the different effects of having an even or an odd number of carbons gave the latter a zigzag-style decrease.

Nonionic surfactants do not tend to be affected by pH as they do not become dissociated in aqueous solution like ionic surfactants. Likewise, there is very little effect of electrolyte on their surface or solution behaviour or in the mixing behaviour of very nonionic-rich mixtures,[19] although Penfold et al[20] found that the addition of a "salting in" electrolyte such as NaCl increased surface adsorption of $C_{12}E_8$, which was attributed to the decreasing solubility of the C_{12} alkyl chain. For $C_{12}E_3/C_{12}E_8$ mixtures[20] both surfactants were affected equally by electrolyte as the alkyl chain length is the same, resulting in no change in surface composition.

The commercial equivalents of nonionic surfactants such as $C_{12}E_8$ are usually polydisperse mixtures of many EO chain lengths, for example Synperionic A5.[21] However, usually they are around EO_8 and higher to ensure sufficient solubility in water.

1.1.2 Linear alkylbenzene sulfonate, LAS

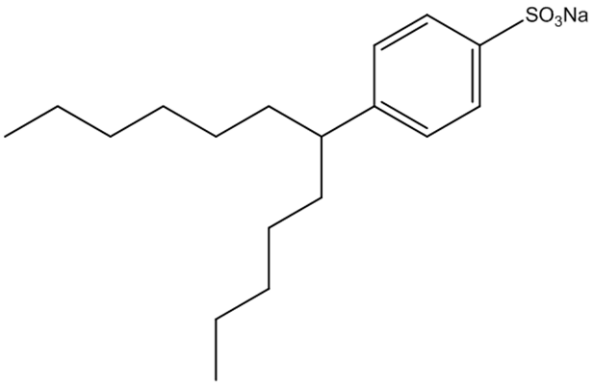

Figure 1.2: Molecular structure of LAS-6

The linear alkylbenzene sulfonates (LAS) such as sodium dodecyl benzene sulfonate, shown in Figure 1.2, are some of the most widely used anionic surfactants today. LAS contains a benzene ring with a sulfonate headgroup on the hydrophilic part and a hydrocarbon chain on the hydrophobic part. Commercial mixtures of LAS usually have components with different alkyl chain lengths, typically an average of C_{12}, with the sulfonate portion attached at the *para* position of the benzene ring, positioned between the 2nd and 6th carbon, giving more than 20 possible isomers.

In this work, LAS-6 is used with the benzene sulfonate headgroup at the 6-position along a C_{12} hydrocarbon chain. LAS-6 has been reported to have a CMC of 1.6 mM[22,23] and 1.8 mM,[24] up to 2.53 mM.[25] The position along the hydrocarbon chain affects the CMC, surface tension, γ, at CMC and area per molecule, due to steric effects.[22] Ma et al[25] conducted a full systematic study of the surface and self-assembly behaviour of the different positional isomers of LAS and the influence of electrolyte. The CMC was 2.53 mM for the 6-isomer and 1.04 mM for the 2-isomer due to its higher hydrophobicity. The Krafft point decreases with headgroup position closer to the centre of the C_{12} hydrocarbon chain and is reported as below 0°C for LAS-4, 5 and 6.[25] This is very low because of the high heat of formation of crystals due to branching of the hydrophobic dodecyl chain. At 25°C, the principal temperature used in this work, the area per molecule of LAS-6 is around 65 Å^2. [25] This decreases as the benzene headgroup is positioned nearer to the terminal carbon. Values for the area per molecule of LAS-4 from Ma et al correspond well to those from Tucker et al[26] (55 Å^2), although

values for LAS-6 are slightly higher than those found using neutron reflectivity (57 $Å^2$) by Penfold et al.[19]

LAS forms micellar aggregates in dilute aqueous solution but liquid crystalline phases in increasingly concentrated solutions.[27] Ma et al[25] found that for LAS-5 and 6 a micellar to lamellar transition exists, with inverse hexagonal structures at the highest concentrations, whereas for LAS-1, 2 and 3 a micellar to hexagonal to lamellar transition exists, occurring at a higher threshold concentration. LAS-6 is effectively a di-chain anionic surfactant with a relatively low spontaneous curvature, so prefers to pack as bilayers. The molecule displays increasing packing constraints as the benzene sulfonate headgroup is positioned closer to the centre of the alkyl chain. On addition of electrolyte, a transition from micelles to vesicles can also occur.[28] The effect of electrolyte will be further discussed in Chapter 5.

The anionic surfactant LAS is rather intolerant to water hardness in the form of divalent counterions such as Ca^{2+} and Mg^{2+}.[29] Precipitation in detergent formulations can be a serious problem and lead to reduced detergency performance. Thus LAS is often used in combination with nonionic surfactants to reduce precipitation effects, to increase detergency and to lower surface tension and mixed CMC values.

1.1.3 Sodium lauryl ether sulfate, SLES

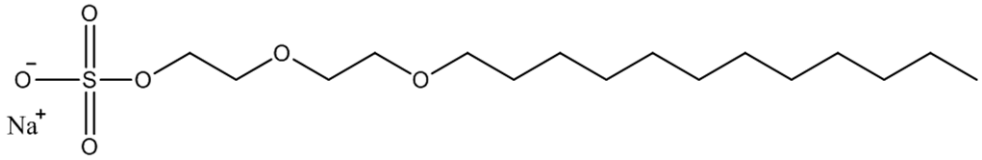

Figure 1.3: Molecular structure of SLES-2EO

Sodium lauryl (dodecyl) ether sulfate (SLES) is another widely-used anionic surfactant of the alkyl ether sulfates (AES) group. SLES is similar to sodium dodecyl sulfate (SDS) in structure, with a polar sulfate headgroup and a hydrophobic dodecyl hydrocarbon chain, but it includes $(C_2H_4O)_n$ (ethylene oxide, EO) groups between the alkyl chain and the headgroup. Xu et al[30] determined the CMC of SLES-2EO to be 2.6 mM. This decreases linearly with increasing carbon number in the alkyl chain. The CMC is much lower than that of SDS (8 mM[13]) due to the presence of the EO groups. Although EO groups would be expected to increase the overall hydrophilicity of the molecule, they become

more hydrophobic in character when adjacent to the sulfate headgroup,[31] which is thought to reduce the headgroup's ionic character.[32] However, Aoudia et al[33] found the degree of ionisation of SLES to be higher than that of SDS and predicted that the presence of the sulfate group reduces the hydration of the EO groups. Vollhardt et al[34] found the presence of EO groups to increase surface activity. The Krafft point for SLES-2EO is -1°C[35] and this decreases as the number of EO groups increases, due to the higher hydrophobicity. However, systematic studies[33,36] found the CMCs of SLES-EO1, 2 and 3 to be comparable, attributed to the fact that the only effective ion-dipole interaction is between the sulfate anion and the first O → CH_2 dipole on the EO group (of either itself or a nearby SLES surfactant). This shows that the ion-dipole interaction does not depend on any additional EO groups.[33]

The area per molecule of SLES-2EO is 46 $Å^2$,[30] which increases with the number of EO groups.[37] SLES forms monolayers at the air/water interface in the absence of electrolyte. However, on the addition of multivalent counterions, in the form of $AlCl_3$, multilayer adsorption occurs due to strong complexation of the Al^{3+} ion with the anionic SLES headgroup.[37]

SLES forms globular micelles in dilute solution, with aggregation numbers found to be independent of the degree of ethoxylation, due to the change from a compact to a looser micelle structure to accommodate the longer headgroup, with a larger volume of the polar layer at the air/water interface.[38] Xu et al[39] investigated the solution behaviour of SLES with a variety of alkyl chain lengths and EO lengths. Weakly interacting, small globular micelles were observed up to 20 mM, with an aggregation number of 87 at 10 mM concentration, which varied very little with the EO group length.

SDS is one of the most intolerant surfactants to the presence of divalent counterions such as Ca^{2+} and Mg^{2+}, but the ethoxylation process to form the SLES molecule makes it much more tolerant to hard water conditions.

1.2 Biosurfactants

Biosurfactants are surfactants synthesised by living microbial cells, with particularly high surface activity and emulsification abilities. They have mainly been used in the processes of enhanced oil recovery and *in situ* bioremediation of hydrocarbons. However, their current uses range more widely from cosmetics to household detergents, paints and coating emulsions. Biosurfactants offer many advantages over conventional surfactants, mainly in their biodegradability,[3] lower toxicity, antimicrobial and antibacterial properties, high foaming[40] and emulsifying[41] abilities. Recent advances in the use of renewable raw materials as feedstocks for biosurfactant growth have also encouraged their use.[42]

Biosurfactants are classified according to their chemical composition and microbial origin, unlike conventional surfactants which are categorised according to the nature of their polar headgroup.[5] A large range of biosurfactants exists, divided into high and low molecular weight categories,[43] and which include glycolipids, lipopeptides, fatty acids and phospholipids.[5] The best-studied of these in the low molecular weight group are the glycolipids, which include mannosylerythritol lipids (MELs), trehalolipids, sophorolipids, and the most familiar, rhamnolipids. In the high molecular weight category, common examples include heteropolysaccharides, such as emulsan and biodispersan, and bacterial lipases.

The focus of this work is on the biosurfactant rhamnolipid, one of the most widely used glycolipids, of which the surface and solution behaviour have already been investigated in detail both individually and as mixtures in the absence[44] and presence[23] of the conventional anionic surfactant LAS.

1.2.1 Rhamnolipids

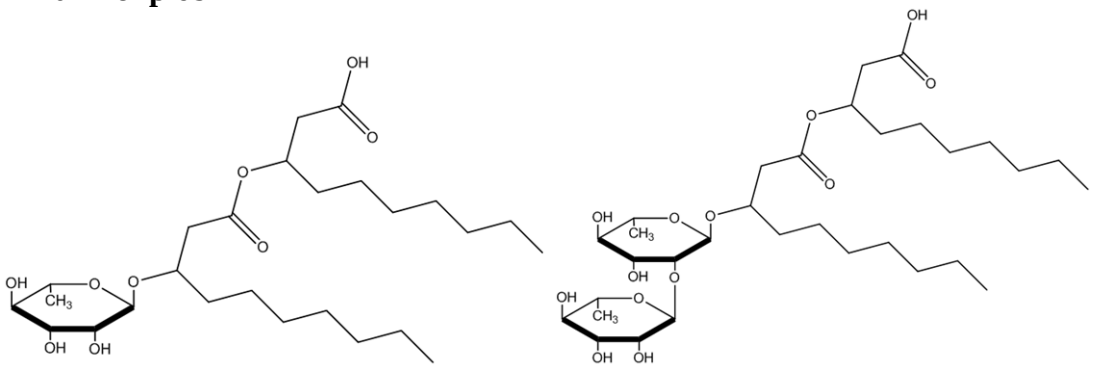

Figure 1.4: Structure of the rhamnolipid biosurfactants, R1 and R2.

The first rhamnolipids were produced by the bacterium *Pseudomonas aeruginosa*[4,45,46] by Bergström et al in 1946.[47,48] *P. aeruginosa* is the primary producer of rhamnolipids, of which hundreds of strains are now known.[49] Rhamnolipids are produced commercially in large quantities, for example, by Jeneil Biosurfactant Co. and Rhamnolipid Inc., with uses ranging from enhanced oil recovery and *in situ* bioremediation of hydrocarbons, to commercial applications such as household cleaners and the cosmetic and food industries.

The rhamnosyl sugar group together with the carboxylic group attached form the hydrophilic part and the alkyl chain forms the hydrophobic part of the molecule. Up to 60 different homologues of rhamnolipids have been identified,[50] differing in their lipid chain lengths and saturation. The two main types are α-L-rhamnopyranosyl-β-hydroxydecanoyl-β-hydroxydecanoate (Rha-C_{10}-C_{10}, mono-rhamnolipid R1) and α-L-rhamnopyranosyl-α-L-rhamnopyranosyl-β-hydroxydecanoyl-β-hydroxydecanoate (Rha-Rha-C_{10}-C_{10}, di-rhamnolipid R2), the difference being in the number of rhamnosyl sugar groups (1 and 2, respectively). Due to its smaller headgroup, R1 has a higher hydrophobicity with a lower micelle curvature than the bulkier R2. R1 is likely to form aggregates at lower concentrations and so has a slightly lower CMC and is more surface-active. Zhong et al[51] found the CMC of R1 to be 7.5×10^{-5} M and R2 to be 1.06×10^{-4} M, at pH 6.5, whilst Peker et al[52] found that R1 and R2 both had a CMC of 1.5×10^{-4} M at pH 6.8. Guo et al[53] found the area per molecule of R1 to be 66 Å^2 and R2 to be 79 Å^2, whereas Chen et al[44] found areas per molecule of 53 Å for R1 and 84 Å for R2, in ultrapure water. The CMCs of R1 and R2 were 4×10^{-5} M and 7×10^{-5} M, respectively.[54] The R1 monolayer is more compact that that of R2 due to the less bulky headgroup of R1 rendering it less

sterically-hindered at the air/water interface than R2. The R1 molecule is more hydrophobic so the rigidity of the R1 monolayer is greater than that of R2.

At lower pH, rhamnolipid molecules are undissociated and the carboxylic acid is not negatively charged, and therefore the monolayer is packed more significantly at the surface as there is less charge repulsion between the headgroups. At a higher pH, the carboxylic acid group on the rhamnolipids become dissociated, so the molecules are more anionic in nature. Ozdemir et al[55] studied the effects of two different pH values (6.8 and 5) on surface behaviour of rhamnolipids. Surface tension measurements gave CMC values of $1x10^{-4}$ M and $1.5x10^{-4}$ M at pH 6.8 for R1 and R2, respectively, decreasing to $4x10^{-5}$ M for both rhamnolipid structures at pH 5, confirming their previous conductivity measurements. Sanchez et al[56] found the CMC of R2 to decrease from $1.1x10^{-4}$ M at pH 7.4 to $0.1x10^{-4}$ M at pH 4. Dahrazma et al[57] found that high curvature rhamnolipid micelles formed at high pH, whereas vesicles of increasing size formed at increasingly lower pH, with a region of coexistence of the two in between. However, Chen et al[44] found rhamnolipids to be no more than weakly ionic and they can almost be viewed as nonionic surfactants, hence their variation with pH is minimal. They also found the addition of 0.5 M NaCl also had little effect on the CMC, confirming their weakly anionic behaviour. There was a weaker dependence of electrolyte and pH on the area per molecule and CMC of R2, confirming the more nonionic-like behaviour of R2 than R1.

1.2.2 Other common biosurfactants

The sophorolipids are a common glycolipid biosurfactant produced by the yeast strain *Candida (Torulopsis) bombicola*, originally found by Gorin et al,[58] with over 20 individual homologues subsequently identified.[59] They contain a hydrophilic sophorose disaccharide unit and a hydrophobic alkyl chain usually 16-18 carbons long. Two types exist, lactonic (LS) and acidic (AS) sophorolipid. The disaccharide units are identical in both but in LS the hydrophobic portion is joined to the sophorose sugar units whereas in AS it is free with a terminal carboxylic acid group. Chen et al[60,61] found LS and AS to exhibit very different mixing behaviour both at the air/water interface and in solution due to the differences in their structure and charge of the headgroup.

Mannosylerythritol lipids (MEL) are another type of glycolipid biosurfactant, produced by the yeast strain *Candida antarctica.*[62] The two main types are MEL-A, 4-O-(4',6'-di-O-acetyl-2',3'-di-O-alkanoyl-β-D-mannopuranosyl)-D-erithritol where R1 = R2 = acetyl (Ac) group and MEL-B, 4-O-(6'-O-acetyl-2',3'-di-O-alkanoyl-β-D-mannopuranosyl)-D-erithritol, where R1 = Ac and R2 = H, with smaller ratios of MEL-C and MEL-D, containing R1 = H and R2 = Ac, and R1 = R2 = H, respectively. Different surface and solution properties are produced by the different types of MEL, as demonstrated by Imura et al[63] where MEL-A formed simple coacervates, whereas MEL-B was seen to form vesicles. The CMC values of MEL-A and MEL-B have been reported as 2.7 $x10^{-6}$ M and 4.5 $x10^{-6}$ M, respectively, with a very low surface tension at CMC of approximately 28 mN/m.[62]

Another common and very surface-active low molecular weight biosurfactant is surfactin, produced by the bacterium *Bacillus Subtilis.*[64] It is a cyclic lipopeptide with a molecular weight of around 1050 and with remarkable surface activity and foaming properties,[40] especially when compared to conventional synthetic surfactants.[65]

Of the high molecular weight category, common examples include the bioemulsifiers such as liposan, from *C. lipolytica*[66] with a molecular weight of 27,600,[41] and emulsan, the heteropolysaccharide produced by *P. fluorescens* strain 378[67] or *Acinetobacter calcoaceticus* RAG-1.[68] Emulsan is composed of a repeating trisaccharide covalently linked to a hydrophobic fatty acid chain.[69] It has a molecular weight of order $1x10^6$ and it can reduce the surface tension of water to 27 mN/m.

Another important type of the high molecular weight biosurfactants are the bacterial lipases (triacylglycerol lipase, EC 3.1.1.3). They catalyse the hydrolysis of triacylglycerol to form glycerol and long-chain fatty acids, as well as the synthesis of esters from these two substances. Lipases have a wide variety of uses from detergents and cosmetics to pharmaceutical, dairy and food applications.[70,71] In detergency applications they are used to break down and remove fat-based stains. They are proteins and are therefore completely biodegradable and non-toxic. Lipolase was the first commercially-available lipase for detergents, launched in 1988 by Novozymes.[72] The bacterial lipase contains an active site which is covered by a surface loop, its "lid". When it is bound to the oil/water interface the

lipase is opened and the active site with a large hydrophobic surface is exposed and available to the solvent. The effectiveness of lipases as successful detergents depends on their stability to extremes of pH and temperature and their low substrate specificity in order for them to break down a variety of triglycerides.

1.3 Surfactant behaviour at interfaces and in solution

The behaviour of surfactants at interfaces and in solution is driven by the hydrophobic effect, which is the tendency of non-polar substances to self-associate in order to remove themselves from aqueous solvent. When a hydrophobic molecule enters water, it disrupts the structure of hydrogen bonds between water molecules. These water molecules are thought to form an ordered “iceberg” structure around the hydrophobic group, which decreases the entropic contribution to the free energy ΔG. At low concentrations, when amphiphilic molecules are present as monomers, they will arrange themselves together into a monolayer at the air/liquid interface to reduce the free energy of the system. However, above a certain concentration (the CMC) there is a saturated monolayer, so the free energy is reduced by the arrangement of molecules into aggregates, with the hydrophobic tails associating together, leaving the hydrophilic polar headgroups exposed to the solvent. This micellisation process of removing the surfactant from the water into the micelle aggregate increases the entropy of the system, because it ruptures the iceberg structure of water, releasing the ordered water molecules.

1.3.1 Surface behaviour of surfactants

Surfactant molecules in aqueous solution congregate at the air/water interface in order to reduce the free energy of the system; this process is spontaneous and thermodynamically favourable. When the interface is saturated with monomers, the surface and solution will be in dynamic equilibrium where there is a continual exchange of monomers between the bulk and the surface, but overall saturation exists. Model adsorption isotherms are used to express this equilibrium, and the best known include the Langmuir and the Volmer adsorption isotherms.

The Gibbs equation relates the change in concentration of a component in solution to the change in the solution's surface or interfacial tension. It can be used to find the amount of surfactant adsorbed per unit area of interface:

$$\Gamma_i = -\frac{1}{nRT}\left(\frac{d\gamma}{d\ln a_i}\right) \tag{1.1}$$

where γ is the surface tension, a_i is the activity of component i which is approximated to concentration in dilute solutions below the CMC, R is the gas constant (8.314 J K^{-1} mol^{-1}) and T is the temperature in Kelvin. The Gibbs pre-factor, n, will either be 2 if the surfactant is fully dissociated, or 1 for nonionic surfactants or surfactants in excess electrolyte. The surface excess of a surfactant monolayer at the interface is used to find the area per adsorbed molecule, A, with units $Å^2$:

$$A = \frac{1}{N_A \Gamma} \tag{1.2}$$

where N_A is the Avogadro's constant (6.022×10^{23} mol^{-1}). The Gibbs equation has been applied to the adsorption of many anionic/nonionic surfactant[73] and nonionic surfactant/polymer systems.[74] The use and limitations of the Gibbs equation to determine surface adsorption is discussed in Chapter 4.

1.3.2 Solution behaviour of surfactants

An array of self-assembled structures exists above the CMC, which can range from micelles, which can be spherical or rod-like, to planar bi- or trilayers, through to inverse micelles. The self-assembled structure that ultimately forms depends on the structure of the individual surfactant and parameters such as the solution concentration, pH, temperature and ionic strength. The aggregate structures are often described as lyotropic, meaning that it is their specific inter-molecular interactions which determine the shape of the mesophase (an intermediate phase with both liquid- and solid-like properties, for example liquid crystals) that forms.

For spherical micelles, the simplest aggregates are formed by molecules such as SDS. Tanford[75] suggested that there is a limit to growth of micelles, beyond which the shape of the aggregate is deformed, and that this depends on both the volume, V, and length, l_c, of the alkyl chain, with n carbon atoms, which are given empirically by Equations 1.3 and 1.4, respectively:

$$V = v(27.4 + 26.9n) \tag{1.3}$$

$$l_c = 1.5 + 1.265n \tag{1.4}$$

Israelachvili, Mitchell and Ninham[76] devised an effective way of determining the preferred geometry for self-assembled molecules, through the use of a critical packing parameter (CPP), which defines the spontaneous curvature of the surfactant:

$$CPP = \frac{V}{Al_c} \tag{1.5}$$

where V defines the average volume of the alkyl chain, A is the headgroup area per molecule and l_c is the extended surfactant chain length. Figure 1.5 shows some examples of the wide variety of structures which may exist, with increasing complexity as the CPP value increases.

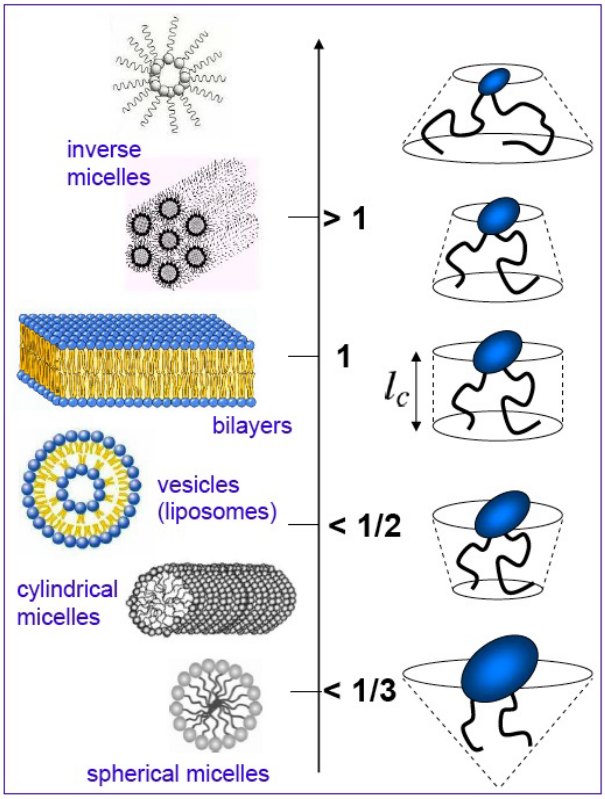

Figure 1.5: Self-assembled aggregate structures in solution.[54]

When CPP ≤ 1/3, the aggregate is in the form of spherical micelles, a value of 1/3 < CPP < 1/2 indicates the formation of more elongated structures such as rod-like micelles, for 1/2 < CPP < 1 vesicles may occur, for CPP = 1 planar bilayers are present, and for CPP ≥ 1 inverse micelles form the aggregate structure.

1.4 Surfactant mixing

Commercial mixtures of surfactants are often composed of mixtures of the ionic, nonionic and zwitterionic forms. They are usually used as mixtures due to the inherent polydispersity of certain surfactants with many different alkyl chain lengths, headgroup lengths, or different isomers. However, they are often combined in a precise formulation to give synergistic interactions such as CMC-lowering, which increase surface-activity and detergency. In addition to surfactants as the main ingredient, co-surfactants, builders, anti-redeposition agents and optical brighteners are included for optimum efficacy.

The addition of nonionic surfactants as co-surfactants to anionic surfactants helps decrease their Krafft temperature and assists in their tolerance to hard water counterions,[77] for example with LAS. A combination of anionic and cationic surfactants is liable to precipitate,[78] and this can also be reduced by the addition of nonionics.[79] It is known that the structure of a surfactant greatly influences its properties at the interface and in solution, for example as seen with the different positional isomers of LAS.[25] Boyd et al[80] found that for dodecyl β-D-glucoside, changes in the intermolecular interactions produced a change in detergency, attributed to packing effects of changing the alkyl chain positioning. It is therefore important to understand fully the behaviour of the individual components so as to optimise their distribution in commercial mixtures and optimise their performance and formulation.

The behaviour of surfactant mixtures has been predicted with many different theories, either ideal or non-ideal. This thesis uses the ideal mixing theory of Clint,[81] and the non-ideal regular solution theory (RST),[82] to predict the mixing behaviour between surfactant mixtures.

1.4.1 Surfactant mixing theories

1.4.1.1 Ideal mixing

In an ideal mixture, the strength of all inter-molecular interactions are equal and the enthalpy of mixing is zero. In this case, the entropy of mixing is:

$$\Delta S_{mix} = -nR\left(x_A \ln x_A + x_B \ln x_B\right) \tag{1.6}$$

where n is the total moles, x_A and x_B are the mole fractions of component A and B, and R is the gas constant (8.314 J K^{-1} mol^{-1}). The activity coefficients, which are a measure of the non-ideality, are unity.

Clint[81] developed a model which could be applied to mixtures of nonionic surfactants, based on the assumption that nonionic mixed micelles behave ideally in terms of thermodynamics, and that the mixed micelle is an ideal combination of the pure nonionic components. In this model, the mixed CMC for a binary mixed surfactant system, C^*, is:

$$\frac{1}{C^*} = \frac{\alpha}{c_1} + \frac{(1-\alpha)}{c_2} \tag{1.7}$$

or in the case of an n-component system:

$$\frac{1}{C^*} = \Sigma \frac{\alpha_n}{c_n} \tag{1.8}$$

where α (or α_n) is the mole fraction of each component (where $\Sigma\alpha_i = 1$) and c_n is the CMC of each pure component in an n-component mixture. However, surfactant mixtures are rarely "ideal" and the presence of non-ideal mixing behaviour is more probable, where the mixed CMC varies distinctly from the predicted mixed CMC obtained by Equation 1.7.

1.4.1.2 Non-ideal mixing

Most models of non-ideal mixing behaviour in binary surfactant mixtures use the pseudophase separation approximation and regular solution theory (RST).[82,83] This has been extended to include more than two components[84,85] and the surface compositions of surfactant mixtures above the CMC have been determined using this approach.[86] The pseudophase separation model treats micelles and the surface as separate "pseudophases". It assumes that the departure from ideal mixing can be expressed in terms of a single interaction parameter, β, and this accounts for the excess free energy of mixing. The excess entropy of mixing is zero, identical to that for ideal mixing, and the enthalpy of mixing is dependent on the solution composition. A negative β value indicates a synergistic departure from ideality, with the size of β describing the extent of non-ideality. Rarely, β may be positive when the surfactants are less compatible, suggesting an antagonistic interaction. Above a certain value this may

lead to phase separation. The ideal mixing Equation 1.7 is amended to include the activity coefficients f_1 and f_2 of the two surfactants, to give the mixed CMC for a non-ideal binary mixture:

$$\frac{1}{C^*} = \frac{\alpha}{f_1 c_1} + \frac{(1-\alpha)}{f_2 c_2} \tag{1.9}$$

These activity coefficients depend on an interaction parameter β, where:

$$\ln f_1 = \beta(1-x_1)^2 \tag{1.10}$$

$$\ln f_2 = \beta x_1^{\,2} \tag{1.11}$$

where x_1 is the mole fraction of component 1 in the micelles, f_1 and f_2 are the activity coefficients for components 1 and 2, and $f_1 = f_2 = 1$ for ideal mixing. Therefore the interaction parameter β can be found for a binary surfactant mixture:

$$\beta = \frac{\ln(\alpha C^* / x_1 c_1)}{(1-x_1)^2} \tag{1.12}$$

In some cases, RST has failed to predict the change in surface composition with solution concentration, and this is often associated with large differences in the β values obtained from NR and surface tension.[87] The surface compositions of mixtures may also often be far from that predicted using the β interaction parameter, as will be discussed in this thesis. RST assumes that the surface is composed of purely a binary surfactant mixture, rather than including hydration, although water must also be part of the interfacial layer. RST also assumes that there is zero excess entropy of mixing, but data for SDS/C_{12}B[87] and for nonionic mixtures[18] showed this assumption to be incorrect. Holland and Rubingh[84] extended the RST approach to the prediction of multicomponent mixtures, although this only describes the more complex interactions in terms of the pairwise interactions of each binary mixture. However, any further discussion on theoretical models is beyond the scope of this thesis.

References: Chapter 1

1. Cserháti, T.; Forgács, E.; Oros, G., *Environment International* **2002,** *28* (5), 337-348.
2. Ying, G.-G., *Environment International* **2006,** *32* (3), 417-431.
3. Zajic, J. E.; Guignard, H.; Gerson, D. F., *Biotecnology and Bioengineering* **1977,** *19* (9), 1303-1320.
4. Banat, I. M.; Makkar, R. S.; Cameotra, S. S., *Applied Microbiology and Biotechnology* **2000,** *53* (5), 495-508.
5. Desai, J. D.; Banat, I. M., *Microbiology and Molecular Biology Reviews* **1997,** *61* (1), 47-64.
6. Banat, I. M.; Franzetti, A.; Gandolfi, I.; Bestetti, G.; Martinotti, M. G.; Fracchia, L.; Smyth, T. J.; Marchant, R., *Applied Microbiology and Biotechnology* **2010,** *87* (2), 427-444.
7. Lyttle, D. J.; Lu, J. R.; Su, T. J.; Thomas, R. K.; Penfold, J., *Langmuir* **1995,** *11* (3), 1001-1008.
8. Hines, J. D.; Thomas, R. K.; Garrett, P. R.; Rennie, G. K.; Penfold, J., *Journal of Physical Chemistry B* **1997,** *101* (45), 9215-9223.
9. Ueno, M.; Takasawa, Y.; Miyashige, H.; Tabata, Y.; Meguro, K., *Colloid and Polymer Science* **1981,** *259* (7), 761-766.
10. Drummond, C.; Warr, G. G.; Grieser, F.; Ninham, B. W.; Fennel Evans, D., *Journal of Physical Chemistry* **1985,** *89* (10), 2103-2109.
11. Rosen, M. J.; Cohen, A. W.; Dahanayake, M.; Hua, X., *Journal of Physical Chemistry* **1982,** *86* (4), 541-545.
12. Shinoda, K., *Journal of Colloid and Interface Science* **1970,** *34* (2), 278-282.
13. Penfold, J.; Tucker, I.; Thomas, R. K.; Staples, E.; Schuermann, R., *Journal of Physical Chemistry B* **2005,** *109* (21), 10760-10770.
14. Penfold, J.; Staples, E.; Tucker, I.; Thomas, R. K., *Journal of Colloid and Interface Science* **1998,** *201*, 223-232.
15. Lu, J. R.; Lee, E. M.; Thomas, R. K.; Penfold, J.; Flitsch, S. L., *Langmuir* **1993,** *9* (5), 1352-1360.
16. Lu, J. R.; Hromadova, M.; Thomas, R. K., *Langmuir* **1993,** *9* (9), 2417-2425.
17. Lu, J. R.; Li, X.; Thomas, R. K.; Staples, E. J.; Thompson, L.; Tucker, I.; Penfold, J., *Journal of Physical Chemistry* **1994,** *98* (26), 6559-6567.
18. Penfold, J.; Staples, E.; Tucker, I.; Thomas, R. K.; Woodling, R.; Dong, C. C., *Journal of Colloid and Interface Science* **2003,** *262* (1), 235-242.
19. Penfold, J.; Thomas, R. K.; Dong, C. C.; Tucker, I.; Metcalfe, K.; Golding, S.; Grillo, I., *Langmuir* **2007,** *23* (20), 10140-10149.
20. Penfold, J.; Staples, E.; Tucker, I.; Thompson, L.; Thomas, R. K., *Journal of Colloid and Interface Science* **2002,** *247* (2), 404-411.
21. Staples, E. J.; Thompson, L.; Tucker, I.; Penfold, J., *Langmuir* **1994,** *10* (11), 4136-4141.
22. Fendler, J. H.; Fendler, E. J., *Catalysis in Micellar and Micromolecular Systems*. Academic Press: New York, 1975.
23. Chen, M.; Penfold, J.; Thomas, R. K.; Smyth, T. J. P.; Perfumo, A.; Marchant, R.; Banat, I. M.; Stevenson, P.; Parry, A.; Tucker, I.; Grillo, I., *Langmuir* **2010,** *26* (23), 17958-17968.
24. Sein, A.; Engberts, J. B. F. N., *Langmuir* **1995,** *11* (2), 455-465.
25. Ma, J.-G.; Boyd, B. J.; Drummond, C. J., *Langmuir* **2006,** *22* (21), 8646-8654.
26. Tucker, I.; Penfold, J.; Thomas, R. K.; Dong, C. C.; Golding, S.; Gibson, C.; Grillo, I., *Langmuir* **2011,** *27* (11), 6674-6682.
27. Težak, D.; Hertel, G.; Hoffmann, H., *Liquid Crystals* **1991,** *10* (1), 15-27.
28. Farquhar, K. D.; Misran, M.; Robinson, B. H.; Steytler, D. C.; Morini, P.; Garrett, P. R.; Holzwarth, J. F., *Journal of Physics: Condensed Matter* **1996,** *8* (47), 9397-9404.
29. Chen, Y.; Xu, G., *Colloids and Surfaces A: Physicochemical and Engineering Aspects* **2013,** *424*, 26-32.
30. Xu, H.; Penfold, J.; Thomas, R. K.; Petkov, J. T.; Tucker, I., *Langmuir* **2013,** *29* (41), 12744-12753.

31. Sowada, R., *Journal für praktische Chemie* **1981,** *323* (2), 269-278.
32. Shiloach, A.; Blankschtein, D., *Langmuir* **1998,** *14* (25), 7166-7182.
33. Aoudia, M.; Al-Maamari, T.; Al-Salmi, F., *Colloids and Surfaces A: Physicochemical and Engineering Aspects* **2009,** *335* (1-3), 55-61.
34. Vollhardt, D.; Czichocki, G.; Rudert, R., *Colloids and Surfaces A: Physicochemical and Engineering Aspects* **1998,** *142* (2-3), 315-322.
35. Schwuger, M. J., Interfacial and Performance Properties of Sulfated Polyoxyethylenated Alcohols. In *Structure/Performance Relationships in Surfactants*, Rosen, M., Ed. ACS Symposium Series; American Chemical Society: Washington, DC, 1984; pp 3-26.
36. Rouse, J. D.; Sabatini, D. A.; Brown, R. E.; Harwell, J. H., *Water Environment Research* **1996,** *68* (2), 162-168.
37. Xu, H.; Penfold, J.; Thomas, R. K.; Petkov, J. T.; Tucker, I.; Webster, J. P. R., *Langmuir* **2013,** *29* (37), 11656-11666.
38. Aoudia, M.; Al-Haddabi, B.; Al-Harthi, Z.; Al-Rubkhi, A., *Journal of Surfactants and Detergents* **2010,** *13* (1), 103-111.
39. Xu, H.; Penfold, J.; Thomas, R. K.; Petkov, J. T.; Tucker, I.; Grillo, I.; Terry, A., *Langmuir* **2013,** *29* (44), 13359-13366.
40. Razafindralambo, H.; Popineau, Y.; Deleu, M.; Hbid, C.; Jacques, P.; Thonart, P.; Paquot, M., *Journal of Agricultural and Food Chemistry* **1998,** *46* (3), 911-916.
41. Cirigliano, M. C.; Carman, G. M., *Applied and Environmental Microbiology* **1985,** *50* (4), 846-850.
42. Zhu, Y.; Gan, J.-j.; Zhang, G.-l.; Yao, B.; Zhu, W.-j.; Meng, Q., *Journal of Zhejiang University SCIENCE A* **2007,** *8* (9), 1514-1520.
43. Rosenberg, E.; Ron, E. Z., *Applied Microbiology and Biotechnology* **1999,** *52* (2), 154-162.
44. Chen, M. L.; Penfold, J.; Thomas, R. K.; Smyth, T. J. P.; Perfumo, A.; Marchant, R.; Banat, I. M.; Stevenson, P.; Parry, A.; Tucker, I.; Grillo, I., *Langmuir* **2010,** *26* (23), 18281-92.
45. Jarvis, F. G.; Johnson, M. J., *Journal of the American Chemical Society* **1949,** *71* (12), 4124-4126.
46. Smyth, T. J.; Perfumo, A.; Marchant, R.; Banat, I. M.; Chen, M.; Thomas, R. K.; Penfold, J.; Stevenson, P. S.; Parry, N. J., *Applied Microbiology and Biotechnology* **2010,** *87* (4), 1347-1354.
47. Bergström, S.; Theorell, H.; Davide, H., *Arkiv. Kemi. Mineral. Geol.* **1946a,** *23A* (13), 1-12.
48. Bergström, S.; Theorell, H.; Davide, H., *Archives of Biochemistry and Biophysics* **1946b,** *10*, 165-166.
49. Rashedi, H.; Jamshidi, E.; Mazaheri Assadi, M.; Bonakdarpour, B., *Int. J. Environ. Sci. Tech.* **2005,** *2* (2), 121-127.
50. Abdel-Mawgoud, A. M.; Lepine, F.; Deziel, E., *Applied Microbiology and Biotechnology* **2010,** *86* (5), 1323-1336.
51. Zhong, H.; Zeng, G. M.; Liu, J. X.; Xu, X. M.; Yuan, X. Z.; Fu, H. Y.; Huang, G. H.; Liu, Z. F.; Ding, Y., *Applied Microbiology and Biotechnology* **2008,** *79* (4), 671-677.
52. Peker, S.; Helvaci, S.; Ozdemir, G., *Langmuir* **2003,** *19* (14), 5838-5845.
53. Guo, Y.-P.; Hu, Y.-Y.; Gu, R. R.; Lin, H., *Journal of Colloid and Interface Science* **2009,** *331* (2), 356-363.
54. Chen, M. DPhil thesis. University of Oxford, 2010.
55. Ozdemir, G.; Peker, S.; Helvaci, S. S., *Colloids and Surfaces A: Physicochemical and Engineering Aspects* **2004,** *234* (1-3), 135-143.
56. Sánchez, M.; Aranda, F. J.; Espuny, M. J.; Marqués, A.; Teruel, J. A.; Manresa, Á.; Ortiz, A., *Journal of Colloid and Interface Science* **2007,** *307* (1), 246-253.
57. Dahrazma, B.; Mulligan, C. N.; Nieh, M.-P., *Journal of Colloid and Interface Science* **2008,** *319* (2), 590-593.
58. Gorin, P. A. J.; Spencer, J. F. T.; Tulloch, A. P., *Canadian Journal of Chemistry* **1961,** *39* (4), 846-855.
59. Davila, A. M.; Marchal, R.; Monin, N.; Vandecasteele, J. P., *Journal of Chromatography A* **1993,** *648* (1), 139-149.

60. Chen, M.; Dong, C. C.; Penfold, J.; Thomas, R. K.; Smyth, T., J. P.; Perfumo, A.; Marchant, R.; Banat, I. M.; Stevenson, P.; Parry, A.; Tucker, I.; Campbell, R. A., *Langmuir* **2011,** *27* (14), 8854-8866.
61. Penfold, J.; Chen, M.; Thomas, R. K.; Dong, C.; Smyth, T. J. P.; Perfumo, A.; Marchant, R.; Banat, I. M.; Stevenson, P.; Parry, A.; Tucker, I.; Grillo, I., *Langmuir* **2011,** *27*, 8867-8877.
62. Kitamoto, D.; Yanagishita, H.; Shinbo, T.; Nakane, T.; Kamisawa, C.; Nakahara, T., *Journal of Biotechnology* **1993,** *29* (1-2), 91-96.
63. Imura, T.; Yanagishita, H.; Kitamoto, D., *Journal of the American Chemical Society* **2004,** *126* (35), 10804-10805.
64. Arima, K.; Kakinuma, A.; Tamura, G., *Biochemical and Biophysical Chemical Research Communications* **1968,** *31* (3), 488-494.
65. Razafindralambo, H.; Paquot, M.; Baniel, A.; Popineau, Y.; Hbid, C.; Jacques, P.; Thonart, P., *Journal of the American Oil Chemists' Society* **1996,** *73* (1), 149-151.
66. Cirigliano, M. C.; Carman, G. M., *Applied and Environmental Microbiology* **1984,** *48* (4), 747-750.
67. Persson, A.; Österberg, E.; Dostalek, M., *Applied Microbiology and Biotechnology* **1988,** *29* (1), 1-4.
68. Rosenberg, E.; Zuckerberg, A.; Rubinovitz, C.; Gutnick, D. L., *Applied and Environmental Microbiology* **1979,** *37* (3), 402-408.
69. Zuckerberg, A.; Diver, A.; Peeri, Z.; Gutnick, D. L.; Rosenberg, E., *Applied and Environmental Microbiology* **1979,** *37* (3), 414-420.
70. Hasan, F.; Shah, A. A.; Hameed, A., *Enzyme and Microbial Technology* **2006,** *39* (2), 235-251.
71. Houde, A.; Kademi, A.; Leblanc, D., *Applied Biochemistry and Biotechnology* **2004,** *118* (1-3), 155-170.
72. Novozymes world wide web page - Novozymes' history. http://www.novozymes.com/en/about-us/facts-about-Novozymes/Novozymes-history/Pages/default.aspx.
73. Hutchinson, E., *Journal of Colloid Science* **1948,** *3* (5), 413-424.
74. Li, P. X.; Li, Z. X.; Shen, H.-H.; Thomas, R. K.; Penfold, J.; Lu, J. R., *Langmuir* **2013,** *29* (30), 9324-9334.
75. Tanford, C., *Journal of Physical Chemistry* **1972,** *76* (21), 3020-3024.
76. Israelachvili, J. N.; Mitchell, D. J.; Ninham, B. W., *Journal of the Chemical Society, Faraday Transactions 2: Molecular and Chemical Physics* **1976,** *72*, 1525-1568.
77. Stellner, K. L.; Scamehorn, J. F., *Langmuir* **1989,** *5* (1), 77-84.
78. Stellner, K. L.; Amante, J. C.; Scamehorn, J. F.; Harwell, J. H., *Journal of Colloid and Interface Science* **1988,** *123* (1), 186-200.
79. Shiau, B.-J.; Harwell, J. H.; Scamehorn, J. F., *Journal of Colloid and Interface Science* **1994,** *167* (2), 332-345.
80. Boyd, B. J.; Drummond, C. J.; Krodkiewska, I.; Weerawardena, A.; Furlong, D. N.; Grieser, F., *Langmuir* **2001,** *17* (20), 6100-6107.
81. Clint, J. H., *Journal of the Chemical Society, Faraday Transactions 1* **1975,** *71*, 1327-1334.
82. Rubingh, D. N., Mixed Micelle Solutions. In *Solution Chemistry of Surfactants*, Mittal, K. L., Ed. Plenum Press: New York, 1979; Vol. 1, pp 337-354.
83. Kamrath, R. F.; Franses, E. I., *Journal of Physical Chemistry* **1984,** *88* (8), 1642-1648.
84. Holland, P. M.; Rubingh, D. N., *Journal of Physical Chemistry* **1983,** *87* (11), 1984-1990.
85. Holland, P. M., *Advances in Colloid and Interface Science* **1986,** *26*, 111-129.
86. Holland, P. M., *Colloids and Surfaces* **1986,** *19* (2-3), 171-183.
87. Hines, J. D.; Thomas, R. K.; Garrett, P. R.; Rennie, G. K.; Penfold, J., *Journal of Physical Chemistry B* **1998,** *102* (44), 8834-8846.

Chapter 2

Theoretical background and experimental procedures

This chapter describes the theoretical background to the techniques of surface tension (ST), neutron reflectivity (NR) and small angle neutron scattering (SANS), and the experimental procedures for all three. The processes of purification of the protonated and deuterated rhamnolipids and deuterated $C_{12}E_8$ are described.

2.1 Surface tension

2.1.1 Theoretical background

The phenomenon of surface tension is related to the cohesive forces between liquid molecules, which cause a greater attraction between molecules in the liquid bulk than in the gaseous phase. At the air/water interface, fewer molecules are in contact with each other than in the bulk solution and so there is a net attraction of water molecules towards the bulk to minimise the contact with air. This is a spontaneous process. The surface tension of a solution is its surface free energy per unit area. The minimum amount of work that is required to expand the interfacial area by dA is the Gibbs free energy:

$$dG = \gamma dA \tag{2.1}$$

where γ is the surface tension measured in force per unit length, and dA is the change in area at the surface. The strength of the intermolecular forces governs the magnitude of the surface tension. In water this value is high[1] due to the hydrogen bonding between the O and H atoms on neighbouring water molecules. The addition of surface active molecules causes the work required to change the area at the interface to be reduced, thus lowering the surface tension.

Surface tension is used principally in this thesis to determine the critical micelle concentration (CMC) of the surfactants and their mixtures, where a sharp break in the surface tension versus log(concentration) curve is observed. It is also possible, using the steepest gradient immediately below

the break in the plot at the CMC, to estimate the surface excess, Γ, i.e. the amount of surfactant adsorbed at the CMC as a monolayer at the interface, using the Gibbs equation:

$$\Gamma_i = \frac{1}{nRT}\left(\frac{d\gamma}{d\ln a_i}\right) \tag{2.2}$$

where a_i is the activity of component i which can be approximated to concentration c_i in mol dm^{-3}, and n is the Gibbs prefactor. If the system contains enough electrolyte to reduce any electrostatic interations, or if the surfactant is nonionic in nature, then the Gibbs prefactor is 1. In the absence of any electrolyte, for ionic surfactants, e.g. A^-X^+, the Gibbs prefactor, will be 2. From this the area per molecule can be determined:

$$A = \frac{1}{N_A\Gamma} \tag{2.3}$$

However, for reasons explained in Chapter 3, the Gibbs equation is not used in this thesis to find the area per molecule. The focus was placed on the variation in mixed CMC values as a function of solution composition and their comparison with ideal and non-ideal mixing models.

2.1.2 Experimental

2.1.2.1 Materials and solution preparation

Protonated $C_{12}E_8$ was obtained from Nikkol Chemicals Group, Tokyo, Japan and was used as received. Protonated LAS-6 was synthesised by S. Golding, Unilever, the synthesis and purification of which is described elsewhere.[2] Protonated SLES-2EO was synthesised and purified through recrystallisation by H. Xu[3] and its purity evaluated by surface tension. NaOH pellets were purchased from Sigma.

Surface tension measurements were made on binary $C_{12}E_8$/LAS, $C_{12}E_8$/SLES and LAS/SLES mixtures at compositions 0.75/0.25, 0.5/0.5 and 0.25/0.75, and the ternary $C_{12}E_8$/LAS/SLES system at solution composition 0.125/0.125/0.75. Solutions were prepared in MilliQ ultrapure water containing $1x10^{-6}$ M NaOH (Section 2.3.3.3).

2.1.2.2 Instrumentation

The surface tension measurements were made on a Krüss K10T maximum pull digital tensiometer, using a Pt/Ir du Nouy ring. Measurements were made at 25 ± 0.1°C with the temperature controlled using a Haake K15 water bath with a manual D30 circulator connected to the waterbath. All surface tension values were referenced to a value of 71.5 ± 0.1 mN/m at 25 ± 0.1°C for ultrapure MilliQ water, which is in good general agreement to literature values (71.99 mN/m at 25°C).[1] To achieve temperature equilibrium, solutions contained in a glass pot (dimensions of 48 mm diameter and 30 mm depth) were kept in the instrument for 10 minutes before the surface tension was measured. The Pt/Ir ring was dipped onto the surface of the solution and the measurement taken from when the ring was in contact with the interface. The most concentrated solution was measured first, approximately 8 x CMC, and subsequent concentrations were obtained by dilution with MilliQ ultrapure water containing $1x10^{-6}$ M NaOH, with all subsequent volumes added verified by weight. The average of three consecutive surface tension measurements was taken and the error was found to be always within 0.5 mN/m. In between measurements, the Pt/Ir ring was washed in MilliQ ultrapure water and flame dried in a Bunsen burner immediately before further use.

2.2 Neutron scattering

Neutron scattering is a powerful and versatile technique to study the adsorption behaviour, bulk aggregate structure and composition of amphiphilic molecules at interfaces and in solution. Neutron scattering techniques include reflectivity, small angle scattering and diffraction methods and probe a wide range of length scales, from angstrom to sub-micrometer dimensions. Small angle neutron scattering is able to probe the larger length scales, up to sub-micrometer dimensions.

Utilising the large difference in scattering power, as characterised by the scattering length, b, between hydrogen and deuterium (H = -3.74×10^{-13} cm and D = 6.67×10^{-13} cm) and by deuterating part or all of one molecule through the technique of D/H isotopic substitution, it is possible to manipulate the scattering length density, ρ, of certain components. The scattering length density is defined as:

$$\rho = \Sigma b_i n_i \tag{2.4}$$

where b_i and n_i are the scattering length and number density, respectively, for atomic species i. Through highlighting certain parts of molecules it is possible to determine the relative compositions of surfactants in a mixture at the air/water interface and in micelles, and to elucidate detailed structural information to a relatively high resolution (around 2 Å).[4,5,6] Isotopic substitution is not generally expected to affect the CMC of the pure protonated and deuterated surfactants.[4] The scattering length of some of the most common elements are given in Table 2.1, with the sum of scattering lengths for the protonated and deuterated version of each surfactant used in this thesis in Table 2.2.

Element	Scattering length b / $\times 10^{-5}$ Å
^{1}H	-3.741
^{2}D	6.671
C	6.646
O	5.803
S	2.847

Table 2.1: Scattering lengths for the elements ^{1}H, ^{2}D, C, O and S.

Surfactant	Molecular formula	Sum of scattering lengths Σb / $x10^{-3}$ Å
h-$C_{12}E_8$	$C_{28}H_{58}O_9$	0.22
d-$C_{12}E_8$	$C_{28}D_{58}O_9$	2.82
h-LAS-6	$C_{12}H_{29}SO_3Na$	0.35
d-LAS-6	$C_{12}D_{29}SO_3Na$	3.48
h-SLES-2EO	$C_{12}H_{25}(OC_2H_4)_2SO_4Na$	0.24
d-SLES-2EO	$C_{12}D_{25}(OC_2H_4)_2SO_4Na$	2.88
h-SDS	$C_{12}H_{25}SO_4Na$	0.33
d-SDS	$C_{12}D_{25}SO_4Na$	6.74
h-R1	$C_{26}H_{48}O_9$	0.45
d-R1 (90 atom% D)	$C_{26}D_{43}H_5O_9$	4.93
d-R1 (78 atom% D)	$C_{26}D_{37}H_{11}O_9$	4.34
h-R2	$C_{32}H_{58}O_{13}$	0.64
d-R2 (90 atom% D)	$C_{32}D_{52}H_6O_{13}$	6.13

Table 2.2: Sum of scattering lengths for all protonated and deuterated surfactants used in this work.

The two main scattering techniques used in this work are neutron reflectivity (NR) and small angle neutron scattering (SANS). For air/water interfacial measurements using NR (Figure 2.1) the scattering length densities of the air and water can be matched by the use of null reflecting water (NRW) as the solvent, composed of 92 vol% H_2O and 8 vol% D_2O, which has a scattering length density, ρ, of 0 and neutron refractive index, n, of 1, identical to air. In a solution containing a deuterium-labelled surfactant, no reflection occurs from the solvent and the only reflected signal will be that of the deuterated molecules in the surfactant monolayer, with their refractive indices and scattering length densities variable depending on the sum of scattering lengths of the molecule. For bulk solution measurements using SANS (Figure 2.2), the natural contrast of micelles in solution is different for the micelle outer shell containing the hydrophilic headgroups, the inner alkyl chain core and the surrounding solvent (D_2O). If the scattering length density of the inner hydrophobic core is contrast matched to the solvent, it is possible to "see" just the outer shell, whereas if the outer shell is contrast matched to the solvent only the hydrophobic core will be visible.

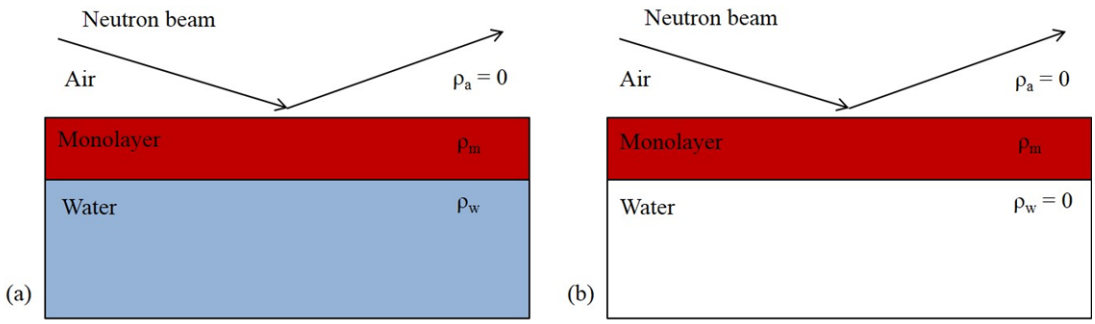

Figure 2.1: Contrast variation for a surfactant monolayer at the air/water interface where (a) the scattering length densities (SLD, ρ) of the air, water and monolayer are all different, and (b) where the scattering length densities of the air and water have been contrast matched so that only the monolayer is visible.[7]

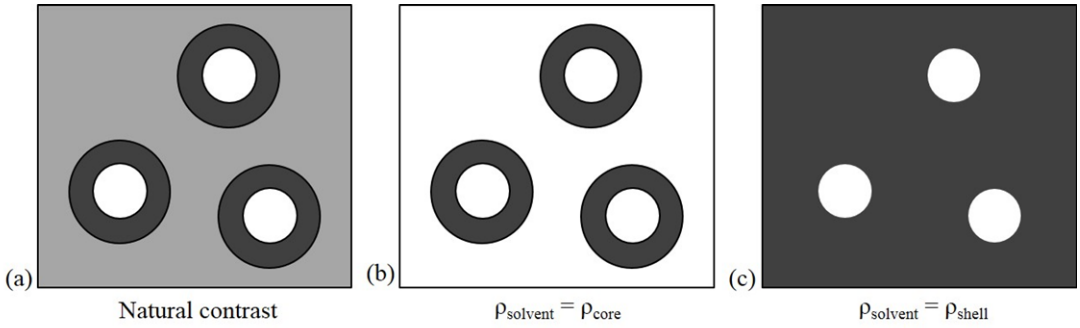

Figure 2.2: Contrast variation for surfactant micelles where (a) the scattering length density, ρ, of the core, shell and solvent are all different, at their natural contrast, (b) the ρ of the core and solvent are contrast matched so only the shell is visible, and (c) the ρ of the shell and solvent are contrast matched so only the core is visible.[8]

2.3 Neutron reflectivity

2.3.1 Theoretical background

Neutron reflectivity (NR) is a depth profiling technique which is able to measure the structure and composition of molecules including surfactants, polymers and solid films, at the interfaces of different media, for example air/liquid, solid/liquid or liquid/liquid interfaces.[9] It provides information on the neutron refractive index n normal to the interface. In specular reflection, the angle of incidence of the radiation at an interface equals the angle of reflection, and therefore the neutron refractive index, n, between the two media, for example air and water, is:

$$n = \frac{k_1}{k_0} \tag{2.5}$$

where k_0 and k_1 are the neutron wave vectors outside and inside the medium, respectively. Figure 2.3 shows the specular reflection of neutrons at the air/water interface, with a surfactant monolayer of refractive index n_1. The refractive index of the medium (for example, water), n_2, is usually below 1, but for air, n_0, it is almost 1.

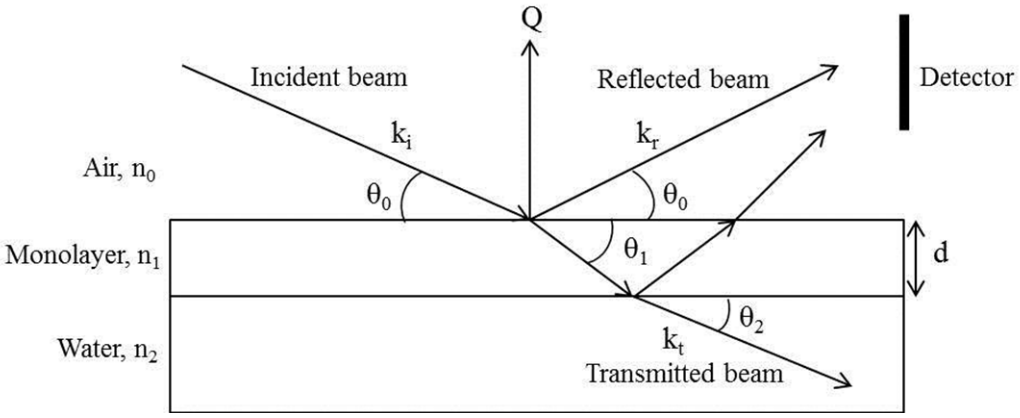

Figure 2.3: Schematic diagram of the specular reflection from a monolayer, where k_i k_r, and k_t are the incident, reflected and transmitted wave vectors, respectively, θ_0 is the incident (and reflected) angle, and θ_1 and θ_2 are the transmitted angles.[10]

The simple relationship between neutron wavelength, λ, the critical angle, θ_c, according to Snell's law, and the scattering length density, ρ (as defined in equation 2.4), of the material which the neutrons are incident to (for example, water at the air/water interface) is:

$$\theta_c = \lambda\sqrt{\frac{\rho}{\pi}} \tag{2.6}$$

Neutron reflectivity measures the variation in specular reflection with wave vector transfer, Q, in the z direction normal to the interface, and so provides structural information in this direction. The wave vector transfer, Q, is defined as:

$$Q = 4\pi \sin\frac{\theta}{\lambda} \tag{2.7}$$

where θ is the grazing angle of incidence and λ is the neutron wavelength. The variation in the reflectivity with Q is related to the composition, or density profile, in the direction normal to the interface. It is possible to manipulate the scattering length density, ρ(z), or neutron refractive index, n, defined in Equation 2.8, of the medium through the use of D/H isotopic substitution:

$$n = 1 - \frac{\lambda^2 \rho(z)}{2\pi} \tag{2.8}$$

For a solution containing a deuterated surfactant in the monolayer, the refractive index of the liquid phase can be matched to that of air (which is 1) by using null reflecting water (NRW) as the solvent, as described in Section 2.2, so that the only reflected signal will be that of the deuterated molecules in the surfactant layer.

2.3.2 Fitting of reflectivity profiles

The Kinematic or Born approximation[11] is often used to analyse reflectivity profiles and can be used when values for Q are sufficiently high and the scattering is weak. It can be used to determine details in surface structure by determination of the scattering length density profile, $\rho(z)$, normal to the interface. The scattering length density is defined as:

$$\rho(z) = \Sigma b_i n_i(z) \tag{2.9}$$

where $n_i(z)$ is the number density profile of species i and b_i is the neutron scattering length. For example, the structure of a surfactant at the air/water interface can be described in terms of the distributions of the hydrocarbon chain (c), the headgroup (h) and the water solvent (s):

$$\rho(z) = b_c n_c(z) + b_h n_h(z) + b_s n_s(z) \tag{2.10}$$

In the kinematic approximation, the reflectivity, R, is related to the square of the one dimensional Fourier transform of the gradient of the scattering length density profile, p(z), normal to the interface:[12]

$$R(Q) = \frac{16\pi^2}{Q^2}\left|\int \rho(z) e^{iQz} dz\right|^2 \tag{2.11}$$

The p(z) can be manipulated by the use of D/H isotopic substitution. The reflected signal of the deuterium-labelled surfactant in NRW gives a slope of reflectivity versus wavevector transfer, Q, which provides information on the adsorbed amount of the surfactant and the thickness of the adsorbed layer. The absolute reflectivity value reflects the actual amount of surfactant adsorbed, whereas the thickness of the adsorbed layer is proportional to the slope of the reflectivity, i.e. a steeper slope will have a thicker adsorbed layer. Neutron reflectivity assumes lateral uniformity across the monolayer being analysed.

Alternatively, the exact optical matrix method[12,13] can be used to model and fit the measured data. The data are compared with a curve calculated by this method. The reflectivity from the deuterated surfactant at the interface is described by a single layer of uniform composition. Reflection from a layer of deuterated material adsorbed at the interface between air and NRW is given by:

$$\frac{\kappa^4}{16\pi^2} R \approx 2\rho^2 - 2\rho^2 \cos(\kappa\tau) = 4b^2 n^2 \sin^2\left(\frac{\kappa\tau}{2}\right) \tag{2.12}$$

where the reflectivity is defined in terms of the momentum transfer, κ:

$$\kappa = \frac{4\pi \sin\theta_0}{\lambda} = 2q_0 \tag{2.13}$$

and where q is the radiation wave vector normal to the interface. The model fitting provides the thickness of the adsorbed layer, d, and the scattering length density, ρ, which determines the absolute level of reflectivity, and from which the area per molecule, A, can be determined using the sum of scattering lengths, Σb:

$$\rho = \frac{\Sigma b}{Ad} \tag{2.14}$$

In a ternary mixture where each component is selectively deuterated, the area per molecule for each surfactant in the mixture is given by:

$$\rho = \Sigma \frac{\Sigma b_n}{A_n d} \tag{2.15}$$

where b_n and A_n are the scattering lengths and area per molecule for each separate component in the n-component mixture. The surface excess, Γ, and subsequently the surface composition of each component are then found by:

$$\Gamma = \frac{1}{N_A A} \tag{2.16}$$

where N_A is Avogadro's constant, which converts the units from Å^2 to mol cm^{-2}. The focus here is on determining the adsorbed amount, Γ, at the interface, which is obtained by the product of d and ρ. The reflectivity is very sensitive to Γ as it depends quadratically on the R value. As the d is varied while fitting the data, there is a compensating inverse relationship with ρ. By varying these two parameters, the subsequent minimum in χ^2 obtained with increasing Γ is much sharper than for either d or ρ. This shows that the Γ product can be determined more accurately than either d or ρ alone as the errors of the product are smaller than the individual components.[12]

2.3.3 Experimental

2.3.3.1 Instrumentation

The neutron reflectivity measurements were made on the SURF[14] and INTER[15] reflectometers at the ISIS pulsed neutron source, Rutherford Appleton Laboratory, Didcot, UK and on the FIGARO[16] reflectometer at the ILL, Grenoble, France. All the reflectometers use the white beam time of flight (TOF) method. Figure 2.4 shows a graphical description of layout of the SURF reflectometer at ISIS.[14]

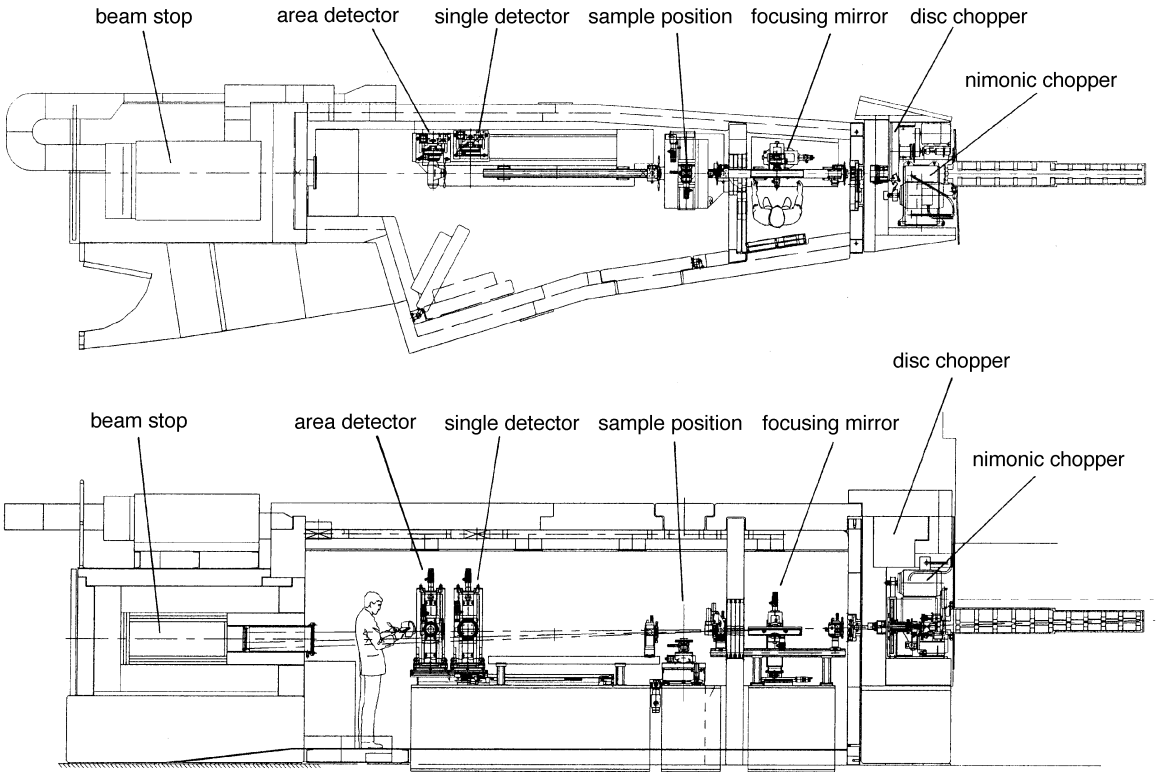

Figure 2.4: Diagram showing the layout of the SURF reflectometer at the ISIS pulsed neutron source, UK, reproduced from literature[14] with the author's permission.

In reflectometers such as SURF, a pulsed white neutron beam passes down the collimation tube at a fixed angle θ of 1.5° inclined to the horizon, over a wide range of wavelengths (TOF method).[17] A nimonic chopper and a double disc chopper at 6 m operate at 50 Hz, which limit the wavelength to 0.5-6.8 Å. Coarse collimation is provided by collimation jaws to obtain a beam of up to 60 x 10 mm dimensions and fine collimation is provided by Cd/B_4C slits positioned before and after the sample position. The reflected neutrons are detected by either a single ^3He gas detector or a two-dimensional area detector, with a variable sample to detector distance of 1.0 to 2.43 m.[14] On SURF all measurements were made using a single detector at a fixed angle θ of 1.5°, using a wavelength, λ,

range of 0.5 - 6.8 Å to provide a wave vector transfer, Q, in the range of 0.048 - 0.57 $Å^{-1}$. INTER has a very similar setup to SURF, but with a flux of an order of magnitude greater.[18] A fixed angle of incidence of 2.3° was used with a wavelength range of 0.5 - 15 Å, to provide a Q range of 0.03 - 0.5 $Å^{-1}$.

The setup of FIGARO is shown in Figure 2.5. Two frame overlap mirrors prevent neutrons from succeeding pulses, above a certain wavelength, from passing through. The neutron beam is pulsed by four choppers and two deflecting mirrors direct the neutrons towards the samples, either upwards or downwards. The beam is transmitted through a collimation tube to direct it towards the sample. Air scattering at the sample is reduced by the presence of an evacuated flight tube after the sample position. The reflected neutrons pass through this to reach the detector, which records a 2D image of the reflectivity.

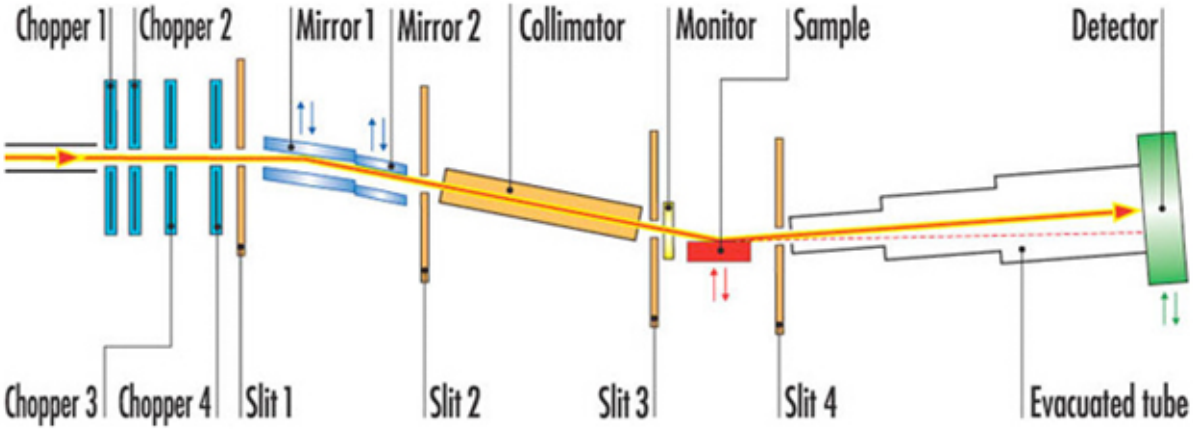

Figure 2.5: Diagram showing the layout of the FIGARO reflectometer at the ILL.[16]

A fixed angle θ of 3.6° was used on FIGARO, but due to the wavelength range being higher (2-30 Å), the Q value remained very similar to those obtained on SURF and INTER. The Q range was ~0.002 to ~0.39 $Å^{-1}$ with the beam deflected downwards and ~0.002 to ~0.27 $Å^{-1}$ with the beam deflected upwards.

2.3.3.2 Materials

Protonated $C_{12}E_8$, LAS and SLES were as described in Section 2.1.2.1. Head-deuterated $hC_{12}dE_8$ and chain-deuterated $dC_{12}hE_8$ were synthesised by R. K. Thomas at the Physical and Theoretical Chemistry Laboratory, University of Oxford, and the synthesis is described elsewhere.[19,20] Chain-deuterated $dC_{12}hE_8$ was purified by medium pressure liquid chromatography (MPLC), as described in Section 2.5.1. Fully-deuterated LAS was synthesised and purified following the same procedures as for protonated LAS and is described elsewhere.[2] Chain-deuterated SLES was synthesised and purified through recrystallisation by H. Xu[3] and its purity evaluated by surface tension and NR (through surface excess measurements of the fully-deuterated and a 50/50 mixture of h/d-SLES; the consistent surface excesses obtained indicated equal and adequate purity for both compounds). Protonated rhamnolipid biosurfactant mixture JBR505 was obtained from Jeneil Biosurfactant Co., Saukville, WI, and deuterated rhamnolipids (~90 atom% D) were produced by the methods described in Chapter 3. Both were subsequently separated into their pure components R1 and R2 by MPLC. NaOH pellets were purchased from Sigma and deuterium oxide, D_2O (99.9 atom%) was obtained from Fluorochem.

2.3.3.3 Sample preparation

It was imperative that all glassware was fully cleaned prior to sample preparation to ensure that no impurities were present. All glassware was soaked overnight in cold 5% Decon 90 solution prepared using deionised water. This was followed by extensive rinsing and soaking in deionised water and further rinsing in MilliQ ultrapure water until hard shaking produced no stable bubbles. The glassware was then rinsed in high-purity ethanol and acetone, dried under nitrogen gas, then stored capped until use.

All surfactant samples were made up in NRW containing $1x10^{-6}$ M NaOH. $1x10^{-6}$ M NaOH corresponded theoretically to pH 8, a slightly alkaline pH originally chosen due to the alkaline pH of commercial detergent formulations, and its compatibility with bacterial lipases, a possible biosurfactant to be used in related work. In reality, using NaOH to keep the pH at 8 was difficult due to atmospheric CO_2 acidifying the aqueous solution over time, and so it was found to be at an almost neutral pH of 6.5 ± 0.5. However, as required, this was higher than if MilliQ ultrapure water was used

alone as its pH was lower, often below pH 6. Buffer was not used to maintain pH 8 due to the introduction of additional counterions (electrolyte) which affected the CMC and area per molecule of the individual surfactants, as well as increasing their surface activity, due to the increased ionic strength in buffer.[10] However, the conventional surfactants are almost independent of pH[21] in the range used in this work, particularly for the nonionic surfactant, and the rhamnolipid molecules in neutral to alkaline pH are, although dissociated, still only weakly anionic and act more like nonionic surfactants at any pH.[22] Therefore a fixed pH using buffer was not required.

n+1 samples were prepared for each solution composition, where n is the number of components, with the following isotopic combinations: for example, dh, hd, and dd for the binary mixtures, and dhhhh, hdhhh, hhdhh, hhhdh, hhhhd and ddddd for the five-component mixtures. This ensured detailed analysis of each surfactant at the interface in turn and the final fully-deuterated contrast was employed to allow for overdetermination and ensure consistency of measurements. A fixed concentration of 2 mM was used throughout, above both the mixed and separate surfactant CMCs.

2.3.3.4 Experimental procedures

The SURF reflectometer housed a sample changer which held 5 Teflon troughs with dimensions 235 x 50 x 2 mm, allowing up to 5 sample loadings at one time. INTER had a similar sample environment with the sample changer holding 7 troughs with the same dimensions. Each trough held 25 ml solution. The FIGARO sample changer held 6 troughs of dimensions 250 x 50 x 1 mm and also held 25 ml solution. In the sample changer the troughs were covered with airtight lids to minimise evaporation and D/H exchange. All measurements were carried out at 25°C, unless otherwise stated.

Prior to measurements, the troughs were disassembled and soaked in 5% Decon 90 solution (prepared in deionised water) overnight, then after extensive rinsing in MilliQ ultrapure water they were dried, reassembled and used immediately. In between sample changes, troughs were washed thoroughly in running ultrapure water for a few minutes and dried. Sample solutions were poured carefully into the Teflon troughs and any visible bubbles removed from the surface with a Pasteur pipette.

The surface was aligned using a laser beam for reference and the heights of each trough adjusted before each measurement until the laser beam was seen to be in the centre of the detector slit. A command file was set up from which it was possible to control the sample heights, positions, and sample names. A reflectivity profile of reflectivity versus wave vector transfer, Q, was obtained for each sample and stored as separate data files.

All data were calibrated with respect to a direct beam and to a reflectivity profile of D_2O, which is compared to a known reflectivity profile. A scale factor was then obtained and used for all further measurements. The reflectivity was corrected for background, which can originate from a variety of different sources, and principally incoherent scattering. The background scattering was approximately $5x10^{-6}$ in NRW, largely independent of Q and was included in the data fitting process.

Data was analysed using the program OpenGenie and the MULF fitting program, assuming monolayer adsorption at the interface, and using Equation 2.11. The fitting and subsequent obtaining of reflectivity parameters layer thickness, ρ, and the scattering length density, d, were obtained as described in Section 2.3.2, from which the area per molecule, surface excess and the relative surface composition for each component in the surfactant mixture were found.

2.4 Small angle neutron scattering

2.4.1 Theoretical background

Small angle neutron scattering (SANS) is a very effective method for characterising the shape and size of many chemical and biological molecules and assemblies in solution, ranging from angstrom to sub-micrometer dimensions. It is a powerful, non-invasive technique which measures the coherent elastic scattering of radiation by a sample in the forwards direction, as shown in Figure 2.6.

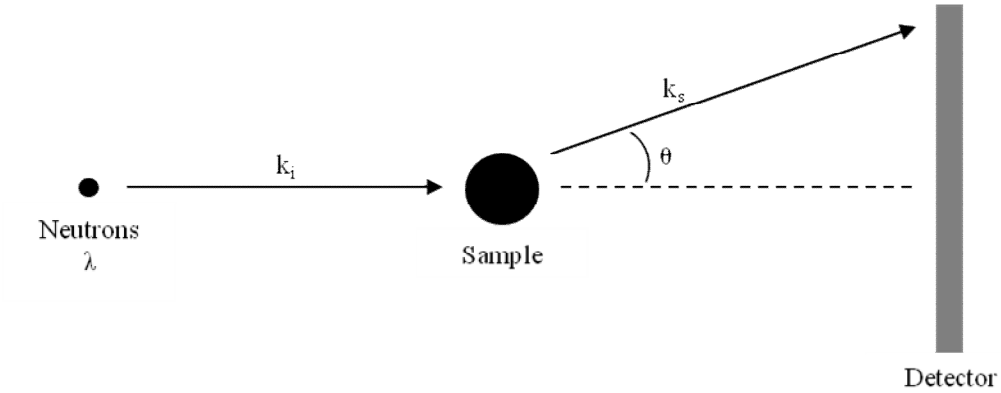

Figure 2.6: Schematic diagram of scattering of a sample in a SANS instrument.

The scattering vector, or wave vector transfer, Q, is a description of the relationship between the incident, k_i, and scattered, k_s, wave vectors. Its modulus is given by the following:

$$Q = |k_s - k_i| = \frac{4\pi n}{\lambda}\sin\left(\frac{\theta}{2}\right) \tag{2.17}$$

where λ is the neutron wavelength and the neutron refractive index, n, can be approximated to 1. If there is a repeating distance, d, in the structure, Bragg's law of diffraction gives:

$$\lambda = 2d\sin\frac{\theta}{2} \tag{2.18}$$

By substituting this into Equation 2.17, the scattering vector, Q, with units usually expressed as $Å^{-1}$, on different length scales, d, can be simply related to Q by:

$$d = \frac{2\pi}{Q} \tag{2.19}$$

It is the large Q range available on the SANS instrument that allows a large range of length scales to be probed. The detector measures the flux of neutrons, I(Q), reaching the detector in a certain amount of time at a certain wavelength, λ, where:

$$I(\lambda,\theta) = I_0(\lambda)\Delta\Omega\eta(\lambda)T(\lambda)V\frac{\delta\Sigma}{\delta\Omega}(Q) \tag{2.20}$$

where I_0 is the incident flux, $\Delta\Omega$ is the solid angle element, η is the detector efficiency, which are all specific to the instrument, and T is the sample transmission, V is the volume, and $\delta\Sigma/\delta\Omega$ (Q) is the macroscopic differential scattering cross section (scattering intensity), usually expressed in cm^{-1}. The scattering cross section is important as it carries all the necessary information on the structural information of the scattering bodies and the interactions between them, and is defined as:

$$\frac{\delta\Sigma}{\delta\Omega}(Q) = N_p V_p^2 (\Delta\rho)^2 P(Q)S(Q) + B_{inc} \tag{2.21}$$

where N_p is the number concentration of scattering bodies, V_p is the volume of one scattering body, $(\Delta\rho)^2$ is the squared difference in neutron scattering length density between the particles and solvent (ρ-$\rho_{solvent}$), i.e. the contrast, P(Q) is the form factor, S(Q) is the inter-particle structure factor, Q is the modulus of the scattering vector and B_{inc} is the incoherent background scattering. The first three terms in Equation 2.18 are independent of Q, but the form factor and structure factor depend on Q.

The form factor P(Q) describes the size and shape of the scattering bodies, by the scattering of neutrons from parts of the same particle. It is modelled here using the standard Core and Shell model for globular micelles.[23] For a spherical particle P(Q) is defined as follows:

$$P(Q) = V_1(\rho_1 - \rho_2)F_0(QR_1) + V_2(\rho_2 - \rho_s)F_0(QR_2) \tag{2.22}$$

where ρ_1, ρ_2 and ρ_3 are the scattering length densities of the micelle core, shell and the solvent, respectively, R_1 is the radius of the inner core of alkyl chains which have fully extended chain length l_c and R_2 is the radius of the outer shell containing the headgroup and associated hydration water. Both use fixed values in modelling using the standard Core-Shell model for interacting globular micelles.[23] The micelle volume is $V_i = 4\pi r_i^3/3$ and F_0(QR) for a spherical object with radius R is:

$$F_0(QR) = \frac{3j_1(QR)}{(QR)} = \frac{3[\sin(QR) - Qr\cos(QR)]}{(QR)^3} \tag{2.23}$$

If micelles have sufficiently large aggregation numbers, ν, the elliptical ratio, e, is included to accommodate the elliptical distortion made by the larger volume. Therefore the inner core dimensions

are R_1, R_1, eR_1 and the outer shell dimensions are R_2, R_2, eR_2. An additional parameter, ext, is included as a packing parameter which allows flexibility in the core partial molar volume values due to packing constraints, and is the division of the radius of the inner core R_1 by the extended alkyl chain length l_c.

The structure factor S(Q) describes the attractions between different particles and the relative positions of the different scattering bodies. This factor is included in the rescaled mean spherical approximation (RMSA) calculation.[24,25] The interaction between the particles depends on a repulsive screened Coulombic potential[24] which is defined by the surface charge, z, the micelle number density, N_p, diameter, d, and the Debye-Huckel screening length, κ^{-1}. In increasingly dilute solutions, S(Q) tends to unity because of the reduction in inter-particle interactions. The structure factor is:

$$S(Q) = 1 + 4\pi N_p \int_0^\infty [g(r) - 1] \frac{\sin(qr)}{qr} r^2 dr \tag{2.24}$$

and g(r) is the pair correlation function for the scattering particles.

The scattering data is analysed using the OpenGENIE fitting program[26] using Equations 2.17 to 2.24, where the fitting is optimised by varying the aggregation number, ν, surface charge, z, and core extension factor, ext, by a process of trial and error until the most satisfactory fit is achieved and χ^2 is minimised by least squares, to obtain values for the R_1, R_2, ellipticity, ee, and scale factor, f.

As with neutron reflectivity, the large differences in scattering lengths of H and D can be utilised to concentrate on certain components in a surfactant mixture through isotopic substitution. Through the use of D_2O as the solvent, it is possible to "see" only the surfactant molecules, which are all protonated, or to selectively deuterate certain components to observe scattering from only the protonated components. The surrounding medium used is D_2O because the larger incoherent scattering cross section for ^1H than ^2D leads to too high a background.

2.4.2 Experimental

2.4.2.1 Instrumentation

SANS measurements were made on the LOQ[27] and SANS2D[28] diffractometers at the ISIS pulsed neutron source, UK, and on the D33[29] diffractometer at the ILL, France. For all measurements the temperature was maintained at 25°C. Figure 2.7 shows the experimental setup for D33.

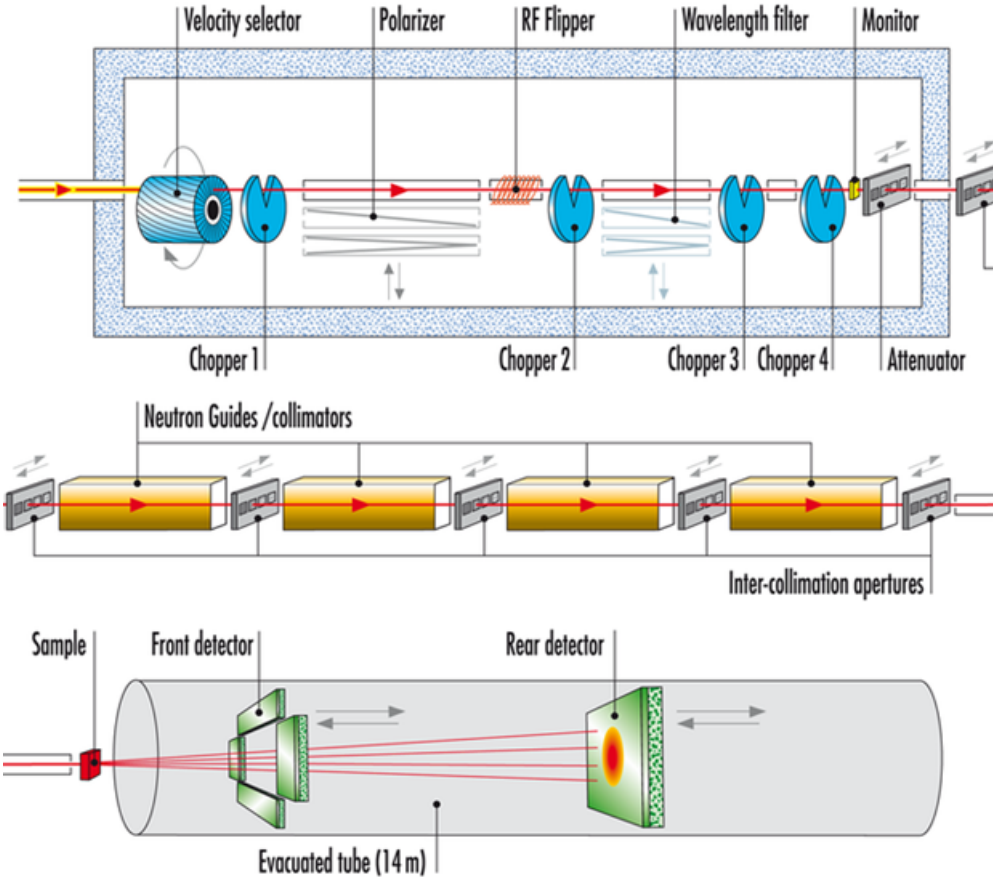

Figure 2.7: Experimental set-up of D33 diffractometer at the ILL, France.[29]

On D33, cold neutrons travel through the neutron guides, and the neutrons are selected either with a velocity selector if in monochromatic mode, or with four choppers if in TOF mode. The neutrons travel through a set of collimators towards the sample and then are reflected towards the front and rear detectors, which move between 1.2 m and 12.8 m after the sample position (in this work distances of 2 m and 12 m from the sample position were used, for the large angles and small angles, respectively.) The extended Q range on D33 is due to the presence of these two detectors at different distances from the sample, instead of just one. Neutrons are then collected by two ^{3}He gas tube detectors. D33 was used for measurements of the five-component biosurfactant mixtures at higher LAS solution

compositions, whereas LOQ and SANS2D were used for both ternary conventional and multicomponent biosurfactant mixtures, with SANS2D more specifically for solutions at the lower concentrations.

On LOQ, measurements were made using the white beam TOF method at a neutron wavelength of 2-10 Å and a sample to detector distance of 4 m which covered a wave vector transfer, Q, between 0.008 and 0.25 $Å^{-1}$. An 8 mm diameter beam was used to make the measurements. SANS data were collected for 15 μA (related to a measurement time of approximately 20 minutes) and transmission for 10 μA (15 minutes). SANS2D also used the white beam TOF method and an 8 mm diameter beam, at a wavelength of 2 - 12 Å to give a Q range of 0.01 – 0.35 Å.

2.4.2.2 Sample preparation

All surfactants used were in their protonated form and prepared in D_2O containing $1x10^{-6}$ M NaOH. Surfactant mixtures were made at a variety of solution compositions, identical to those used for neutron reflectivity (Figure 4.9, Chapter 4). 2 ml solutions were prepared at a fixed concentration of 50 mM and subsequent lower concentrations were prepared by dilution with D_2O containing $1x10^{-6}$ M NaOH. 0.5 ml solution was added to and held in Hellma quartz spectrophotometer cells with 1 mm path length. Each cell was stoppered to minimise contamination and evaporation. Prior to filling with solution, cells were cleaned thoroughly by soaking in dilute (~2%) Decon 90 for approximately 2 hours, then rinsing with copious amounts of MilliQ ultrapure water, rinsing with acetone and air-dried using an air pump. All cells were checked visually for cleanliness before use.

2.4.2.3 Experimental procedures

Samples in the Hellma quartz cells were held in a sample changer. On SANS2D the sample changer consisted of two decks holding a total of 40 samples, whereas LOQ and D33 held 20 samples, on one deck only. The horizontal and vertical positions for each sample in the decks were inputted and changed remotely using a command file on the computer. The scattering for each sample was measured and each scattering result stored as a separate data file.

A straight through beam and a measurement of D_2O was carried out beforehand. Corrections were made for the sample transmission and background scattering, which may originate from the quartz sample cell, incoherent scattering from the solvent, and from neutron noise. The raw scattering data was then converted to absolute scattering cross section ($I(Q) / cm^{-1}$), by reference to a standard scatterer.

2.5 Surfactant purification and separation

2.5.1 Medium pressure liquid chromatography

Medium pressure liquid chromatography (MPLC) was used for the purification of protonated and deuterated rhamnolipids and the separation of these into their two components, R1 and R2. Chain-deuterated $dC_{12}hE_8$ was also purified by the same method.

For the purification and separation of protonated rhamnolipids, a column 35 x 230 mm was prepared by the addition of 100 g silica gel 60 (230-400 μm mesh) made up as a slurry in chloroform. 4 g rhamnolipid mixture JBR505 (freeze-dried from aqueous solution beforehand) was dissolved in approximately 20 ml chloroform and loaded into the top of the column. The column was washed with 100% chloroform and 50:3 v/v chloroform: methanol until all neutral lipids were eluted. Subsequently 50:6 and 50:8 v/v were used to elute R1 and 50:15 and 50:20 v/v to elute R2. 40 ml fractions were collected throughout and those containing pure R1 were combined, and likewise with R2. The composition and purity of each fraction was tested by thin layer chromatography (TLC) and also mass spectrometry (ESI-MS) at regular intervals (Sections 2.5.2 and 2.5.3, respectively). A lengthy overlap period existed between the elution of pure R1 and R2, where a mixture of the two eluted together. Care was taken to ensure all traces of R1 had been removed before increasing the proportion of methanol in the solvent system. Due to the high proportion of methanol required to elute R2, some of the silica stationary phase in the column became dissolved in solution. To overcome this problem, the solvent containing combined R2 fractions was dried by rotary evaporation, R2 was redissolved in chloroform, filtered to remove the (now undissolved) silica and the solvent was evaporated once again. Care was taken to ensure as little as possible of the rhamnolipids were lost in the process.

For the separation of deuterated rhamnolipids, 4 g rhamnolipid mixture was dissolved in approximately 50 ml chloroform containing an equal mass of silica gel 60, then rotary evaporated to dryness. This was mixed to a fine powder and loaded dry into the top of a 35 x 230 mm column, packed with 100 g silica gel 60 as a slurry in chloroform, then the column was washed with pure chloroform. A slightly different solvent system was required for the deuterated rhamnolipids, which was preliminarily found through TLC screening in a variety of ratios of chloroform to methanol. The optimised procedure involved pure chloroform and 50:3 v/v chloroform: methanol to elute the neutral lipids, 50:4 v/v to elute R1 and 50:6 and 50:10 v/v to elute R2. The column was run in 50:50 v/v afterwards to recover all traces of rhamnolipids from the column. Again, combined R2 fractions were redissolved in chloroform, filtered and dried by rotary evaporation to remove any previously dissolved silica. As with the protonated rhamnolipids, a long period of overlap existed between eluting pure R1 and R2, so once again care was taken to ensure as much R1 as possible had eluted before proceeding to use 50:6 v/v chloroform: methanol.

For the purification of deuterated $C_{12}E_8$, a solvent system of diethyl ether: acetone was used. Both solvents were rotary evaporated beforehand to remove any impurities and stabilisers in the solvent. A 35 x 230 mm column was packed with 120 g silica gel 60 in diethyl ether and approximately 9 g crude mixture of $C_{12}E_8$, the preparation of which is described in detail elsewhere,[19,20] was loaded into the top of the column. The column was first washed with diethyl ether to elute all short chain homologues (E_6 and below), then 90:10 v/v diethyl ether: acetone to elute $C_{12}E_{6\text{-}7}$, and 85:15 v/v to elute $C_{12}E_{7\text{-}9}$, the required product. 20 ml fractions were collected throughout to ensure as monodisperse a product as possible, but it was not possible to separate the three homologues further as their polarities are so similar. However, $C_{12}E_{7\text{-}9}$ is seen as effectively monodisperse because of their very similar properties and only if lower members were introduced, for example $C_{12}E_5$ and below, would the compound count as polydisperse.[30] In addition, as the concentrations used are above the CMC of $C_{12}E_8$ and the mixed CMC, the more surface-active components with lower EO numbers would be solubilised within the micelle and have no effect on the surface excess determined.[31] The purity of the separated $C_{12}E_8$ was evaluated prior to neutron reflectivity measurements and was found to be adequate.

2.5.2 Thin layer chromatography

Thin layer chromatography (TLC) was carried out on silica gel 60 TLC aluminium plates (Merck), using a solvent system of 65:15:2 chloroform: methanol: water as the mobile phase. Phosphomolybdic acid solution in ethanol was used as a staining reagent and on heating showed four spots in the crude mixture with different retention factor (R_f) values. The retention factor is a measure of the polarity of a compound, defined as the ratio between the distance travelled by the compound. d_c, and the total distance travelled by the solvent along the TLC plate, d_s:

$$R_f = \frac{d_c}{d_s} \tag{2.25}$$

with higher R_f values for the less polar compounds. Two spots with R_f values 0.2 and 0.5 indicated the presence of R1 and R2, respectively, similar to that found by M. Chen,[10] with spots at 0.6 and 0.8 indicating the presence of other neutral compounds.

For TLC of deuterated $C_{12}E_8$, a solvent system of diethyl ether: acetone was used as the mobile phase. As the spots were so close together, varying ratios from 90:10 v/v to 60:40 v/v were used, depending on the solvent system used in the column, in order to observe the spots eluted as the mobile phase in the column was made progressively more polar. TLC plates were stained with phosphomolybdic acid solution and heated to reveal each congener.

2.5.3 Mass spectrometry, ESI-MS

2.5.3.1 Rhamnolipid

ESI-MS analysis was carried out at the Chemistry Research Laboratory, University of Oxford. Figure 2.8 shows the ESI-MS traces for the (a) crude protonated rhamnolipid mixture JBR505 before purification, (b) pure separated R1 and (c) pure separated R2. Purities were consistently higher than 99% (i.e. less than 1% R1 remained), as evaluated using HPLC-MS. All MS traces are in negative mode. HPLC-MS traces for the separation of deuterated rhamnolipids R1 and R2 are given in Chapter 3, which includes in detail the tandem MS-MS analysis of each congener in the mixture.

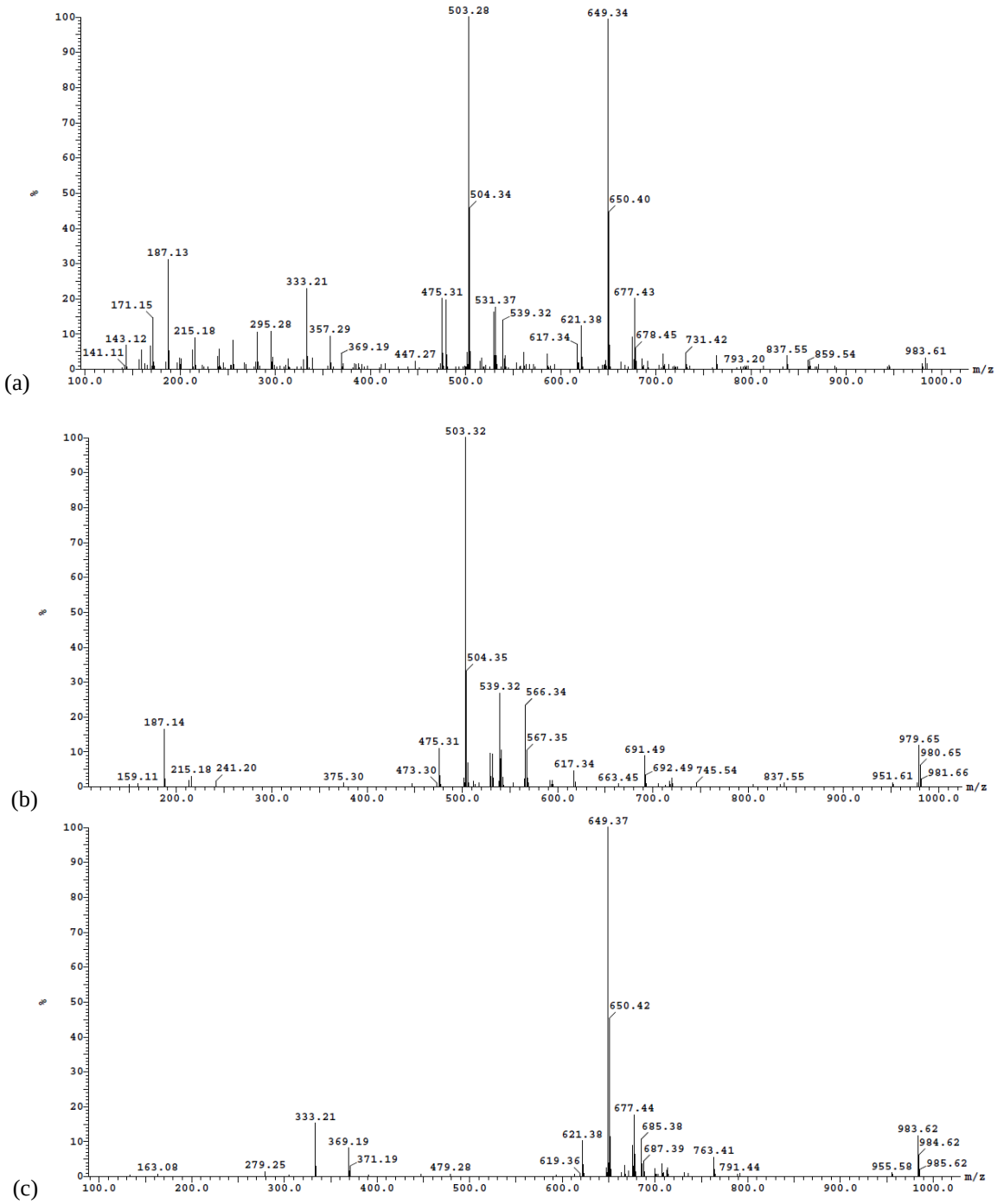

Figure 2.8: ESI-MS traces for (a) crude protonated rhamnolipid mixture JBR505 before purification, (b) pure separated R1 and (c) pure separated R2.

2.5.3.2 Octaethylene glycol monododecyl ether, $dC_{12}hE_8$

Figure 2.9 shows the ESI-MS analysis of (a) a crude chain-deuterated $dC_{12}hE_8$ mixture before purification and (b) the separated $C_{12}E_8$ after purification (predominantly $C_{12}E_8$). All MS traces are in positive mode. As described in Section 2.5.1, a product of $C_{12}E_{7\text{-}9}$ was obtained, its purity found to be of adequate quality for neutron reflectivity measurements.

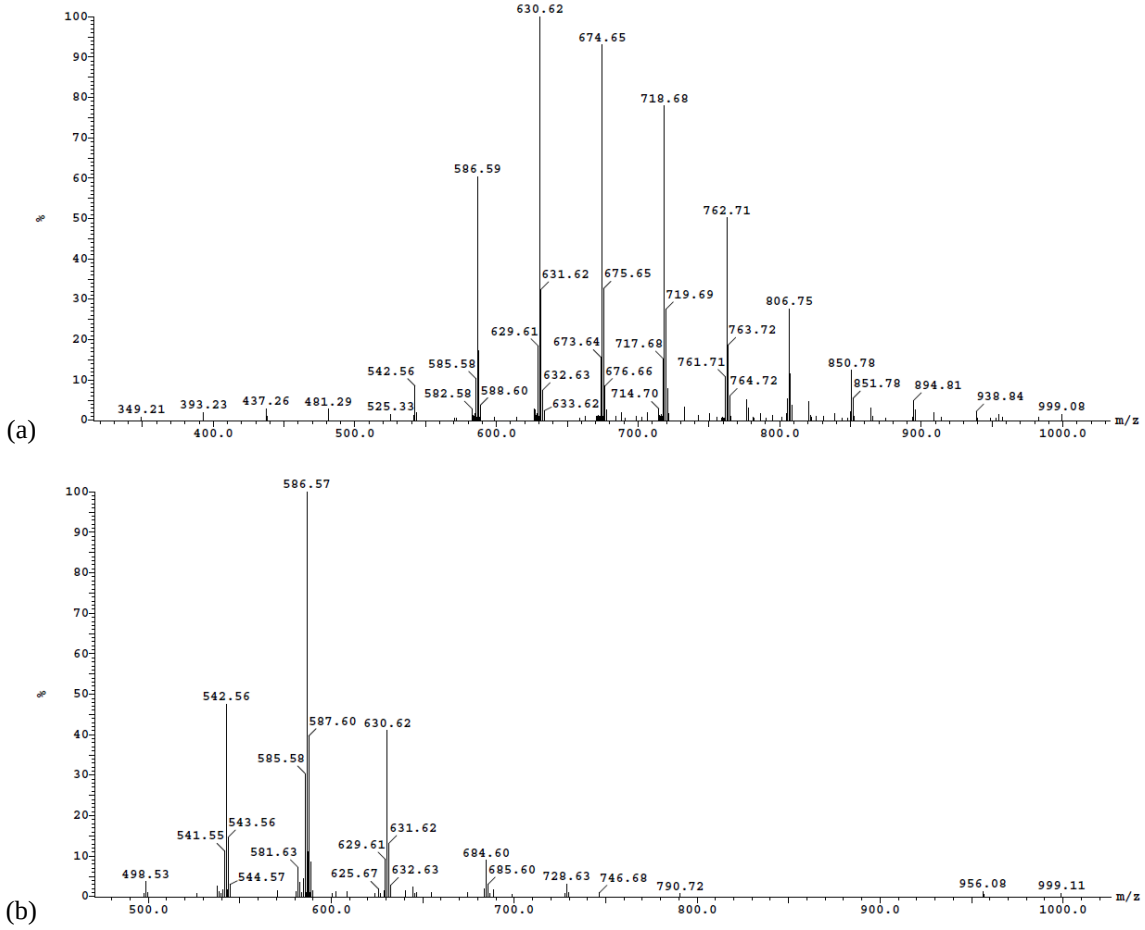

Figure 2.9: ESI-MS traces for deuterated $C_{12}E_8$ (a) before and (b) after purification.

References: Chapter 2

1. Vargaftik, N. B.; Volkov, B. N.; Voljak, L. D., *Journal of Physical and Chemical Reference Data* **1983,** *12* (3), 817-820.
2. Penfold, J.; Thomas, R. K.; Dong, C. C.; Tucker, I.; Metcalfe, K.; Golding, S.; Grillo, I., *Langmuir* **2007,** *23* (20), 10140-10149.
3. Xu, H. DPhil thesis. University of Oxford, 2013.
4. Lu, J. R.; Hromadova, M.; Thomas, R. K.; Penfold, J., *Langmuir* **1993,** *9* (9), 2417-2425.
5. Lu, J. R.; Li, Z. X.; Smallwood, J.; Thomas, R. K.; Penfold, J., *Journal of Physical Chemistry* **1995,** *99* (20), 8233-8243.
6. Thomas, R. K., *Annual Review of Physical Chemistry* **2004,** *55*, 391-426.
7. RKT group website, Physical and Theoretical Chemistry Laboratory, University of Oxford. http://rkt.chem.ox.ac.uk/research.html.
8. Jackson, A. J., Introduction to Small-Angle Neutron Scattering and Neutron Reflectometry. NIST Center for Neutron Research, 2008.
9. Penfold, J.; Thomas, R. K., *Journal of Physics: Condensed Matter* **1990,** *2* (6), 1369-1412.
10. Chen, M. DPhil thesis. University of Oxford, 2010.
11. Crowley, T. L.; Lee, E. M.; Simister, E. A.; Thomas, R. K., *Physica B: Condensed Matter* **1991,** *173* (1-2), 143-156.
12. Lu, J. R.; Thomas, R. K.; Penfold, J., *Advances in Colloid and Interface Science* **2000,** *84* (1-3), 143-304.
13. Lu, J. R.; Lee, E. M.; Thomas, R. K., *Acta Crystallographica* **1996,** *52* (1), 11-41.
14. Penfold, J.; Richardson, R. M.; Zarbakhsh, A.; Webster, J. R. P.; Bucknall, D. G.; Rennie, A. R.; Jones, R. A. L.; Cosgrove, T.; Thomas, R. K.; Higgins, J. S.; Fletcher, P. D. I.; Dickonson, E.; Roser, S. J.; McLure, I. A.; Hillman, A. R.; Richards, R. W.; Staples, E. J.; Burgess, A. N.; Simister, E. A.; White, J. W., *Journal of the Chemical Society, Faraday Transactions* **1997,** *93* (22), 3899-3917.
15. INTER Reflectometer at ISIS. http://www.isis.stfc.ac.uk/instruments/inter/inter2471.html.
16. FIGARO Reflectometer at ILL. http://www.ill.eu/instruments-support/instruments-groups/instruments/figaro/.
17. Penfold, J.; Ward, R. C.; Williams, W. G., *Journal of Physics E: Scientific Instruments* **1987,** *20* (11), 1411-1417.
18. Webster, J.; Holt, S.; Dagliesh, R., *Physica B: Condensed Matter* **2006,** *385-386* (2), 1164-1166.
19. Lu, J. R.; Lee, E. M.; Thomas, R. K.; Penfold, J.; Flitsch, S. L., *Langmuir* **1993,** *9* (5), 1352-1360.
20. Lu, J. R.; Li, Z. X.; Su, T. J.; Thomas, R. K.; Penfold, J., *Langmuir* **1993,** *9* (9), 2408-2416.
21. Rahman, A.; Brown, C. W., *Journal of Applied Polymer Science* **1983,** *28* (4), 1331-1334.
22. Chen, M. L.; Penfold, J.; Thomas, R. K.; Smyth, T. J. P.; Perfumo, A.; Marchant, R.; Banat, I. M.; Stevenson, P.; Parry, A.; Tucker, I.; Grillo, I., *Langmuir* **2010,** *26* (23), 18281-92.
23. Hayter, J. B.; Penfold, J., *Colloid and Polymer Science* **1983,** *261* (12), 1022-1030.
24. Hayter, J. B.; Penfold, J., *Molecular Physics: An International Journal at the Interface Between Chemistry and Physics* **1981,** *42* (1), 109-118.
25. Hansen, J.-P.; Hayter, J. B., *Molecular Physics: An International Journal at the Interface Between Chemistry and Physics* **1982,** *46* (3), 651-656.
26. Penfold, J. OpenGENIE. http://www.isis.rl.ac.uk/OpenGENIE/.
27. Heenan, R. K.; Penfold, J.; King, S. M., *Journal of Applied Crystallography* **1997,** *30* (6), 1140-1147.
28. SANS2D Diffractometer at ISIS, http://www.isis.stfc.ac.uk/instruments/sans2d/sans2d3000.html.
29. D33 Diffractometer at ILL. http://www.ill.eu/instruments-support/instruments-groups/instruments/d33/description/layout/.

30. Warr, G. G.; Grieser, F.; Healy, T. W., *Journal of Physical Chemistry* **1983,** *87* (7), 1220-1223.
31. Lu, J. R.; Li, X.; Thomas, R. K.; Staples, E. J.; Thompson, L.; Tucker, I.; Penfold, J., *Journal of Physical Chemistry* **1994,** *98* (26), 6559-6567.

Chapter 3

Deuteration of rhamnolipid biosurfactant

This chapter describes the production of highly deuterated (around 90%) rhamnolipid molecules from a strain of *Pseudomonas aeruginosa* (*P. aeruginosa*), a well-known rhamnolipid producer, for use in the study of multicomponent biosurfactant-containing mixtures using neutron reflectivity. The deuterated rhamnolipids were used in their purified and separated forms, mono- and di-rhamnolipid (abbreviated as R1 and R2, respectively). In combination with protonated R1 and R2 and through the use of isotopic substitution, it was possible to investigate the surface behaviour of rhamnolipids in the presence of $C_{12}E_8$, LAS and SLES, well known conventional surfactants used in many detergent formulations.

The procedure by Smyth et al[1] successfully generated rhamnolipids with up to 90% deuteration (atom% D) at a yield of 0.56 g/L. In this work, using fully-deuterated feedstocks of D_2O and deuterated glycerol, and after adaption of the *P. aeruginosa* to their new deuterated environment, rhamnolipids of approximately 90 atom% D were obtained, high enough to give an excellent signal for use in neutron reflectivity studies.

3.1 Introduction

3.1.1 Microbiology of *P. aeruginosa*

P.aeruginosa is a gram-negative bacterium of the family *Pseudomonadaceae*, often found in soils and water. It has a flagellum which aids in its movement and also in helping it attach to surfaces or other *P. aeruginosa* cells. Under stress, the *P. aeruginosa* cells may bond together and to surfaces to form a biofilm, surrounded by Extracellular Polymeric Substance (EPS). EPS is the extracellular matrix which protects the cells and aids in the bacteria's survival. There is great physiological relevance to the production of the rhamnolipid biosurfactant. Examples of the role of the rhamnolipids include assistance in penetrating cell membranes for bacteria to attack cell walls of various fungi (thus making

them fungicides), lowering of surface tension of aqueous media to aid bacterial dispersal in the media, and assistance in maintaining open channels during biofilm production for nutrient delivery.

The first rhamnolipids were produced by the bacterium *P. aeruginosa*,[2] by Bergstrom and co-workers in 1946,[3,4] of which hundreds of strains are now known. *P. aeruginosa* is the primary producer of rhamnolipids,[5] although recent reviews[6,7] point to many non-*Pseudomonas* bacterial strains which are also rhamnolipid-producers. Rhamnolipids are now produced commercially in large quantities, for example, Jeneil Biosurfactant Co. and Rhamnolipid Inc., and are becoming increasingly incorporated in applications which range from household cleaners, the cosmetic and food industries, to enhanced oil recovery and *in situ* bioremediation of hydrocarbons.

3.1.2 Production of rhamnolipids by *P. aeruginosa*

There are three stages to bacterial growth; lag phase, involving the adaption of bacteria to their environment, log phase, where the number of cells increase exponentially, and stationary phase where one of the components in the media becomes limited and there is no more cell growth. A final death phase also occurs where cells die as a result of lack of sufficient nutrients.

Rhamnolipids are secondary metabolites,[8, 9] in that they are supportive for the growth of the bacteria but not necessary or directly involved.[10] In the exponential growth phase of *P. aeruginosa*, the poly(β-hydroxyalkanoic acids), PHAs, are produced.[11] The transformation to production of rhamnolipids then occurs at the onset of the stationary phase[12] through addition of the rhamnose sugar group(s).

The production of rhamnolipids is promoted in an environment of limiting concentrations of nitrogen or "essential multivalent cations."[11,12,13,14,15] Therefore for the commercial biosynthesis of rhamnolipids, *P. aeruginosa* is often grown up in a minimal salts medium (MSM) with limiting amounts of nitrogen and trace elements such as iron (0.001 g/L). It is also the limiting iron concentration which is responsible for the production of the blue pigment Pyocyanin.[16] Also present in the MSM is the carbon substrate, the "food" for the bacteria. Whilst originally being grown on hydrocarbons, the bacteria have since been successfully grown on a variety of different hydrophilic carbon substrates, including carbohydrates such as glucose,[13] olive oil,[17] soybean oil[18] and canola oil.[19]

Many different homologues have been found to be present in a typical mixture of rhamnolipids produced by *P. aeruginosa*, with the two most abundant congeners being α-L-rhamnopyranosyl-α-L-β-hydroxydecanoyl-β-hydroxydecanoate and α-L-rhamnopyranosyl-α-L-rhamnopyranosyl-β-hydroxydecanoyl-β-hydroxydecanoate, termed Rha-C_{10}-C_{10} (R1) and Rha-Rha-C_{10}-C_{10} (R2), respectively. They contain a hydrophilic headgroup with either one or two rhamnosyl sugar groups, and two β-hydroxydecanoic acid residues acting as the hydrophobic tail. These C_{10}-C_{10} congeners comprise 60-80% of the total abundance[20] yet new congeners are frequently being reported, including the unusual mono-rhamnolipids with unsaturated fatty acid chains $C_{8:2}$ and $C_{12:2}$[21,22] in other *P. aeruginosa* strains. The compositional ratio of R1:R2 is usually around 1:3,[23] although the exact chemical composition is very dependent on the strain of *P. aeruginosa* used (Abdel-Mawgoud et al found one strain to contain 56% R1 and 44% R2)[24] and the cultivation conditions,[25] for example the carbon source,[26] pH,[11] temperature, agitation speed and the availability of oxygen. R1 is a precursor to R2.[27,28] The *alg*C gene is known to have a strong importance in rhamnolipid production, and it is thought that an overexpression of this specific gene leads to a larger proportion of rhamnolipid molecules with two rhamnose sugar groups, due to the higher synthesis of the deoxy-thymidine-diphospho-L-rhamnose (dTDP-L-rhamnose), the precursor to the rhamnose moiety.[29]

3.1.3 Biosurfactant deuteration and the toxicity of D_2O

By metabolic reaction and through cleavage of C-H bonds, deuterated biosurfactant molecules are formed over time. However, the primary obstacle in deuteration of these molecules is the inevitable toxicity of D_2O to the prokaryotic cells. Under stress, the *P. aeruginosa* cells may bond together and to surfaces to form a biofilm, surrounded by Extracellular Polymeric Substance (EPS), the extracellular matrix which protects the bacterial cells. This can be observed as a collection of cells along the rim of the culture flasks at the air/media interface. There are a number of reasons why D_2O is toxic to cells, the two main ones being Solvent Isotope Effects (SIE) and Deuterium Isotope Effects (DIE).[30] SIE are due to properties such as the density of the D_2O itself, which is higher in deuterated than protonated water. DIE involve the ability of the D_2O to replace H with D. The stretching frequency of O-D is 0.7 that of O-H, and the difference in zero point energy effectively makes the O-D bond stronger. D_2O

affects mitosis, thus slowing bacterial growth, and also the function of membranes and motility of the flagellae.[31] However, D_2O does not fully inhibit growth, and through adaption of the bacteria to increasing percentages of deuterated media, successful growth is possible, as found by Paliy et al[32] in the adaption of *E. coli*.

3.2 Experimental

3.2.1 Materials and media preparation

Deuterated water, D_2O >99.92 Atom% D, was obtained from Eurisotop. Deuterated glycerol, 1, 1, 2, 3, 3-D5 98%, was obtained from Sigma. Yeast extract was obtained from DIFCO and all salts were purchased from Sigma.

The MSM used for both the adaption procedure and production of rhamnolipids in fully-deuterated media was prepared in either MilliQ deionised water, D_2O or a certain composition of the two, and contained (in g/L): 2.0 $NaNO_3$, 0.9 Na_2HPO_4, 0.7 KH_2PO_4, 0.4 $MgSO_4.7H_2O$, 0.1 $CaCl_2$ (added as 1 ml/L of a filter-sterilised 100 g/L solution (0.20 µm Sartorius Minisart syringe filter, Fisher Scientific, UK) due to $CaCl_2$ precipitating out during autoclaving), 0.001 $FeSO_4.7H_2O$, 2% w/v (20 g/L) glycerol as carbon substrate (either protonated or deuterated) and trace element solution (added as a 1 ml/L filter-sterilised solution (0.20 µm Sartorius Minisart syringe filter, Fisher Scientific, UK) using deionised water) containing (g/L): 0.7 $ZnSO_4.7H_2O$, 0.5 $CuSO_4.5H_2O$, 0.5 $MnSO_4.H_2O$, 0.26 H_3BO_3, 0.06 $Na_2MoO_2.2H_2O$. 0.5 g/L yeast extract was added to all fully-deuterated media (i.e. containing 100% D_2O and 100% d-glycerol) to enhance cell growth and hence speed up the lag phase.[9] Yeast extract has been seen to decrease yield slightly,[13] but here it had no effect on deuteration levels (Section 3.3.2), with satisfactory yields to supply sufficient amounts for neutron experiments. All media were sterilised by autoclaving at 121°C for 15 minutes prior to inoculation. For MSM used in the adaption procedure, all salts and glycerol were added as filter-sterilised stock solutions, to minimise any precipitation during autoclaving and also for greater accuracy of salt concentration addition due to the solutions being made on such a small scale.

3.2.2 Inoculation and adaptation of *P. aeruginosa* to deuterated media

The adaptation process is summarised in Figure 3.1. The *P. aeruginosa* ST5 strain was initially streaked on agar plates and incubated at 37°C until inoculation. Inoculation involved transferring a loopful of *P. aeruginosa* from the agar plate to 100 ml MSM medium, split into two 50 ml portions, each in a 250 ml Erlenmeyer flask. All stages were carried out in duplicate to ensure at least one was successfully grown without contamination. All culture fermentation was carried out in Erlenmeyer flasks and incubated in a reciprocal shaker at 37°C with shaking at 200 rpm. It was necessary to fill no more than 20% of a flask with culture media (10% filled in the present work) for enough oxygen to be available to the bacteria. Initial growth was seen as clumps of cells and cloudiness of the media and with pigment formation, as was seen with *P. aeruginosa* growing in the rich phosphate-deficient proteose peptone-glucose-ammonium salts medium (PPGAS).[33] After 72 hours, 100 ml fully-protonated MSM media was inoculated with 10% of the previous culture by the following method: 10 ml of the initial culture grown in MSM was removed, cells were spun down in a centrifuge for 15 minutes at 10,000 xg and at 4°C, the supernatant was removed, cells were resuspended in 10 ml of the new MSM medium by vortexing, and finally 5 ml was transferred into each of two 50 ml fully protonated MSM each in 500 ml flask (hence 10% inoculum in the total volume of new media). These first two cultures acted as the control against which the growth of bacteria in the adaptation procedure was measured. Sterile conditions were kept at all times by flaming all pipettes and the rim of each flask with a Bunsen burner immediately before and after inoculation.

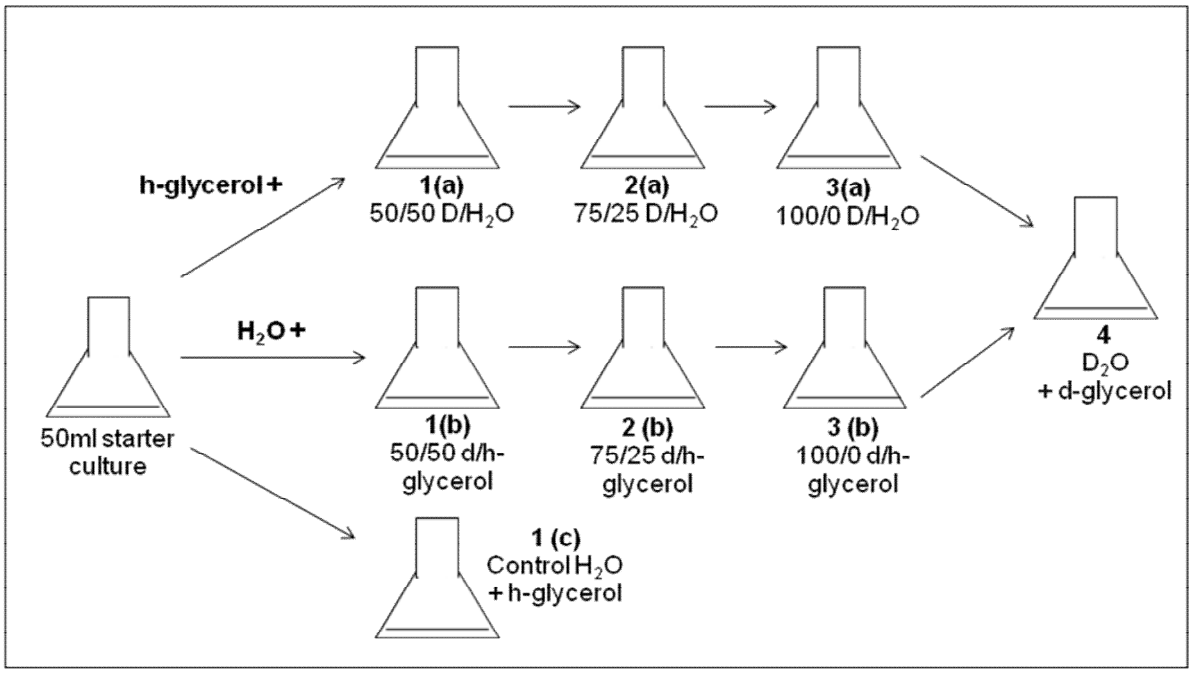

Figure 3.1: Adaptation procedure for *P. aeruginosa* on increasingly deuterated media.

To adapt the *P. aeruginosa* to deuterated media, the bacteria were grown separately on increasing percentages of both D_2O and d-glycerol (stages 1, 2 and 3, Figure 3.1) and then collectively in one medium containing 100% D_2O and d-glycerol (stage 4, Figure 3.1), prior to the scale-up of production. Each stage of the adaption procedure was carried out in duplicate, as with the control, to ensure successful growth without contamination.

Each 50 ml MSM contained 10% inoculum of resuspended cells from the previous media, and cultures were grown for 48 hours in 500 ml Erlenmeyer flasks, shaking at 200 rpm at 37°C. For each transfer, cells were spun down in a centrifuge for 15 minutes at 10,000 xg and at 4°C, supernatant was removed and kept for later analysis (Section 3.3.2), and then cells were resuspended and transferred to the increasingly deuterated media. Finally, culture media from (a) and (b) (50 ml each) in stage 3 were spun down by centrifuging, cells were resuspended in fully-deuterated MSM and all cells were combined, before inoculating into 200 ml (in triplicate) of fully-deuterated MSM (stage 4).

Once the adaptation procedure had been completed, the production was scaled up by culturing *P. aeruginosa* in 500 ml batches in 5 L Erlenmeyer flasks using cells from stage 4. As described in Section 3.2.1, 0.5 g/L yeast extract was added to all culture flasks to encourage cell growth. A total of 6 L fully-deuterated media was successfully grown with an average yield of over 1 g/L. *P. aeruginosa*

culture was also grown in 2.5 L media containing 100% D_2O and h-glycerol, in order to gain as much crude product as possible. Using protonated glycerol with D_2O previously gave very satisfactory deuteration levels of over 70%.[1] This will be further discussed in the results section.

3.2.3 Optical density

Optical density measurements were used to follow the rate of growth of *P. aeruginosa*. 100 µl of culture broth was taken at known time intervals and diluted by a factor of 10 with MSM by mixing with MSM inside a quartz cuvette. The optical density was measured at a fixed wavelength of 600 nm on a Novaspec II Pharmacia Biotech spectrophotometer (Cambridge, UK).[34] All measurements were made in triplicate and calibrated to a blank of MSM.

3.2.4 Surface tension

Surface tension was used as a qualitative procedure to follow the production of surface active molecules in the culture media. Surface tension measurements were made using a Krüss digital tensiometer K10ST using a *du* Nuoy Pt-Ir ring. 1 ml of culture broth was taken from a specific flask at known time intervals and diluted by a factor of 10 with MilliQ ultrapure water to give a total volume of 10 ml. The measurements, although only able to be used qualitatively, proved very useful as a measure of the ability and speed of *P. aeruginosa* to produce rhamnolipids. A reduction in surface tension was seen from around 70 mN/m to around 30 mN/m once in stationary phase.

3.2.5 Extraction of rhamnolipids

To obtain the crude extract from the aqueous culture medium, a solvent extraction technique was used.[35] Firstly, the culture media was centrifuged at 10,000 xg for 15 minutes to remove cell precipitate. The supernatant was collected and acidified using concentrated HCl to pH 2.0, to precipitate out the (now fully-protonated) rhamnolipids. The aqueous supernatant containing the precipitate was transferred to a separating funnel and extracted at least four times with equal volumes of ethyl acetate. After addition of $MgSO_4$ to remove any traces of water (approximately 0.5 g per 100 ml solution), twice-filtration and rotary evaporation of the solvent, a brown extract was obtained,

transferred to a pre-weighed vial and dried under N_2 gas. Crude yields were calculated using the volume of supernatant extracted.

3.2.6 Analysis of rhamnolipids

3.2.6.1 Thin layer chromatography

Thin layer chromatography (TLC) was carried out on silica plates, using a solvent system of 65:15:2 chloroform: methanol: water. The TLC plate was sprayed with an anthrone mixture (prepared with 63 ml sulphuric acid, 25 ml water and 0.125 g anthrone, under ice conditions)[35] and developed in the oven at 120°C for 10 minutes. Two spots were obtained, indicating the presence of R1 and R2, with R_f values 0.2 and 0.5, respectively, similar to those observed by M. Chen.[36]

3.2.6.2 Mass spectrometry

Direct infusion ESI-MS was carried out at the University of Ulster and University of Oxford and was used to estimate the level of deuteration of the extracted rhamnolipids. Q-TOF HPLC-MS analysis was carried out at Teagasc Research Company, Dublin, under the supervision of Dr Thomas Smyth, to find the deuteration levels of the rhamnolipids achieved at each step in the adaption procedure and the location of d-atoms on the rhamnolipid molecules. Measurements were made on a Waters Alliance 2695 HPLC system coupled to a Waters Q-TOF Premier mass spectrometer. An injection volume of 2 µl was introduced into the HPLC system through a C_{18} column (agilent poroshell EC-C_{18}, 2.1x100 mm, 2.7 µm particle size.) Mobile phase A (HPLC-grade H_2O + 4 mM ammonium acetate): mobile phase B (MeCN) were used for chromatographic separation as follows: 0-10 min: 50 - 55% B, 10-14 min: 55% - 70% B, 14-16 min: held at 70% B, 16 – 18 min: 70% - 50% B, 18 – 20 min: held at 50% B. The flow rate was 0.5 ml/min. The column oven temperature was set at 40°C. The source temperature was 120° C and the desolvation temperature was 300°C. In each case, nitrogen was used as the desolvation gas (800 L/hr) and cone gas (50 L/hr). The cone voltage was 30 V and capillary voltage to 2.5 kV. Collision induced dissociation (CID) of the analytes was achieved in MS^e mode with argon by ramping up the collision energy from 20 eV to 30 eV. Samples were analysed in negative mode in the range *m/z* 150 – 1200. All Q-TOF MS was conducted in negative mode ESI. The

addition of yeast extract to culture media had no effect on the percentage deuteration levels, as values obtained were almost identical to those reported by Smyth et al.[1]

3.3 Results

3.3.1 Optical density and surface tension

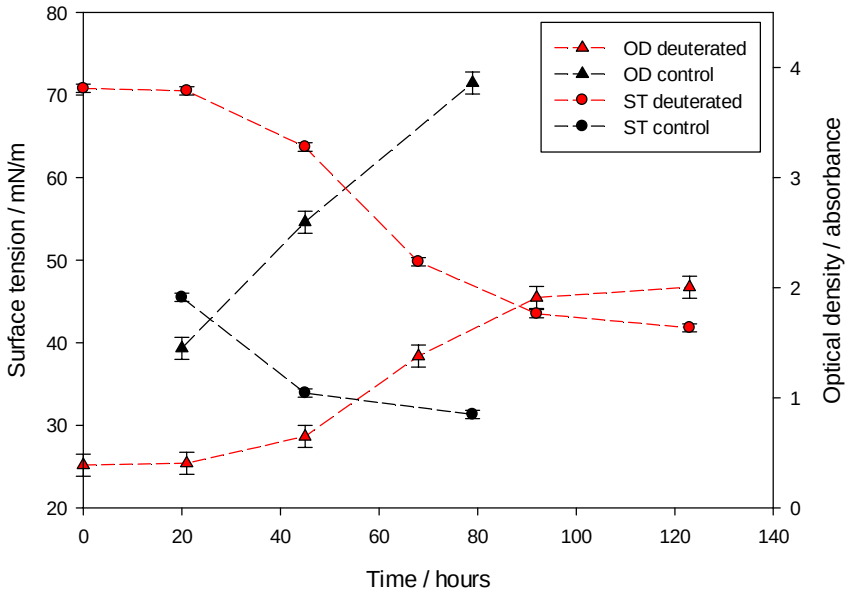

Figure 3.2: The change in optical density and surface tension with time, for a culture of P. aeruginosa growing in fully protonated control (black) and fully deuterated (red) MSM media.

Figure 3.2 provides optical density and surface tension data for cultures grown in fully-deuterated MSM (stage 4, Figure 3.1), with some data values from the control culture (stage 1 (c), Figure 3.1) for comparison. The vast difference in the timescales between growing *P. aeruginosa* in fully-protonated and fully-deuterated media is evident. Cultures grown in protonated MSM reach stationary phase soon after 80 hours, with a very high optical density of 3.8 and a large reduction in surface tension reaching 31 mN/m. However, after 80 hours growing in fully deuterated media, the surface tension only decreases to 46 mN/m and the optical density rises to just 1.6. Stationary phase is not reached until approximately 120 hours. It is clear that, even by subjecting the *P. aeruginosa* to a comprehensive adaption procedure prior to growth in fully-deuterated media, the effects of toxicity of D_2O are still great enough to hinder the growth of cells and production of rhamnolipids.

3.3.2 Mass spectrometry

HPLC-MS and tandem MS-MS analysis was carried out on all the rhamnolipids produced from the adaption procedure, and those made in fully-deuterated media. All the analysis was done at Teagasc Research Company, Dublin, under the supervision of Dr Thomas Smyth.

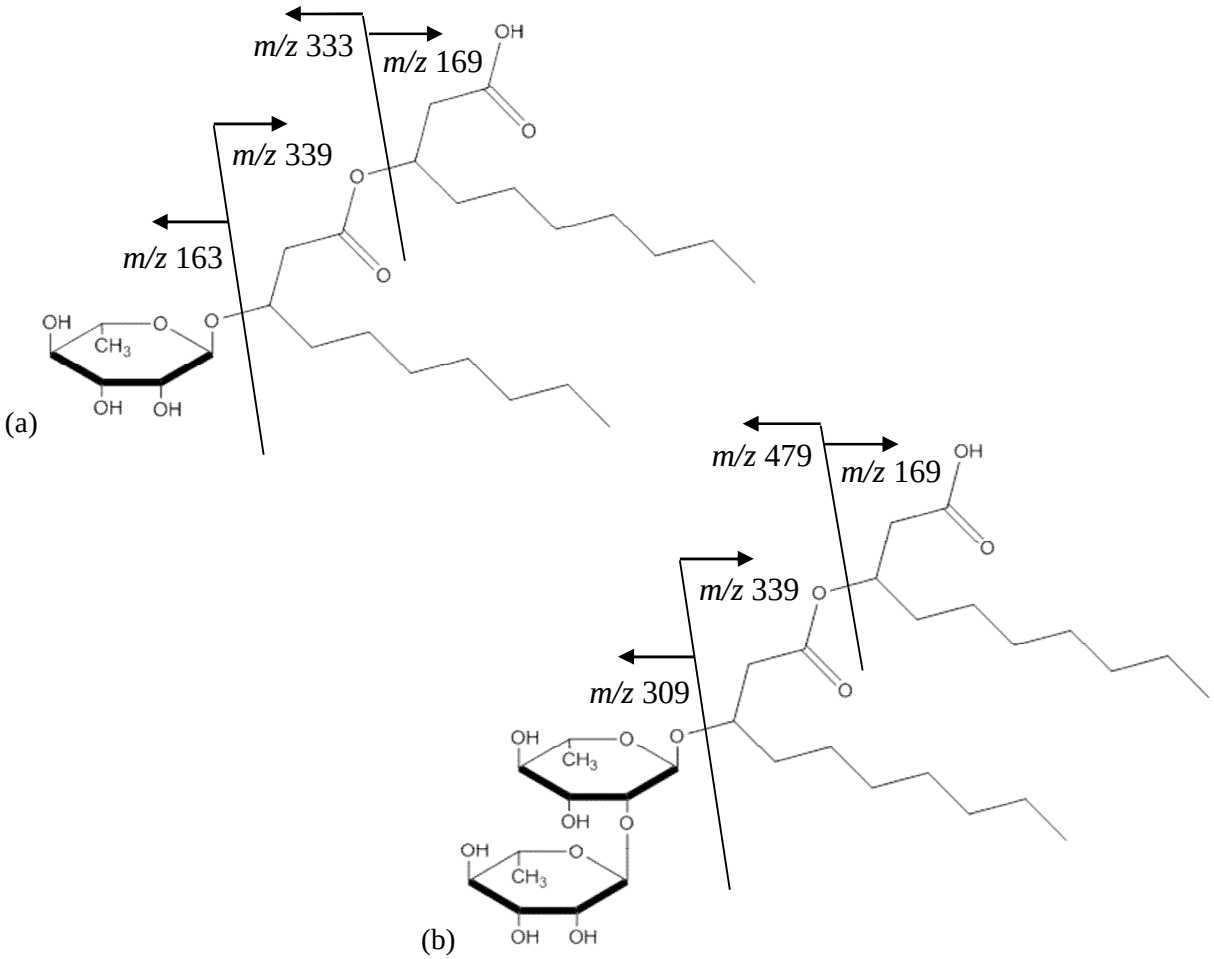

Figure 3.3: Molecular structures and fragmentation patterns of (a) Rha-C_{10}-C_{10} (R1), (b) Rha-Rha-C_{10}-C_{10} (R2).

In MS-MS fragmentation of fully protonated rhamnolipids containing C_{10}-C_{10} hydrocarbon chains, an *m/z* value of 333 signifies the loss of outer C_{10} fatty acid group (the first fragment lost) in R1 and *m/z* 479 signifies this loss in R2. This information is vital in order to decipher the number of d-atoms on both the lipid and sugar part of the deuterated molecules. For example, fragmentation of the R2 molecule Rha-Rha-C_{10}-C_{10} produced in 100/0 D_2O/H_2O and h-glycerol yielded a peak at *m/z* 505, which relates to the deuterated version of *m/z* 479, belonging to the sugar and inside lipid portion of the molecule, as can be seen in Figure 3.3 (b). With an *m/z* value of 691 (molecular weight of 692 g/mol), the difference of 186 (691-505) will be the *m/z* of the outer fatty acid. In a protonated R2

molecule, the *m/z* for the outer fatty acid is 169, and for the total fatty acid portion it is 339. Thus, there are 17 deuterons on the outer fatty acid and a total of 34 deuterons on the overall lipid part of the molecule, giving *m/z* 373 for the lipid (339+34). The difference between 691 and 373 belongs to the sugar part of the molecule (*m/z* 318), and since a fully protonated R2 molecule will have *m/z* 309 on the sugar portion, there are 9 deuterons on this part of the rhamnolipid.

3.3.2.1 Effect of increasing deuteration in water

Tables 3.1 to 3.3 give the range and average number of d-ions, percentage of d-atoms, percentage total of each homologue and the number of d-atoms on both the sugar and lipid parts of the R1 and R2 rhamnolipid molecules, for the adaptation procedure with increasing percentage of D_2O in the MSM (stage 1 (a), 2 (a) and 3 (a), Figure 3.1).

RL	Molecular formula	Range of d-ions	Average	Range	% d-atoms	% Total	Sugar	Lipid
Rha-C_{10}-C_8/ C_8-C_{10}	$C_{24}H_{44}O_9$	486 (11d) – 494 (19d)	490 (15d)	8	35	1.1		
Rha-C_{10}-C_{10}	$C_{26}H_{48}O_9$	515 (12d) – 525 (22d)	520 (17d)	10	36	18.6	166 (3d)	353 (14d)
Rha-$C_{12:1}$-C_{10}/C_{10}-$C_{12:1}$	$C_{28}H_{50}O_9$	542 (13d) – 551 (22d)	547 (18d)	9	37	1.4		
Rha-C_{12}-C_{10}/C_{10}-C_{12}	$C_{28}H_{52}O_9$	545 (14d) – 554 (23d)	550 (19d)	9	37	2.7		
Rha_2-C_{10}-C_8/C_8-C_{10}	$C_{30}H_{54}O_{13}$	634 (13d) – 642 (22d)	638 (17d)	8	32	5.6		
Rha_2-C_{10}-C_{10}	$C_{32}H_{58}O_{13}$	663 (14d) – 673 (24d)	668 (19d)	10	33	50	313 (4d)	354 (15d)
Rha_2-$C_{12:1}$-C_{10}/ C_{10}-$C_{12:1}$	$C_{34}H_{60}O_{13}$	689 (14d) – 699 (24d)	695 (20d)	10	34	4.3		
Rha_2-C_{12}-C_{10}/C_{10}-C_{12}	$C_{34}H_{62}O_{13}$	692 (15d) – 703 (26d)	697 (20d)	11	33	16.3		

Table 3.1: %D levels and position of d-atoms for R1 and R2 grown in 50/50 D_2O/H_2O & h-glycerol.

RL	Molecular formula	Range of d-ions	Average	Range	% d-atoms	% Total	Sugar	Lipid
Rha-C_{10}-C_8/ C_8-C_{10}	$C_{24}H_4{}_4O_9$	495 (20d) – 503 (28d)	490 (23d)	8	54	5.4		
Rha-C_{10}-C_{10}	$C_{26}H_{48}O_9$	525 (22d) – 534 (31d)	530 (27d)	9	57	10.6	167 (3d)	362 (23d)
Rha-$C_{12:1}$-C_{10}/C_{10}-$C_{12:1}$	$C_{28}H_{50}O_9$	Not detected	N/A	N/A	0	0.0		
Rha-C_{12}-C_{10}/C_{10}-C_{12}	$C_{28}H_{52}O_9$	556 (25d) – 565 (34d)	562 (31d)	9	61	1.8		
Rha2-C_{10}-C_8/C_8-C_{10}	$C_{30}H_{54}O_{13}$	643 (22d) – 653 (32d)	648 (27d)	10	51	5.4		
Rha_2-C_{10}-C_{10}	$C_{32}H_{58}O_{13}$	673 (24d) – 684 (35d)	679 (30d)	11	53	60.4	316 (7d)	362 (23d)
Rha_2-$C_{12:1}$-C1$_0$/ C_{10}-$C_{12:1}$	$C_{34}H_{60}O_{13}$	702 (27d) – 710 (35d)	706 (31d)	8	53	0.2		
Rha_2-C_{12}-C_{10}/C_{10}-C_{12}	$C_{34}H_{62}O_{13}$	704 (27d) – 714 (37d)	709 (32d)	10	52	13.8		

Table 3.2: %D levels and position of d-atoms for R1 and R2 grown in 75/25 D_2O/H_2O & h-glycerol.

RL	Molecular formula	Range of d-ions	Average	Range	% d-atoms	% Total	Sugar	Lipid
Rha-C_{10}-C_8/ C_8-C_{10}	$C_{24}H_{44}O_9$	506 (31d) – 512 (37d)	509 (34d)	6	79	1.4		
Rha-C_{10}-C_{10}	$C_{26}H_{48}O_9$	538 (35d) – 544 (41d)	520 (38d)	6	81	19.1	167 (4d)	372 (33d)
Rha-$C_{12:1}$-C_{10}/C_{10}-$C_{12:1}$	$C_{28}H_{50}O_9$	566 (37d) – 572 (43d)	569 (40d)	6	82	1.9		
Rha-C_{12}-C_{10}/C_{10}-C_{12}	$C_{28}H_{52}O_9$	569 (38d) – 576 (45d)	573 (42d)	7	82	3.9		
Rha_2-C_{10}-C_8/C_8-C_{10}	$C_{30}H_{54}O_{13}$	656 (35d) – 663 (42d)	660 (39d)	7	74	5.2		
Rha_2-C_{10}-C_{10}	$C_{32}H_{58}O_{13}$	687 (38d) – 695 (46d)	691 (42d)	8	74	48.3	318 (9d)	372 (33d)
Rha_2-$C_{12:1}$-C$_{10}$/ C_{10}-$C_{12:1}$	$C_{34}H_{60}O_{13}$	716 (41d) – 722 (47d)	719 (44d)	6	75	1.7		
Rha_2-C_{12}-C_{10}/C_{10}-C_{12}	$C_{34}H_{62}O_{13}$	719 (42d) – 726 (49d)	723 (46d)	7	75	18.5		

Table 3.3: %D levels and position of d-atoms for R1 and R2 grown in 100/0 D_2O/H_2O & h-glycerol.

With an increasing percentage of deuterated water in the media, the percentage of d-atoms on the rhamnolipid molecules increases dramatically, even though the carbon source is protonated. A fully-protonated R1 will have 35 hydrogens on the lipid and 11 hydrogens on the sugar, whilst R2 will have 35 hydrogens on the lipid and 21 on the sugar. Looking at Rha-Rha-C_{10}-C_{10}, it is evident that once 100% D_2O is used, even with protonated glycerol, almost every proton is changed to deuteron giving an almost fully-deuterated lipid chain. Thus, H_2O must have a large effect on the production of the lipid portion of the molecule. Smyth et al[1] found H_2O to be strongly involved in the production of the hydrophobic lipid part of the molecule when no alkanes were present as the carbon source.

Conversely, on the sugar portion only 9 d-atoms exchange with hydrogen, out of the total 21 available on R2.

A significant decrease in the range of d-ions can be seen when increasing the proportion of D_2O in the media. The largest range (12d) is seen for rhamnolipids grown in 50/50 D_2O/H_2O with h-glycerol, whereas the smallest is seen for homologues grown in 100% D_2O with h-glycerol (6d).

3.3.2.2 Effect of increasing deuteration in glycerol

Tables 3.4 to 3.6 give the range and average number of ions, percentage of d-atoms, percentage total of each homologue and the number of d-atoms on both the sugar and lipid parts of the R1 and R2 rhamnolipid molecules, for the adaptation procedure with an increasing percentage of d-glycerol in the MSM (stages 1 (b), 2 (b) and 3 (b), Figure 3.1).

RL	Molecular formula	Range of d-ions	Average	Range	% d-atoms	% Total	Sugar	Lipid
Rha-C_{10}-C_8/ C_8-C_{10}	$C_{24}H_{44}O_9$	477 (2d) – 484 (9d)	481 (6d)	7	14	1.7		
Rha-C_{10}-C_{10}	$C_{26}H_{48}O_9$	505 (2d) – 514 (11d)	510 (7d)	9	15	24.1	166 (3d)	343 (4d)
Rha-$C_{12:1}$-C_{10}/C_{10}-$C_{12:1}$	$C_{28}H_{50}O_9$	532 (3d) – 539 (10d)	536 (7d)	7	14	1.1		
Rha-C_{12}-C_{10}/C_{10}-C_{12}	$C_{28}H_{52}O_9$	534 (3d) – 541 (10d)	538 (7d)	7	14	2.4		
Rha_2-C_{10}-C_8/C_8-C_{10}	$C_{30}H_{54}O_{13}$	625 (4d) – 633 (12d)	629 (8d)	8	15	5		
Rha_2-C_{10}-C_{10}	$C_{32}H_{58}O_{13}$	653 (4d) – 662 (13d)	658 (9d)	9	16	51.1	314 (5d)	343 (4d)
Rha_2-$C_{12:1}$-C_{10}/ C_{10}-$C_{12:1}$	$C_{34}H_{60}O_{13}$	679 (4d) – 688 (13d)	683 (8d)	9	14	2.5		
Rha_2-C_{12}-C_{10}/C_{10}-C_{12}	$C_{34}H_{62}O_{13}$	681 (4d) – 691 (14d)	685 (8d)	10	13	12.1		

Table 3.4: %D levels and position of d-atoms for R1 and R2 grown in 50/50 d/h-glycerol & H_2O.

RL	Molecular formula	Range of d-ions	Average	Range	% d-atoms	% Total	Sugar	Lipid
Rha-C_{10}-C_8/ C_8-C_{10}	$C_{24}H_{44}O_9$	480 (5d) – 488 (13d)	484 (9d)	8	21	5.2		
Rha-C_{10}-C_{10}	$C_{26}H_{48}O_9$	508 (5d) – 517 (14d)	512 (9d)	9	19	32.3	166 (3d)	345 (6d)
Rha-$C_{12:1}$-C_{10}/C_{10}-$C_{12:1}$	$C_{28}H_{50}O_9$	535 (6d) – 544 (15d)	539 (10d)	9	20	4.6		
Rha-C_{12}-C_{10}/C_{10}-C_{12}	$C_{28}H_{52}O_9$	537 (6d) – 546 (15d)	541 (10d)	9	20	6.3		
Rha_2-C_{10}-C_8/C_8-C_{10}	$C_{30}H_{54}O_{13}$	629 (8d) – 638 (17d)	633 (12d)	9	23	5.5		
Rha_2-C_{10}-C_{10}	$C_{32}H_{58}O_{13}$	657 (8d) – 666 (17d)	661 (12d)	9	21	30.0	315 (6d)	345 (6d)
Rha_2-$C_{12:1}$-C_{10}/ C_{10}-$C_{12:1}$	$C_{34}H_{60}O_{13}$	684 (9d) – 692 (17d)	688 (13d)	8	22	4.3		
Rha_2-C_{12}-C_{10}/C_{10}-C_{12}	$C_{34}H_{62}O_{13}$	686 (9d) – 695 (18d)	690 (13d)	9	21	11.9		

Table 3.5: %D levels and position of d-atoms for R1 and R2 grown in 75/25 d/h-glycerol & H_2O.

RL	Molecular formula	Range of d-ions	Average	Range	% d-atoms	% Total	Sugar	Lipid
Rha-C_{10}-C_8/ C_8-C_{10}	$C_{24}H_{44}O_9$	485 (10d) – 492 (17d)	489 (14d)	7	33	1.9		
Rha-C_{10}-C_{10}	$C_{26}H_{48}O_9$	513 (10d) – 521 (18d)	517 (14d)	8	30	39.3	167 (4d)	349 (10d)
Rha-$C_{12:1}$-C_{10}/C_{10}-$C_{12:1}$	$C_{28}H_{50}O_9$	540 (11d) – 548 (19d)	544 (15d)	8	31	1.2		
Rha-C_{12}-C_{10}/C_{10}-C_{12}	$C_{28}H_{52}O_9$	542 (11d) – 550 (19d)	546 (15d)	8	29	6.2		
Rha_2-C_{10}-C_8/C_8-C_{10}	$C_{30}H_{54}O_{13}$	634 (13d) – 643 (22d)	638 (17d)	9	32	2.6		
Rha_2-C_{10}-C_{10}	$C_{32}H_{58}O_{13}$	662 (13d) – 671 (22d)	667 (18d)	9	32	41.7	317 (8d)	348 (9d)
Rha_2-$C_{12:1}$-C_{10}/ C_{10}-$C_{12:1}$	$C_{34}H_{60}O_{13}$	689 (14d) – 698 (23d)	693 (18d)	9	31	1.2		
Rha_2-C_{12}-C_{10}/C_{10}-C_{12}	$C_{34}H_{62}O_{13}$	691 (14d) – 700 (23d)	696 (19d)	9	31	5.7		

Table 3.6: %D levels and position of d-atoms for R1 and R2 grown in 100/0 d/h-glycerol & H_2O.

When rhamnolipids are grown in increasing percentages of deuterated glycerol, the average number of d-ions increases, but to a much lesser extent than is seen for rhamnolipids growing under increasing percentages of D_2O. An R1 molecule grown in 50/50 d/h-glycerol with H_2O gains an average of 7 d-atoms (15% deuterated), which increases to just 14 d-atoms (30% deuterated) once in 100/0 d/h-glycerol with H_2O. Approximately 35% of the sugar portion is deuterated, in both R1 and R2, in media containing 100% d-glycerol with H_2O. This is almost the same as for rhamnolipids growing in 100% D_2O with h-glycerol. However, here only 25% of the lipid portion is deuterated, whereas when grown in deuterated water, almost the entire lipid portion is deuterated. Deuteration of the glycerol carbon source thus gives a significantly lower overall percentage deuteration than using deuterated water.

3.3.2.3 Rhamnolipids grown in fully-deuterated media

Figure 3.4 shows the HPLC-MS analysis of a typical rhamnolipid mixture produced in fully deuterated media (stage 4, Figure 3.1) and table 3.7 gives a summary of the percentage and position of d-atoms.

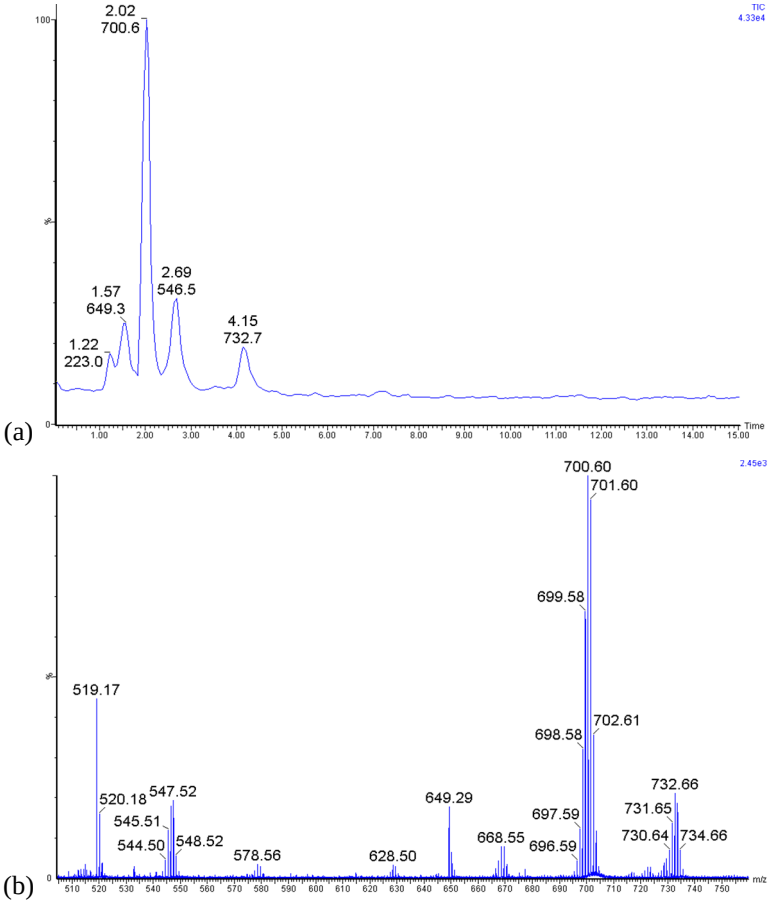

Figure 3.4: Example (a) HPLC and (b) MS traces of rhamnolipids grown in fully-deuterated media.

RL	Molecular formula	Range of d-ions	Average	Range	% d-atoms	% Total	Sugar	Lipid
Rha-C_{10}-C_8/ C_8-C_{10}	$C_{24}H_{44}O_9$	512 (37d) – 516 (41d)	514 (39d)	4	89	1.8	172 (9d)	341 (30d)
Rha-C_{10}-C_{10}	$C_{26}H_{48}O_9$	544 (41d) – 548 (45d)	546 (43d)	4	91	9.8	172 (9d)	373 (34d)
Rha-$C_{12:1}$-C_{10}/C_{10}-$C_{12:1}$	$C_{28}H_{50}O_9$	572 (43d) – 576 (47d)	574 (45d)	4	90	0.2	172 (9d)	402 (36d)
Rha-C_{12}-C_{10}/C_{10}-C_{12}	$C_{28}H_{52}O_9$	576 (45d) – 580 (49d)	576 (47d)	4	90	0.1	172 (9d)	404 (38d)
Rha_2-C_{10}-C_8/C_8-C_{10}	$C_{30}H_{54}O_{13}$	666 (45d) – 670 (49d)	668 (47d)	4	89	5.6	326 (17d)	341 (30d)
Rha_2-C_{10}-C_{10}	$C_{32}H_{58}O_{13}$	698 (49d) – 702 (53d)	700 (51d)	4	89	50	326 (17d)	373 (34d)
Rha_2-$C_{12:1}$-C_{10}/ C_{10}-$C_{12:1}$	$C_{34}H_{60}O_{13}$	726 (51d) – 730 (55d)	728 (53d)	4	88	4.3	326 (17d)	403 (36d)
Rha_2-C_{12}-C_{10}/C_{10}-C_{12}	$C_{34}H_{62}O_{13}$	730 (53d) – 734 (57d)	732 (55d)	4	90	12.3	326 (17d)	405 (38d)
h-Rha_2-C_{10}-C_{10}	$C_{32}H_{58}O_{13}$	N/A	N/A	N/A	0	2.8		

Table 3.7: Percentage deuteration levels and position of d-atoms for R1 and R2 grown in 100% D_2O & d-glycerol.

The percentage abundance of the R1 and R2 C_{10}-C_{10} congeners is 9.8% and 50%, respectively, similar to the values in the literature for protonated rhamnolipids produced by *P. aeruginosa.*[23] The range of d-ions (shown in the fifth column of Table 3.7) is known to be significantly smaller for rhamnolipids grown in fully-deuterated media than under conditions of lower percentages of deuterated media.[1] This is significant for the use of deuterated rhamnolipids in neutron scattering studies, as it gives a more accurate and reliable value for the sum of scattering lengths, as in this work the molecular weight of only the single most abundant C_{10} congener is used.

References: Chapter 3

1. Smyth, T. J.; Perfumo, A.; Marchant, R.; Banat, I. M.; Chen, M.; Thomas, R. K.; Penfold, J.; Stevenson, P. S.; Parry, N. J., *Applied Microbiology and Biotechnology* **2010,** *87* (4), 1347-1354.
2. Jarvis, F. G.; Johnson, M. J., *Journal of the American Chemical Society* **1949,** *71* (12), 4124-4126.
3. Bergström, S.; Theorell, H.; Davide, H., *Arkiv. Kemi. Mineral. Geol.* **1946a,** *23A* (13), 1-12.
4. Bergström, S.; Theorell, H.; Davide, H., *Archives of Biochemistry and Biophysics* **1946b,** *10*, 165-166.
5. Rashedi, H.; Jamshidi, E.; Mazaheri Assadi, M.; Bonakdarpour, B., *Int. J. Environ. Sci. Tech.* **2005,** *2* (2), 121-127.
6. Toribio, J.; Escalante, A. E.; Soberón- Chávez, G., *European Journal of Lipid Science and Technology* **2010,** *112* (10), 1082-1087.
7. Abdel-Mawgoud, A. M.; Lepine, F.; Deziel, E., *Applied Microbiology and Biotechnology* **2010,** *86*, 1323-1336.
8. Deziel, E. P. G.; Villemur, R.; Lepione, F.; Bisaillon, J., *Applied and Environmental Microbiology* **1996,** *62* (6), 1908-1912.
9. Ramana, K. V.; Karanth, N. G., *Journal of Chemical Technology and Biotechnology* **1989,** *45* (4), 249-257.
10. Fraenkel, G. S., *Science* **1959,** *129* (3361), 1466-1470.
11. Chayabutra, C.; Ju, L.-K., *Biotechnology Progress* **2001,** *17* (3), 419-423.
12. Guerra-Santos, L. H.; Kapelli, O.; Fiechter, A., *Applied Microbiology and Biotechnology* **1986,** *24* (6), 443-448.
13. Guerra-Santos, L.; Käppeli, O.; Fiechter, A., *Applied and Environmental Microbiology* **1984,** *48* (2), 301-305.
14. Mulligan, C. N.; Gibbs, B. F., *Applied and Environmental Microbiology* **1989,** *55* (11), 3016-3019.
15. Manresa, M. A.; Bastida, J.; Mercadé, M. E.; Robert, M.; de Andrés, C.; Espuny, M. J.; Guinea, J., *Journal of Industrial Microbiology* **1991,** *8* (2), 133-136.
16. Kovacs, N., *Nature* **1956,** *178* (4535), 703.
17. Robert, M.; Mercadé, M. E.; Bosch, M. P.; Parra, J. L.; Espuny, M. J.; Manresa, M. A.; Guinea, J., *Biotechnology Letters* **1989,** *11* (12), 871-874.
18. Lang, S.; Wullbrandt, D., *Applied Microbiology and Biotechnology* **1999,** *51* (1), 22-32.
19. Sim, L.; Ward, O. P.; Li, Z. Y., *Journal of Industrial Microbiology and Biotechnology* **1997,** *19* (4), 232-238.
20. Déziel, E.; Lépine, F.; Milot, S.; Villemur, R., *Biochimica et Biophysica Acta* **2000,** *1485* (2-3), 145-152.
21. Abalos, A.; Pinazo, A.; Infante, M. R.; Casals, M.; Garcia, F.; Manresa, A., *Langmuir* **2001,** *17* (5), 1367-1371.
22. Haba, E.; Abalos, A.; Jauregui, O.; Espuny, M. J.; A., M., *Journal of Surfactants and Detergents* **2003a,** *6* (2), 155-161.
23. Arino, S.; Marchal, R.; Vandecasteele, J. P., *Applied Microbiology and Biotechnology* **1996,** *45* (1-2), 162-168.
24. Abdel-Mawgoud, A. M.; Aboulwafa, M. M.; Hassouna, N. A.-H., *Applied Biochemistry and Biotechnology* **2009,** *157* (2), 329-345.
25. Chen, S.-Y.; Wei, Y.-H.; Chang, J.-S., *Applied Microbiology and Biotechnology* **2007,** *76* (1), 67-74.
26. Déziel, E.; Lépine, F.; Dennie, D.; Boismenu, D.; Mamer, O. A.; Villemur, R., *Biochimica et Biophysica Acta* **1999,** *1440* (2-3), 244-252.
27. Itoh, S.; Honda, H.; Tomita, F.; Suzuki, T., *Journal of Antibiotics* **1971,** *24* (12), 855-859.
28. Burger, M. M.; Glaser, L.; Burton, R. M., *Journal of Biological Chemistry* **1963,** *238* (8), 2595-2602.

29. Olvera, C.; Goldberg, J. B.; Sánchez, R.; Soberón-Chávez, G., *FEMS Microbiology Letters* **1999,** *179* (1), 85-90.
30. Hirai, K.; Tomida, M.; Kikuchi, Y.; Ueda, O.; Ando, H.; Asanuma, N., *The Bulletin of Tokyo Dental College* **2010,** *51* (4), 175-183.
31. Kushner, D. J.; Baker, A.; Dunstall, T. G., *Canadian Journal of Physiology and Pharmacology* **1999,** *77* (2), 79-88.
32. Paliy, O.; Bloor, D.; Brockwell, D.; Gilbert, P.; Barber, J., *Journal of Applied Microbiology* **2003,** *94*, 580-586.
33. Cheng, K.-J.; Ingram, J. M.; Costerton, J. W., *Journal of Bacteriology* **1970,** *104* (2), 748-753.
34. Perfumo, A.; Rudden, M.; Smyth, T. J. P.; Marchant, R.; Stevenson, P. S.; Parry, N. J.; Banat, I. M., *Applied Microbiology and Biotechnology* **2013,** *97* (16), 7297-7306.
35. Smyth, T. J. P.; Perfumo, A.; Marchant, R.; Banat, I. M., Isolation and Analysis of Low Molecular Weight Microbial Glycoloipids. In *Handbook of Hydrocarbon and Lipid Microbiology*, Timmis, K. N., Ed. Springer: Berlin, 2010; pp 3705-324.
36. Chen, M. DPhil thesis. University of Oxford, 2010.

Chapter 4

Surface adsorption behaviour of a ternary conventional surfactant mixture

The surface adsorption behaviour of a ternary mixture of octaethylene glycol monododecyl ether ($C_{12}E_8$), linear alkylbenzene sulfonate (LAS) and sodium lauryl ether sulfate (SLES) has been investigated in detail at the air/water interface using surface tension and NR. These are three of the most widely used surfactants in current home and personal care formulations and are frequently used as ternary mixtures. Hence it is of great importance to characterise their behaviour at both the interface and in solution. This is also an essential precursor to the study of systems with more than three components; through, for example, the addition of biosurfactants as reported later in this thesis.

4.1 Literature review

There are many reports concerning the non-ideal mixing behaviour of surfactant mixtures, with most theoretical treatments based on binary mixtures[1] using the Pseudophase Separation Approximation and Regular Solution Theory (RST) approach.[2,3] This has been extended to include more than two components[4,5] and comparisons between the RST and Molecular Thermodynamic (MT) theories have been used to determine the mixed CMCs in ternary surfactant mixtures.[6] For investigating the mixing behaviour, surface tension has provided estimates of individual surface excesses through the use of the Gibbs adsorption isotherm.[7] However, neutron reflectivity has proved a much more successful and direct technique for determining the surface composition of multicomponent mixtures, through the use of deuterium labelling and exploiting contrast variation. The surface composition has been analysed in detail for many nonionic-nonionic[8,9] anionic-nonionic,[10] zwitterionic-nonionic[11] and cationic-nonionic[12] surfactant mixtures. The non-ideal interactions between nonionic polyethoxylate surfactants with SDS[13] and with LAS[10,14] are particularly important and relate specifically to this study. The non-ideal interactions of ternary mixtures such as SDS/C_{12}B/C_{12}M,[11] previously explored using surface tension and neutron reflectivity, are also important to this work.

However, very little has been published concerning the mixing behaviour of the nonionic surfactant $C_{12}E_8$ with LAS and/or SLES; apart from the detailed analysis of a binary mixture of $C_{12}E_8$ and $C_{12}E_{23}$ with LAS by Penfold et al.[10] They found mixed monolayer adsorption at the air/water interface, with the mixing behaviour broadly consistent with the predictions of RST. This will be discussed in more detail in Section 4.3. The mixing behaviour of LAS with the nonionics $C_{12}E_3$ and $C_{12}E_7$ was studied as a function of temperature and time by Verma and Kumar.[15] However, this was investigated at the oil/water interface and was restricted to the evaluation of interfacial tension. The binary and ternary mixtures of LAS with the cationic surfactant tetradecyltrimethylammonium bromide, TTAB, and the nonionic polyoxyethylene octylphenols ($OP(EO)_8$) were also investigated, and related to approximations using Regular Solution Theory.[16] Highly non-ideal mixing behaviour was also found by Tucker et al[12] in binary mixtures between the nonionic surfactants $C_{12}E_3$, $C_{12}E_6$, $C_{12}E_{10}$ and the di-alkyl cationic DHDAB.

An in-depth investigation into the surface behaviour of the ternary system of $C_{12}E_8$/LAS/SLES is investigated here for the first time. This chapter focuses on the surface behaviour of this system in ultrapure water/NRW containing $1x10^{-6}$ M NaOH (theoretical pH 8 value, as explained in Chapter 2) using surface tension and neutron reflectivity.

4.2 Surface tension

The surface adsorption behaviour of the binary mixtures $C_{12}E_8$/LAS, $C_{12}E_8$/SLES and LAS/SLES, at compositions 0.75/0.25, 0.5/0.5 and 0.25/0.75, and the ternary mixture $C_{12}E_8$/LAS/SLES at composition 0.375/0.375/0.25, were investigated using surface tension. All solutions were made in MilliQ ultrapure water containing $1x10^{-6}$ M NaOH. The variation in CMC with surfactant composition was related to the theoretical change in CMC for an ideal solution, according to the Clint equation:[17]

$$\frac{1}{C^*} = \frac{\alpha}{c_1} + \frac{(1-\alpha)}{c_2} \tag{4.1}$$

where α is the surfactant mole fraction, c_1 and c_2 are the CMC of the pure components 1 and 2 and C* is the mixed CMC. For a ternary mixture, this is:

$$\frac{1}{C^*} = \frac{\alpha_1}{c_1} + \frac{\alpha_2}{c_2} + \frac{\alpha_3}{c_3} \tag{4.2}$$

Surface tension data here have also been compared to regular solution approximations using the non-ideal mixed micelle model.[4] RST treats the surface and bulk phases as separate pseudophases, and the departure from ideality can be expressed in terms of an interaction parameter, β, which accounts for the excess free energy of mixing. A strongly negative β value indicates a large departure from ideality and therefore a highly synergistic relationship. On the other hand, a small interaction parameter means the relationship is closer to an ideal one. In very few cases, β may be positive indicating a tendency to phase-separate and that the surfactants are not compatible. All RST calculations to find the β interaction parameter, for both surface tension and NR data, were carried out by J. Penfold at the University of Oxford.

4.2.1 Binary surfactant mixtures

4.2.1.1 $C_{12}E_8$/LAS

The surface tension of $C_{12}E_8$, LAS and its binary mixtures at compositions 0.75/0.25, 0.5/0.5 and 0.25/0.75 was studied and the variation in surface tension with log(surfactant concentration) is shown in Figure 4.1 (a). Figure 4.1 (b) gives the variation in CMC with increasing mole fraction of LAS. A summary of the CMC values and surface tension, γ, at CMC is given in Table 4.1.

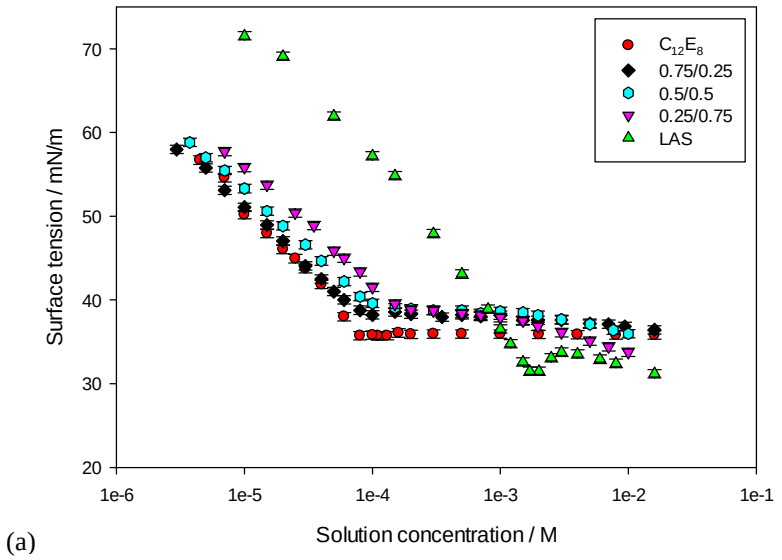

(a)

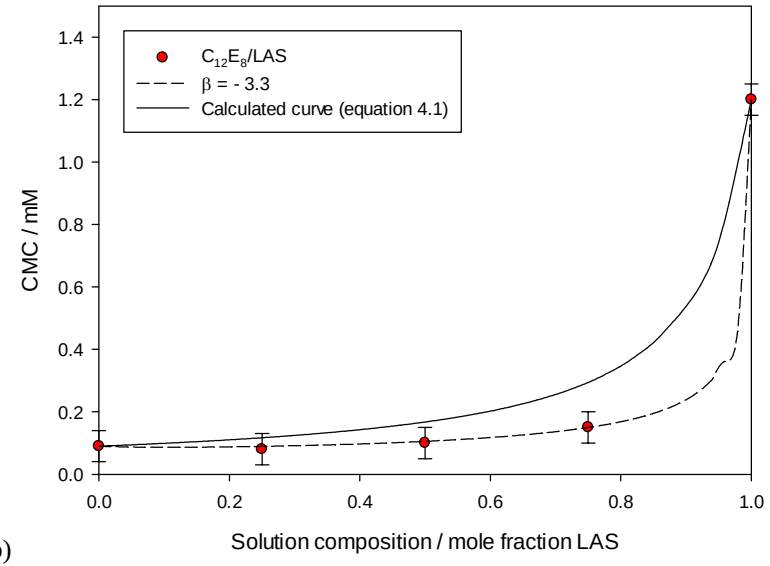

(b)

Figure 4.1: Variation in (a) surface tension for $C_{12}E_8$, LAS and their binary mixtures at compositions 0.75/0.25, 0.5/0.5, 0.25/0.75 and (b) CMC with increasing mole fraction LAS for $C_{12}E_8$/LAS binary mixtures, at 25°C, in ultrapure water containing $1x10^{-6}$ M NaOH. Results are compared with theoretical values according to the Clint equation (black line) and the predicted non-ideal mixing parameter β = -3.3 (dashed line).

Mole fraction LAS	CMC / ± 0.05 mM	γ at CMC / ± 0.5 mN/m
0	0.09	36.0
0.25	0.08	38.4
0.5	0.10	39.1
0.75	0.15	39.0
1	1.20	34.9

Table 4.1: Parameters for surface tension analysis of $C_{12}E_8$/LAS mixtures.

Figure 4.1 (b) shows that the mixed CMC increases with mole fraction of LAS, due to the higher CMC and lower surface activity of LAS. The surface tension at CMC for LAS is in general agreement with that found in literature.[18] The mixed CMC values are systematically lower than those predicted with ideal mixing (using Equation 4.1). The departure from ideal mixing has a non-ideality parameter β of

-3.3, suggesting a synergistic interaction between the $C_{12}E_8$ and LAS at the interface. $C_{12}E_8$ is nonionic and LAS is negatively-charged in aqueous solution. The area per molecule of LAS is around 57 Å^2, smaller than $C_{12}E_8$ (~62 Å^2)[19] due to the smaller headgroup and di-chain properties of the LAS-6 isomer. It is to be expected that non-ideal mixing may occur between these two surfactants due to their different hydrophobic tail properties, headgroup sizes and charge; similar to, for example, the non-ideal mixing behaviour between SDS and $C_{12}M$, which had a β interaction parameter of -4.1,[11] and the interactions between $C_{12}E_6$/SDS[20] and $C_{12}E_8$/LAS[10] with similar interaction parameters.

Above the mixed CMC, $C_{12}E_8$/LAS mixtures show a slight decrease in surface tension, especially for the more LAS-rich solutions. This could be due to exchange between the surfactant at the air/water interface and the other surfactant in the bulk solution. This was seen by Takasugi and Esumi[21] where in binary mixtures of the nonionic surfactants $C_{10}E_8$ or $C_{10}E_6$ with bis(2-hydroxyethyl)(2-hydroxy-3-perfluorooctylpropyl)methylammonium chloride (DEFUMAC), a cationic fluorocarbon surfactant, the nonionic was replaced by DEFUMAC in concentrations above the CMC, further lowering the surface tension above the CMC.

A slight minimum around the CMC of LAS is usually indicative of the presence of impurities. However, after TLC, NMR and ESI-MS analysis, the LAS was found to be of high purity. It is thought that the minimum may be due to the presence of small amounts of other LAS isomers, i.e LAS-4 or LAS-5. This is assumed not to be a major concern as the surface behaviour of these three isomers is very similar[18] and the CMC value and γ at CMC are in broad agreement with the literature.[22] Furthermore, the subsequent NR measurements are made well above the mixed CMC.

4.2.1.2 $C_{12}E_8$/SLES

The variation in surface tension with solution concentration for $C_{12}E_8$, SLES and their binary mixtures at compositions 0.75/0.25, 0.5/0.5 and 0.25/0.75 is shown in Figure 4.2 (a). Figure 4.2 (b) gives the variation in CMC with increasing mole fraction of SLES. A summary of the CMC values and surface tension, γ, at CMC is given in Table 4.2.

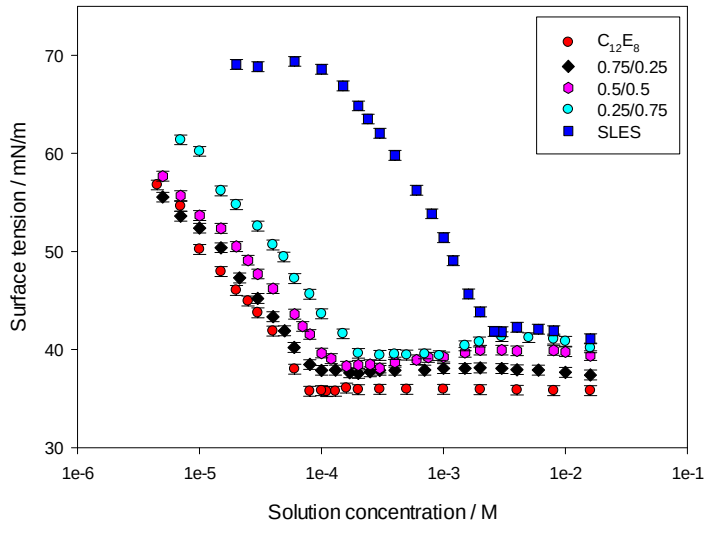

(a)

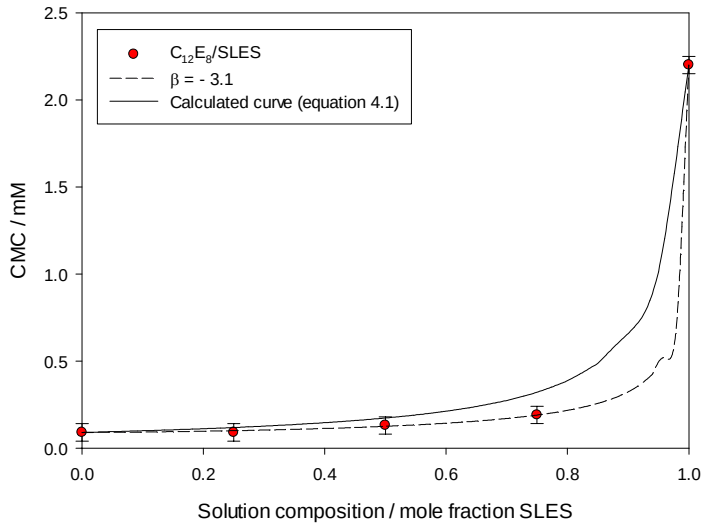

(b)

Figure 4.2: Variation in (a) surface tension with surfactant concentration for $C_{12}E_8$, SLES and their binary mixtures at compositions 0.75/0.25, 0.5/0.5 and 0.25/0.75 and (b) mixed CMC of $C_{12}E_8$/SLES as a function of SLES solution composition, at 25°C, in ultrapure water containing $1x10^{-6}$ M NaOH. Results are compared with theoretical values according to the Clint equation (black line) and the predicted non-ideal mixing parameter β = -3.1 (dashed line).

Mole fraction SLES	CMC / ± 0.05 mM	γ at CMC / ± 0.5 mN/m
0	0.09	36.0
0.25	0.09	37.7
0.5	0.13	38.1
0.75	0.19	39.5
1	2.17	42.6

Table 4.2: Parameters for surface tension analysis of $C_{12}E_8$/SLES mixtures.

The variation in surface tension with increasing log(surfactant concentration) for $C_{12}E_8$/SLES is given in Figure 4.2 (a). For SLES, at very low concentrations, there is a region where there is a minimal decrease in surface tension with increasing concentration, before the steep decrease in surface tension between solution concentrations $1x10^{-4}$ M and $2.17x10^{-4}$ M, the CMC. This is possibly due to the "increased activity of the surfactant in the bulk phase rather than at the interface"[23] although it could be attributed to the phenomenon of co-operative adsorption of the surfactant molecules to the interface (Frumkin kinetics),[24,25] where an increased concentration of molecules in solution is thought to increase the favourable intra-molecular hydrophobic interactions, encouraging further surface adsorption.

The mixed CMC increases with a higher proportion of SLES, explained by the relative surface activities of the two surfactants. In very $C_{12}E_8$-rich solutions, the experimental values are close to the ideal values, but with increasing mole fraction of SLES, there is an increasingly prominent negative deviation from ideality and mixed CMC values are systematically lower than those theoretically predicted. The areas per molecule for $C_{12}E_8$ and SLES are rather different, and due to their different headgroup sizes, charges, and a difference in CMC of over an order of magnitude, non-ideal mixing behaviour would be expected between these two surfactants. The change in mixed CMC with composition follows predictions from RST,[26] with a predicted non-ideal mixing parameter $\beta = -3.1$. This is almost the same as with $C_{12}E_8$/LAS and indicates a positive interaction between the $C_{12}E_8$ and SLES.

4.2.1.3 LAS/SLES

The variation in surface tension with solution concentration for LAS, SLES and their binary mixtures at compositions 0.75/0.25, 0.5/0.5 and 0.25/0.75 is shown in Figure 4.3 (a). Figure 4.3 (b) gives the variation in CMC with increasing mole fraction of SLES. A summary of the CMC values and surface tensions at the CMC is given in Table 4.3.

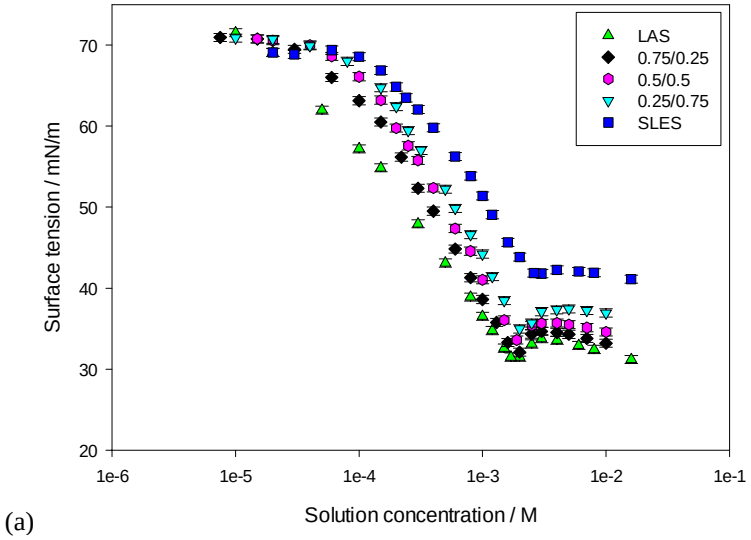

(a)

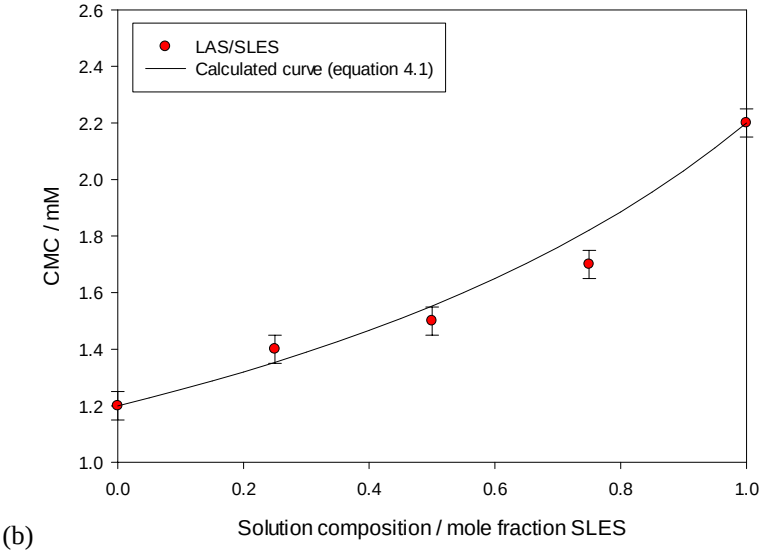

(b)

Figure 4.3: Variation in (a) surface tension with surfactant concentration for LAS, SLES and their binary mixtures at solution compositions 0.75/0.25, 0.5/0.5 and 0.25/0.75 and (b) mixed CMC of $C_{12}E_8$/SLES as a function of SLES solution composition, at 25°C, in ultrapure water containing $1x10^{-6}$ M NaOH. Results are compared with theoretical values according to the Clint equation (black line).

Mole fraction SLES	CMC / ± 0.05 mM	γ at CMC / ± 0.5 mN/m
0	1.17	34.9
0.25	1.35	35.3
0.5	1.50	35.9
0.75	1.72	37.6
1	2.17	43.2

Table 4.3: Parameters for surface tension analysis of LAS/SLES mixtures.

The variation in surface tension with log(solution concentration) is shown in Figure 4.3(a) for LAS, SLES and their binary mixtures at compositions 0.75/0.25, 0.5/0.5 and 0.25/0.75. An increase in mixed CMC and γ at CMC is seen with increasing mole fraction of SLES. Within error, these data correlate well with those predicted for ideal mixing. This may be expected due to the similarities in CMC of LAS and SLES and their negatively-charged headgroups in water, even though their areas per molecule are rather dissimilar (57 and 46 $Å^2$, respectively).

4.2.2 Ternary surfactant mixtures

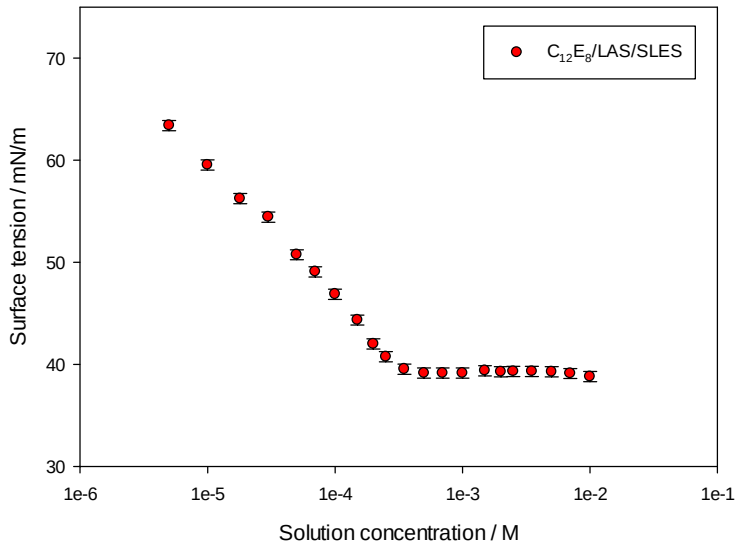

Figure 4.4: Variation in surface tension with solution concentration for $C_{12}E_8$/LAS/SLES at solution composition 0.125/0.125/0.75, at 25°C, in ultrapure water containing $1x10^{-6}$ M NaOH.

The variation in surface tension with log(solution concentration) for an example $C_{12}E_8$/LAS/SLES ternary mixture was measured to find the mixed CMC and to confirm that the solution concentration of 2 mM used throughout was above the mixed CMC. At solution composition 0.125/0.125/0.75 $C_{12}E_8$/LAS/SLES, 75% of which had a CMC higher than 2 mM (SLES), the mixed CMC was $3.4x10^{-4}$ M, well below the solution concentration used throughout this work.

4.3 Neutron reflectivity

Neutron reflectivity measurements were carried out at the air/water interface on the binary mixtures $C_{12}E_8$/SLES and LAS/SLES, and on the ternary mixture $C_{12}E_8$/LAS/SLES, at 2 mM solution concentration, in null reflecting water (NRW) containing $1x10^{-6}$ M NaOH, at a variety of solution compositions. Three isotopic combinations were measured for the binary mixtures, e.g. for $C_{12}E_8$/SLES: d-$C_{12}E_8$/h-SLES, h-$C_{12}E_8$/d-SLES, d-$C_{12}E_8$/d-SLES, and four isotopic combinations for the ternary mixtures: d-$C_{12}E_8$/h-LAS/h-SLES, h-$C_{12}E_8$/d-LAS/h-SLES, h-$C_{12}E_8$/h-LAS/d-SLES, d-$C_{12}E_8$/d-LAS/d-SLES. By selectively deuterating each component (where the solvent is NRW and hence contributes zero scattering) the only reflected signal will be from the deuterated component at the interface. The reflectivity profile obtained is then compared to one calculated using the optical matrix method for a single monolayer of uniform composition, to give the parameters adsorbed layer thickness, d, and scattering length density, ρ. From this, the surface composition for each surfactant at the interface can be determined. The dd and ddd combinations were required as a consistency check of the measurements and to allow for overdetermination in order to use the simplex least squares method to extract the area per molecule of each component. Using Equation 4.3 for binary mixtures and Equation 4.4 for ternary mixtures, and through the use of contrast variation, the area per molecule for each component in the mixture could be determined from:

$$d\rho = \frac{\Sigma b_1}{A_1} + \frac{\Sigma b_2}{A_2} \tag{4.3}$$

$$d\rho = \frac{\Sigma b_1}{A_1} + \frac{\Sigma b_2}{A_2} + \frac{\Sigma b_3}{A_3} \tag{4.4}$$

where Σb_n is the sum of scattering lengths, A_n is the area per molecule for each component n, and d and ρ are defined as above. The surface excess, Γ, of each surfactant in the mixture is then found by:

$$\Gamma = \frac{1}{N_A A} \tag{4.5}$$

which leads to relative values of surface composition for each component in the mixture.

4.3.1 Binary surfactant mixtures

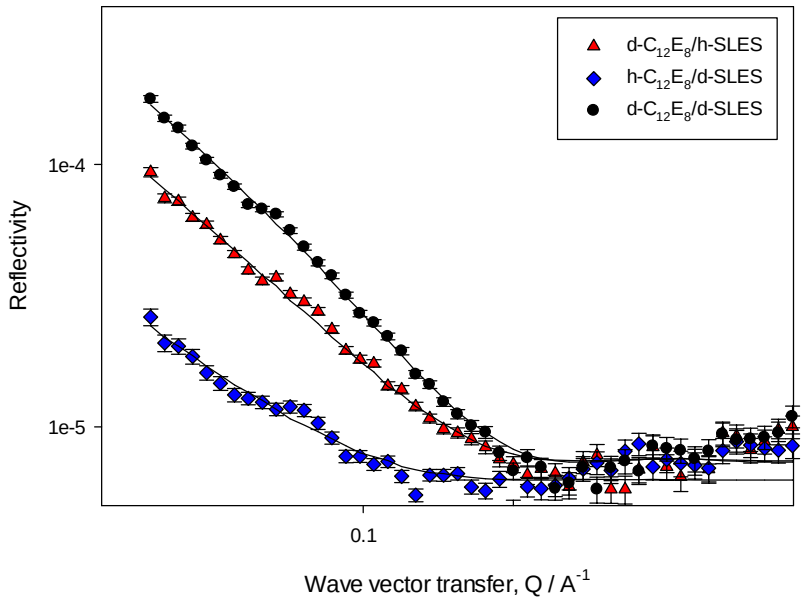

Figure 4.5: Example reflectivity curve with associated model fits for the isotopic combinations dh, hd and dd for 2mM $C_{12}E_8$/SLES at solution composition 0.25/0.75, at 25°C, in NRW containing $1x10^{-6}$ M NaOH.

Binary mixtures of $C_{12}E_8$/SLES and LAS/SLES were studied at solution composition 0.75/0.25, 0.5/0.5, 0.25/0.75 and 0.1/0.9, at 2 mM concentration, in NRW containing $1x10^{-6}$ M NaOH. Comparisons have been made with the mixing behaviour of $C_{12}E_8$/LAS, which was investigated in detail by Penfold et al.[10] Figure 4.5 shows an example reflectivity curve of the three isotopic combinations dh, hd and dd for 0.25/0.75 $C_{12}E_8$/SLES. The absolute level of reflectivity indicates the amount of surfactant adsorbed at the interface and the steepness of the slope relates to the thickness of the adsorbed layer; the steeper the slope of reflectivity, the thicker the adsorbed layer. Here, the absolute amount of $C_{12}E_8$ adsorbed at the interface is much greater than that of SLES, even though the solution composition of $C_{12}E_8$ is lower. The steepest curve (black) for the dd component gives the reflectivity for both surfactants at the interface. The following results in this chapter explore the relationship between $C_{12}E_8$ and SLES in detail.

4.3.1.1 $C_{12}E_8$/SLES

The variation in adsorbed amount and surface composition for $C_{12}E_8$ and SLES, as a function of SLES solution composition, is shown in Figure 4.6 and summarised in Table 4.4.

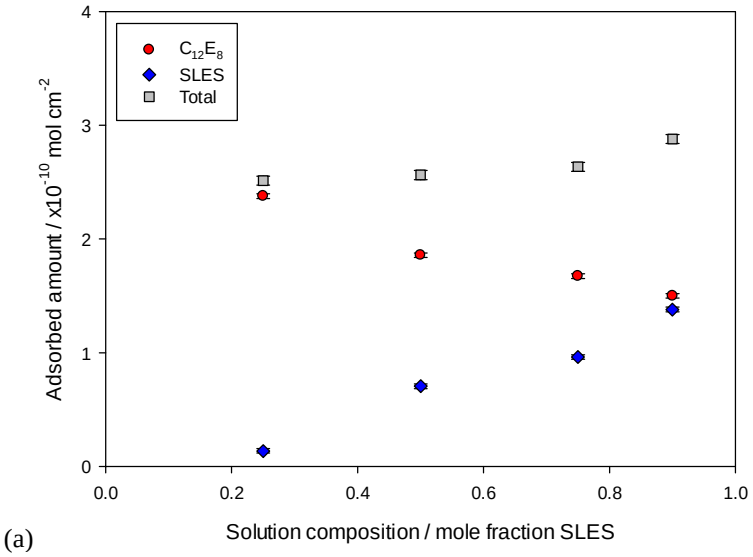

(a)

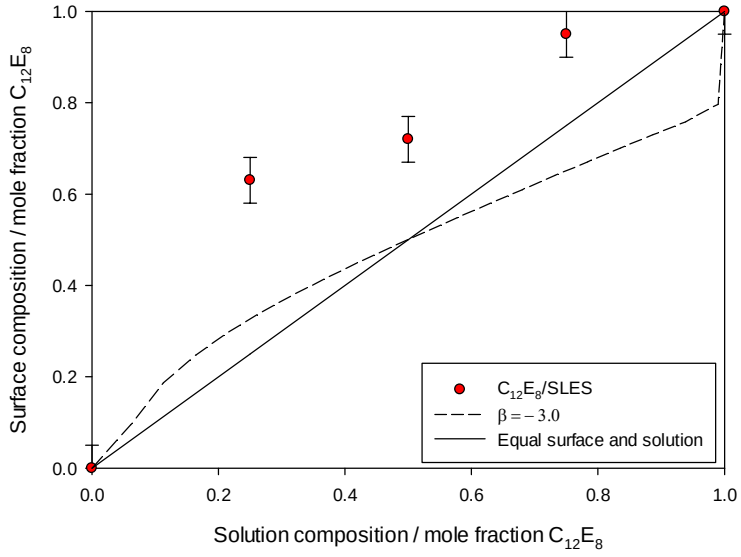

(b)

Figure 4.6: Variation in (a) adsorbed amount and (b) surface composition, with solution composition for 2 mM $C_{12}E_8$/SLES, at 25°C, in NRW containing 1x10^{-6} M NaOH. Surface composition data are compared with equal surface and solution composition (black line) and predicted non-ideal mixing parameter β = - 3.0 (dashed line).

Ratio	Contrast	d (± 1)	ρ (± 0.02 x10^{-6} Å^{-2})	A (± 2Å^2)	Γ (± 0.02 x10^{-10} mol cm^{-2})	Γ_{total} (± 0.04 x10^{-10} mol cm^{-2})	Solution compos-ition	Surface composition (± 0.02)
0.75/0.25	dh	27	1.85	70	2.38	2.51	0.75	0.95
	hd	53	0.07	1218	0.14		0.25	0.05
	dd	24	2.32					
0.5/0.5	dh	23	1.63	89	1.86	2.56	0.5	0.72
	hd	50	0.23	236	0.71		0.5	0.28
	dd	26	2.13					
0.25/0.75	dh	24	1.53	99	1.67	2.63	0.25	0.63
	hd	34	0.55	173	0.96		0.75	0.37
	dd	28	1.89					
0.1/0.9	dh	28	1.16	111	1.50	2.88	0.1	0.52
	hd	25	1.00	120	1.38		0.9	0.48
	dd	26	2.21					

Table 4.4: Key model parameters for 2 mM $C_{12}E_8$/SLES mixtures, at 25°C in NRW containing 1x10^{-6} M NaOH.

For binary $C_{12}E_8$/SLES mixtures, the nonionic component dominates the interface at all the solution compositions studied, resulting in highly non-ideal mixing. At a solution composition of 0.75 nonionic, the interface contains 95 mol% $C_{12}E_8$. As the solution becomes progressively richer in SLES, the amount of SLES at the interface only increases very marginally and even at 90 mol% SLES, the amount of SLES adsorbed at the interface does not reach 0.5. Clearly there is little attraction of SLES to the interface and it may be that there is a stronger interaction for this component to form aggregates in solution. The total surface excess slightly increases with increasing SLES mole fraction and in SLES-rich solutions reaches 2.88 $x10^{-10}$ mol cm^{-2}, with an average value of 2.64 $x10^{-10}$ mol cm^{-2}. When compared to the $C_{12}E_8$/LAS total surface excess data,[10] where an average total adsorption of 3.0 $x10^{-10}$ mol cm^{-2} was found, independent of the anionic composition, this is rather low.

The solid line in Figure 4.6 (b) represents the line of equal surface and solution compositions, and the dashed line is a RST calculation for a β value of -3.0. Clearly the surface composition deviates strongly from the solution composition. Furthermore it is highly non-ideal and not consistent with the application of RST.

4.3.1.2 LAS/SLES

The variation of adsorbed amount and surface composition with increasing solution composition of SLES is shown in Figure 4.7 and summarised in Table 4.5.

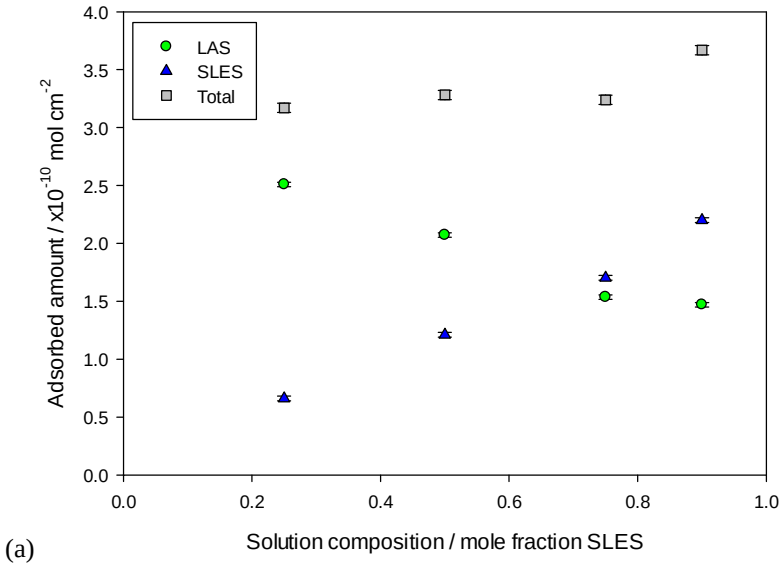

(a)

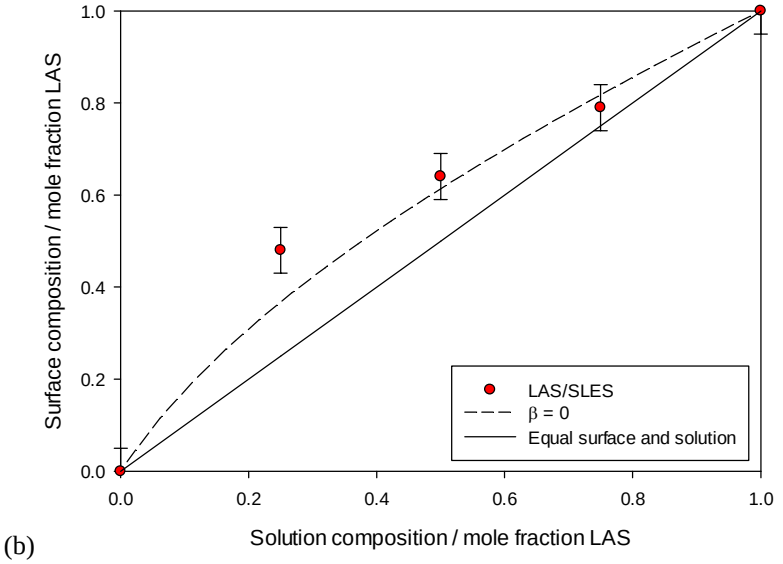

(b)

Figure 4.7: Variation in (a) adsorbed amount and (b) surface composition with solution composition for 2mM LAS/SLES mixtures, at 25°C, in NRW containing 1x10^{-6}M NaOH. Surface composition data are compared with equal surface and solution composition (black line) and the predicted nonideal mixing parameter β = 0 (dashed line).

Ratio	Contrast	d (± 1)	ρ (± 0.02 x10^{-6} Å^{-2})	A (± 2 Å^2)	Γ (± 0.02 x10^{-10} mol cm^{-2})	Γ_{total} (± 0.04 x10^{-10} mol cm^{-2})	Solution compos-ition	Surface compos-ition (± 0.02)
0.75/0.25	dh	20	2.60	66	2.51	3.17	0.75	0.79
	hd	27	0.58	251	0.66		0.25	0.21
	dd	22	3.00					
0.5/0.5	dh	19	2.32	80	2.07	3.28	0.5	0.63
	hd	25	0.98	137	1.21		0.5	0.37
	dd	20	3.25					
0.25/0.75	dh	18	1.82	108	1.54	3.24	0.25	0.47
	hd	18	1.65	98	1.70		0.75	0.53
	dd	20	3.26					
0.1/0.9	dh	26	1.30	113	1.49	3.67	0.1	0.40
	hd	23	1.71	76	2.16		0.9	0.60
	dd	21	3.27					

Table 4.5: Key model parameters for 2 mM LAS/SLES mixtures, at 25°C, in NRW containing 1x10^{-6} M NaOH.

With increasing mole fraction of SLES, there is an almost linear decrease in adsorbed amount of LAS and an increase of SLES. Although there is no significant change in total surface excess over the solution compositions analysed, the absolute surface excess is around 25% higher than for the $C_{12}E_8$/SLES mixtures. Here the average is 3.33×10^{-10} mol cm^{-2}, whereas for $C_{12}E_8$/SLES it was 2.64×10^{-10} mol cm^{-2}. The variation in total surface excess is described in more detail in Section 4.3.2 for the ternary $C_{12}E_8$/LAS/SLES system.

Solutions progressively richer in the SLES component deviate increasingly from "ideal" mixing behaviour. At 0.75/0.25 LAS/SLES, the surface compositions of both are similar to that of their solution compositions, but with increasing solution composition of SLES, the LAS component becomes increasingly dominant at the interface and at a SLES solution composition of 0.75 mole fraction, only around 50% of the interface is composed of SLES. This deviation from "ideal" mixing is not as extreme as with $C_{12}E_8$/SLES binary mixtures previously described, which can be rationalised in terms of the relative surface activities of $C_{12}E_8$, LAS and SLES.

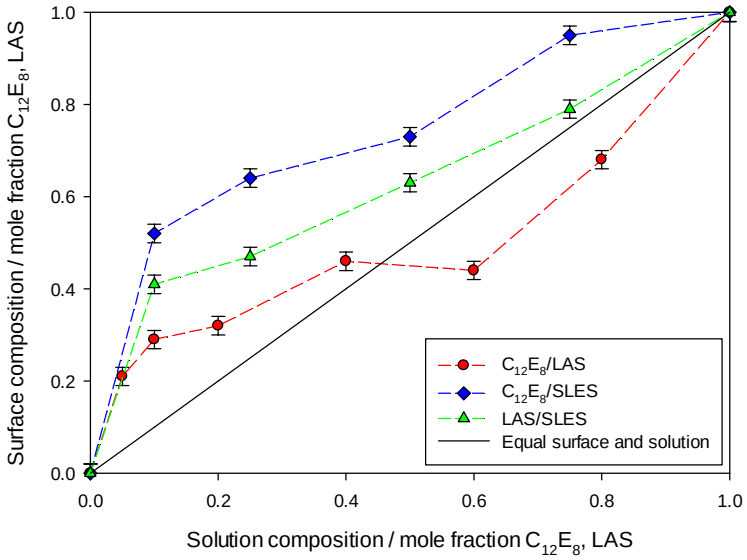

Figure 4.8: Variation in surface composition with solution composition for 2 mM binary conventional surfactant mixtures, compared with "ideal" mixing behaviour (straight line). Dashed lines are guides to the eye only.

The variation in surface composition with solution composition for all three binary conventional surfactant mixtures is summarised in Figure 4.8, this time as a function of solution composition of either $C_{12}E_8$ or LAS. Penfold et al used neutron reflectivity to investigate the surface behaviour of binary mixtures of LAS with $C_{12}E_8$ and $C_{12}E_{23}$,[10] in NRW, 6 mM NaCl and 2 mM $CaCl_2$, at a

surfactant concentration of 2 mM. In the absence of electrolyte they found mixed monolayer adsorption at the air/water interface. The $C_{12}E_8$/LAS data reproduced above showed a departure from the "ideal mixing" line which was broadly consistent with RST, with a large negative interaction parameter β between -7 and -10. As RST predicted, in the (less surface-active) LAS-rich solutions (0.6-0.95 mole fraction LAS), the nonionic component was dominant at the interface, but as the solution became progressively richer in the more surface-active nonionic, the LAS component began to dominate surface adsorption.

The $C_{12}E_8$/SLES and LAS/SLES mixtures both show a large departure from ideality, more prominent in more SLES-rich solutions and more pronounced for $C_{12}E_8$/SLES. At a solution composition of 0.1/0.9 $C_{12}E_8$/SLES and LAS/SLES, the surface compositions are 0.52/0.48 and 0.41/0.59, respectively. This mixing behaviour does not seem to be consistent with RST. The total adsorption ranged between 2.5 and 3.6 $x10^{-10}$ mol cm^{-2} for the solution compositions analysed. No synergy in total adsorption was observed for the binary mixtures as the total adsorbed amounts scaled with those of the individual components.

The data in Figures 4.6 to 4.8, and subsequent Figures 4.13 and 4.14, are compared to a theoretical "ideal mixing" line corresponding to the surface and solution compositions being equal at all solution compositions. However, in reality, this line of equal surface and solution compositions does not necessarily mean ideal mixing behaviour is present. At the concentration of 2 mM used here, which is far in excess of the mixed CMC, the surface composition may be expected to have evolved to become identical to its solution composition, whether ideal or non-ideal mixing is present. However at lower concentrations, the surface compositions of the components could be very different, as the surface which initially forms (and micelles) may be dominated by the more surface-active component. Here this trend clearly extends to the concentration used in this study. Hence in general the surface mixing is highly non-ideal, and in some cases it is outside that which can be predicted by theories such as RST. This is in contrast to the CMC variation, which is readily accounted for in terms of RST.

4.3.2 Ternary surfactant mixtures

The surface behaviour of the ternary $C_{12}E_8$/LAS/SLES system was investigated at a variety of solution compositions, and Figure 4.9 gives a graphical description of each data point, including the binary data described earlier. Data points were spread evenly across the ternary diagram over a wide composition range in order to give a complete picture of the surface properties of the system.

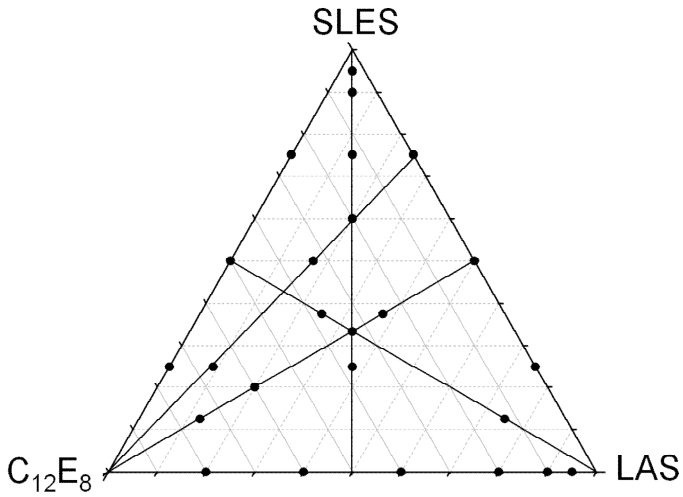

Figure 4.9: Ternary diagram displaying the wide range of solution compositions investigated for the ternary $C_{12}E_8$/LAS/SLES system. Data points investigated are shown by black dots.

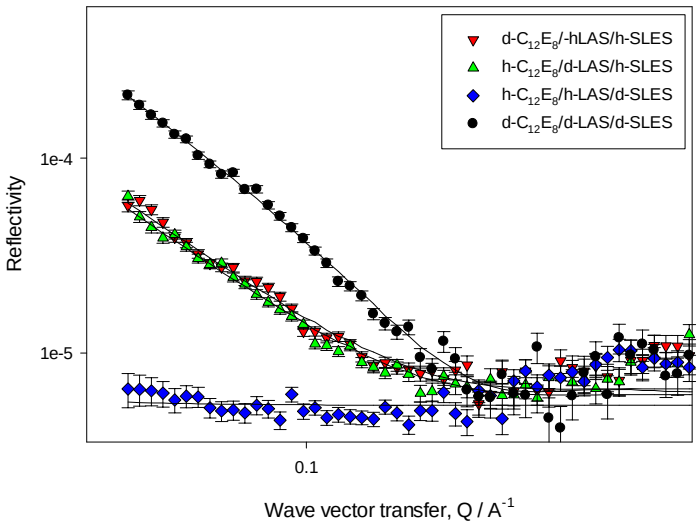

Figure 4.10: Example reflectivity curve with associated model fitting for $C_{12}E_8$/LAS/SLES at solution composition 0.375/0.375/0.25 for the isotopic combinations dhh, hdh, hhd and ddd, at 2 mM concentration, at 25°C, in NRW containing $1x10^{-6}$ M NaOH.

A typical reflectivity curve is shown in Figure 4.10 at solution composition 0.375/0.375/0.25 $C_{12}E_8$/LAS/SLES. The ddd component gives the steepest curve and thus the thickest adsorbed layer, as expected. The $C_{12}E_8$ and LAS, both with solution composition 0.375, have very similar reflectivity curves, indicating similar amounts of surfactant at the air water interface and thicknesses of adsorbed

layer. There is almost no reflectivity signal for SLES, indicating qualitatively that almost no SLES adsorbs to the interface, even when it comprises 0.25 of the overall solution composition. The variation in adsorbed amounts of the individual components $C_{12}E_8$, LAS and SLES in the ternary $C_{12}E_8$/LAS/SLES system with increasing solution composition of each component, respectively, is shown in Figure 4.11 and summarised in Table 4.6.

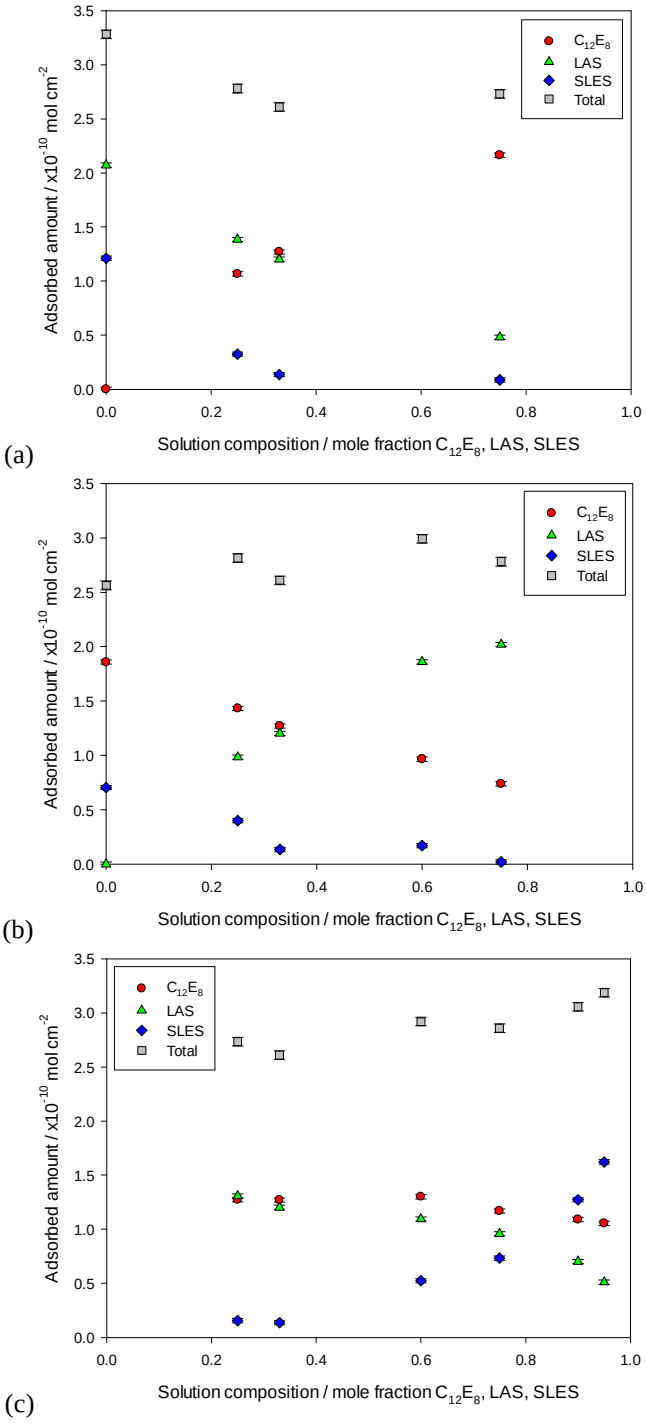

Figures 4.11: Variation in adsorbed amount with solution composition for the individual components $C_{12}E_8$, LAS and SLES as a function of (a) $C_{12}E_8$, (b) LAS and (c) SLES solution composition, for 2 mM $C_{12}E_8$/LAS/SLES, at 25°C, in NRW containing 1x10^{-6} M NaOH.

Ratio	Contrast	d (± 1)	ρ (± 0.02 x10^{-6} Å^{-2})	A (± 2 Å^2)	Γ (± 0.02 x10^{-10} mol cm^{-2})	Γ_{total} (± 0.04 x10^{-10} mol cm^{-2})	Solution compos-ition	Surface compos-ition (± 0.02)
0.375/0.375/ 0.25	dhh	21	1.40	131	1.27	2.73	0.375	0.46
	hdh	21	1.35	127	1.31		0.375	0.48
	hhd	48	0.13	1071	0.16		0.25	0.06
	ddd	24	2.46					
0.33/0.33/ 0.33	dhh	21	1.40	31	1.27	2.61	0.33	0.49
	hdh	20	1.35	138	1.20		0.33	0.46
	hhd	40	0.15	1224	0.14		0.33	0.05
	ddd	26	2.11					
0.2/0.2/0.6	dhh	25	1.24	128	1.30	2.92	0.2	0.45
	hdh	19	1.35	152	1.09		0.2	0.37
	hhd	30	0.42	317	0.52		0.6	0.18
	ddd	22	2.70					
0.125/0.125/ 0.75	dhh	30	0.86	142	1.16	2.86	0.125	0.41
	hdh	23	0.88	173	0.96		0.125	0.34
	hhd	16	0.86	227	0.73		0.75	0.25
	ddd	27	2.27					
0.05/0.05/ 0.9	dhh	34	0.69	164	1.01	2.81	0.05	0.36
	hdh	28	0.53	270	0.62		0.05	0.22
	hhd	23	0.95	140	1.19		0.9	0.42
	ddd	24	2.35					
0.025/0.025/ 0.95	dhh	32	0.79	161	1.03	3.16	0.025	0.33
	hdh	44	0.33	310	0.54		0.025	0.17
	hhd	28	1.06	104	1.59		0.95	0.50
	ddd	23	2.71					

Table 4.6: Key model parameters for 2 mM $C_{12}E_8$/LAS/SLES mixtures, as a function of SLES solution composition, at 25°C, in NRW containing 1x10^{-6}M NaOH.

With a solution composition increasingly rich in each component $C_{12}E_8$, LAS and SLES, the adsorbed amount of each component increases whilst that of the other two decreases. However, quantitatively there are subtle differences between the data. With increasing solution composition of LAS (Figure 4.11 (b)), its amount adsorbed increases at a similar rate to that seen with $C_{12}E_8$ (Figure 4.11(a)), with an almost linear decrease in both $C_{12}E_8$ and SLES. The absolute surface composition of $C_{12}E_8$ is much higher than SLES, reflecting the relative surface activities of each pure surfactant. With increasing SLES solution composition (Figure 4.11 (c)), a relatively constant surface composition is observed up to 0.33 mole fraction of SLES, where it then increases only moderately to a maximum of 1.6x10^{-10} mol cm^{-2}. The adsorbed amounts of $C_{12}E_8$ and LAS decrease very little, and at relatively the same rate.

The total surface excess ranges between 2.5 and 3.6 x10^{-10} mol cm^{-2} over the solution composition range measured, with the highest total adsorbed amount in only very SLES-rich solutions and the lower total adsorption in more $C_{12}E_8$-rich solutions. The values scale well with the adsorbed amounts

of the individual components $C_{12}E_8$, LAS and SLES, which are 2.9, 3.1 and 3.3 $x10^{-10}$ mol cm^{-2}, respectively.[14,27] No synergy is observed in the total adsorption of the mixtures when compared to the adsorption of the pure components.

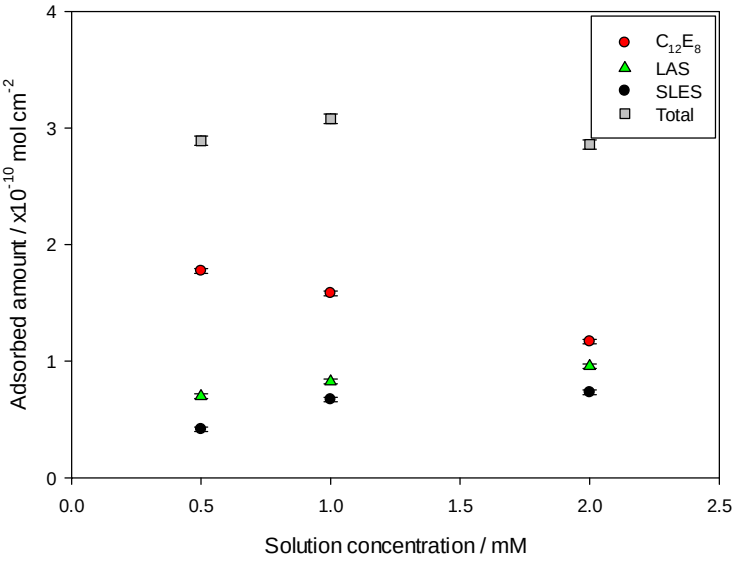

Figure 4.12: Variation in adsorbed amount $C_{12}E_8$, LAS, SLES, and the total adsorption, with increasing solution concentration, at solution composition 0.125/0.125/0.75, for the ternary mixture $C_{12}E_8$/LAS/SLES, at 25°C, in NRW containing $1x10^{-6}$M NaOH.

Figure 4.12 shows the variation in the adsorption with concentration for the $C_{12}E_8$/LAS/SLES ternary mixture at solution composition 0.125/0.125/0.75, from 0.5 mM, close to the mixed CMC (Figure 4.4, Section 4.2.2), to 2 mM, in excess of the mixed CMC. With increasing solution concentration, the adsorbed amounts of LAS and SLES increase, but that of $C_{12}E_8$ decreases. These data are broadly consistent with the general trends of RST and the pseudophase approximation. This dictates that surfactants adsorbed at the air/water interface and the micelles that first form at the CMC will be richer in the more surface active component; $C_{12}E_8$ in this case, but that the surface composition should tend towards the bulk composition at higher concentrations. As the concentration of the surfactant mixture increases, the surface composition will evolve towards that of the solution composition because an increasing amount of the surfactant present is in micelle form. The $C_{12}E_8$ concentration will decrease as the $C_{12}E_8$ molecules become adsorbed into the micelles, while the less surface active LAS and SLES will increase in adsorption at the interface. Here they move towards the same composition as in the bulk, but do not reach it. However, the surface compositions of all three components do tend towards a constant value. From 2 mM and above, it is expected that the surface

composition of all three components will be invariant, so they present "representative solutions of a high concentration limit."[28] The total adsorption remains approximately the same, within error, for the range of concentrations investigated as the $C_{12}E_8$ decreases at roughly the same rate as the combination of LAS and SLES is increasing.

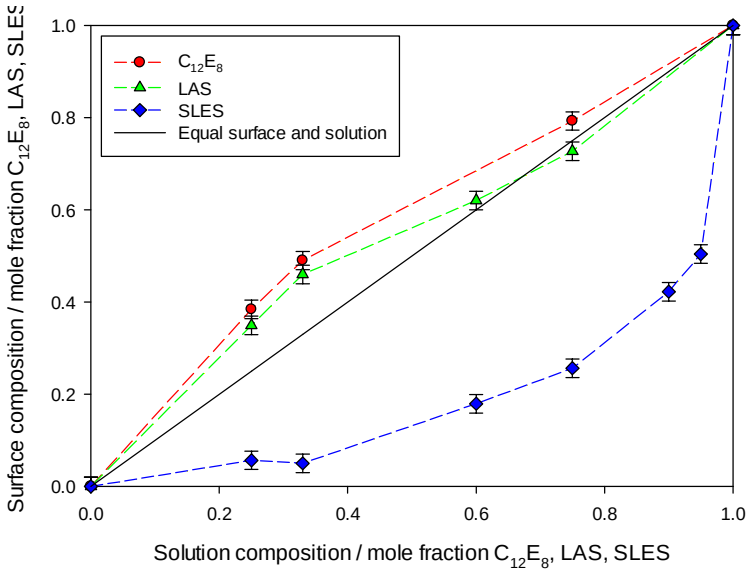

Figure 4.13: Variation in surface composition as a function of solution composition of $C_{12}E_8$, LAS and SLES, for 2 mM $C_{12}E_8$/LAS/SLES, at 25°C, in NRW containing $1x10^{-6}$ M NaOH.

The variation in surface composition for all three surfactants is summarised in Figure 4.13 and when plotted together, the strikingly different behaviour of SLES can be seen clearly. Over all solution compositions studied, $C_{12}E_8$ dominates the air/water interface as its surface composition is systematically higher than its solution composition. A slight positive deviation from the ideal mixing line is seen for LAS, but above 0.6 mole fraction, the surface composition of LAS closely resembles its solution composition. Almost no SLES adsorbs to the interface below 0.3 mole fraction. Above this, the surface composition of SLES increases exponentially. However, even when 95% of the solution is composed of SLES, its surface composition comprises only 50% of the total.

As summarised in Figure 4.14, in increasingly SLES-rich solutions (from 0.5/0.5 to 0.25/0.75 LAS/SLES) the surface composition of $C_{12}E_8$ becomes increasingly higher than its solution composition, representing a dominance of $C_{12}E_8$ and reluctance of SLES to adsorb at the interface.

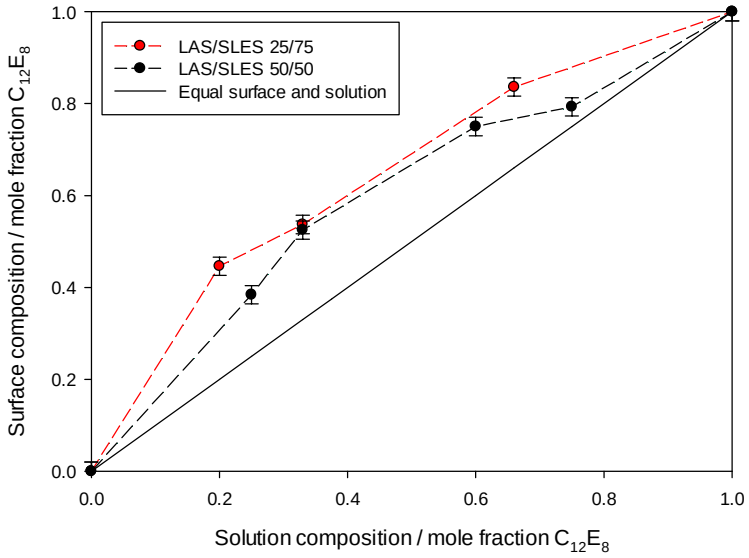

Figure 4.14: Variation in surface composition with solution composition for ternary mixture at LAS/SLES compositions 0.25/0.75 and 0.5/0.5, compared with "ideal" mixing behaviour (straight line).

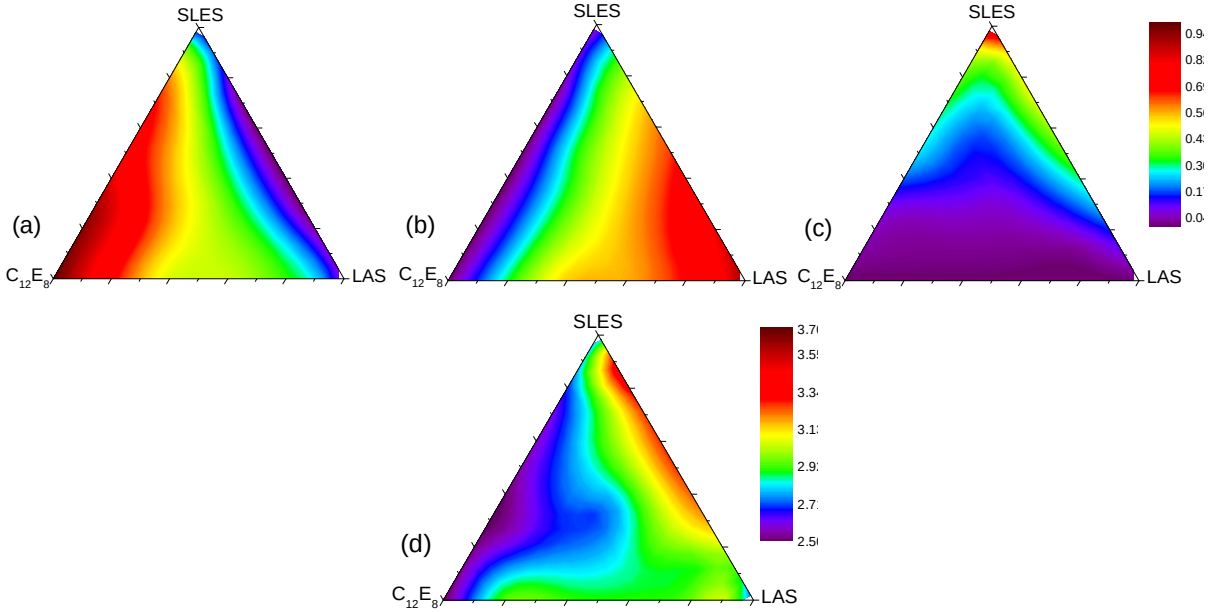

Figure 4.15: Surface compositions as a function of solution composition for (a) $C_{12}E_8$, (b) LAS and (c) SLES, with (d) the variation in total surface adsorption. The surface compositions and adsorbed amounts are given as a variation in colour, as shown by the keys on the right (units are $x10^{-10}$ mol cm^{-2} for adsorbed amounts.)

The ternary contour diagrams in Figure 4.15 (a) to (c) show a graphical description of the surface compositions of $C_{12}E_8$, LAS and SLES, as a function of solution composition. $C_{12}E_8$ (and LAS to a slightly lesser extent) is largely dominant at the surface over much of the solution composition. Even with as little as 25% solution composition, the most surface-active component $C_{12}E_8$ dominates nearly 40% of the interface. However, Figure 4.15 (c) displays the surprisingly low affinity of SLES to the surface. A solution composition of 0.05/0.05/0.9 $C_{12}E_8$/LAS/SLES gives a surface composition is 0.36/0.22/0.42, with SLES solution and surface compositions of 0.9 and 0.42, respectively. This

remarkably low proportion of SLES is a surprising and important result and indicates its preference for incorporation into aggregate phases. Interestingly there also appears to be an area of lower than expected surface composition of SLES in ternary mixtures containing around 50% SLES, when the $C_{12}E_8$/LAS composition is approximately 0.4/0.6. However, a more extensive data set may be needed to establish this effect.

No synergy in total adsorption is observed for the ternary conventional surfactant mixtures, when compared to adsorption of the single components, as described earlier in Figure 4.11. However, interestingly a decrease in total adsorption is observed towards more $C_{12}E_8$-rich solution compositions and conversely a higher proportion of LAS/SLES provides a higher total adsorbed amount, as shown in Figure 4.15 (d).

4.4 Surface adsorption of a $C_{12}E_8$/LAS/SDS ternary mixture

Sodium dodecyl sulfate (SDS) is another common anionic surfactant used in many current detergent formulations. It contains a C_{12} hydrocarbon chain and an anionic sulfate headgroup, as with SLES, but an absence of ethylene oxide (EO) groups in between the hydrocarbon tail and anionic head.

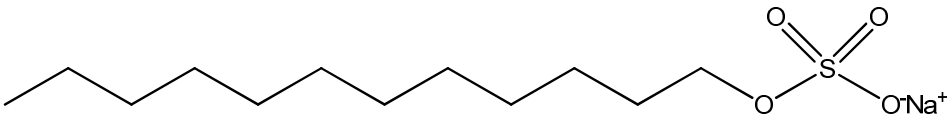

Figure 4.16: Molecular structure of sodium dodecyl sulfate (SDS)

The CMC of SDS is 8 mM.[20] The addition of the hydrophilic EO groups between the hydrophobic hydrocarbon chain and the anionic sulfate headgroup results in a CMC of almost an order of magnitude lower than the value for SDS, even though the EO groups would be expected to increase the overall hydrophilicity of the molecule. This is because when adjacent to the sulfate headgroup, the EO groups become hydrophobic in character.[29] Through investigation of the $C_{12}E_8$/LAS/SLES ternary system using surface tensiometry and neutron reflectivity, SLES was found to be surprisingly reluctant to adsorb to the air/water interface in the presence of $C_{12}E_8$ and LAS. Replacement of the SLES with SDS was used to investigate whether the presence of EO groups was the reason for the ineffectiveness of SLES at competing for the air/water interface. Table 4.7 provides a comparison for two solution compositions 0.375/0.375/0.25 and 0.125/0.125/0.75 for $C_{12}E_8$/LAS/SDS, with the results for $C_{12}E_8$/LAS/SLES shown on the two far right hand columns for comparison.

Ratio	Contrast	d (± 1)	ρ (± 0.02 x10^{-6} Å^{-2})	A (± 2 Å^2)	Γ (± 0.02 x10^{-10} mol cm^{-2})	Γ_{total} (± 0.04 x10^{-10} mol cm^{-2})	Solution compos-ition	Surface composition (± 0.02)
0.375/0.375 /0.25	dhh	11	2.93	95	1.74	3.05 (2.73)	0.375	0.57 (0.46)
	hdh	26	1.04	140	1.19		0.375	0.39 (0.48)
	hhd	20	0.30	1391	0.12		0.25	0.04 (0.06)
	ddd	10	5.80					
0.125/0.125 /0.75	dhh	24	1.33	94	1.76	3.08 (2.86)	0.125	0.56 (0.41)
	hdh	19	1.04	201	0.83		0.125	0.27 (0.34)
	hhd	15	0.80	323	0.51		0.75	0.17 (0.25)
	ddd	14	4.00					

Table 4.7: Key model parameters for 2mM $C_{12}E_8$/LAS/SDS at solution compositions 0.375/0.375/0.25 and 0.125/0.125/0.75, at 25°C, in NRW containing 1x10^{-6} M NaOH. Data in brackets shows the equivalent data for the $C_{12}E_8$/LAS/SLES mixtures for comparison.

Qualitatively, the results with SLES and SDS ternary mixtures at both compositions are similar, but subtle differences between the data can be seen. For the ternary $C_{12}E_8$/LAS/SLES system, the $C_{12}E_8$ and LAS components both dominate surface adsorption, with the SLES component almost non-existent at the interface. However, on replacement with SDS, the $C_{12}E_8$ component dominates adsorption to a larger extent than it does with SLES, and the difference between the surface composition of $C_{12}E_8$ and LAS becomes much greater. For example, at a solution composition of 0.375/0.375/0.25, the surface composition of $C_{12}E_8$ increases from 0.47 to 0.57 while the LAS composition decreases from 0.46 to 0.39. The SLES/SDS component remains approximately the same, within error. Replacement with SDS also brings about a higher total adsorption of around 10%. However, total adsorption is not higher in solutions richer in SDS, as was found in the $C_{12}E_8$/LAS/SLES system.

Non-ideal mixing behaviour is observed with a strong attractive interaction between LAS, the highly charged SDS and the nonionic $C_{12}E_8$ at the interface. This is to be expected due to their very different headgroup sizes and the intermolecular alkyl chain-EO group interactions.[30] Similarly non-ideal mixing behaviour has been reported for SDS/$C_{12}E_6$,[13] SDS/C_{12}B/C_{12}M,[11] and the multicomponent mixture of SDS, dodecanol and $C_{12}E_n$ with varying EO lengths.[31] In the ternary SDS/C_{12}B/C_{12}M system,[11] the low proportion of SDS at the interface, as found in this work, was thought to be due to relatively weak interactions between the SDS itself and the C_{12}B and C_{12}M.

4.5 Discussion

The surface adsorption behaviour of $C_{12}E_8$/LAS/SLES binary and ternary mixtures was studied using surface tension and neutron reflectivity and a marked departure from ideal mixing at the air/water interface was observed. For binary and ternary mixtures, the more surface-active $C_{12}E_8$ and LAS dominated much of the surface composition over SLES, which was surprisingly unable to compete for the interface. The interface is dominated by the components in the order $C_{12}E_8$>LAS>SLES. Clearly there is little attraction of SLES to the interface and it may be that there is a stronger tendency for this component to form aggregates in solution. Further insight is given in Chapter 5 where this system is investigated in the presence of electrolyte.

Similarly unusual non-ideal behaviour was found by Tucker et al[12] with a dominance of one particular component at the air/water interface in binary mixtures of the di-alkyl cationic surfactant DHDAB with nonionic surfactants $C_{12}E_3$, $C_{12}E_6$ and $C_{12}E_{12}$. In $C_{12}E_3$/DHDAB mixtures up to 0.2 solution composition $C_{12}E_3$, no $C_{12}E_3$ was present the interface and the surface was composed entirely of the more surface-active DHDAB (CMC = $4x10^{-5}$ M [12]). Only above 0.2 mole fraction nonionic did adsorption of the nonionic component begin. In binary mixtures with $C_{12}E_6$ this pattern was more extreme, with adsorption of the nonionic occurring at only 0.4 - 0.5 mole fraction. Nonionic adsorption in binary mixtures of $C_{12}E_{12}$ and DHDAB only occurred at 0.5 mole fraction and above. This highly non-ideal behaviour at the interface depended greatly on the nonionic surfactant involved. It is thought that this non-ideality was due to changes in the solution behaviour because the evolution in surface composition towards its solution composition with increasing mole fraction of nonionic corresponded to distinct changes in aggregate structure. In excess of the mixed CMC, small changes in the bulk can often manifest themselves into extreme changes in the monomer composition at the surface.

In this work the surface excess of each component at the air/water interface was measured directly by neutron reflectivity. Many comparisons in literature have been made between surface excess values determined by surface tension and through neutron reflectivity. The determination of surface excesses

through surface tension relies on the gradient of surface tension versus log(solution concentration) immediately below the CMC. Frumkin kinetics[24] implies that saturation can be found once the cooperation curve has levelled off, i.e. at the break in surface tension versus log(concentration) curve and not before. This assumes that throughout the decreasing part of the surface tension plot, the interface is saturated. Recent literature by Menger et al[25,32,33,34] indicates that saturation is not actually reached at the CMC. For example, they found that the percentage surface coverage of SDS was still increasing in this linear part, albeit by only up to 10%.[32]

However, Thomas et al[35] state that the saturation of the interface by nonionic surfactants may occur prior to the CMC, giving a linear plot below the CMC from which is it relatively easy to find an accurate surface excess. It is thought that the break in surface tension versus concentration plot can occur at concentrations lower than the real CMC due to the most surface-active component in the mixture causing saturation at the air/water interface before micelles actually begin to form in the bulk solution. It is possible that a "bulk" measurement such as conductivity[36] or PGSE-NMR[37] may be more accurate in determining the CMC for mixed surfactant systems.

The ternary $C_{12}E_8$/LAS/SDS system has been studied to further analyse the reluctance of SLES and/or SDS to adsorb at the air/water interface. On replacement of SLES with SDS, qualitatively similar results in surface behaviour are found in that very little SDS adsorbed to the interface while the nonionic and LAS components dominate adsorption. Quantitatively there are some subtle differences between the two sets of data, as the more surface-active $C_{12}E_8$ becomes even more dominant at the surface when in combination with SDS rather than SLES, and the LAS becomes less dominant. Further discussion is postponed until Chapter 5 which discusses the effect of electrolyte on surfactant mixtures with both SLES and SDS and comparisons are made with literature data of SDS with nonionic surfactants[13] which were also carried out in electrolyte.

The current ratio of $C_{12}E_8$/LAS/SLES used in many current detergent formulations is 0.42/0.31/0.27. The closest ratio investigated here is 0.375/0.375/0.25 which gives a surface composition of 0.46/0.48/0.06, giving a remarkably low surface adsorption of SLES when in combination with

nonionic ethoxylate surfactants, which are vastly more surface active and hence dominate surface adsorption. In the six-component mixture with a similar solution composition to that of the commercial "Synperionic A5"[31] there was a very high dominance of the more surface-active components even at concentrations one hundred times greater than the CMC. This is unlike what would be expected from the pseudophase approximation and RST, where above the CMC the most surface-active components are expected to become preferentially solubilised into the micelles rather than at the interface.

Until now, complex multicomponent surfactant mixtures such as this have not been explored in detail and it is encouraging to observe such interesting results. Highly non-ideal behaviour was observed for binary and ternary mixtures of the $C_{12}E_8$/LAS/SLES system which cannot be described by current non-ideal mixing theories such as RST. This work provides a good basis for the investigation of the impact of electrolyte on the ternary system, and for the exploration of the surface behaviour of multicomponent mixtures containing the rhamnolipid biosurfactant.

References: Chapter 4

1. Holland, P. M.; Rubingh, D. N., Mixed Surfactant Systems. In *Mixed Surfactant Systems*, ACS: Washington DC, 1992; pp 2-30.
2. Rubingh, D. N., Mixed Micelle Solutions. In *Solution Chemistry of Surfactants*, Mittal, K. L., Ed. Plenum Press: New York, 1979; Vol. 1, pp 337-354.
3. Kamrath, R. F.; Franses, E. I., *Journal of Physical Chemistry* **1984,** *88* (8), 1642-1648.
4. Holland, P. M.; Rubingh, D. N., *Journal of Physical Chemistry* **1983,** *87* (11), 1984-1990.
5. Holland, P. M., *Advances in Colloid and Interface Science* **1986,** *26*, 111-129.
6. Shiloach, A.; Blankschtein, D., *Langmuir* **1998,** *14* (15), 4105-4114.
7. Hutchinson, E., *Journal of Colloid Science* **1948,** *3* (5), 413-424.
8. Penfold, J.; Staples, E.; Tucker, I.; Thompson, L.; Thomas, R. K., *Journal of Colloid and Interface Science* **2002,** *247*, 404-411.
9. Penfold, J.; Staples, E.; Tucker, I.; Thomas, R. K.; Woodling, R.; Dong, C. C., *Journal of Colloid and Interface Science* **2003,** *262*, 235-242.
10. Penfold, J.; Thomas, R. K.; Dong, C. C.; Tucker, I.; Metcalfe, K.; Golding, S.; Grillo, I., *Langmuir* **2007,** *23* (20), 10140-10149.
11. Hines, J. D.; Thomas, R. K.; Garrett, P. R.; Rennie, G. K.; Penfold, J., *Journal of Physical Chemistry B* **1998,** *102* (48), 9708-9713.
12. Tucker, I.; Penfold, J.; Thomas, R. K.; Tildesley, D. J., *Langmuir* **2009,** *25* (7), 3924-3931.
13. Penfold, J.; Staples, E.; Thompson, L.; Tucker, I.; Hines, J.; Thomas, R. K.; Lu, J. R., *Langmuir* **1995,** *11* (7), 2496-2503.
14. Tucker, I.; Penfold, J.; Thomas, R. K.; Dong, C. C.; Golding, S.; Gibson, C.; Grillo, I., *Langmuir* **2010,** *26* (13), 10614-10626.
15. Verma, S.; Kumar, W., *Journal of Colloid and Interface Science* **1998,** *207* (1), 1-10.
16. Graciaa, A.; Ben Ghoulam, M.; Marion, G.; Lachaise, J., *Journal of Physical Chemistry* **1989,** *93* (10), 4167-4173.
17. Clint, J. H., *Journal of the Chemical Society, Faraday Transactions 1* **1975,** *71*, 1327-1334.
18. Ma, J.-G.; Boyd, B. J.; Drummond, C. J., *Langmuir* **2006,** *22* (21), 8646-8654.
19. Rosen, M. J.; Cohen, A. W.; Dahanayake, M.; Hua, X.-y., *Journal of Physical Chemistry* **1982,** *86*, 541-545.
20. Penfold, J.; Tucker, I.; Thomas, R. K.; Staples, E.; Schuermann, R., *Journal of Physical Chemistry B* **2005,** *109* (21), 10760-10770.
21. Takasugi, K.; Esumi, K., *Journal of Physical Chemistry* **1996,** *100* (48), 18802-18807.
22. Chen, M.; Dong, C. C.; Penfold, J.; Thomas, R. K.; Smyth, T., J. P.; Perfumo, A.; Marchant, R.; Banat, I. M.; Stevenson, P.; Parry, A.; Tucker, I.; Campbell, R. A., *Langmuir* **2011,** *27* (14), 8854-8866.
23. Rosen, M. J., Surfactants and Interfacial Phenomena, 3rd edition. John Wiley and Sons: New York, 2004; p 464.
24. Hsu, C.-T.; Chang, C.-H.; Lin, S.-Y., *Langmuir* **1997,** *13* (23), 6204-6210.
25. Menger, F. M.; Shi, L.; Rizvi, S. A. A., *Journal of the American Chemical Society* **2009,** *131* (30), 10380-10381.
26. Penfold, J.; Staples, E.; Thompson, L.; Tucker, I.; Hines, J.; Thomas, R. K.; Lu, J. R., *Langmuir* **1995,** *11* (7), 2496-2503.
27. Xu, H.; Penfold, J.; Thomas, R. K.; Petkov, J. T.; Tucker, I.; Webster, J. P. R., *Langmuir* **2013,** *29* (37), 11656-11666.
28. Penfold, J.; Thomas, R. K., *Physical Chemistry Chemical Physics* **2013,** *15*, 7017-7027.
29. Sowada, R., *Journal für praktische Chemie* **1981,** *323* (2), 269-278.
30. Lu, J. R.; Thomas, R. K.; Penfold, J., *Advances in Colloid and Interface Science* **2000,** *84*, 143-304.
31. Staples, E. J.; Thompson, L.; Tucker, I.; Penfold, J., *Langmuir* **1994,** *10* (11), 4136-4141.
32. Menger, F. M.; Rizvi, S. A. A., *Langmuir* **2011,** *27* (23), 13975-13977.
33. Menger, F. M.; Shi, L.; Rizvi, S. A. A., *Langmuir* **2010,** *26* (3), 1588-1589.

34. Menger, F. M.; Rizvi, S. A. A.; Shi, L., *Langmuir* **2011,** *27* (12), 7963-7965.
35. Li, P. X.; Li, Z. X.; Shen, H.-H.; Thomas, R. K.; Penfold, J.; Lu, J. R., *Langmuir* **2013,** *29* (30), 9324-9334.
36. Menger, F. M.; Shi, L., *Journal of the American Chemical Society* **2009,** *131* (19), 6672-6673.
37. Misselyn-Bauduin, A. M.; Thibaut, A.; Grandjean, J.; Broze, G.; Jérôme, R., *Langmuir* **2000,** *16* (10), 4430-4435.

Chapter 5

The impact of electrolyte on the surface adsorption behaviour of conventional surfactant mixtures

The effect of mono- and multivalent counterions on surfactants often have negative consequences on the performance of detergent mixtures, by, for example, causing precipitation of anionic components on complexation with counterions of opposite charge. Therefore it is important to investigate the surface behaviour of multicomponent surfactant mixtures in the presence of these counterions as a model for how the surfactants' performance can be affected in hard water environments. This chapter discusses the effect of Na^+ and Ca^{2+} ions, in the form of NaCl and $CaCl_2$, on the surface adsorption behaviour of the binary mixtures $C_{12}E_8$/SLES and LAS/SLES, and the ternary $C_{12}E_8$/LAS/SLES and $C_{12}E_8$/LAS/SDS mixtures.

5.1 Literature review

The effect of electrolyte on surface adsorption in surfactant mixtures is well known. It produces a decrease in CMC and surface tension, γ, at CMC, increases micellar aggregation numbers and enhances surface adsorption.[1] An extensive amount of literature has focused on the effects of mono- and divalent counterions on surfactant mixtures, which range from the non-ideal mixing behaviour in nonionic/anionic,[2,3] nonionic/cationic[4] and zwitterionic/anionic mixtures at the air/water interface, to those at the solid/liquid interface.[5] The behaviour of $C_{12}E_8$/LAS[2] in the presence of Na^+ and Ca^{2+}, and $C_{12}E_{12}$/SLES[3] in the presence of Al^{3+}, are especially important in the context of the work presented in this chapter.

In terms of the individual components $C_{12}E_8$, LAS and SLES used here, the addition of a "salting out" electrolyte such as NaCl has the effect of increasing adsorption of pure $C_{12}E_8$ and decreasing its area per molecule.[6] This is attributed to a decrease in the solubility of the alkyl chain, changing its conformation, increasing surface activity and reducing CMC values.[7] It has been possible, through

selective deuteration of the head and chain on the surfactant molecule, to determine its exact conformation at the interface.[8]

Ma et al[9] demonstrated the impact of 0.1 M NaCl on pure LAS at 50°C. The CMC decreased from 2.53 to 0.25 mM, γ at CMC decreased from 32.1 to 24.8 mN/m, and the area per molecule decreased from 67 to 51 $Å^2$, all due to weakened headgroup repulsions. The Krafft point also increased but it was still well below the 25°C used here. Micellar L_1 aggregates were present at the relatively low concentration used in this work, although lamellar/micellar L_α/L_1 coexistence was found above ~10 w/w% concentration due to the low preferred curvature of LAS. Zhu et al[10] investigated LAS in hard water conditions, in an aqueous solution containing $CaCl_2$, $MgSO_4$, $NaHCO_3$, KH_2PO_4 and $NaNO_3$ at pH 7.5, and found an almost 10-fold decrease in CMC to 2.69 $x10^{-4}$ M at 30°C, with an area per molecule of 52.7 $Å^2$. The chain length and position of the phenyl sulfonate headgroup greatly affected the CMC and γ at CMC.

The valency and type of alkali metal ion also greatly affects the surface and solution behaviour of surfactants. Xu et al[11,12] found that the presence of the more highly valent Al^{3+} was able to induce multilayer formation in SLES of over 20 layers in aqueous solution, which could be further manipulated by the variation in alkyl chain lengths and ethoxylate (EO) group sizes of the SLES. From surface tension measurements, Alagorva et al[13] found that the incorporation of multivalent cations into SLES (containing two EO groups, as used in this study) affected the surface and aggregate properties and that the overall electrolyte concentration had a large effect on the CMC, whereas the ion valency greatly affected the aggregate structure. The onset of micellar growth occurs at the point at which the counterion charge is in excess. Sein and Engberts[14] observed different types of aggregate phase behaviour depending on the cation valency, on addition of Li^+ or Ca^{2+} chlorides to LAS, and Missel et al[15] showed that the type of alkali metal ion strongly affects SDS micelle growth.

The surface behaviour of multicomponent surfactant mixtures is also greatly affected by the addition of counterions, and this is more relevant in the context of this work. The effect of Na^+ and Ca^{2+} on the interaction of $C_{10}E_3$/LAS was investigated by Tucker et al,[16] and highly non-ideal mixing behaviour

was found. In the presence of Ca^{2+}, this was no longer compatible with non-ideal mixing theories such as RST. The addition of Ca^{2+} counterions to mixtures of the rhamnolipid biosurfactant R2 with LAS[17] induced a reversal in charge. This was attributed to the Ca^{2+} binding only to single LAS molecules in R2-rich mixtures due to the steric hindrance associated with the bulky R2 headgroup, thus giving an excess of the free positive charges.

The effects of calcium ions on mixtures of LAS with $C_{12}E_8$ and $C_{12}E_{23}$ is also important in the context of the present work.[2] The strong counterion binding to the surfactants at the interface caused a reduction in the area per molecule and induced multilayer formation in LAS-rich solutions. For solutions richer in $C_{12}E_8$ (and even more so with EO_{23}), steric hindrance and hydration of the EO groups made it increasingly difficult to form multilayers, and higher $CaCl_2$ concentrations were required to induce multilayer formation. In LAS-rich solutions, a transition from micelles to lamellae occurred.

The effect of divalent and multivalent counterions are more important in the context of detergent performance in hard water environments as their presence is known to cause precipitation[18] and monovalent ions such as Na^+ require significantly higher concentrations to induce this effect.[19] Out of the three conventional surfactants used here, LAS is the most susceptible to precipitation,[20,21] but in the presence of nonionic surfactants such as $C_{12}E_8$ precipitation is reduced due to mixed micelle formation.[22] Furthermore the EO groups on SLES make it much more stable than SDS to precipitation in the presence of multivalent counterions.[13] Hence it is often used as a co-surfactant with LAS. These three conventional surfactants are often used in combination with each other in detergent formulations.

There is a paucity of literature examining the effects of electrolyte on nonionic or anionic surfactants mixed with SLES, apart from the binary mixtures of $C_{12}E_{12}$/SLES[3] in the presence of $AlCl_3$. In this chapter the detailed impact of monovalent and divalent counterions, in the form of NaCl and $CaCl_2$, on the surface adsorption behaviour of binary and ternary mixtures of $C_{12}E_8$/LAS/SLES and $C_{12}E_8$/LAS/SDS is presented, at 2 mM, above the mixed CMC. The impact of increasing electrolyte concentration on the surface behaviour is also discussed.

5.2 Sodium chloride

The surface adsorption behaviour of the binary mixtures $C_{12}E_8$/SLES and LAS/SLES at compositions 0.75/0.25, 0.5/0.5 and 0.25/0.75, and the ternary $C_{12}E_8$/LAS/SLES mixture using the same solution composition range as described in the previous chapter (Figure 4.9, Chapter 4) were studied in the presence of 0.1 M NaCl. The measurements were made using neutron reflectivity at a fixed solution concentration of 2 mM containing $1x10^{-6}$ M NaOH. The electrolyte concentration was high enough to ensure screening of all possible electrostatic interactions. The following isotopic combinations were used at each composition: for binary mixtures, e.g. $C_{12}E_8$/SLES, the d-$C_{12}E_8$/h-SLES, h-$C_{12}E_8$/d-SLES, d-$C_{12}E_8$/d-SLES combinations, and for ternary mixtures the d-$C_{12}E_8$/h-LAS/h-SLES, h-$C_{12}E_8$/d-LAS/h-SLES, h-$C_{12}E_8$/h-LAS/d-SLES and d-$C_{12}E_8$/d-LAS/d-SLES combinations. The data are compared to those in the absence of electrolyte, which are included in brackets in Tables 5.1 to 5.3.

5.2.1 Binary surfactant mixtures

Figure 5.1 (a) shows the original binary surface composition data in the absence of electrolyte and 5.1 (b) shows the variation in surface composition with solution composition for $C_{12}E_8$/SLES and LAS/SLES in the presence of 0.1 M NaCl. Tables 5.1 and 5.2 summarise the key model parameters of the neutron reflectivity data for the binary mixtures. The results are compared to literature data[2] for the $C_{12}E_8$/LAS system (red data), studied in the presence of 6 mM NaCl.

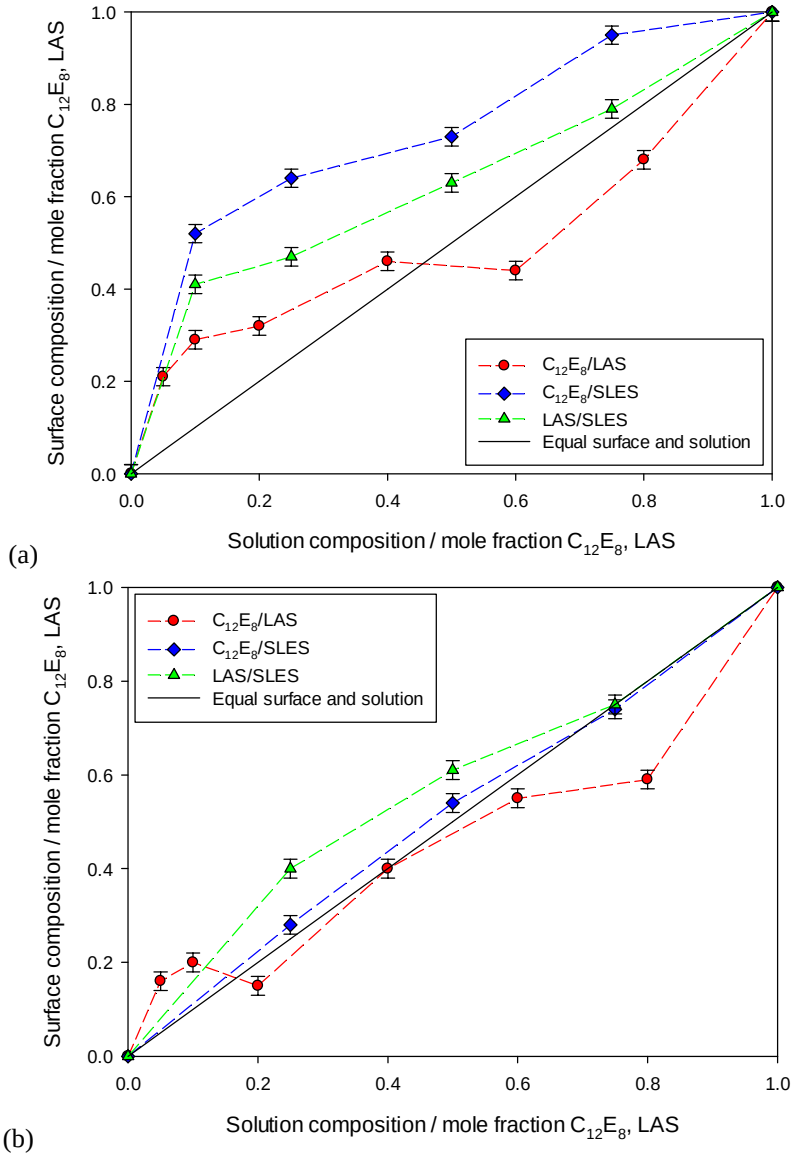

Figure 5.1: (a) Original surface versus solution composition data in the absence of eletrolyte, and (b) surface composition as a function of solution composition (mole fraction $C_{12}E_8$, LAS) in the presence of 0.1 M NaCl, for $C_{12}E_8$/SLES and LAS/SLES, at 2 mM concentration, at 25°C, in NRW containing $1x10^{-6}$ M NaOH. Literature data for $C_{12}E_8$/LAS[2] (red data) is included for comparison. Lines are guides to the eye only.

Ratio	Contrast	d (± 1)	ρ (± 0.02x10^{-6} Å^{-2})	A (± 2 Å^2)	Γ (± 0.02x10^{-10} mol cm^{-2})	Γ_{total} (± 0.04x10^{-10} mol cm^{-2})	Solution compos-ition	Surface composition (± 0.02)
0.75/0.25	dh	18	2.54	63	2.65 (2.38)	3.57 (2.51)	0.75	0.74 (0.95)
	hd	45	0.41	180	0.92 (0.14)		0.25	0.26 (0.05)
	dd	20	3.10					
0.5/0.5	dh	21	1.58	86	1.94 (1.86)	3.58 (2.56)	0.5	0.54 (0.72)
	hd	26	1.12	101	1.64 (0.71)		0.5	0.46 (0.28)
	dd	20	3.22					
0.25/0.75	dh	23	0.88	164	1.01 (1.67)	3.61 (2.63)	0.25	0.28 (0.63)
	hd	23	2.02	64	2.60 (0.96)		0.75	0.72 (0.37)
	dd	20	3.14					

Table 5.1: Key model parameters for 2 mM $C_{12}E_8$/SLES binary mixtures in 0.1 M NaCl at compositions 0.75/0.25, 0.5/0.5 and 0.25/0.75, at 25°C, in NRW containing $1x10^{-6}$ M NaOH.

Ratio	Contrast	d (± 1)	ρ (± 0.02x10^{-6} Å^{-2})	A (± 2 Å^2)	Γ (± 0.02x10^{-10} mol cm^{-2})	Γ_{total} (± 0.04x10^{-10} mol cm^{-2})	Solution compos-ition	Surface composition (± 0.02)
0.75/0.25	dh	18	3.44	59	2.81 (2.51)	3.77 (3.17)	0.75	0.75 (0.79)
	hd	33	0.69	173	0.96 (0.66)		0.25	0.25 (0.21)
	dd	18	4.25					
0.5/0.5	dh	16	3.09	72	2.32 (2.07)	3.82 (3.28)	0.5	0.61 (0.63)
	hd	23	1.34	111	1.50 (1.21)		0.5	0.39 (0.37)
	dd	21	3.52					
0.25/0.75	dh	19	1.99	100	1.67 (1.54)	4.15 (3.24)	0.25	0.40 (0.47)
	hd	22	2.08	67	2.48 (1.70)		0.75	0.60 (0.53)
	dd	17	4.52					

Table 5.2: Key model parameters for 2 mM LAS/SLES binary mixtures in 0.1 M NaCl at compositions 0.75/0.25, 0.5/0.5 and 0.25/0.75, at 25°C, in NRW containing 1x10^{-6} M NaOH.

In the $C_{12}E_8$/LAS mixtures analysed by Penfold et al,[2] mixed monolayer adsorption was found in both the absence and presence of 6 mM NaCl. A strong departure from ideal mixing, broadly consistent with RST, was observed, which was more pronounced in NaCl. In LAS-rich solutions, the addition of Na^+ resulted in the surface and solution compositions being more comparable. However, electrolyte had little effect on $C_{12}E_8$-rich solutions, as would be expected for a nonionic-rich surfactant mixture.[23] The total adsorption remained relatively constant at approximately 3.0x10^{-10} mol cm^{-2} in the absence and presence of 6 mM NaCl. This was slightly higher when the NaCl concentration was increased to 30 mM, but still only monolayer adsorption was observed.

The impact of Na^+ on $C_{12}E_8$/SLES and LAS/SLES binary mixtures is very different to that of $C_{12}E_8$/LAS. The most profound impact is seen in SLES-rich solutions for the $C_{12}E_8$/SLES mixtures. This is expected as the electrolyte will not affect the surface behaviour of $C_{12}E_8$ as much due to its nonionic nature. However, even in nonionic-rich solutions the addition of Na^+ results in the surface composition being much closer to the solution composition.

The increase in total adsorption on addition of electrolyte is considerably greater in LAS/SLES than in $C_{12}E_8$/SLES mixtures, presumably due to the higher proportion of anionic surfactant present. The total adsorption is also higher in increasingly SLES-rich solutions for both mixtures. This is expected for $C_{12}E_8$/SLES but the reason for this result for LAS/SLES is less obvious. The impact of Na^+ on the total adsorption is discussed further in Section 5.2.2.

5.2.2 Ternary surfactant mixtures

The variation in adsorbed amount with increasing solution composition of $C_{12}E_8$, LAS and SLES for the ternary $C_{12}E_8$/LAS/SLES system, in the presence of 0.1 M NaCl, is shown in Figures 5.2 (a), (b) and (c), respectively, and the associated key model parameters are summarised in Table 5.3.

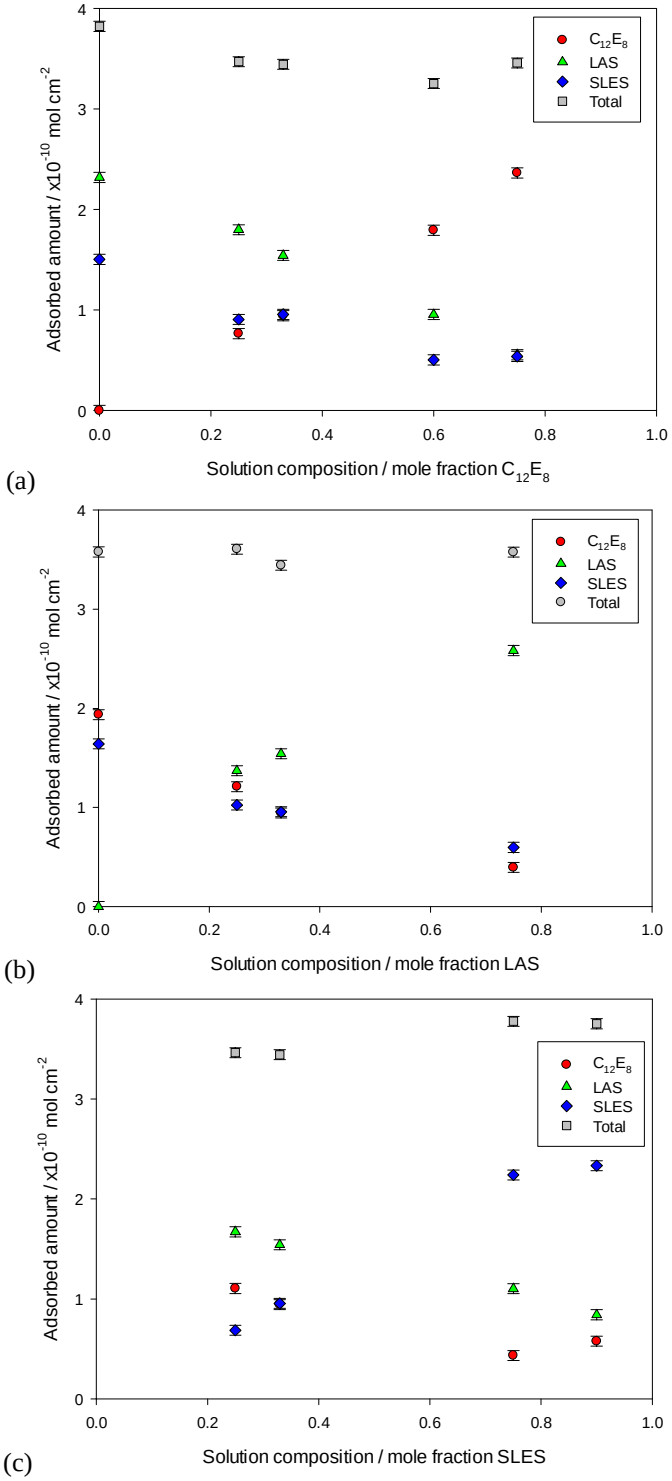

Figure 5.2: The variation in adsorbed amounts of $C_{12}E_8$, LAS and SLES and the total adsorption, as a function of solution composition of (a) $C_{12}E_8$, (b) LAS and (c) SLES, in 0.1 M NaCl, for $C_{12}E_8$/LAS/SLES at 2 mM concentration, at 25°C, in NRW containing 1x10^{-6} M NaOH.

Ratio	Contrast	d (± 1)	ρ (± 0.02x10^{-6} Å^{-2})	A (± 2 Å^2)	Γ (± 0.02x10^{-10} mol cm^{-2})	Γ_{total} (± 0.04x10^{-10} mol cm^{-2})	Solution compos-ition	Surface composition (± 0.02)
0.375/0.375/ 0.25	dhh	22	0.97	150	1.11 (1.27)	3.46 (2.73)	0.375	0.32 (0.46)
	hdh	17	2.02	99	1.67 (1.31)		0.375	0.48 (0.48)
	hhd	36	0.41	242	0.69 (0.16)		0.25	0.20 (0.06)
	ddd	19	3.52					
0.33/0.33/ 0.33	dhh	24	0.86	176	0.94 (1.27)	3.44 (2.61)	0.33	0.27 (0.49)
	hdh	19	1.83	108	1.54 (1.20)		0.33	0.45 (0.46)
	hhd	46	0.46	174	0.96 (0.14)		0.33	0.28 (0.05)
	ddd	20	3.19					
0.125/0.125/ 0.75	dhh	30	0.41	383	0.43 (1.16)	3.78 (2.86)	0.125	0.12 (0.41)
	hdh	24	1.09	151	1.10 (0.96)		0.125	0.29 (0.34)
	hhd	20	2.09	74	2.24 (0.73)		0.75	0.59 (0.25)
	ddd	20	3.50					
0.05/0.05/ 0.9	dhh	29	0.35	287	0.58 (1.01)	3.75 (2.81)	0.05	0.15 (0.36)
	hdh	22	0.78	197	0.84 (0.62)		0.05	0.22 (0.22)
	hhd	17	2.22	71	2.33 (1.19)		0.9	0.62 (0.42)
	ddd	20	3.66					

Table 5.3: Key model parameters for 2 mM $C_{12}E_8$/LAS/SLES in 0.1 M NaCl, as a function of SLES solution composition, at 25°C, in NRW containing 1x10^{-6} M NaOH. Data are compared to that in the absence of electrolyte, shown in brackets.

In the original $C_{12}E_8$/LAS/SLES system, the $C_{12}E_8$ and LAS were found to dominate surface adsorption over much of the solution composition, whereas the SLES was highly depleted at the air/water interface. The addition of electrolyte in the form of NaCl has a profound effect on the surface adsorption behaviour of these three components by drawing the surface composition much closer to its solution composition.

With increasing $C_{12}E_8$ solution composition, the adsorbed amount of $C_{12}E_8$ at the interface increases and that of LAS and SLES decrease at different rates. The absolute adsorbed amount of LAS is higher at all compositions. However, these changes in absolute adsorption values are very different to those observed in the absence of electrolyte (Figure 4.11 (a), Chapter 4). With increasing solution composition of LAS, the $C_{12}E_8$ and SLES adsorbed amounts, which are very similar, decrease at approximately the same rate. This is also very different to what was found in the absence of electrolyte (Figure 4.11 (b), Chapter 4) where the absolute value of $C_{12}E_8$ at the interface was much higher than SLES. The addition of electrolyte in this case clearly has a large effect on the relative adsorption of $C_{12}E_8$ and SLES and results in them behaving in a more similar manner at the interface. With increasing SLES solution composition, the SLES adsorption increases, and that of $C_{12}E_8$ and LAS both

decrease. Surprisingly, the absolute adsorbed amount of LAS here is higher than that of $C_{12}E_8$, the opposite result to what was observed in the absence of electrolyte (Figure 4.11 (c), Chapter 4).

In the absence of electrolyte, although a slightly higher total adsorption was observed in more LAS and SLES-rich solutions, no significant change in total adsorption was observed over the solution composition range or when compared to that of the individual components. In the presence of Na^+, the overall total adsorption increases. The total adsorption is higher in more SLES-rich solutions and lower in nonionic-rich solutions. No significant change is seen as a function of LAS solution composition, although an increase might have been expected due to its anionic nature.

Figure 5.3 shows the variation in surface behaviour for the ternary system in the (a) absence and (b) presence of 0.1 M NaCl. The ternary contour diagrams in Figure 5.4 provide an alternative description of the surface behaviour in the presence of electrolyte.

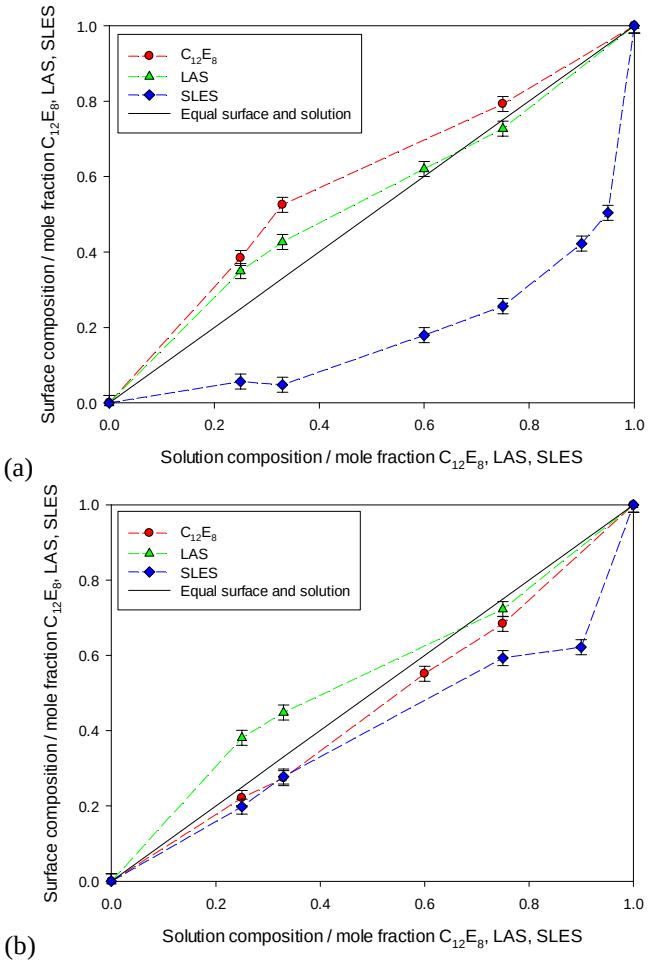

Figure 5.3: (a) Original ternary surface composition data in the absence of electrolyte. (b) The variation in surface composition with solution composition in 0.1 M NaCl for $C_{12}E_8$, LAS and SLES for 2 mM $C_{12}E_8$/LAS/SLES, at 25°C, in NRW containing $1x10^{-6}$ M NaOH. Dashed lines are guides to the eye only.

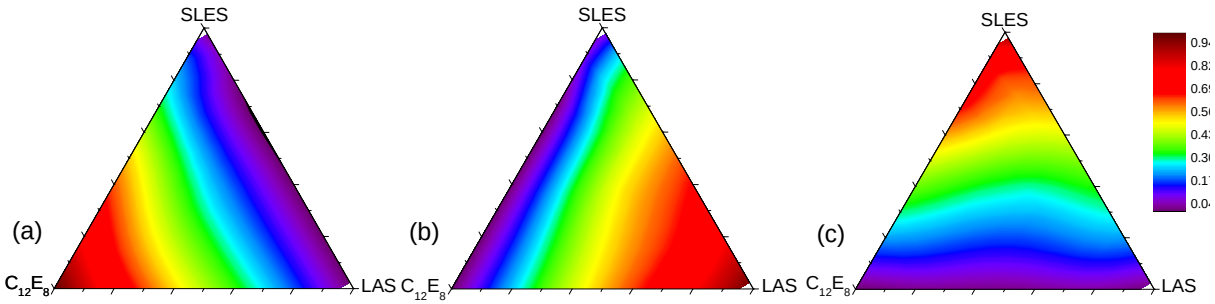

Figure 5.4: Ternary contour diagrams showing the surface composition of (a) $C_{12}E_8$, (b) LAS and (c) SLES as a function of solution composition, for $C_{12}E_8$/LAS/SLES in 0.1 M NaCl.

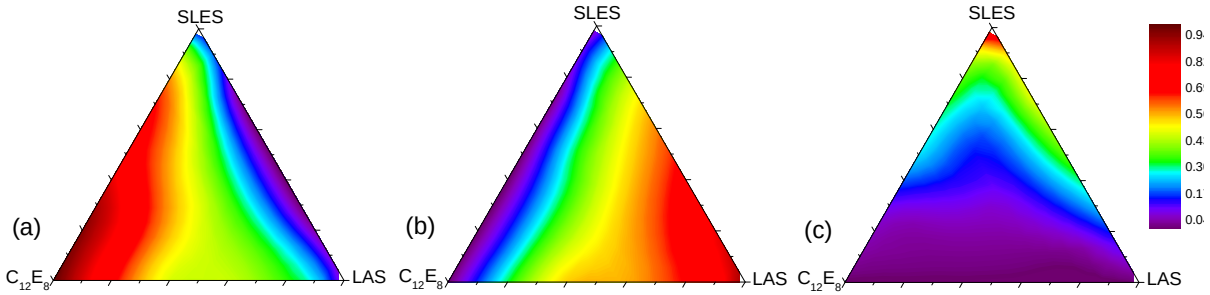

Figure 5.5: Original ternary contour diagrams showing the surface composition of (a) $C_{12}E_8$, (b) LAS and (c) SLES as a function of solution composition, for $C_{12}E_8$/LAS/SLES in the absence of electrolyte.

Figure 5.4 shows contour diagrams that are visually very different to those of the original ternary mixtures (Figure 5.5), which can also be viewed by comparing Figures 5.3 (a) and (b). In the presence of electrolyte, the surface composition of each component more closely resembles its solution composition, the most dramatic change being with SLES. In the absence of electrolyte, 0.9 mole fraction SLES gives a surface composition of only 0.42, but on addition of 0.1 M NaCl its surface composition increases to 0.62.

An electrolyte titration was carried out in order to investigate at which concentration the electrolyte begins to affect surface behaviour. The ternary $C_{12}E_8$/LAS/SLES system at composition 0.125/0.125/0.75 and at 2 mM concentration was analysed at the four isotopic combinations d-$C_{12}E_8$/h-LAS/h-SLES, h-$C_{12}E_8$/d-LAS/h-SLES, h-$C_{12}E_8$/h-LAS/d-SLES and d-$C_{12}E_8$/d-LAS/d-SLES, with subsequent *in situ* addition of a concentrated stock solution of NaCl. The variation in adsorbed amount and surface composition of each component and the total adsorption as a function of NaCl concentration are shown in Figure 5.6, with the relevant data summarised in Table 5.4.

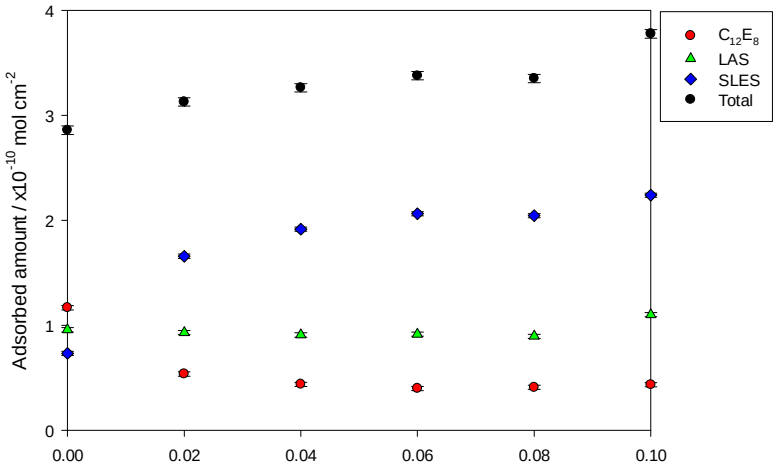

(a)

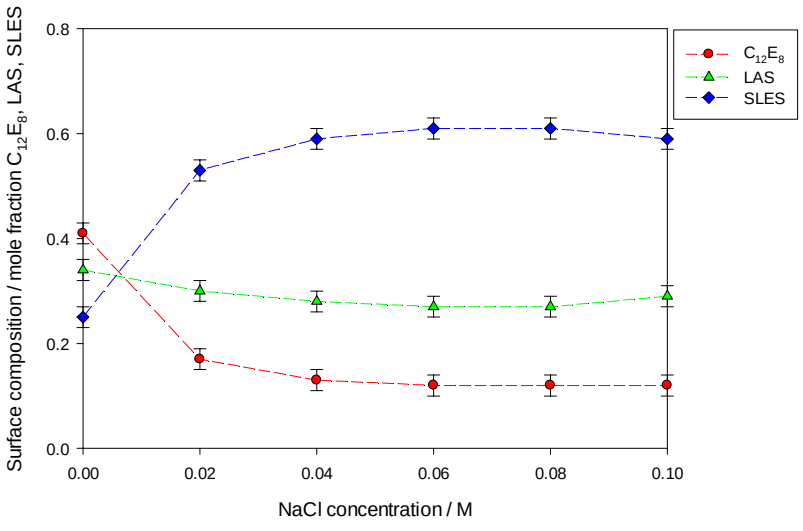

(b)

Figure 5.6: Variation in (a) adsorbed amount and (b) surface composition, respectively, with increasing NaCl concentration, for the $C_{12}E_8$/LAS/SLES ternary mixture at solution composition 0.125/0.15/0.75, at 2 mM concentration, at 25°C, in NRW containing $1x10^{-6}$ M NaOH. Lines are guides to the eye only.

[NaCl] / M	Contrast	d (± 1)	ρ (± $0.02x10^{-6}$ Å^{-2})	A (± 2 Å^2)	Γ (± $0.02x10^{-10}$ mol cm^{-2})	Γ_{total} (± $0.04x10^{-10}$ mol cm^{-2})	Solution compos-ition	Surface composition (± 0.02)
0	dhh	30	0.86	142	1.17	2.86	0.125	0.41
	hdh	23	0.88	173	0.96		0.125	0.34
	hhd	16	0.86	227	0.73		0.75	0.25
	ddd	27	2.27					
0.02	dhh	17	1.19	309	0.54	3.13	0.125	0.17
	hdh	16	1.37	178	0.93		0.125	0.30
	hhd	13	2.33	100	1.66		0.75	0.53
	ddd	17	3.79					
0.04	dhh	19	0.93	378	0.44	3.26	0.125	0.13
	hdh	17	1.31	183	0.91		0.125	0.28
	hhd	14	2.62	87	1.92		0.75	0.59
	ddd	16	4.08					
0.06	dhh	18	0.86	417	0.40	3.38	0.125	0.12
	hdh	16	1.37	181	0.92		0.125	0.27
	hhd	14	2.76	81	2.06		0.75	0.61
	ddd	17	3.99					
0.08	dhh	19	0.90	405	0.41	3.35	0.125	0.12
	hdh	16	1.37	185	0.90		0.125	0.27
	hhd	14	2.77	81	2.05		0.75	0.61
	ddd	15	4.40					
0.10	dhh	30	0.41	383	0.43	3.78	0.125	0.12
	hdh	24	1.09	151	1.10		0.125	0.29
	hhd	20	2.09	74	2.24		0.75	0.59
	ddd	20	3.50					

Table 5.4: Key model parameters for the variation in adsorption and surface composition for 0.125/0.125/0.75 $C_{12}E_8$/LAS/SLES as a function of NaCl concentration, at 25°C, at 2 mM, in NRW containing $1x10^{-6}$ M NaOH.

In the absence of electrolyte, $C_{12}E_8$ and LAS dominate surface adsorption, with a surface composition of 0.41/0.34/0.25, which is very different to its solution composition of 0.125/0.125/0.75. On addition of just 20 mM NaCl, the relative surface compositions of $C_{12}E_8$ and SLES appear to switch. Above 20 mM $C_{12}E_8$ is largely unaffected by the addition of electrolyte, as expected due to its nonionic nature.

No significant change is seen in the adsorbed amount of LAS, which remains close to $1x10^{-10}$ mol cm^{-2} throughout the NaCl concentration range. However, the adsorbed amount of SLES increases with increasing NaCl concentration. A similar pattern is observed for the variation in surface composition. The progressive addition of NaCl drives the surface composition much closer to its solution composition and above 40 mM NaCl the overall surface composition is invariant with electrolyte concentration. However the LAS component now dominates adsorption with a surface composition of 0.29 (0.125 solution composition) and SLES is still systematically lower than its solution composition.

A large increase in total adsorption of over 30% is observed on progressive addition of electrolyte, from 2.86 to 3.78 $x10^{-10}$ mol cm^{-2}. This is attributed to the screening of the electrostatic charges on the anionic LAS and SLES, allowing the surfactant molecules to become closer together and resulting in a closer packed surfactant monolayer. Monolayer adsorption was observed at all electrolyte concentrations.

5.2.3 The effect of replacement with SDS

The anionic surfactant SLES was replaced with SDS in the ternary $C_{12}E_8$/LAS/SLES system to investigate whether the presence of ethylene oxide (EO) groups was the reason for the ineffectiveness of SLES at competing for the interface. It was therefore also important to analyse the impact of Na^+ on $C_{12}E_8$/LAS/SDS. This was studied at the fixed solution compositions 0.375/0.375/0.25 and 0.125/0.125/0.75 at 2 mM concentration, above the mixed CMC, as with the previous $C_{12}E_8$/LAS/SLES system. Table 5.5 summarises the impact of Na^+ on 0.375/0.375/0.25 $C_{12}E_8$/LAS/SDS, with the $C_{12}E_8$/LAS/SLES data in brackets for comparison.

		No NaCl		0.1 M NaCl	
Surfactant	Solution composition	Surface composition (± 0.02)	Γ_{total} (± $0.04x10^{-10}$ mol cm^{-2})	Surface composition (± 0.02)	Γ_{total} (± $0.04x10^{-10}$ mol cm^{-2})
$C_{12}E_8$	0.375	0.57 (0.46)	3.05 (2.73)	0.36 (0.32)	3.36 (3.46)
LAS	0.375	0.39 (0.48)		0.49 (0.48)	
SDS	0.25	0.04 (0.06)		0.15 (0.20)	

Table 5.5: Surface compositions and total adsorbed amount data for 0.375/0.375/0.25 $C_{12}E_8$/LAS/SDS, in the absence and presence of 0.1 M NaCl. Original $C_{12}E_8$/LAS/SLES data is given in brackets for comparison.

Firstly, when comparing $C_{12}E_8$/LAS/SDS and $C_{12}E_8$/LAS/SLES in the absence of electrolyte, qualitatively similar results are observed with the $C_{12}E_8$ and LAS dominating surface adsorption and the SLES/SDS depleted at the interface. However, in detail there are some differences in the $C_{12}E_8$/LAS/SDS system; the $C_{12}E_8$ is more dominant at the surface and the LAS surface composition is very close to its solution composition.

On addition of Na^+ to the $C_{12}E_8$/LAS/SDS system, the surface composition of the nonionic component decreases and that of the anionic LAS and SDS increases. This is similar to the mixtures containing SLES, but the increase in SDS adsorption is more gradual than mixtures with SLES. The total adsorption increases by 10% on addition of Na^+ to $C_{12}E_8$/LAS/SDS, much lower than with $C_{12}E_8$/LAS/SLES where an increase of over 25% was observed.

There is no literature data discussing the mixing behaviour of a ternary anionic/nonionic mixture involving SDS, although binary mixture data do exist that can be used as a comparison with the present work. In a similar system of SDS with the nonionic surfactant nonylphenol polyethoxylate $NP(EO)_{10}$, the nonionic-rich solutions were more tolerant to salinity in the form of NaCl because of mixed micelle formation and lower abundance of anionic monomers.[19] However, unlike in this work, the addition of Na^+ had little impact on the total adsorption or the variation in adsorption with solution composition.

An electrolyte titration was carried out at solution composition 0.125/0.125/0.75 $C_{12}E_8$/LAS/SDS, in order to make comparisons with the $C_{12}E_8$/LAS/SLES adsorption isotherm at this composition. The variation in surface composition with NaCl concentration for $C_{12}E_8$/LAS/SDS is shown in Figure 5.7 and the data are summarised in Table 5.6.

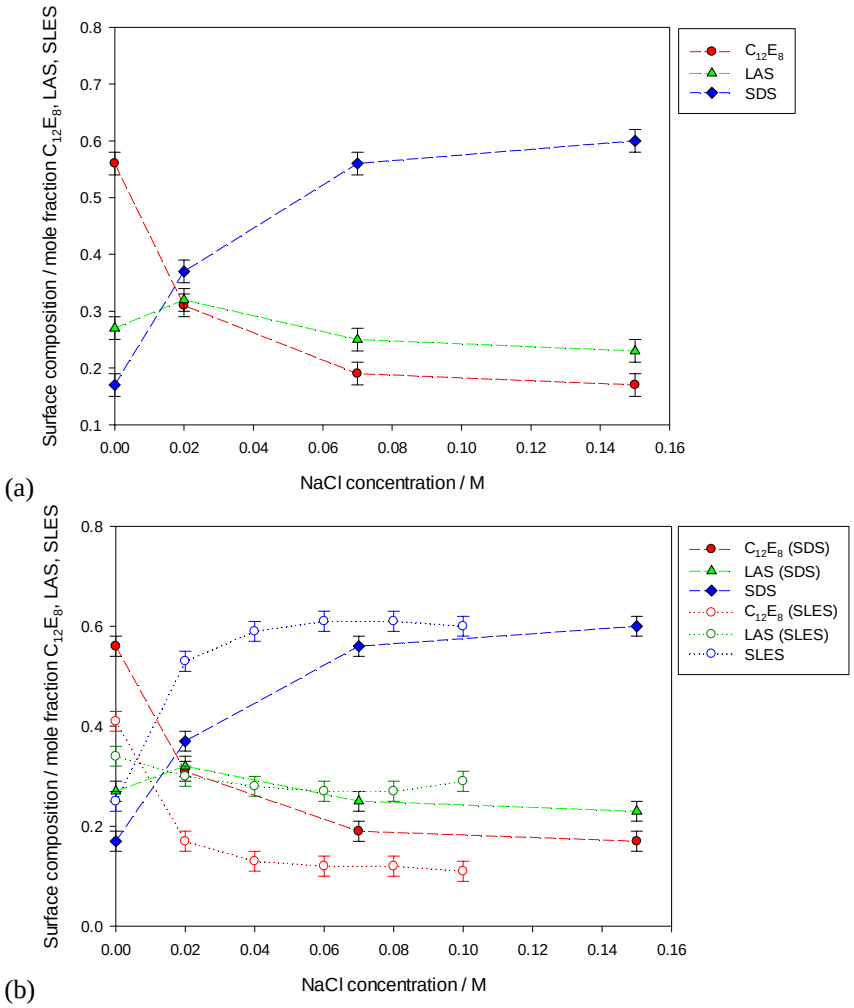

Figure 5.7: Variation in surface composition with NaCl concentration for (a) $C_{12}E_8$/LAS/SDS and (b) $C_{12}E_8$/LAS/SDS and $C_{12}E_8$/LAS/SLES, both at 0.125/0125/0.75 solution composition, at 2 mM solution concentration, at 25°C, in NRW containing 1x10^{-6} M NaOH. Lines are guides to the eye only.

[NaCl] / M	Contrast	d (± 1)	ρ (± 0.02 x10^{-6} Å^{-2})	A (± 2 Å^2)	Γ (± 0.02 x10^{-10} mol cm^{-2})	Γ_{total} (± 0.04 x10^{-10} mol cm^{-2})	Solution compos-ition	Surface composition (± 0.02)
0	dhh	24	1.33	94	1.76	3.08 (2.86)	0.125	0.56 (0.41)
	hdh	19	1.04	201	0.83		0.125	0.27 (0.34)
	hhd	15	0.80	323	0.51		0.75	0.17 (0.25)
	ddd	14	4.00					
0.02	dhh	26	0.79	159	1.05	3.39 (3.13)	0.125	0.31 (0.17)
	hdh	25	1.01	153	1.09		0.125	0.32 (0.30)
	hhd	24	1.01	132	1.26		0.75	0.37 (0.53)
	ddd	16	3.93					
0.07	dhh	30	0.52	232	0.72	3.75	0.125	0.19
	hdh	25	0.90	175	0.95		0.125	0.25
	hhd	20	1.81	80	2.08		0.75	0.56
	ddd	14	4.65					
0.15	dhh	25	0.60	245	0.68	3.94	0.125	0.17
	hdh	26	0.81	185	0.90		0.125	0.23
	hhd	21	2.01	70	2.37		0.75	0.60
	ddd	17	4.12					

Table 5.6: Key model parameters for the variation in adsorbed amount and surface composition with increasing NaCl concentration, for 2 mM 0.125/0.125/0.75 $C_{12}E_8$/LAS/SDS, at 25°C, in NRW containing 1x10^{-6} M NaOH. Data in brackets are the equivalent values in the $C_{12}E_8$/LAS/SLES system.

A qualitatively similar pattern is observed with $C_{12}E_8$/LAS/SDS and $C_{12}E_8$/LAS/SLES in NaCl (Section 5.2.2). With increasing electrolyte concentration, the surface composition evolves to one that more closely resembles its solution composition. The CMCs of all components become more comparable in the presence of electrolyte due to the screening of electrostatic repulsions between the ionic molecules and the resultant lack of non-ideal mixing behaviour. On addition of just 70 mM NaCl, the surface composition of SDS increases dramatically from 0.17 to 0.56. Even though the surface compositions reach a constant value by this concentration, the surface and solution compositions are still rather different. The surface composition of $C_{12}E_8$ is close to its solution value, but the surface is richer in LAS, and less rich in SLES or SDS. The evolution in surface composition with electrolyte is also more gradual for SDS than for SLES. The surface composition becomes invariant above 70 mM NaCl in mixtures with SDS whereas with SLES this is reached by approximately 40 mM. SLES is less anionic than SDS due to the addition of EO groups.[11,23] Xu et al[11] found that SLES adsorption was constant at concentrations above the CMC and SLES micelles had a low degree of ionisation. This implies that SLES counterions are strongly bound and the molecule is only weakly ionic. Therefore the impact of electrolyte observed on SLES is rather unexpected.

5.3 Calcium chloride

The impact of divalent Ca^{2+} ions, in the form of $CaCl_2$, was investigated at the air/water interface for the binary mixtures $C_{12}E_8$/SLES and LAS/SLES and the ternary $C_{12}E_8$/LAS/SLES system using neutron reflectivity, with the same isotopic combinations and solution composition as in the system containing NaCl. The effect of Ca^{2+} ions on surface behaviour acts as a model for how the surfactant mixture may perform in hard water environments, a subject with great commercial relevance.

5.3.1 Binary surfactant mixtures

The variation in adsorbed amount and surface composition for $C_{12}E_8$/SLES and LAS/SLES at solution compositions 0.5/0.5 and 0.25/0.75 was measured in the presence of 2 mM $CaCl_2$, at a fixed solution concentration of 2 mM. Figure 5.8 (b) shows the variation in surface composition with solution composition, alongside the original binary surface composition data in the absence of electrolyte in Figure 5.8 (a). Tables 5.7 and 5.8 give a summary of the key model parameters from the reflectivity data. Results are compared to literature data[2] for the $C_{12}E_8$/LAS binary mixtures (red data), studied in 2 mM $CaCl_2$. Data obtained in the absence of electrolyte are included in brackets for comparison.

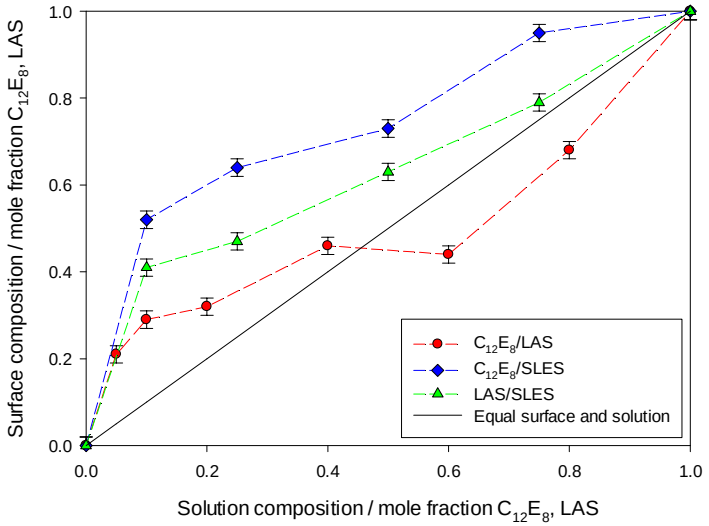

(a)

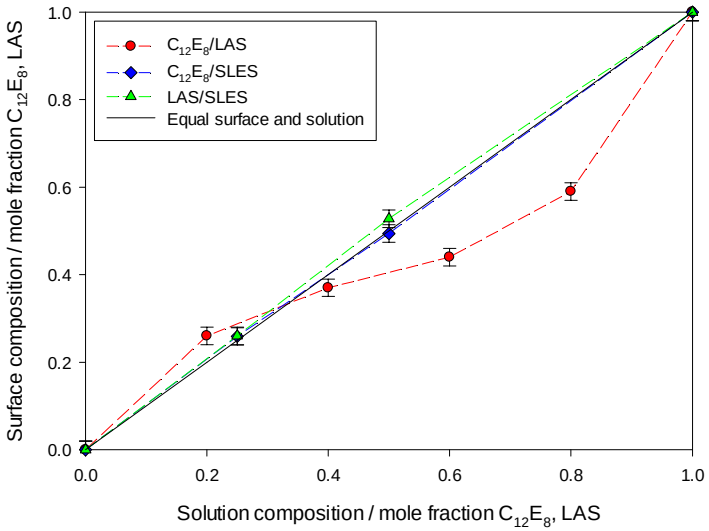

(b)

Figure 5.8: (a) Original surface versus solution composition data in the absence of eletrolyte, including literature $C_{12}E_8$/LAS data.[2] (b) Surface versus solution composition data for 2 mM $C_{12}E_8$/SLES and LAS/SLES in 2 mM $CaCl_2$, at 25°C, in NRW containing $1x10^{-6}$ M NaOH. Dashed lines are guides to the eye only.

Ratio	Contrast	d (± 1)	ρ (± 0.02x10^{-6} Å^{-2})	A (± 2 Å^2)	Γ (± 0.02x10^{-10} mol cm^{-2})	Γ_{total} (± 0.04x10^{-10} mol cm^{-2})	Solution compos-ition	Surface compos-ition
0.5/0.5	dh	24	1.37	92	1.81 (1.86)	3.66 (2.56)	0.5	0.49 (0.72)
	hd	20	1.69	90	1.85 (0.71)		0.5	0.51 (0.28)
	dd	17	3.70					
0.25/0.75	dh	21	0.96	166	1.00 (1.67)	3.87 (2.63)	0.25	0.26 (0.63)
	hd	17	2.89	58	2.87 (0.96)		0.75	0.74 (0.37)
	dd	19	3.49					

Table 5.7: Key model parameters for $C_{12}E_8$/SLES binary mixtures at compositions 0.5/0.5 and 0.25/0.75, in 2 mM $CaCl_2$, at 2 mM concentration, at 25°C, in NRW containing 1x10^{-6} M NaOH.

Ratio	Contrast	d (± 1)	ρ (± 0.02x10^{-6} Å^{-2})	A (± 2 Å^2)	Γ (± 0.02x10^{-10} mol cm^{-2})	Γ_{total} (± 0.04x10^{-10} mol cm^{-2})	Solution compos-ition	Surface compos-ition
0.5/0.5	dh	19	2.43	81	2.05 (2.07)	3.89 (3.28)	0.5	0.53 (0.63)
	hd	21	1.71	90	1.84 (1.21)		0.5	0.47 (0.37)
	dd	17	4.34					
0.25/0.75	dh	23	1.74	95	1.75 (1.54)	3.99 (3.24)	0.25	0.44 (0.47)
	hd	16	2.58	74	2.24 (1.70)		0.75	0.56 (0.53)

Table 5.8: Key model parameters for LAS/SLES binary mixtures at compositions 0.5/0.5 and 0.25/0.75, in 2 mM $CaCl_2$, at 2 mM concentration, at 25°C, in NRW containing 1x10^{-6} M NaOH.

Figure 5.7 shows that Ca^{2+} induces similar effects to those found in the presence of Na^+. Firstly, for the $C_{12}E_8$/LAS mixtures,[2] in NRW the surface behaviour was broadly consistent with RST. In NaCl and even more so in $CaCl_2$, especially in solutions richer in the nonionic, RST was increasingly inadequate. In the presence of Ca^{2+} the adsorbed layer structure became increasingly complex in solutions containing over 0.8 mole fraction LAS, and a transition from monolayers to bi/trilayers and finally to multilayers in above 0.95 solution composition was observed, shown by the presence of pronounced "Bragg" peaks in the reflectivity curves. The steric hindrance associated with the large E_8 headgroup meant that formation of multilayers at the interface was inhibited in more nonionic-rich solutions. The pattern in adsorbed layer structure also corresponded with a change in solution behaviour from micelles (L_1) to mixed micellar/lamellar (L_1/L_α) and lamellar (L_α). The overall total adsorption increased in the presence of Ca^{2+} and this was significantly higher than on the addition of Na^+ and more prominent in solutions rich in LAS. The addition of multivalent counterions is thought to compress the electrical double layer of anionic surfactants[23] and so increase interfacial adsorption.

For both $C_{12}E_8$/SLES and LAS/SLES, non-ideal mixing behaviour is seen, but which cannot be accounted for by RST. The addition of Ca^{2+} has the effect of drawing the surface composition very close to its solution composition, especially for $C_{12}E_8$/SLES, and to an overall greater extent than is

seen with Na^+. The greatest change in surface composition is seen in solutions richer in the less surface-active SLES. Monolayer adsorption is observed at all solution compositions for the $C_{12}E_8$/SLES and LAS/SLES binary mixtures. It may be that the SLES/Ca^{2+} binding is not strong enough to displace the already present SLES/Na^+ interaction at the air/water interface.[12] For $C_{12}E_8$/LAS, a transition to bilayers only occurred above 0.8 mole fraction LAS, and here only up to 0.75 LAS was investigated for LAS/SLES, so it is possible that above this mole fraction a transition towards multilayers might be observed, as was seen previously.[2]

The effects seen on $C_{12}E_8$/SLES and LAS/SLES appear similar to those observed in $C_{10}E_3$/LAS mixtures by Tucker et al.[16] In the absence of electrolyte the surface was dominated by the nonionic $C_{10}E_3$, to a greater extent in more LAS-rich solutions, but in the presence of 1 mM $CaCl_2$ the surface composition was drawn very close to the solution composition. The electrolyte depresses the CMC of LAS so that the CMCs of both components are more comparable at around $1x10^{-4}$ M and the two surfactants mix more ideally; that is, closer to the solution composition. This more ideal behaviour is also attributed to the promotion to more planar-like structures by the addition of Ca^{2+} due to a reduction in the curvature of LAS.[16] The concentration at which the divalent counterion had these effects was much lower than with the monovalent counterions. For $C_{12}E_8$/SLES, the very different CMCs in the absence of electrolyte become much more alike in the presence of Ca^{2+}. For LAS/SLES, the CMCs are already relatively similar, but the addition of electrolyte still has a profound effect on surface behaviour.

An increase in total surface excess is observed for $C_{12}E_8$/SLES with increasing SLES solution composition. Although SLES is only weakly anionic, it will still be more affected by electrolyte than the nonionic component, as electrolyte decreases the repulsion between anionic headgroup charges, allowing for a more closely-packed monolayer. When comparing Tables 5.7 and 5.8 it can also be seen that consistently higher absolute total adsorption values are obtained for LAS/SLES mixtures than $C_{12}E_8$/SLES.

5.3.2 Ternary surfactant mixtures

The ternary $C_{12}E_8$/LAS/SLES system was investigated in the presence of 2 mM $CaCl_2$ over the same solution composition range as for NaCl. Figure 5.9 shows the variation in adsorption for $C_{12}E_8$, LAS and SLES as a function of each respective solution composition, as well as the variation in total adsorption. A selection of the data is summarised in Table 5.9 as a function of SLES solution composition.

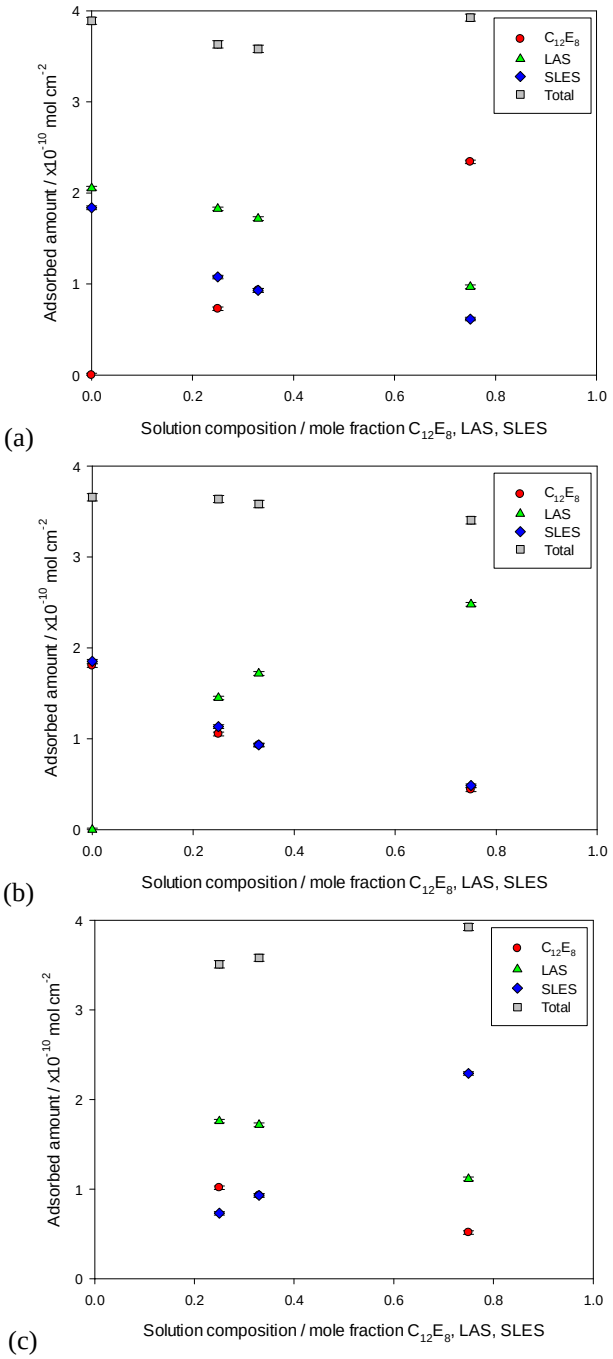

Figure 5.9: Adsorbed amounts and total adsorption for 2 mM $C_{12}E_8$/LAS/SLES as a function of (a) $C_{12}E_8$, (b) LAS and (c) SLES solution composition, in 2 mM $CaCl_2$, at 25°C, in NRW containing 1x10^{-6} M NaOH.

Ratio	Contrast	d (± 1)	ρ (± 0.02x10^{-6} Å^{-2})	A (± 2 Å^2)	Γ (± 0.02 x10^{-10} mol cm^{-2})	Γ_{total} (± 0.04x10^{-10} mol cm^{-2})	Solution compos-ition	Surface composition (± 0.02)
0.375/0.375/ 0.25	dhh	24	0.93	163	1.02 (1.27)	3.51 (2.73)	0.375	0.29 (0.46)
	hdh	18	2.16	94	1.76 (1.31)		0.375	0.50 (0.48)
	hhd	28	0.64	227	0.73 (0.16)		0.25	0.21 (0.06)
	ddd	17	3.97					
0.33/0.33/ 0.33	dhh	22	0.94	178	0.93 (1.27)	3.58 (2.61)	0.33	0.26 (0.49)
	hdh	19	2.01	97	1.72 (1.20)		0.33	0.48 (0.46)
	hhd	23	0.91	178	0.93 (0.14)		0.33	0.26 (0.05)
	ddd	19	3.67					
0.125/0.125/ 0.75	dhh	21	0.70	321	0.52 (1.16)	3.93 (2.86)	0.125	0.13 (0.41)
	hdh	21	1.29	149	1.12 (0.96)		0.125	0.28 (0.34)
	hhd	19	2.31	73	2.29 (0.73)		0.75	0.58 (0.25)
	ddd	17	4.25					

Table 5.9: Key model parameters for 2 mM $C_{12}E_8$/LAS/SLES in 2 mM $CaCl_2$, as a function of SLES solution composition, at 25°C, in NRW containing 1x10^{-6} M NaOH. Data are compared to that in the absence of electrolyte, shown in brackets.

With increasing solution composition of each component, the adsorbed amount of that component increases while that of the other two components decreases. The variation is qualitatively very similar to that for the mixtures in the presence of NaCl (Figure 5.2). For example, on increasing LAS solution composition, the adsorbed amounts of $C_{12}E_8$ and SLES are almost the same, and decrease at exactly the same rate, indicating very similar adsorption at the interface. This is very different to data seen in the absence of electrolyte (Figure 4.11 (b), Chapter 4) where the $C_{12}E_8$ adsorption is vastly higher than that of SLES. These results are displayed as the variation in surface composition with $C_{12}E_8$, LAS and SLES solution compositions, shown in Figure 5.10, with surface composition data displayed as ternary contour diagrams in Figure 5.11, and compared to the original ternary contour diagrams (Figure 5.12).

Total adsorption values are systematically higher in the presence of Ca^{2+} than Na^+, for example, at 0.125/0.125/0.75 $C_{12}E_8$/LAS/SLES, the total adsorbed amount is 3.78x10^{-10} mol cm^{-2} in Na^+ but 3.93x10^{-10} mol cm^{-2} in Ca^{2+}. The total adsorption is higher in solutions richer in SLES or LAS/SLES in the presence of both Na^+ and Ca^{2+}. This is considerably higher in the presence of Ca^{2+}. As would be expected, there is no significant effect of Ca^{2+} on the relative adsorption of $C_{12}E_8$ due to its nonionic nature.

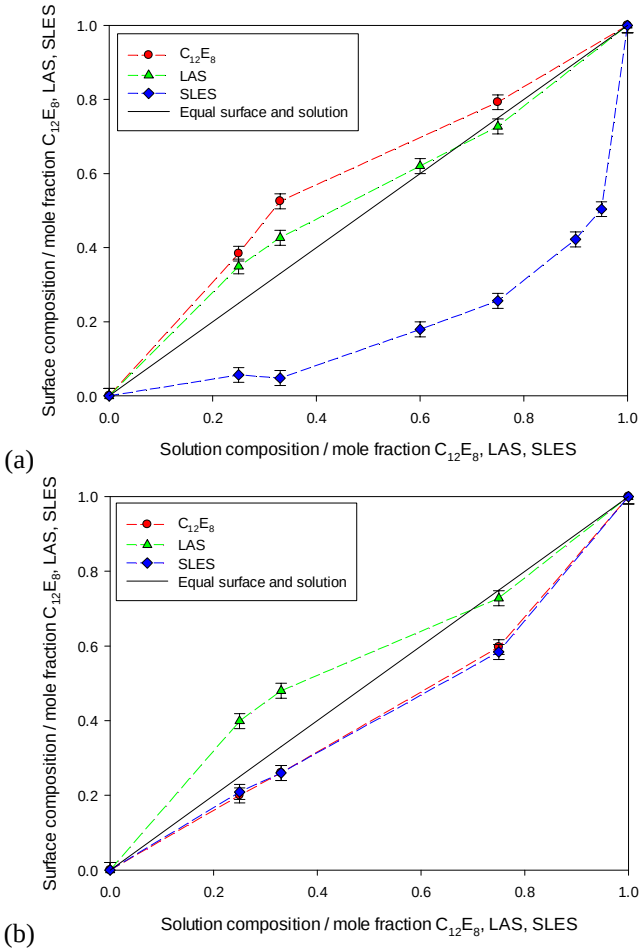

Figure 5.10: (a) Original surface versus solution composition data in the absence of eletrolyte, and (b) surface composition as a function of solution composition of $C_{12}E_8$, LAS and SLES, for 2 mM $C_{12}E_8$/LAS/SLES in 2 mM $CaCl_2$, at 25°C, in NRW containing $1x10^{-6}$ M NaOH. Lines are guides to the eye only.

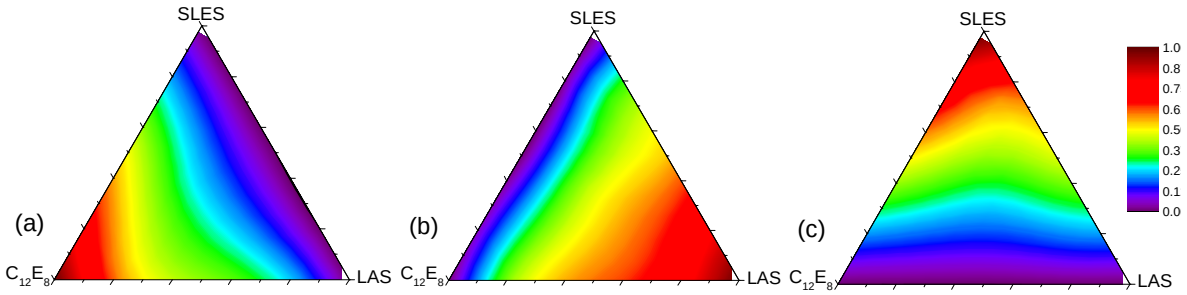

Figure 5.11: Ternary contour diagrams showing surface composition for (a) $C_{12}E_8$, (b) LAS and (c) SLES as a function of solution composition, for ternary $C_{12}E_8$/LAS/SLES mixtures in 2 mM $CaCl_2$.

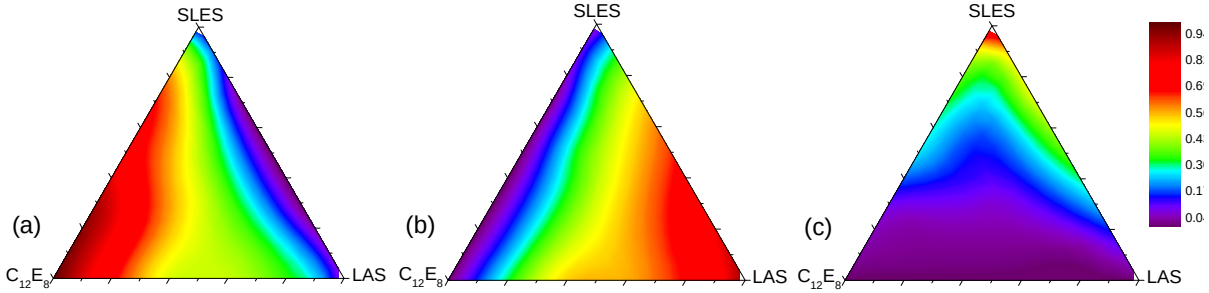

Figure 5.12: Original ternary contour diagrams showing surface composition for (a) $C_{12}E_8$, (b) LAS and (c) SLES as a function of solution composition, for ternary $C_{12}E_8$/LAS/SLES mixtures in the absence of electrolyte.

The addition of Ca^{2+} results in very different surface behaviour to that observed in the absence of electrolyte, with the most pronounced change seen in the surface composition of SLES. With a solution composition of 0.9, the surface composition of SLES increases from 0.42 to 0.86, almost exactly the same as the solution composition. Monolayer adsorption is observed at all solution compositions for the ternary mixtures, as observed in the binary surfactant mixtures.

5.4 Discussion

Monovalent and divalent counterions, in the form of NaCl and $CaCl_2$, were found to have a profound effect on the mixing behaviour of the $C_{12}E_8$/LAS/SLES system. Na^+ and Ca^{2+} were both very effective at driving the surface composition closer to the solution composition, promoting significantly more ideal-like behaviour. The Ca^{2+} counterion is more efficient than Na^+ in promoting this change. In the binary $C_{12}E_8$/SLES and LAS/SLES mixtures and the ternary $C_{12}E_8$/LAS/SLES system in the absence of electrolyte, a large departure from ideality is seen which is not possible to explain using current non-ideal mixing theories such as RST. A similarly large departure from ideality was seen in mixtures of the dialkyl chain cationic DHDAB with $C_{12}E_6$[24] and also for $C_{10}E_3$/LAS[16] as described in Section 5.3.1, where in the absence of electrolyte the much more surface-active DHDAB and $C_{10}E_3$, respectively, dominated surface adsorption. However, in the latter example, the addition of Ca^{2+} caused the less surface-active LAS to become more dominant at the interface so that the surface and solution compositions were very similar. This was due to the promotion to more planar-like structures attributed to a reduction in the intrinsic curvature of LAS. In the present system, a switch in relative surface activities is seen where the SLES is able to adsorb to the interface more easily and the relative amount of the nonionic $C_{12}E_8$ at the interface diminishes. The presence of electrolyte makes all components more comparable, so the original requirement for SLES to be in the bulk rather than at the interface is no longer as important, thus giving the SLES more comparable surface and solution compositions.

A switch in the relative surface activities of two surfactants was also seen by Chen et al[17] who studied the impact of Ca^{2+} on the mixing behaviour of the rhamnolipid biosurfactant R2 with LAS. In the

absence of electrolyte, LAS dominated surface adsorption, but on addition of $CaCl_2$ the surface changed to becoming more dominant in the R2. The Ca^{2+} bound more strongly to the anionic headgroup of LAS than to the less anionic and bulkier R2 molecule. Only monolayer adsorption was observed in the presence of Ca^{2+}, even though in pure LAS multilayers have been found.[2] This was attributed to the bulky headgroup of R2 preventing LAS/Ca^{2+} complexation and so disrupting multilayer formation. Calcium ions can introduce positive charges to the system. Chen et al[17] observed a charge reversal when Ca^{2+} was added to the system of a R2-rich binary mixture with LAS. This was due to the larger headgroup of R2, so that with a higher proportion of R2, the anionic parts of the LAS were sterically hindered for complexation with the calcium ions, meaning only one of the anionic sites were complexed to Ca^{2+}, leaving a net positive charge. Similarly, with $C_{12}E_{12}$/SLES in the presence of the trivalent Al^{3+}, the large headgroup of $C_{12}E_{12}$ disrupted complex formation with the Al^{3+} counterion.[3]

The total adsorbed amounts significantly increase on addition of electrolyte by approximately 30%, with total adsorption values systematically higher in the presence of the divalent Ca^{2+} than Na^+. The presence of more highly valent counterions is known to drive a larger micellar growth[13] and it has been shown that a significantly lower concentration of multivalent counterions are required to give similar effects.

It is important to note the relative concentrations of the two salts used in the present work. Although 0.1 M NaCl was used, surface compositions are invariant above 40 mM NaCl, which corresponds to an equivalent ionic strength of around 13mM $CaCl_2$. However, $CaCl_2$ concentrations as low as 2 mM have produced even better results than with the NaCl. This indicates that the divalent Ca^{2+} ions are better at driving the surface composition towards its solution composition than the Na^+ ions and much higher concentrations of Na^+ are needed in order to create these effects.

In the $C_{12}E_8$/LAS system investigated by Penfold et al[2], multilayer adsorption occurred on addition of 2 mM $CaCl_2$. However, only monolayer adsorption was observed in all mixtures investigated here. It

is expected that more complex surface behaviour would be observed in the $C_{12}E_8$/LAS/SLES system only in much higher surfactant and/or electrolyte concentrations and in very LAS-rich solutions.

When SLES is replaced with SDS in the presence of NaCl, the same effects on surface composition and total adsorption occur, albeit at a slightly lower level. SDS is much more anionic than SLES, which acts more like a nonionic surfactant due to its relatively low degree of ionisation (≤ 0.15), of which typical values are of the order 0.3.[25] The results obtained here are therefore expected for $C_{12}E_8$/LAS/SDS but more surprising for mixtures with SLES, as the counterion is strongly bound and SLES is only weakly anionic.[12]

Further information on the solution aggregate behaviour of $C_{12}E_8$/LAS/SLES mixtures, as a function of type and concentration of electrolyte, using SANS, would be valuable. Through the preparation of the solutions in Ca^{2+} electrolyte, it was found that solutions containing less than 0.5 mole fraction LAS were clear and colourless. However, better wetting properties were observed at higher LAS mole fractions, and above 0.6 mole fraction LAS, the solutions were increasingly cloudy as the LAS solution composition increased. This shows that there are some interesting phase behaviour changes occurring on addition of multivalent electrolyte which do not occur in monovalent electrolyte. Furthermore, at a fixed mole fraction of LAS, cloudier solutions were observed in solutions containing more SLES than $C_{12}E_8$. The presence of $C_{12}E_8$ may disrupt complex aggregate or multilayer formation due to its larger hydrophilic headgroup, as was seen with SLES and $C_{12}E_{12}$ in the presence of Al^{3+}.[13]

Although multivalent counterions bring about negative effects such as precipitation, it is possible that a controlled addition of certain electrolytes may be beneficial for detergency. The surface tension and CMC-lowering abilities of the presence of electrolyte, as well as the promotion of more complex aggregate structures, are advantageous for cleaning and can be controlled by the structure of the actual surfactant, particularly with LAS.[9]

References: Chapter 5

1. Lu, J. R.; Thomas, R. K.; Penfold, J., *Advances in Colloid and Interface Science* **2000,** *84*, 143-304.
2. Penfold, J.; Thomas, R. K.; Dong, C. C.; Tucker, I.; Metcalfe, K.; Golding, S.; Grillo, I., *Langmuir* **2007,** *23* (20), 10140-10149.
3. Petkov, J. T.; Tucker, I. M.; Penfold, J.; Thomas, R. K.; Petsev, D. N.; Dong, C. C.; Golding, S.; Grillo, I., *Langmuir* **2010,** *26* (22), 16699-16709.
4. Javadian, S.; Gharibi, H.; Bromand, Z.; Sohrabi, B., *Journal of Colloid and Interface Science* **2008,** *318* (2), 449-456.
5. Penfold, J.; Staples, E.; Tucker, I.; Thomas, R. K., *Langmuir* **2002,** *18* (15), 5755-5760.
6. Penfold, J.; Staples, E.; Tucker, I.; Thompson, L.; Thomas, R. K., *Journal of Colloid and Interface Science* **2002,** *247* (2), 404-411.
7. Carale, T. R.; Pham, Q. T.; Blankschtein, D., *Langmuir* **1994,** *10* (1), 109-121.
8. Penfold, J.; Staples, E.; Tucker, I.; Thomas, R. K., *Journal of Colloid and Interface Science* **1998,** *201*, 223-232.
9. Ma, J.-G.; Boyd, B. J.; Drummond, C. J., *Langmuir* **2006,** *22* (21), 8646-8654.
10. Zhu, Y.-P.; Rosen, M. J.; Morrall, S. W.; Tolls, J., *Journal of Surfactants and Detergents* **1998,** *1* (2), 187-193.
11. Xu, H.; Penfold, J.; Thomas, R. K.; Petkov, J. T.; Tucker, I., *Langmuir* **2013,** *29* (41), 12744-12753.
12. Xu, H.; Penfold, J.; Thomas, R. K.; Petkov, J. T.; Tucker, I.; Webster, J. P. R., *Langmuir* **2013,** *29* (37), 11656-11666.
13. Alargova, R. G.; Petkov, J. T.; Petsev, D. N., *Journal of Colloid and Interface Science* **2003,** *261* (1), 1-11.
14. Sein, A.; Engberts, J. B. F. N., *Langmuir* **1995,** *11* (2), 455-465.
15. Missel, P. J.; Mazer, N. A.; Carey, M. C.; Benedek, G. B., *Journal of Physical Chemistry* **1989,** *93* (26), 8354-8366.
16. Tucker, I.; Penfold, J.; Thomas, R. K.; Dong, C. C.; Golding, S.; Gibson, C.; Grillo, I., *Langmuir* **2010,** *26* (13), 10614-10626.
17. Chen, M.; Penfold, J.; Thomas, R. K.; Smyth, T. J. P.; Perfumo, A.; Marchant, R.; Banat, I. M.; Stevenson, P.; Parry, A.; Tucker, I.; Grillo, I., *Langmuir* **2010,** *26* (23), 17958-17968.
18. Chou, S. I.; Bae, J. H., *Journal of Colloid and Interface Science* **1983,** *96* (1), 192-203.
19. Stellner, K. L.; Scamehorn, J. F., *Journal of the American Oil Chemists Society* **1986,** *63* (4), 566-574.
20. Yu, Y.; Zhao, J.; Bayly, A. E., *Chinese Journal of Chemical Engineering* **2008,** *16* (4), 517-527.
21. Scheibel, J. J., *Journal of Surfactants and Detergents* **2004,** *7* (4), 319-328.
22. Stellner, K. L.; Scamehorn, J. F., *Langmuir* **1989,** *5* (1), 77-84.
23. Schwuger, M. J., Interfacial and Performance Properties of Sulfated Polyoxyethylenated Alcohols. In *Structure/Performance Relationships in Surfactants*, Rosen, M., Ed. ACS Symposium Series; American Chemical Society: Washington, DC, 1984; pp 3-26.
24. Penfold, J.; Staples, E.; Tucker, I.; Thomas, R. K., *Langmuir* **2004,** *20* (4), 1269-1283.
25. Hayter, J. B., *Langmuir* **1992,** *8* (12), 2873-2876.

Chapter 6

Surface adsorption behaviour of multicomponent biosurfactant / conventional surfactant mixtures

This chapter discusses the impact of the partial replacement of the ternary conventional surfactant mixture $C_{12}E_8$/LAS/SLES with the rhamnolipid biosurfactants Rha-C_{10}-C_{10} (R1) and Rha-Rha-C_{10}-C_{10} (R2) on the surface adsorption behaviour at the air/water interface using neutron reflectivity. The mixing behaviour of binary and ternary rhamnolipid/conventional surfactant mixtures is studied and the effect of altering the R1:R2 ratio at a fixed rhamnolipid/conventional surfactant (R/C) ratio of 30/70 for the five-component mixture is presented.

6.1 Literature review

There is limited literature concerning the adsorption of rhamnolipids at the air/water interface. Ozdemir et al[1] studied the effects of pH on the surface behaviour of both Rha-C_{10}-C_{10} (R1) and Rha-Rha-C_{10}-C_{10} (R2) and found it reduced the CMC of R1 and R2 from $1x10^{-4}$ M and $1.5x10^{-4}$ M, respectively, at pH 6.8, to $4x10^{-5}$ M at pH 5. The rhamnolipid carboxyl groups are undissociated at lower pH, which reduces their anionic nature and the repulsion between the electrostatic charges on the carboxyl headgroups. Hence a more highly compacted monolayer was also present at lower pH. Helvaci et al[2] found that electrolyte also impacted the carboxyl group on both R1 and R2, allowing the rhamnolipids to form a closer packed monolayer of more nonionic-like surfactants due to the screening of the repulsive headgroup charges. R1 formed more rigid monolayers due to its higher hydrophobicity than R2. Peker et al[3] showed that the differences in headgroup sizes of R1 and R2 greatly affected their surface behaviour. However, Chen et al[4] showed from NR measurements that R1 and R2 are only weakly ionic at all pH values investigated, with minimal effect of electrolyte.

The only recent literature reporting on the mixing behaviour of rhamnolipids is by Chen et al[4,5] who investigated the surface behaviour of R1/R2 mixtures, as well as binary and ternary mixtures of rhamnolipids with the conventional surfactant linear alkylbenzene sulfonate (LAS-6). In the R1/R2

binary system, R1 dominated surface adsorption over the whole composition range, even at concentrations far above the CMC. Similarities in surface behaviour have been linked to that of $C_{12}E_3/C_{12}E_8$[6] due to the large differences in headgroup size of R1 and R2 and the effectively nonionic nature of the rhamnolipids.[4] A synergy in adsorption was found in R1/R2/LAS at a 1:1 ratio of R1:R2. This synergy was not observed in any of the binary mixtures. The data presented by Chen et al[4,5] for the binary and ternary mixtures of rhamnolipids R1 and R2 with LAS are used to make direct comparisons with the data presented here. The solution behaviour of this system was also investigated but discussion of this is deferred to Chapter 7. In terms of the mixing behaviour of other biosurfactants with conventional surfactants, the surface behaviour of the two forms of the sophorolipid biosurfactant, acidic sophorolipid (AS) and lactonic sophorolipid (LS) with LAS has also been studied.[7] Variations in mixing behaviour were observed as a result of the two forms of sophorolipid having different alkyl chain structures.

There are very few reports on mixtures with more than three components, and none on those containing biosurfactants. Staples et al[8] investigated a six-component mixture of the nonionic ethoxylate surfactants $C_{12}E_3$, $C_{12}E_5$, $C_{12}E_8$, $C_{12}E_{12}$ with the anionic SDS and the impurity dodecanol. The average EO length, which was ~5 in solution, became ~3.5 at the interface, indicating an interface composed mainly of the most surface-active components, primarily dodecanol, with a corresponding synergistic increase in total adsorption.

In this chapter, a model ternary system of the conventional surfactants $C_{12}E_8$/LAS/SLES, commonly used in detergent formulations, is partially replaced with the rhamnolipid biosurfactants (R1, R2) to form the five-component biosurfactant/conventional surfactant mixture R1/R2/$C_{12}E_8$/LAS/SLES. The surface behaviour of the binary, ternary and five-component biosurfactant mixtures is studied and the addition of highly surface-active rhamnolipids, as well as the increase in the number of components in the system, is expected to have a positive effect on overall surface activity.

6.2 Binary biosurfactant / conventional surfactant mixtures

Binary mixtures of R1 and R2 with the conventional surfactant $C_{12}E_8$ and SLES were investigated at the air/water interface at solution compositions 0.75/0.25, 0.5/0.5, 0.25/0.75 and 0.1/0.9, at 2 mM concentration, using neutron reflectivity. Two contrasts were measured for each composition: d-R/h-C, h-R/d-C, R representing rhamnolipid R1 or R2, and C representing the conventional surfactant $C_{12}E_8$ or SLES. Figure 6.1 gives the variation in adsorbed amount for the rhamnolipids R1 and R2 with $C_{12}E_8$, with the data shown in Tables 6.1 and 6.2. Figure 6.2 shows the variation in adsorbed amount for the rhamnolipids with SLES, with the relevant data presented in Tables 6.3 and 6.4.

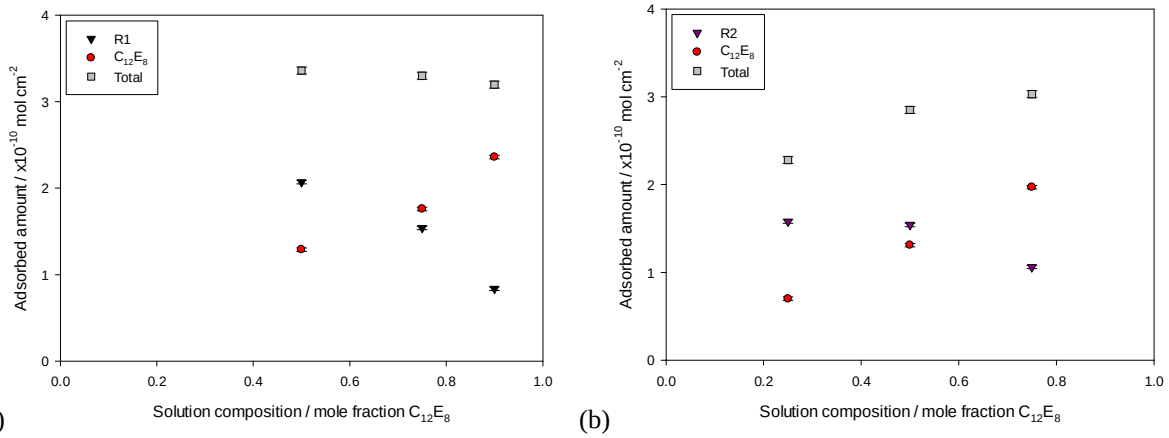

Figure 6.1: Variation in adsorbed amount for (a) R1/$C_{12}E_8$ and (b) R2/$C_{12}E_8$ with solution composition of $C_{12}E_8$, at 2 mM concentration, at 25°C, in NRW containing 1x10^{-6} M NaOH.

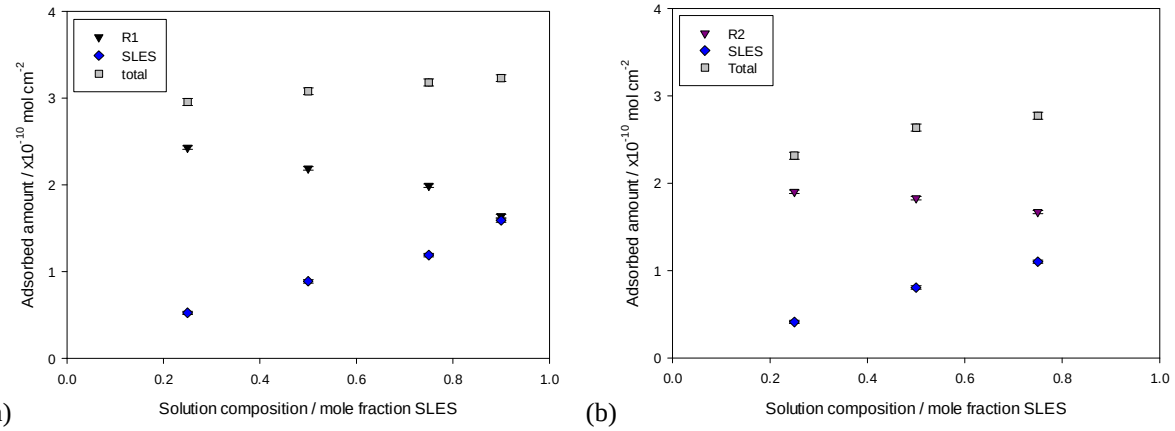

Figure 6.2: Variation in adsorbed amount for (a) R1/SLES and (b) R2/SLES with solution composition of SLES, at 2 mM concentration, at 25°C, in NRW containing 1x10^{-6} M NaOH.

Ratio	Contrast	d (± 1)	ρ (± 0.02x10^{-6} Å^{-2})	A (± 2 Å^2)	Γ (± 0.02x10^{-10} mol cm^{-2})	Γ_{total} (± 0.04x10^{-10} mol cm^{-2})	Solution composition	Surface composition (± 0.02)
0.5/0.5	dh	20	3.18	80	2.07	3.36	0.5	0.62
	hd	25	1.33	129	1.29		0.5	0.38
0.25/0.75	dh	20	2.36	108	1.54	3.30	0.25	0.47
	hd	26	1.57	94	1.76		0.75	0.53
0.1/0.9	dh	26	1.09	199	0.84	3.20	0.1	0.26
	hd	21	2.00	70	2.36		0.9	0.74

Table 6.1: Key model parameters for 2 mM R1/$C_{12}E_8$, at 25°C, in NRW containing 1x10^{-6} M NaOH.

Ratio	Contrast	d (± 1)	ρ (± 0.02x10^{-6} Å^{-2})	A (± 2 Å^2)	Γ (± 0.02x10^{-10} mol cm^{-2})	Γ_{total} (± 0.04x10^{-10} mol cm^{-2})	Solution composition	Surface composition (± 0.02)
0.75/0.25	dh	20	3.04	105	1.58	2.28	0.75	0.69
	hd	32	0.57	237	0.70		0.25	0.31
0.5/0.5	dh	19	3.09	108	1.54	2.85	0.5	0.54
	hd	32	0.89	127	1.31		0.5	0.46
0.25/0.75	dh	15	2.70	157	1.06	3.03	0.25	0.35
	hd	19	1.95	84	1.97		0.75	0.65

Table 6.2: Key model parameters for 2 mM R2/$C_{12}E_8$, at 25°C, in NRW containing 1x10^{-6} M NaOH.

Ratio	Contrast	d (± 1)	ρ (± 0.02 x10^{-6} Å^{-2})	A (± 2 Å^2)	Γ (± 0.02x10^{-10} mol cm^{-2})	Γ_{total} (± 0.04x10^{-10} mol cm^{-2})	Solution composition	Surface composition (± 0.02)
0.75/0.25	dh	20	3.68	68	2.43	2.96	0.75	0.82
	hd	33	0.47	316	0.52		0.25	0.18
0.5/0.5	dh	20	3.32	75	2.20	3.10	0.5	0.71
	hd	34	0.63	185	0.90		0.5	0.29
0.25/0.75	dh	20	3.02	86	1.99	3.18	0.25	0.63
	hd	28	0.91	139	1.19		0.75	0.37
0.1/0.9	dh	18	2.84	101	1.64	3.23	0.1	0.51
	hd	25	1.27	105	1.59		0.9	0.49

Table 6.3: Key model parameters for 2 mM R1/SLES, at 25°C, in NRW containing 1x10^{-6} M NaOH.

Ratio	Contrast	d (± 1)	ρ (± 0.02 x10^{-6} Å^{-2})	A (± 2 Å^2)	Γ (± 0.02x10^{-10} mol cm^{-2})	Γ_{total} (± 0.04x10^{-10} mol cm^{-2})	Solution composition	Surface composition (± 0.02)
0.75/0.25	dh	19	3.67	87	1.90	2.32	0.75	0.82
	hd	32	0.45	402	0.41		0.25	0.18
0.5/0.5	dh	18	3.77	91	1.83	2.64	0.5	0.63
	hd	30	0.69	206	0.81		0.5	0.31
0.25/0.75	dh	18	3.43	100	1.67	2.77	0.25	0.60
	hd	26	0.99	151	1.10		0.75	0.40

Table 6.4: Key model parameters for 2 mM R2/SLES, at 25°C, in NRW containing 1x10^{-6} M NaOH.

Figure 6.1 shows that for rhamnolipid (R)/$C_{12}E_8$ binary mixtures, the absolute adsorbed amount of R1 is higher than R2 at a particular solution composition of conventional surfactant. With increasing solution composition of rhamnolipids, the adsorbed amount of R1 increases at a faster rate than R2 does. This is also observed for R1/SLES and R2/SLES (Figure 6.2). This means that R1 is more effective than R2 at displacing the conventional nonionic surfactant as the R mole fraction increases. This is attributed to the bulkier headgroup of R2, which contains one more rhamnose sugar group than

R1. This introduces packing constraints and makes it more difficult for R2 to reach the interface and displace other surfactants, hence its lower level of surface activity.

Significant differences can also be seen between the binary mixtures of R with either $C_{12}E_8$ or SLES. The absolute amount of rhamnolipid adsorbed at the interface is higher in the presence of SLES than $C_{12}E_8$. This is due to the lower surface activity of SLES than the nonionic component. This results in the rhamnolipids dominating surface adsorption to a greater extent in R/SLES mixtures. As a result, the absolute amount of SLES at the interface in R/SLES mixtures is systematically lower than that of $C_{12}E_8$ in R/$C_{12}E_8$ mixtures.

The total adsorption increases with all binary mixtures except R1/$C_{12}E_8$ where a slight decrease is seen. The increase is greater for R2/C than R1/C due to the packing problems associated with the larger headgroup on R2. Compared to the adsorption values of the pure components (pure R1, R2 and $C_{12}E_8$ and SLES = 2.9, 1.9, 2.7 and 3.5 x10^{-10} mol cm^{-2}, respectively) no synergy in total adsorption is observed. However, interestingly the highest absolute adsorption values are observed for R1/$C_{12}E_8$ whereas the lowest values are observed for the R2/SLES. This may be due to the steric hindrance of the R2 hindering adsorption, as well as the fact that the nonionic $C_{12}E_8$ is more surface-active than SLES.

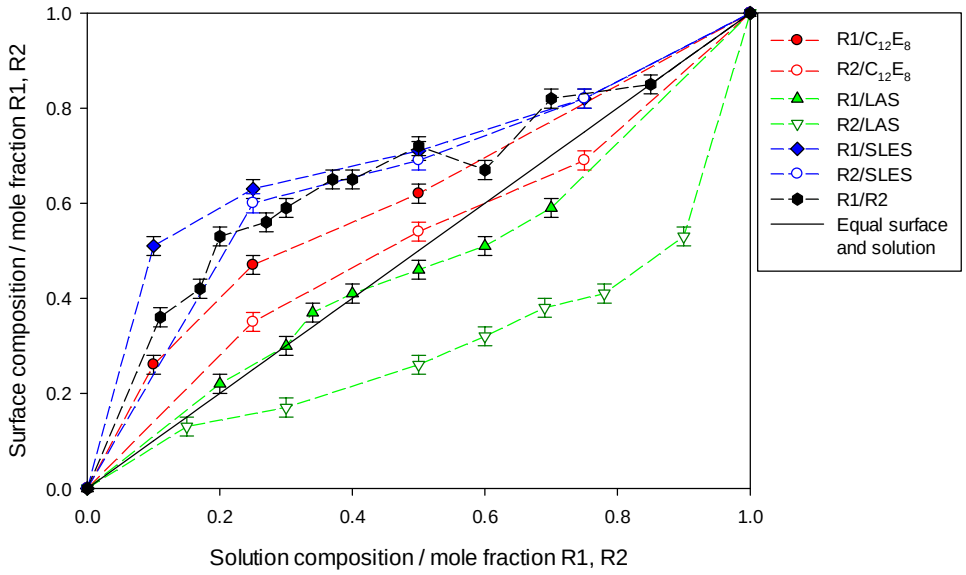

Figure 6.3: Variation in surface composition with solution composition for binary rhamnolipid/conventional surfactant mixtures, compared with ideal mixing (straight line). Literature R1/R2 data (1 mM at pH in buffer) are included for a qualitative comparison. Dashed lines are guides to the eye only.

Figure 6.3 shows R2/$C_{12}E_8$ as a mixture which closely follows the solution composition. This may be expected, due to the fact that R2 acts more like a nonionic surfactant than R1[4] and because their headgroup areas are close in size relative to the other surfactants. However, for all other binary mixtures there is a dominance of R1 at the air/water interface and this is most prominently seen with the rhamnolipid/SLES mixtures. For all R/C binary mixtures, R1 dominates adsorption much more than R2 due to the packing constraints of the larger headgroup on R2. This is explained clearly in the literature R1/R2 data by Chen et al[4] (black data points) where R1 dominates surface adsorption over the whole composition range. The measurements were made far in excess of the mixed CMC, but the large dominance of R1, especially for R1/SLES, shows an extreme departure from ideality which cannot be accounted for by non-ideal mixing theories such as RST. $C_{12}E_8$ has a higher surface activity than SLES, hence R1 is not quite so dominant at the interface of R1/$C_{12}E_8$ mixtures. The non-ideal mixing behaviour observed with rhamnolipids and SLES is similar to that of the $C_{12}E_8$/SLES binary mixtures described in Chapter 4. R1 and R2 are very mildly anionic and can be viewed almost as nonionic surfactants.[4] No synergy in total adsorption is observed when compared to adsorption values of the individual components for any of the binary mixtures.

Previous data for the mixing of rhamnolipids with LAS by Chen et al[5] (green data) are reproduced in Figure 6.3 for comparison. The surface composition of R1/LAS was consistently close to its solution composition, whereas for R2/LAS mixtures it was not. The surface was dominated by LAS, especially in R2-rich solutions, due to the packing constraints introduced by the larger headgroup of R2. This is similar to the packing constraints in R1/R2 binary mixtures[4] as described above. Although no synergy in total adsorption was observed in either binary mixture, in R1/R2/LAS a synergy was seen, as will be discussed in Section 6.3.

6.3 Ternary biosurfactant / conventional surfactant mixtures

The ternary mixtures R1/R2/$C_{12}E_8$ and R1/R2/SLES were investigated at the air/water interface, at a solution concentration of 2 mM and at a fixed R1:R2 ratio of 1:1, using neutron reflectivity. For each solution composition, four measurements were made with the following isotopic combinations: d-R1/h-R2/h-C, h-R1/d-R2/h-C, h-R1/h-R2/d-C, d-R1/d-R2/d-C, where C is the conventional surfactant $C_{12}E_8$ or SLES. The data are compared with the R1/R2/LAS ternary data previously reported.[5]

6.3.1 R1/R2/$C_{12}E_8$

The variation in adsorbed amount for each component in the R1/R2/$C_{12}E_8$ ternary mixture, and the total adsorption are shown in Figure 6.4 (a). The variation in surface composition as a function of the solution composition of each component is displayed in Figure 6.4 (b). The data parameters are summarised in Table 6.5.

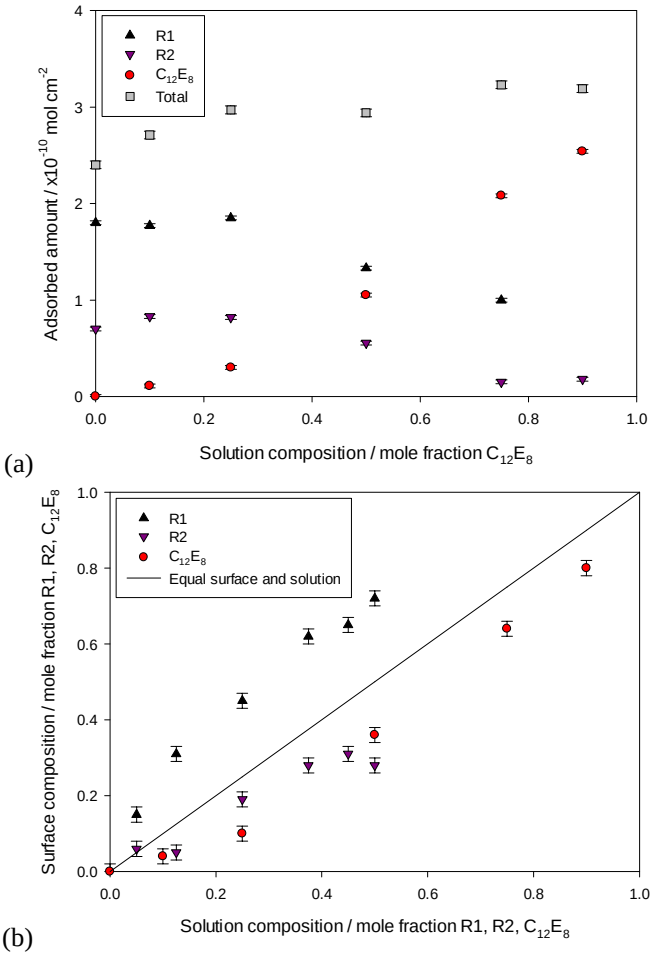

Figure 6.4: (a) Adsorbed amounts of R1, R2 and $C_{12}E_8$, and the total adsorption, as a function of $C_{12}E_8$ solution composition. (b) Surface versus solution behaviour for R1, R2 and $C_{12}E_8$ in a ternary mixture.

Ratio	Contrast	d (± 1)	ρ (± 0.02x10^{-6} Å^2)	A (± 2 Å^2)	Γ (± 0.02x10^{-10} mol cm^{-2})	Γ_{total} (± 0.02x10^{-10} mol cm^{-2})	Solution composition	Surface composition (± 0.02)
0.45/0.45/0.1	dhh	22	2.32	94	1.77	2.71	0.45	0.65
	hdh	18	2.02	199	0.83		0.45	0.31
	hhd	20	0.55	1555	0.11		0.1	0.04
	ddd	20	3.92					
0.375/0.375/0.25	dhh	22	2.39	90	1.85	2.97	0.375	0.62
	hdh	21	1.73	203	0.82		0.375	0.28
	hhd	24	0.59	555	0.30		0.25	0.10
	ddd	15	5.48					
0.25/0.25/0.5	dhh	19	2.41	125	1.33	2.94	0.25	0.45
	hdh	22	1.22	299	0.55		0.25	0.19
	hhd	25	1.02	158	1.05		0.5	0.36
	ddd	17	4.43					
0.125/0.125/0.75	dhh	21	1.45	167	1.00	3.23	0.125	0.31
	hdh	39	0.23	1097	0.15		0.125	0.05
	hhd	19	1.90	80	2.08		0.75	0.64
	ddd	18	4.09					
0.05/0.05/0.9	dhh	24	0.72	354	0.47	3.19	0.05	0.15
	hdh	21	0.50	921	0.18		0.05	0.06
	hhd	19	2.36	65	2.54		0.9	0.80
	ddd	18	3.53					

Table 6.5: Key model parameters for the variation in adsorption and surface composition for R1/R2/$C_{12}E_8$ at 2 mM concentration, at 25°C, in NRW containing 1x10^{-6} M NaOH.

As the mole fraction of $C_{12}E_8$ increases, its surface composition increases whilst that of R1 and R2 decreases. The R1 adsorption values are consistently higher than those of R2, as would be expected because of the different sizes of their hydrophilic headgroups and relative surface activity. An increase in total adsorption is observed from 2.7x10^{-10} mol cm^{-2} [4] to 3.2x10^{-10} mol cm^{-2} as the nonionic component increases. The addition of $C_{12}E_8$ gives a higher total adsorption than for R1/R2 alone[4] where the total adsorption there was between 2.1x10^{-10} and 2.7x10^{-10} mol cm^{-2}, depending on the solution composition. This is attributed to the nonionic surfactant acting as a buffer between the repulsive headgroup charges.

Figure 6.4 shows a system in which R1 dominates surface adsorption and $C_{12}E_8$ is depleted at the air/water interface. The surface composition of R2 generally follows its solution composition. The absolute amount of R1 adsorbed is consistently higher than that of R2 at all solution compositions, even though their solution compositions are equal.

6.3.2 R1/R2/SLES

The variation in adsorbed amount for each component in the R1/R2/SLES ternary mixture, and the total adsorption are shown in Figure 6.5 (a), with the variation in surface composition as a function of the solution composition of each component in Figure 6.5 (b). The key model parameters are summarised in Table 6.6.

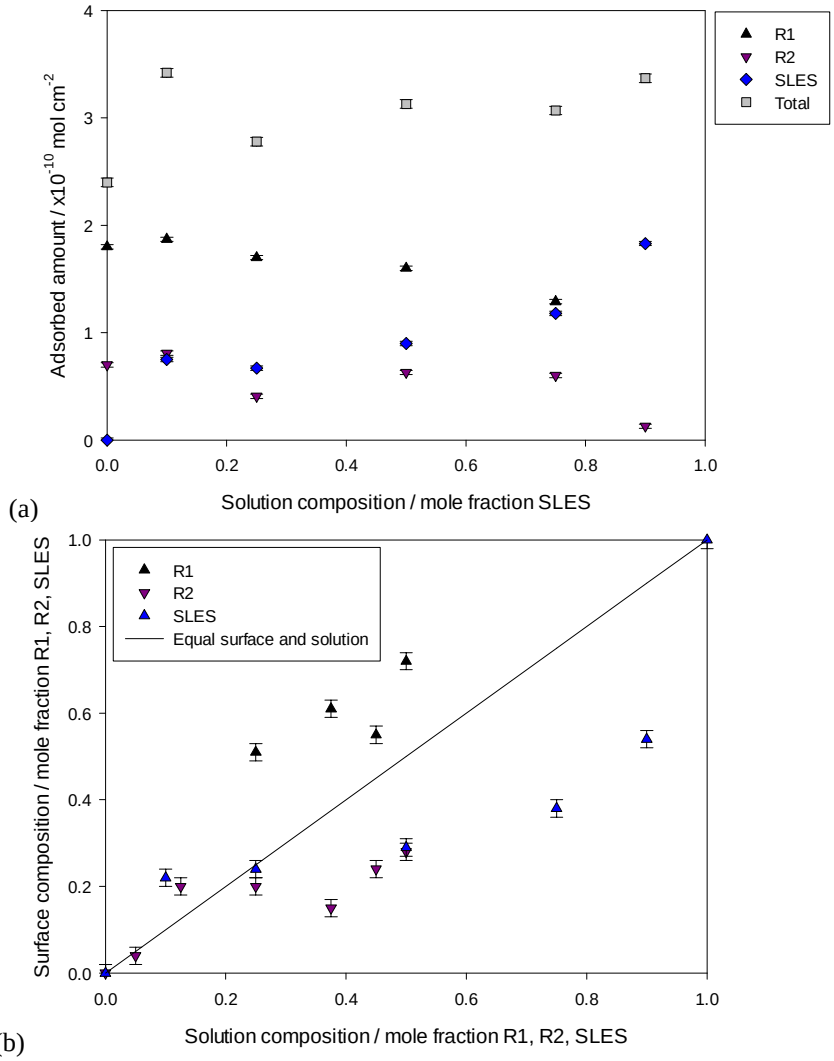

Figure 6.5: (a) Adsorbed amounts of R1, R2 and SLES, and the total adsorption, as a function of SLES solution composition. (b) Surface versus solution behaviour for R1, R2 and SLES in a ternary mixture.

Ratio	Contrast	d (± 1)	ρ (± 0.02x 10^{-6} Å^2)	A (± 2 Å^2)	Γ (± 0.02x10^{-10} mol cm^{-2})	Γ_{total} (± 0.04x10^{-10} mol cm^{-2})	Solution compos-ition	Surface composition (± 0.02)
0.45/0.45/ 0.1	dhh	20	2.65	89	1.87	3.42	0.45	0.55
	hdh	19	1.94	206	0.81		0.45	0.24
	hhd	32	0.34	222	0.75		0.1	0.22
	ddd	18	4.37					
0.375/0.375/ 0.25	dhh	17	3.12	97	1.71	2.78	0.375	0.61
	hdh	20	0.93	410	0.41		0.375	0.15
	hhd	25	0.64	250	0.67		0.25	0.24
	ddd	17	4.79					
0.25/0.25/ 0.5	dhh	21	2.47	104	1.60	3.13	0.25	0.51
	hdh	22	1.17	264	0.63		0.25	0.20
	hhd	24	0.82	185	0.90		0.5	0.29
	ddd	19	4.36					
0.125/0.125/ 0.75	dhh	18	2.46	129	1.29	3.07	0.125	0.42
	hdh	20	1.49	276	0.60		0.125	0.20
	hhd	22	1.31	141	1.18		0.75	0.38
	ddd	16	4.93					
0.05/0.05/ 0.9	dhh	18	2.50	117	1.42	3.37	0.05	0.42
	hdh	23	0.49	1297	0.13		0.05	0.04
	hhd	20	1.84	91	1.83		0.9	0.54
	ddd	16	4.92					

Table 6.6: Key model parameters showing the variation in adsorption and surface composition for 2 mM R1/R2/SLES, at 25°C, in NRW containing 1x10^{-6} M NaOH.

On increasing solution composition of SLES, its adsorbed amount increases, but to a much lesser extent than was observed for $C_{12}E_8$. As was observed with R1/R2/$C_{12}E_8$, R1 competes more favourably for the interface than R2, due to its smaller headgroup size. The total adsorption values increase in solutions progressively richer in SLES, and are up to 40% higher than those of only R1/R2, indicating synergistic behaviour between the rhamnolipids and SLES which is not observed in the binary R1/R2 mixtures.[4] Figure 6.5 (b) shows that R1 dominates surface adsorption, R2 has a surface composition similar to its solution behaviour at the compositions investigated, and SLES is always depleted at the surface. When comparing these data to Figure 6.4 (b) of R1/R2/$C_{12}E_8$, the SLES is more depleted at the interface than the $C_{12}E_8$ is, explained by the relative surface activities of the two surfactants.

For the ternary system of R1/R2/LAS,[5] LAS dominated surface adsorption, with the adsorbed amount of R1 consistently higher than that of R2, as observed here with R1/R2/$C_{12}E_8$ and R1/R2/SLES. A synergy in total adsorption was observed in R1/R2/LAS, with a maximum adsorption value of 3.85x10^{-10} mol cm^{-2} at an R1:R2 ratio of 1:1 when the R/LAS ratio was approximately 40/60. This value is higher than ternary rhamnolipid mixtures with either the nonionic or SLES.

The variation in the surface composition of the conventional surfactant $C_{12}E_8$ and SLES, as a function of their solution compositions, for the ternary R1/R2/$C_{12}E_8$ and R1/R2/SLES mixtures, is shown in Figure 6.6. The data for R1/R2/LAS from Chen et al[5] is included for comparison.

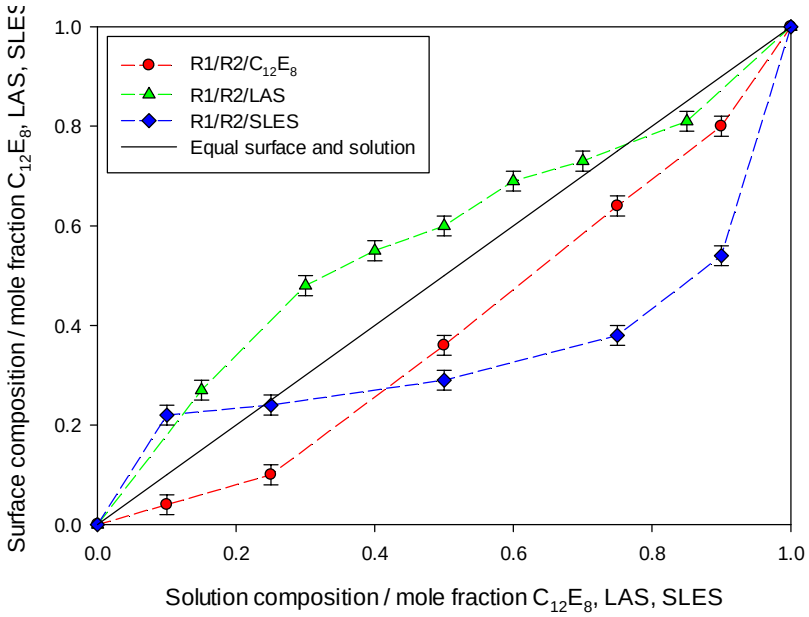

Figure 6.6: Variation in surface composition with solution composition for ternary R1/R2/C mixtures, where C is $C_{12}E_8$, LAS or SLES, at 2 mM concentration, at 25°C, in NRW containing $1x10^{-6}$ M NaOH. R1/R2/LAS data (green) is reproduced from Chen et al.[5]

Figure 6.6 shows $C_{12}E_8$ and SLES to be depleted at the interface, at almost all conventional surfactant solution compositions. The rhamnolipids compete favourably for the interface, to a greater extent in mixtures with SLES due to its lower surface activity than the nonionic $C_{12}E_8$. However, in the R1/R2/LAS[5] mixtures it is the LAS which competes favourably for the interface. This is attributed to its smaller area per molecule and compacted shape, which allows it to reach the interface more easily. The behaviour of LAS with R1 and R2 is similar to the interaction between LAS with both $C_{12}E_8$ and $C_{12}E_{23}$. The nonionic surfactants have very different sized headgroups, and steric interactions affect the interaction at the interface with LAS.[9]

6.4 Five-component biosurfactant / conventional surfactant mixtures

The five-component mixture R1/R2/$C_{12}E_8$/LAS/SLES was investigated at 2 mM concentration, above the mixed CMC over a wide solution composition range and at two R1:R2 ratios, 1:1 and 1:2, to investigate the effect of the rhamnose headgroup on surface behaviour of each of the five components. Each solution composition was measured at the following six isotopic combinations: d-R1/h-R2/h-$C_{12}E_8$/h-LAS/h-SLES, h-R1/d-R2/h-$C_{12}E_8$/h-LAS/h-SLES, h-R1/h-R2/d-$C_{12}E_8$/h-LAS/h-SLES, h-R1/h-R2/h-$C_{12}E_8$/d-LAS/h-SLES, h-R1/h-R2/h-$C_{12}E_8$/h-LAS/d-SLES and d-R1/d-R2/d-$C_{12}E_8$/d-LAS/d-SLES. The areas per molecule for each component were found using a least squares solution to the corresponding six simultaneous equations and from this the surface excess and hence the surface composition of each component could be determined.

6.4.1 R1:R2 ratio 1:1

The variation in adsorbed amount and surface composition with solution composition of the five-component mixture at a 1:1 R1:R2 ratio is shown in Figures 6.7 and 6.8, respectively, and the key model data summarised in Table 6.7. The x axis in the figures indicates the solution composition of the 70% conventional surfactant mole fraction. For example, "0.375/0.375/0.25 $C_{12}E_8$/LAS/SLES" corresponds to a five-component mole fraction of 0.15/0.15/0.26/0.26/0.18 R1/R2/$C_{12}E_8$/LAS/SLES.

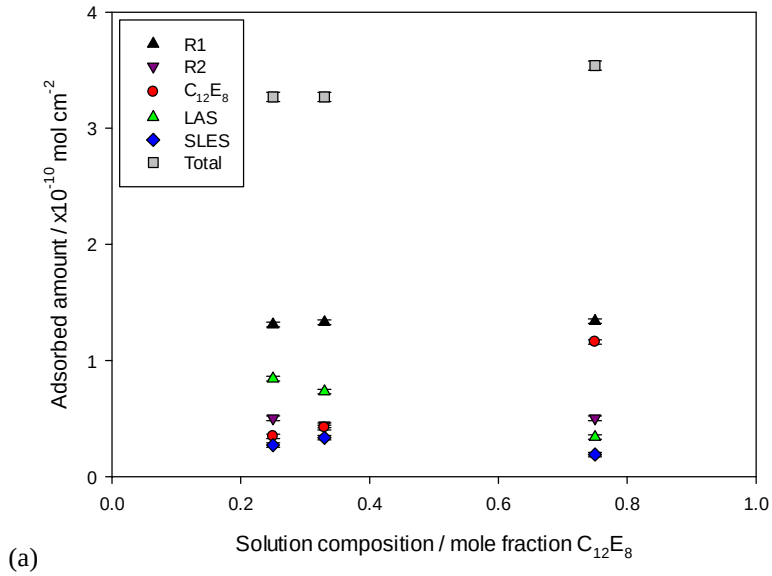

(a)

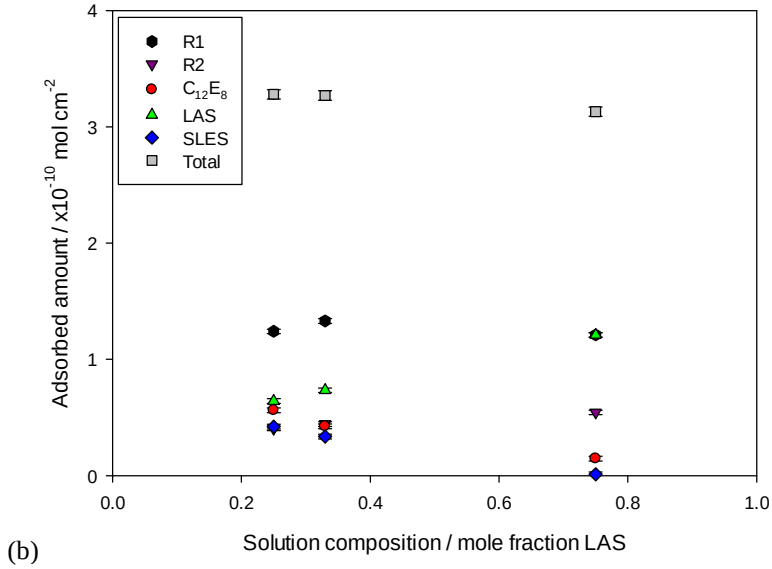

(b)

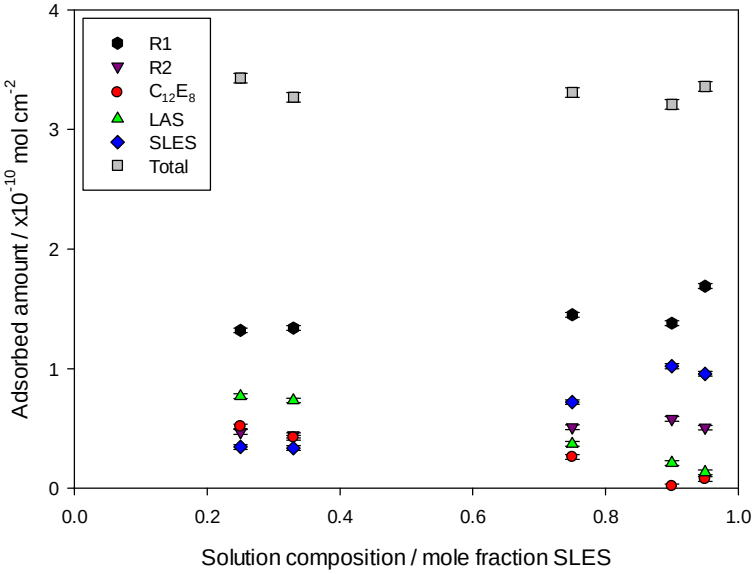

(c)

Figure 6.7: Adsorbed amounts of R1, R2, $C_{12}E_8$, LAS and SLES, and the total adsorption, as a function of (a) $C_{12}E_8$, (b) LAS and (c) SLES solution composition, for 2 mM R1/R2/$C_{12}E_8$/LAS/SLES at 1:1 R1:R2, at 25°C, in NRW containing 1x10^{-6} M NaOH.

Ratio	Contrast	d (± 1)	ρ (± 0.02x10^{-6} Å^2)	A (± 2 Å^2)	Γ (± 0.02x10^{-10} mol cm^{-2})	Γ_{total} (± 0.04x10^{-10} mol cm^{-2})	Solution compos-ition	Surface composition (± 0.02)
0.375/0.375/ 0.25	dhhhh	21	1.95	125	1.32	3.43	0.15	0.39
	hdhhh	30	0.83	355	0.47		0.15	0.14
	hhdhh	32	0.53	322	0.52		0.26	0.15
	hhhdh	31	0.77	216	0.77		0.26	0.22
	hhhhd	42	0.34	481	0.35		0.18	0.10
	ddddd	19	4.24					
0.33/0.33/ 0.33	dhhhh	19	2.20	125	1.33	3.27	0.15	0.41
	hdhhh	30	0.81	375	0.44		0.15	0.14
	hhdhh	36	0.45	392	0.42		0.23	0.13
	hhhdh	30	0.77	226	0.73		0.23	0.22
	hhhhd	46	0.33	495	0.34		0.23	0.10
	ddddd	19	4.20					
0.125/0.125/ 0.75	dhhhh	23	2.13	115	1.45	3.31	0.15	0.44
	hdhhh	31	0.85	325	0.51		0.15	0.15
	hhdhh	40	0.34	638	0.26		0.09	0.08
	hhhdh	35	0.48	449	0.37		0.09	0.11
	hhhhd	31	0.68	230	0.72		0.52	0.22
	ddddd							
0.05/0.05/ 0.9	dhhhh	23	2.02	120	1.38	3.21	0.15	0.43
	hdhhh	23	1.25	286	0.58		0.15	0.18
	hhdhh	53	0.17	11360	0.02		0.035	0.01
	hhhdh	45	0.29	777	0.21		0.035	0.07
	hhhhd	30	0.84	163	1.02		0.63	0.32
	ddddd	19	4.48					
0.025/0.025/ 0.95	dhhhh	21	2.38	99	1.69	3.36	0.15	0.50
	hdhhh	26	1.06	328	0.51		0.15	0.15
	hhdhh	65	0.16	2181	0.08		0.017	0.02
	hhhdh	51	0.27	1248	0.13		0.017	0.04
	hhhhd	32	0.84	174	0.96		0.66	0.29
	ddddd	19	4.05					

Table 6.7: Key model parameters for 2 mM R1/R2/$C_{12}E_8$/LAS/SLES at 1:1 R1:R2, as a function of SLES solution composition, at 25°C, in NRW containing 1x10^{-6} M NaOH.

Figure 6.7 shows a system where R1 competes most favourably for the interface. The surface excesses of R2 are consistently lower than R1 in all cases, due to the packing constraints associated with its bulkier headgroup. This is similar to the behaviour observed between the mixing of $C_{12}E_3$ and $C_{12}E_8$[10,11] where the bulkier E_8 headgroup of $C_{12}E_8$ rendered it less able to adsorb to the interface.

No significant change in total adsorption can be seen upon changing of any conventional component. However the absolute total adsorption is considerably higher than that of the original ternary mixtures or any of the individual components (pure R1, R2 and LAS adsorbed amounts are 2.89, 1.91 and 3.1 x 10^{-10} mol cm^{-2}, respectively.)[12] The introduction of rhamnolipids to the conventional system thus induces a pronounced synergy in total adsorption. In the ternary system at 0.05/0.05/0.9 $C_{12}E_8$/LAS/SLES, the total surface excess was 2.82x10^{-10} mol cm^{-2}, but with 30% of the total

surfactant replaced by rhamnolipids, a dramatic 20% increase to $3.36x10^{-10}$ mol cm^{-2} occurs. The addition of the very surface-active rhamnolipids, combined with the greater number of components in the system, appears to have a large effect on optimising the packing of surfactants at the air/water interface.

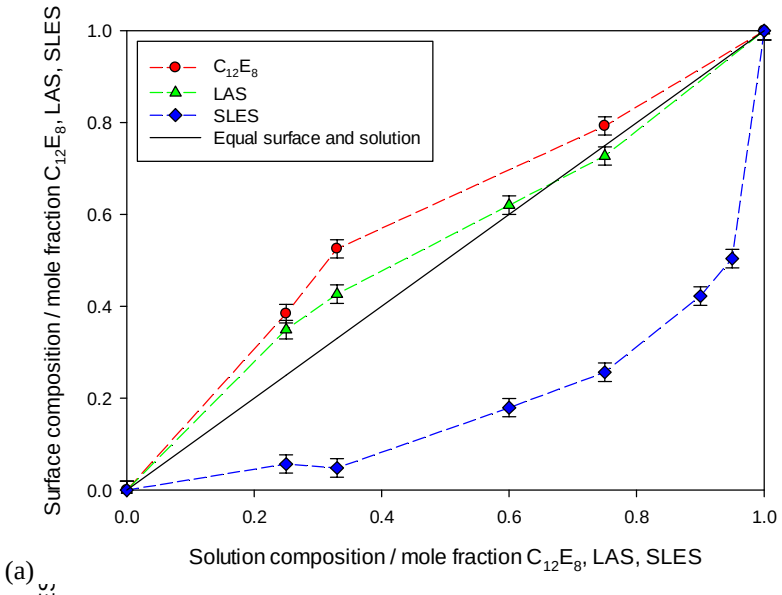

(a)

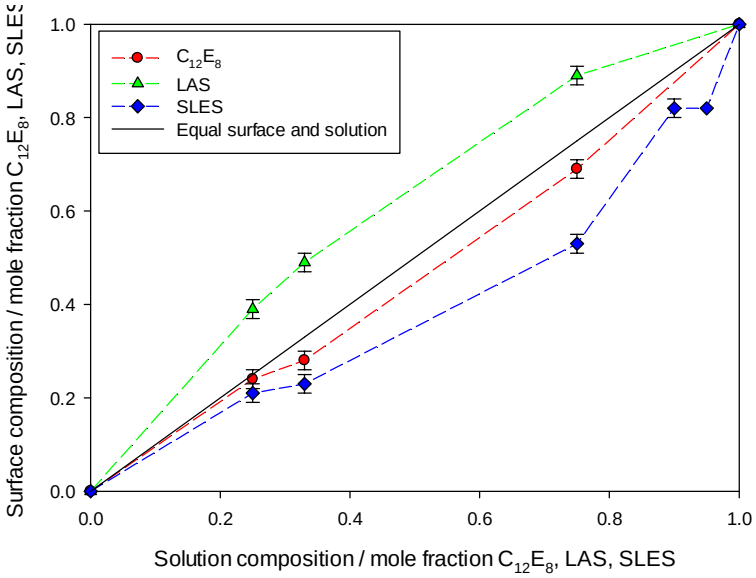

(b)

Figure 6.8: Surface composition of $C_{12}E_8$, LAS, SLES as (a) $C_{12}E_8$/LAS/SLES mixture and (b) 70% of the equivalent ternary proportion of the five-component R1/R2/$C_{12}E_8$/LAS/SLES mixture at 1:1 R1:R2, both as a function of $C_{12}E_8$, LAS and SLES solution compositions, at 2 mM, at 25°C, in NRW containing $1x10^{-6}$ M NaOH.

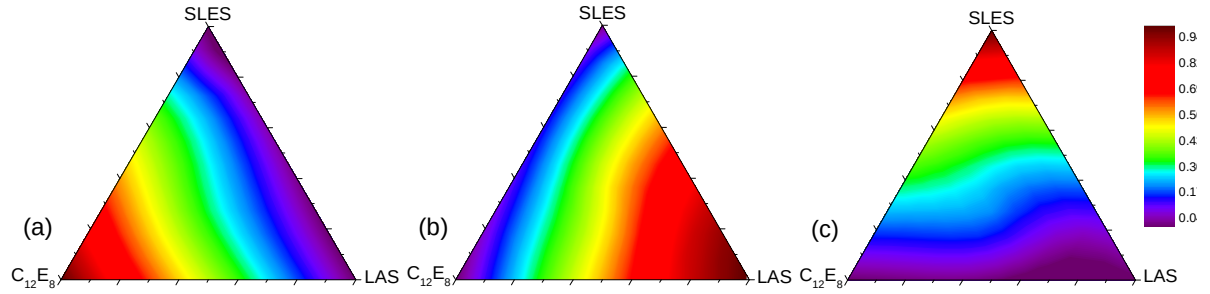

Figure 6.9: The variation in surface composition with solution composition of (a) $C_{12}E_8$, (b) LAS and (c) SLES in the 5-component mixture at R1:R2 ratio 1:1.

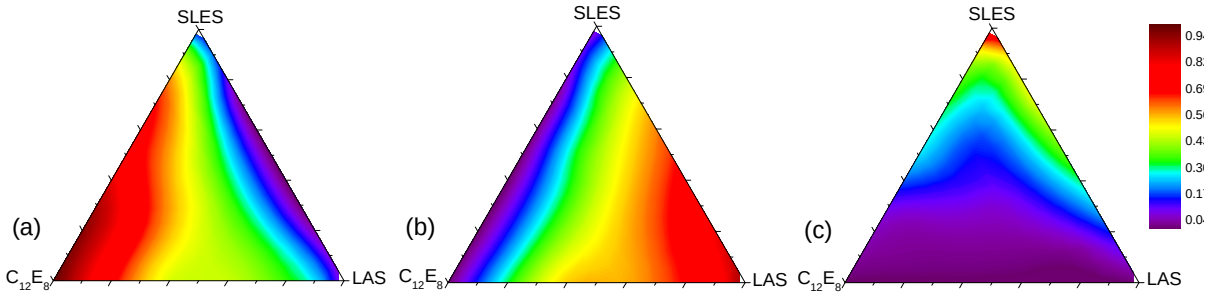

Figure 6.10: Original ternary contour diagrams showing the variation in surface composition with solution composition of (a) $C_{12}E_8$, (b) LAS and (c) SLES in the ternary $C_{12}E_8$/LAS/SLES system.

In the original $C_{12}E_8$/LAS/SLES ternary system, $C_{12}E_8$, and to a lesser extent LAS, dominate surface adsorption over much of the solution composition and very little SLES is present at the interface even at very high SLES solution compositions. However, when 30% of the conventional surfactants are replaced by rhamnolipids in the ratio 1:1 R1:R2, the rhamnolipids dominate the interface, but a rather unexpected behaviour occurs as this dominance is now at the expense of the $C_{12}E_8$ and LAS rather than the SLES. At a solution composition of 0.15/0.15/0.035/0.035/0.63 (i.e. 0.05/0.05/0.9 solution composition for the ternary conventional surfactant mixture) the surface composition is 0.36/0.17/0.08/0.10/0.29, with an effective ternary surface composition of 0.17/0.21/0.62. The original ternary conventional surface composition at this solution composition 0.05/0.05/0.9 was 0.36/0.22/0.42. On addition of rhamnolipids, the SLES surface composition appears to be closer to its solution composition, the $C_{12}E_8$ composition is now much lower than it was in the absence of rhamnolipids, and the LAS composition is almost unchanged.

Figures 6.9 and 6.10 show that the surface composition of SLES is most affected by the addition of rhamnolipids and it is now much closer to its solution composition, but also the $C_{12}E_8$ is affected in that it shows mixing behaviour closer to the solution composition over the solution composition range. The pronounced surface dominance of $C_{12}E_8$ over SLES in the original contour diagram (Figure

6.10 (a)) is no longer observed. These effects are similar to those observed for the ternary mixtures in the presence of Na^+ and Ca^{2+} electrolyte (Chapter 5).

6.4.2 R1:R2 ratio 1:2

The surface adsorption behaviour for the five-component mixture was also studied at a 1:2 R1:R2 ratio, close to the natural ratio of abundance of R1:R2 in rhamnolipids produced by *P. aeruginosa*. The variation in the adsorbed amount of each component as a function of solution composition of $C_{12}E_8$, LAS and SLES, and the total adsorption, is shown in Figure 6.11, with a selection of the data summarised in Table 6.8, as a function of SLES solution composition. As described in Section 6.4.1, the conventional surfactant solution composition given in Table 6.8 and Figures 6.11 and 6.12 is the effective composition of the remaining 70% conventional surfactant mole fraction.

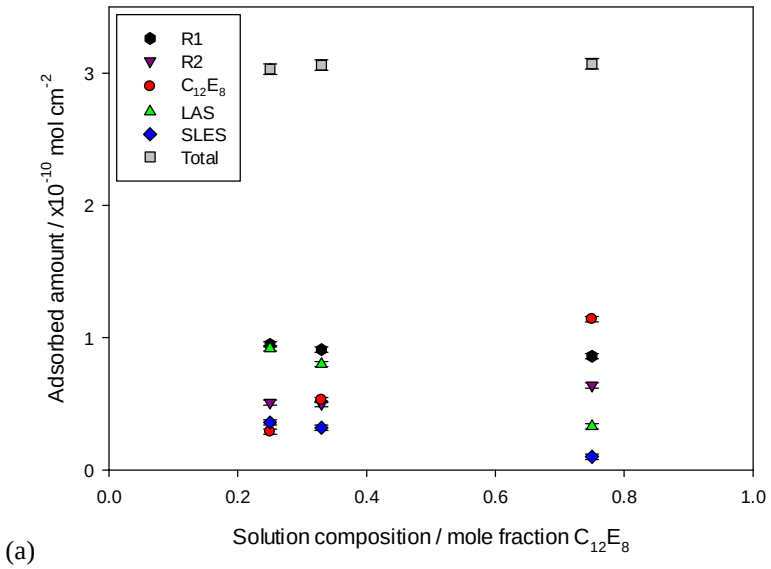

(a)

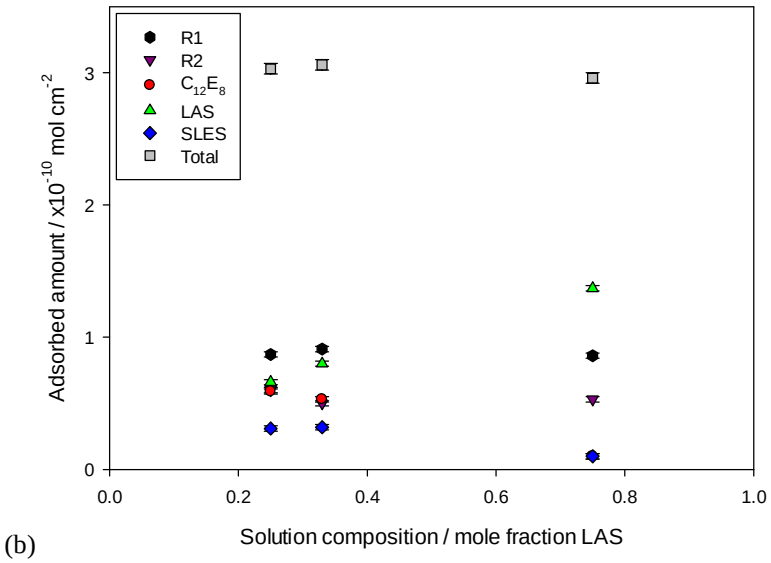

(b)

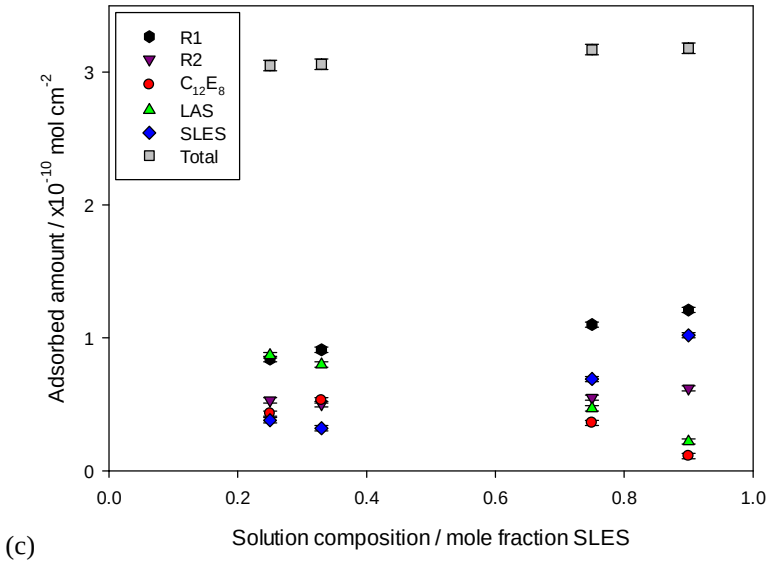

(c)

Figure 6.11: Adsorbed amounts of R1, R2, $C_{12}E_8$, LAS and SLES, and the total adsorption, as a function of (a) $C_{12}E_8$, (b) LAS and (c) SLES solution composition, for 2 mM R1/R2/$C_{12}E_8$/LAS/SLES at 1:2 R1:R2, at 25°C, in NRW containing 1x10^{-6} M NaOH.

Ratio	Contrast	d (± 1)	ρ (± 0.02x10^{-6} Å^2)	A (± 2 Å^2)	Γ (± 0.05x10^{-10} mol cm^{-2})	Γ_{total} (± 0.04x10^{-10} mol cm^{-2})	Solution compos-ition	Surface composition (± 0.02)
0.375/0.375/ 0.25	dhhhh	17	1.56	198	0.84	3.05	0.1	0.28
	hdhhh	16	1.51	311	0.53		0.2	0.17
	hhdhh	18	0.78	383	0.43		0.26	0.14
	hhhdh	22	1.06	190	0.87		0.26	0.29
	hhhhd	37	0.35	441	0.38		0.18	0.12
	ddddd	15	4.92					
0.33/0.33/ 0.33	dhhhh	16	1.72	182	0.91	3.06	0.1	0.30
	hdhhh	20	1.11	332	0.50		0.2	0.16
	hhdhh	28	0.51	315	0.53		0.23	0.17
	hhhdh	13	1.57	208	0.80		0.23	0.26
	hhhhd	20	0.55	522	0.32		0.23	0.11
	ddddd	17	4.46					
0.125/0.125/ 0.75	dhhhh	18	1.81	151	1.10	3.17	0.1	0.35
	hdhhh	21	1.17	303	0.55		0.2	0.17
	hhdhh	35	0.35	463	0.36		0.09	0.11
	hhhdh	24	0.65	355	0.47		0.09	0.15
	hhhhd	14	1.28	240	0.69		0.52	0.22
	ddddd	17	4.67					
0.05/0.05/ 0.9	dhhhh	21	1.66	137	1.21	3.18	0.1	0.38
	hdhhh	28	1.07	268	0.62		0.2	0.19
	hhdhh	45	0.193	1556	0.11		0.035	0.03
	hhhdh	21	0.53	751	0.22		0.035	0.07
	hhhhd	20	1.19	163	1.02		0.63	0.32
	ddddd	17	4.61					

Table 6.8: Key model parameters for 2 mM R1/R2/$C_{12}E_8$/LAS/SLES at 1:2 R1:R2, at 25°C, in NRW containing 1x10^{-6} M NaOH.

Figure 6.11 with a R1:R2 ratio of 1:2 shows a system qualitatively very similar system to that where the R1:R2 ratio was 1:1 (Figure 6.7). However, here the changes observed on the partial replacement of rhamnolipids are not as great as they were with 1:1 R1:R2 ratio, due to the higher relative solution composition of the less surface-active R2.

The total adsorbed amount for five-component mixtures containing R1:R2 at a ratio of 1:2 are significantly higher than those of the original ternary surfactant system. However, these values are systematically lower than when the R1:R2 ratio is 1:1 (Section 6.4.1). For example at composition 0.375/0.375/0.25 at an R1:R2 ratio of 1:1 the total adsorption is 3.42x10^{-10} mol cm^{-2}, but at a 1:2 ratio it is only 3.05x10^{-10} mol cm^{-2}. This is attributed to a higher proportion of R2 in solution, which has a larger hydrophilic headgroup and thus a lower surface activity.

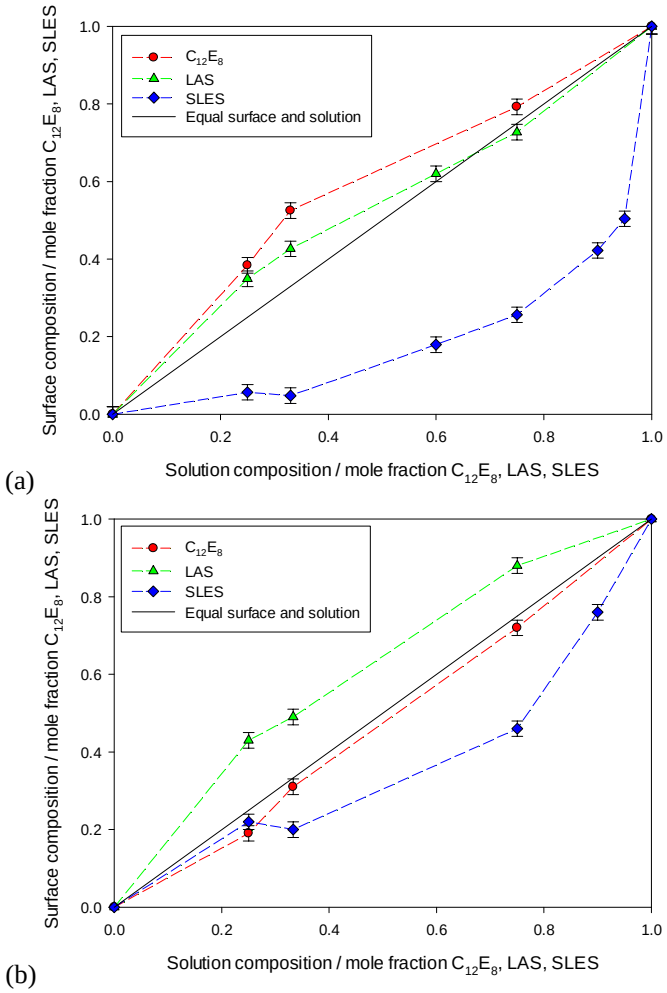

Figure 6.12: Surface composition of $C_{12}E_8$, LAS, SLES as (a) $C_{12}E_8$/LAS/SLES mixture and (b) 70% of the equivalent ternary proportion of the five-component R1/R2/$C_{12}E_8$/LAS/SLES mixture at 1:2 R1:R2. Both are as a function of $C_{12}E_8$, LAS and SLES solution composition, at 2 mM, 25°C, in NRW containing 1x10^{-6} M NaOH.

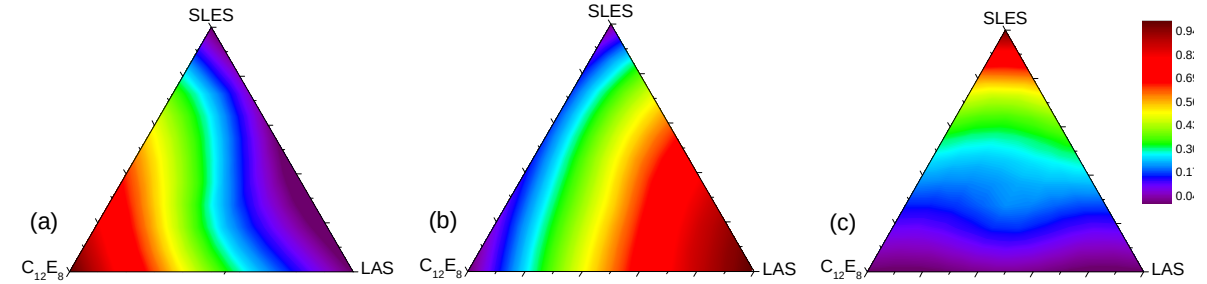

Figure 6.13: The variation in surface composition with solution composition of (a) $C_{12}E_8$, (b) LAS and (c) SLES in the 5-component mixture at R1:R2 ratio 1:2.

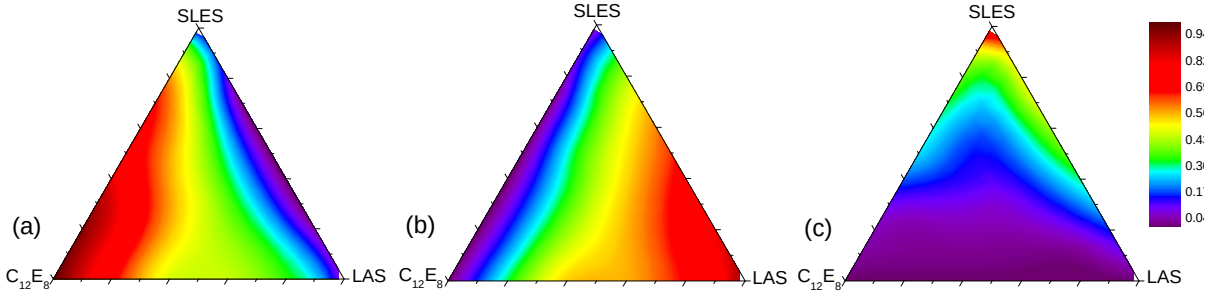

Figure 6.14: Original ternary contour diagrams showing the variation in surface composition with solution composition of (a) $C_{12}E_8$, (b) LAS and (c) SLES in the ternary $C_{12}E_8$/LAS/SLES system.

Figure 6.12 shows a variation in surface composition which is similar to that observed with an R1:R2 ratio of 1:1 (Figure 6.8), where the surface composition of each of the three conventional surfactants is drawn closer to its solution composition on the addition of rhamnolipids. However, the extent to which this occurs is less than with a 1:1 ratio.

The ternary contour diagrams show a summary of the variation in the surface composition of the three conventional surfactants $C_{12}E_8$, LAS and SLES, in the presence of 30% replacement of rhamnolipids in the ratio R1:R2 1:2 (Figure 6.13), and, for comparison, in the absence of any rhamnolipids (Figure 6.14). The greatest change is seen with SLES where it has a higher affinity for the interface in the presence of added rhamnolipids, similar to that observed on the addition of electrolyte.

	1:1 R1:R2	1:2 R1:R2
Average R1	0.41 (0.15)	0.31 (0.1)
Average R2	0.15 (0.15)	0.18 (0.2)
Ratio R1:R2 at surface	2.7 : 1	1.7 : 1
Ratio R:C at surface	1.3 : 1 (0.4:1)	1 : 1 (0.4:1)

Table 6.9: Average rhamnolipid surface compositions for the five-component mixture R1/R2/$C_{12}E_8$/LAS/SLES at R1:R2 ratios 1:1 and 1:2. Data in brackets are the solution compositions values included for comparison.

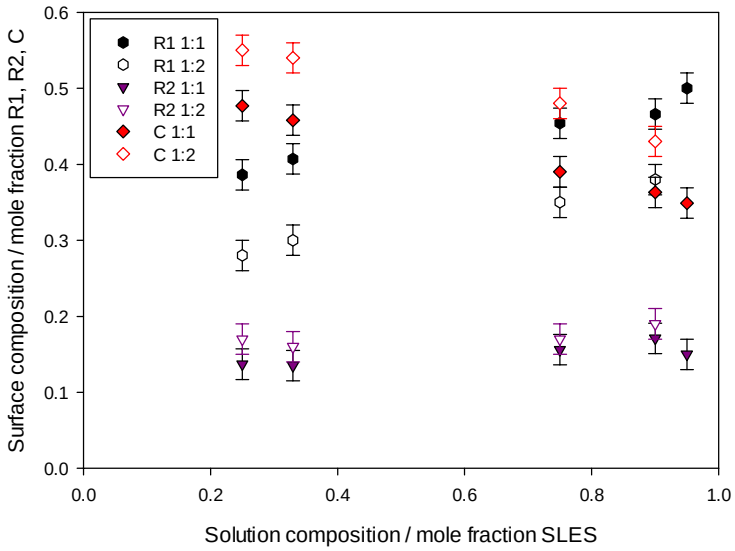

Figure 6.15: Change in surface composition of R1, R2 and total conventional surfactant with variation of SLES solution composition, for 2 mM R1/R2/$C_{12}E_8$/LAS/SLES at 1:1 and 1:2 R1:R2, at 25°C, in NRW containing $1x10^{-6}$ M NaOH.

The key surface data for the rhamnolipids summarised in Table 6.9 clearly show the favourable interfacial adsorption of the rhamnolipids. At a solution composition of 0.3, the average total surface composition of the rhamnolipids is almost twice as high at 0.56 for 1:1, but lower at 0.49 for 1:2, indicating the preferential adsorption of R1 over R2. Interestingly, in increasingly SLES-rich

solutions, R1 becomes increasingly dominant at the interface whilst the surface composition of the total conventional surfactant actually decreases. This effect is more pronounced at an R1:R2 ratio of 1:1 than 1:2, as shown in Figure 6.15. The variation in SLES solution composition has little effect on the surface behaviour of R2 and, within error, it is independent of the R1:R2 ratio.

6.5 Discussion

The replacement of conventional synthetic surfactants with "greener", biocompatible alternatives is of increasing interest. Rhamnolipids, the most well-known glycolipid biosurfactants, have been shown to exhibit high emulsifying properties,[13] excellent surface tension-lowering abilities[14] as well as biocompatibility and biodegradability. All of these characteristics render them potentially very useful as commercial detergents. It is possible that the blending of biosurfactants with conventional surfactants would initially be used, so a thorough understanding of their surface adsorption and solution behaviour as multicomponent mixtures is crucial.

On partial replacement of the ternary conventional surfactant mixture $C_{12}E_8$/LAS/SLES with the highly surface-active rhamnolipid biosurfactants to give a five-component mixture, a very different surface behaviour has been observed. The rhamnolipids are found to always dominate the surface adsorption, with a surface composition almost twice as high as its solution composition. R1 adsorption is favoured over R2 due to the packing constraints associated with the larger R2 molecule which contains an extra rhamnosyl group on its hydrophilic portion. The addition of rhamnolipids results in a surface composition of the ternary mixture much closer to its solution composition, similar to that observed on the addition of electrolyte to the ternary conventional surfactant system. The impact upon the SLES adsorption is particularly pronounced. In the ternary mixture it is more favourable for the SLES (or SDS) to be in the bulk rather than at the interface, but the addition of the weakly anionic rhamnolipids mitigates any unfavourable interactions.

The most remarkable change on addition of rhamnolipids to the ternary conventional surfactant mixture is in the pronounced synergy in terms of enhanced adsorption. It is possible that the increased number of components in the system and the packing arrangements of the multicomponent mixtures

mitigate the unfavourable interactions between the anionic headgroups and lessen the packing constraints seen in the ternary surfactant mixture. A synergistic enhancement in adsorption was also observed by Chen et al[5] with R1/R2/LAS which was not observed in the binary R1/R2 or R2/LAS mixtures. Conversely, due to the more extreme packing constraints of the sophorolipid biosurfactants AS and LS with LAS, no such synergy was reported.[7] This confirms the importance of the size and hydrophobicity of the headgroup in dictating surface adsorption behaviour.

The barriers to using rhamnolipids and other biosurfactants as commercial surfactants include the costs of large-scale production, low production yields and the difficulty and cost-effectiveness of purifying and separating the biosurfactant mixtures into their separate components. Manufacturing costs are often extremely high[15] and much higher than that of current conventional alternatives, with the raw materials comprising up to 30% of the production cost.[16] In addition, *P. aeruginosa*, one of the main rhamnolipids producers, is an opportunistic human pathogen, which brings about understandable safety concerns for large-scale production. However, non-pathogenic rhamnolipids producers such as *P. chlororaphis*[17] and *P. alcaligenes*[18] are becoming increasingly viable as substitutes for future use in industry. Establishing sufficiently high and viable yields is stimulating much activity, as recently filed patents indicate.[19] More importantly, the many positive attributes which come from using biosurfactants such as rhamnolipids, particularly their high biodegradability, low toxicity, ability to be grown on renewable hydrophobic and hydrophilic feedstocks[20] and their exceptional surface activity, mean that the use of rhamnolipids is increasingly becoming a serious alternative to petroleum-derived chemical surfactants.[21]

References: Chapter 6

1. Ozdemir, G.; Peker, S.; Helvaci, S. S., *Colloids and Surfaces A: Physicochemical and Engineering Aspects* **2004,** *234* (1-3), 135-143.
2. Helvaci, S. S.; Peker, S.; Ozdemir, G., *Colloids and Surfaces B: Biointerfaces* **2004,** *35* (3-4), 225-233.
3. Peker, S.; Helvaci, S.; Ozdemir, G., *Langmuir* **2003,** *19* (14), 5838-5845.
4. Chen, M. L.; Penfold, J.; Thomas, R. K.; Smyth, T. J. P.; Perfumo, A.; Marchant, R.; Banat, I. M.; Stevenson, P.; Parry, A.; Tucker, I.; Grillo, I., *Langmuir* **2010,** *26* (23), 18281-92.
5. Chen, M.; Penfold, J.; Thomas, R. K.; Smyth, T. J. P.; Perfumo, A.; Marchant, R.; Banat, I. M.; Stevenson, P.; Parry, A.; Tucker, I.; Grillo, I., *Langmuir* **2010,** *26* (23), 17958-17968.
6. Penfold, J.; Staples, E.; Thompson, L.; Tucker, I.; Hines, J.; Thomas, R. K.; Lu, J. R., *Langmuir* **1995,** *11* (7), 2496-2503.
7. Chen, M.; Dong, C. C.; Penfold, J.; Thomas, R. K.; Smyth, T., J. P.; Perfumo, A.; Marchant, R.; Banat, I. M.; Stevenson, P.; Parry, A.; Tucker, I.; Campbell, R. A., *Langmuir* **2011,** *27* (14), 8854-8866.
8. Staples, E. J.; Thompson, L.; Tucker, I.; Penfold, J., *Langmuir* **1994,** *10* (11), 4136-4141.
9. Penfold, J.; Thomas, R. K.; Dong, C. C.; Tucker, I.; Metcalfe, K.; Golding, S.; Grillo, I., *Langmuir* **2007,** *23* (20), 10140-10149.
10. Penfold, J.; Staples, E.; Thompson, L.; Tucker, I., *Colloids and Surfaces A: Physicochemical and Engineering Aspects* **1995,** *102*, 127-132.
11. Penfold, J.; Staples, E.; Tucker, I.; Thomas, R. K., *Journal of Colloid and Interface Science* **1998,** *201*, 223-232.
12. Chen, M. DPhil thesis. University of Oxford, 2010.
13. Patel, R. M.; Desai, A. J., *Journal of Basic Microbiology* **1997,** *37* (4), 281-286.
14. Guerra-Santos, L.; Käppeli, O.; Fiechter, A., *Applied and Environmental Microbiology* **1984,** *48* (2), 301-305.
15. Lang, S.; Wullbrandt, D., *Applied Microbiology and Biotechnology* **1999,** *51* (1), 22-32.
16. Cameotra, S. S.; Makkar, R. S., *Applied Microbiology and Biotechnology* **1998,** *50* (5), 520-529.
17. Gunther IV, N. W.; Nuñez, A.; Fett, W.; Solaiman, D. K. Y., *Applied and Environmental Microbiology* **2005,** *71* (5), 2288-2293.
18. Oliveira, F. J. S.; Vazquez, L.; de Campos, N. P.; de França, F. P., *Process Biochemistry* **2009,** *44* (4), 383-389.
19. Gunther, N. W.; Solaiman, D. K. Y.; Fett, F. W. Processes for the production of rhamnolipids. 2007.
20. Zhu, Y.; Gan, J.-J.; Zhang, G.-L.; Yao, B.; Zhu, W.-J.; Meng, Q., *Journal of Zhejiang University SCIENCE A* **2007,** *8* (9), 1514-1520.
21. Banat, I. M.; Makkar, R. S.; Cameotra, S. S., *Applied Microbiology and Biotechnology* **2000,** *53* (5), 495-508.

Chapter 7

Solution behaviour of multicomponent biosurfactant / conventional surfactant mixtures

The solution self-assembly behaviour of the ternary conventional surfactant mixture $C_{12}E_8$/LAS/SLES and the effect of its partial replacement with the rhamnolipid biosurfactants R1 and R2 have been investigated using SANS at relatively low concentrations (up to 50 mM). In this chapter, the effect of the R1:R2 ratio, rhamnolipid/conventional surfactant (R/C) ratio, LAS solution composition and overall solution concentration on the solution aggregate behaviour is presented and discussed.

7.1 Literature review

Small angle neutron scattering has proven to be an extremely successful technique for investigating the structure and composition of aggregate microstructures across a wide range of length scales. Through the use of D/H isotopic substitution, it has been possible to probe the composition of mixed micelles in nonionic/nonionic,[1] anionic/nonionic,[2,3,4,5] and cationic/nonionic surfactant mixtures.[6] The techniques of light scattering,[7,8] fluorescence[7,9] and NMR[10] have also proved to be useful in obtaining information on micelle compositions as well as their shape and size.

The solution aggregate behaviour of nonionic polyethylene glycol surfactants such as $C_{12}E_8$[3,11] and linear alkylbenzene sulfonates[11,12,13] have been well studied. Recently Xu et al[14,15] investigated the solution behaviour of SLES as a function of the alkyl chain length and size of the ethylene oxide (EO) group. In dilute aqueous solution, $C_{12}E_8$, LAS and SLES all form small globular micelles in their pure forms, with aggregation numbers of $C_{12}E_8$ reported as 105 at 25 mM,[3,11] ~40 for LAS at 25 mM[11,13] and ~90 for SLES at 20 mM.[16] At higher concentrations $C_{12}E_8$ and SLES still form globular micelles due to their relatively large headgroup areas and high spontaneous curvatures, but LAS has a much lower spontaneous curvature and tends to form planar structures at higher concentrations.[12,17]

A wide range of solution microstructures are formed in anionic/nonionic mixtures, and the structure and composition of mixed micelles can be determined using contrast variation and the selective deuteration of different surfactant components.[2,4] The aggregation behaviour for the binary mixtures $C_{10}E_3$/LAS,[18] $C_{12}E_8$/LAS,[11] and SDS with $C_{12}E_6$ and $C_{12}E_8$[3] are qualitatively relevant to this work. For all mixtures, modest micellar growth and a reduction in the charge on the micelle was observed in solutions richer in the nonionic surfactant. For SDS/$C_{12}E_6$ and SDS/$C_{12}E_8$, growth is more evident in solutions with $C_{12}E_6$ because of its smaller headgroup and lower spontaneous micelle curvature than $C_{12}E_8$. The electrostatic (for anionic-rich) and steric (for nonionic-rich) contributions play a large role in these anionic/nonionic mixtures.

There is very little literature concerning the mixing behaviour in solution for mixtures of biosurfactants on their own and with conventional ionic or nonionic surfactants. Exceptions to this include work by Chen et al, who studied the mixing behaviour in solution of the rhamnolipids R1 and R2[19] and those with the anionic surfactant LAS.[17] For R1 and R2, small globular micelles existed for both biosurfactants at relatively low concentrations with aggregation numbers at 20 mM of 47 and 26, respectively, at pH 9 controlled by buffer. At higher concentrations (50 mM) R1 formed lamellar L_α structures, whereas R2 remained as small globular micelles up to 100 mM due to its higher micelle curvature from the extra rhamnosyl sugar group on its hydrophilic portion. Thus it followed that R1-rich solutions formed more planar aggregates whilst R2-rich solutions formed predominately micellar structures. Although R1 micelles are slightly more ionic than those of R2, both were found to be only weakly ionic even at high pH, as shown by their relatively low degrees of ionisation. The degree of ionisation decreased as the concentration increased, which can be attributed to micellar growth taking precedence over micellar surface charge. This was also observed by Kuwamoto et al[20] for the growth of spherical micelles of the gemini surfactant 6-methoxy-*N*-(3-sulfopropyl)quinolinium (SPQ).

For the binary and ternary mixtures of the rhamnolipids with LAS,[17] the size of the rhamnolipid rhamnosyl headgroup was found to have a profound effect on the aggregate behaviour of the mixtures. R1/LAS mixtures formed small globular micelles at lower concentrations, which changed to lamellar and unilamellar/multilamellar vesicles (ULV/MLV) at higher concentrations. However, in R2/LAS the

higher preferred curvature of R2 prevented anything but mostly micellar structures forming, unless at very high LAS compositions where lamellar structures formed. In the ternary R1/R2/LAS system, the variation from micellar to more planar structures depended on the size of the rhamnolipid headgroup and the proportion of rhamnolipids to LAS, with R1-rich and LAS-rich solutions forming more planar structures. Chen et al also studied the solution behaviour of LAS with the two forms of the biosurfactant sophorolipid (lactonic, LS, and acidic, AS)[21] which share the same headgroup but a different fatty acid tail structure. The weakly anionic AS formed small globular micelles up to 30 mM concentration, whilst the more hydrophobic, nonionic LS formed unilamellar vesicles at concentrations as low as 2 mM, and a dilute tubules phase at higher concentrations. In binary and ternary mixtures with LAS, micelles, L_1, dominated in both AS and LAS-rich solutions, whilst complex planar structures evolved in increasingly LS-rich solutions.

The work presented in this chapter builds on the work by Chen et al.[17,19] The solution behaviour of a model ternary conventional surfactant mixture, of which the surface behaviour is now well studied (see Chapter 4), is analysed in the absence and presence of the biosurfactant R1 and R2, to form the complex five-component mixture R1/R2/$C_{12}E_8$/LAS/SLES. The impact of varying the rhamnolipid/conventional surfactant (R/C) ratio is studied to observe the effect of varying the proportion of the highly surface-active rhamnolipids, and varying the R1:R2 ratio to indicate the impact of their very different headgroup sizes.

7.2 Conventional surfactant mixtures

The solution behaviour of the binary mixtures $C_{12}E_8$/LAS, $C_{12}E_8$/SLES and LAS/SLES at solution compositions 0.75/0.25, 0.5/0.5 and 0.25/0.75 and the ternary $C_{12}E_8$/LAS/SLES system over the same composition range as with neutron reflectivity measurements (Figure 4.9, Chapter 4), was studied using SANS at relatively low concentrations (10, 25 and 50 mM), at 25°C, in D_2O containing $1x10^{-6}$ M NaOH. Measurements at the lowest concentration (10 mM) were carried out on the SANS2D diffractometer at the ISIS pulsed neutron source at the Rutherford Appleton Laboratory, UK and all other measurements were carried out on the LOQ diffractometer at ISIS, UK and the D33

diffractometer at the ILL, France. All scattering data were fitted using the standard Hayter-Penfold Core-Shell model for interacting globular micelles.[22]

7.2.1 Binary surfactant mixtures

7.2.1.1 $C_{12}E_8$/LAS

Figure 7.1 shows typical $C_{12}E_8$/LAS SANS scattering data as a function of (a) solution concentration and (b) solution composition, with the associated model parameters given in Tables 7.1 and 7.2, respectively.

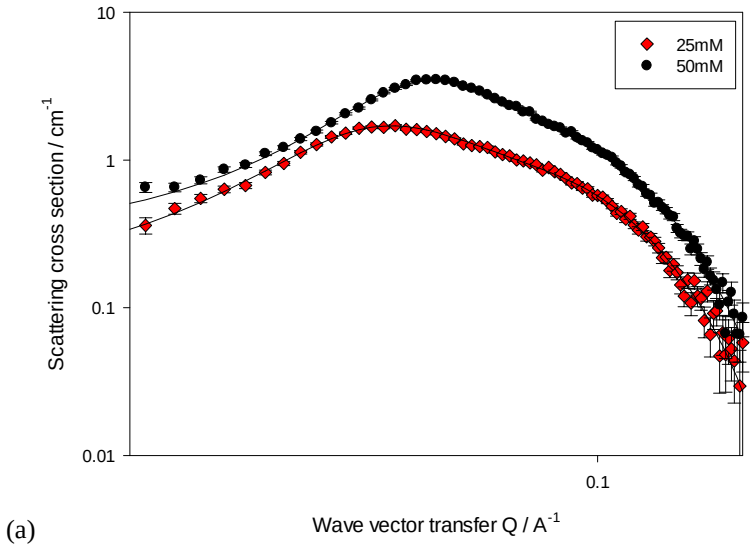

(a)

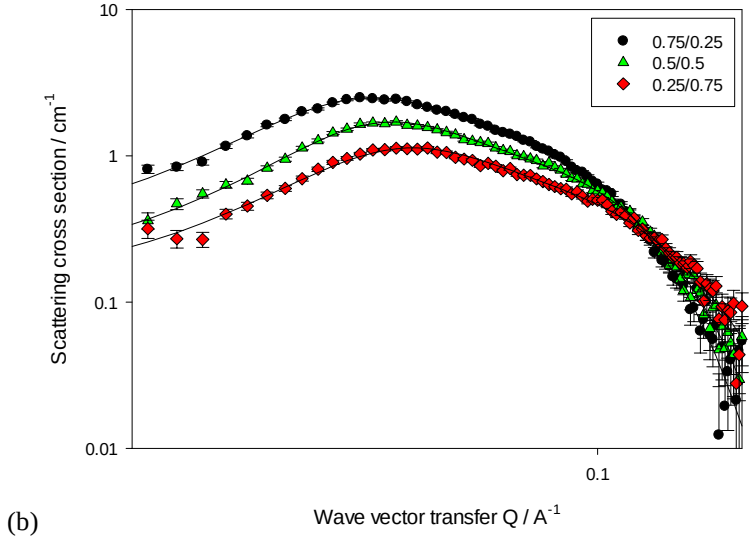

(b)

Figure 7.1: (a) SANS data for 0.5/0.5 $C_{12}E_8$/LAS at 25mM and 50mM, (b) $C_{12}E_8$/LAS at solution compositions 0.75/0.25, 0.5/0.5, 0.25/0.75 at 25mM, both with the associated model fitting (solid lines). All measurements were made at 25°C, in D_2O containing $1x10^{-6}$ M NaOH.

Concentration / mM	Aggregation number, ν ± 5	Surface charge, z ± 1	R1 / ± 1 Å	R2 / ± 1 Å	ext / ± 0.05	ee / ± 0.02
25	76	13	16	21	1.10	1.64
50	81	15	16	21	1.10	1.73

Table 7.1: Core-Shell analysis parameters for 0.5/0.5 $C_{12}E_8$/LAS, at 25 and 50 mM, at 25°C, in D_2O containing $1x10^{-6}$M NaOH.

Solution composition $C_{12}E_8$/LAS	Aggregation number, ν ± 5	Surface charge, z ± 1	R_1 / ± 1 Å	R_2 / ± 1 Å	ext / ± 0.05	ee / ± 0.02
0.75/0.25	98	12	17	24	1.10	1.59
0.5/0.5	76	13	16	21	1.10	1.64
0.25/0.75	62	12	15	19	1.10	1.95

Table 7.2: Core-Shell analysis parameters for $C_{12}E_8$/LAS at solution compositions 0.75/0.25, 0.5/0.5 and 0.25/0.75, at 25mM, at 25°C, in D_2O containing $1x10^{-6}$M NaOH.

The scattering data in Figure 7.1 (a) is consistent with the presence of small globular interacting micelles at 25 mM and 50 mM, indicated by the pattern of scattering at high Q (greater than 0.02 $Å^{-1}$). The micelle Core-Shell model describes the scattering data well. The micelle ellipticity (ee) increases slightly as the solution concentration increases, with values similar to those reported in the literature.[11]

For 25 mM $C_{12}E_8$/LAS, from LAS-rich to $C_{12}E_8$-rich, the scattering at high Q shows a trend of decreasing charge on the micelle, and hence a reduction in the contribution from the interparticle structure factor S(Q), as the solution becomes richer in the nonionic component. The peak in the scattering is shifted to lower Q in increasingly nonionic-rich solutions, indicative of micellar growth. The ellipticity ranges from 1.59 to 1.95 at 25mM as shown in Table 7.2 and these values are similar to those previously reported (between 1.6 and 1.8).[11] Here the micelles become less elliptical in increasingly nonionic-rich solutions, whereas Penfold et al[11] found the ellipticity to increase. It is possible that here the rate of increase in aggregation number in more $C_{12}E_8$-rich solutions is not large enough compared to the change in the effective l_c value (the constraint on the dimensions of R_1) for the ellipticity to increase. The variation in aggregation number for $C_{12}E_8$/LAS mixed micelles at 25 and 50 mM is shown in Figure 7.2.

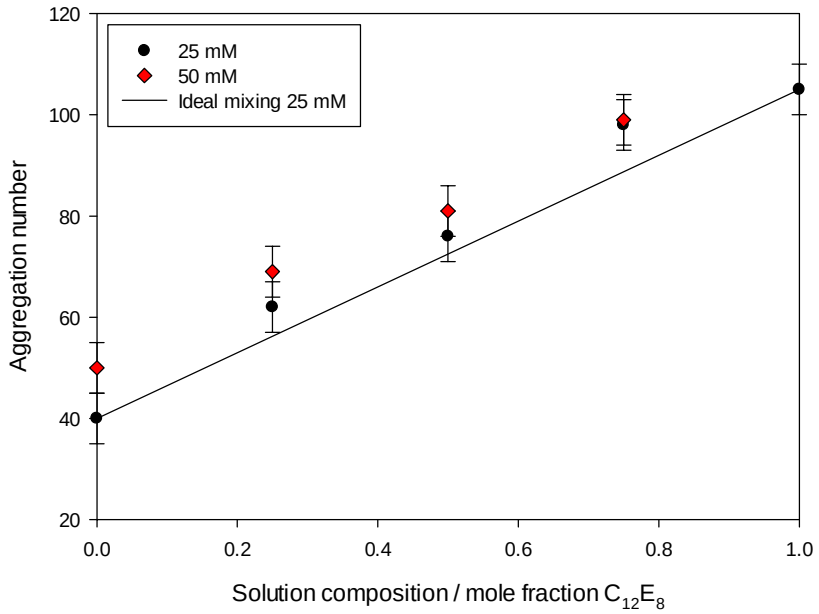

Figure 7.2: Variation in aggregation number for $C_{12}E_8$/LAS at 25 and 50 mM, at 25°C, in D_2O containing $1x10^{-6}$ M NaOH. Literature data for $C_{12}E_8$ and LAS at 25 mM[11] are included for comparison. Data are compared to an ideal mixing line at 25 mM.

The aggregation numbers of pure $C_{12}E_8$ and LAS have been reported as 105 and ~40 at 25 mM, respectively.[11] There is a linear increase in aggregation number in increasingly nonionic-rich solutions, as shown in Figure 7.2, due to the higher number of uncharged molecules screening the anionic charges of the LAS and so reducing the importance of the inter-headgroup electrostatic repulsions. A similar increase in the aggregation number with increasing solution composition of the nonionic component was observed for $C_{10}E_3$/LAS,[18] $C_{12}E_8$/LAS[11] in both D_2O and 0.1 M NaCl, and mixtures of SDS with $C_{12}E_6$ and $C_{12}E_8$.[3] The increase in aggregation number with mole fraction of the nonionic component is very similar at both concentrations, and the values are close to those expected for an ideal variation in aggregation number with solution composition (black line), where the composition of the mixed micelle is the same as that of the bulk solution.

The degree of micelle ionisation, δ, is expressed as the surface charge, z, divided by the aggregation number, ν:

$$\delta = \frac{z}{\nu} \tag{7.1}$$

Table 7.3 shows the variation in degree of ionisation for $C_{12}E_8$/LAS as a function of solution concentration and composition.

Solution composition $C_{12}E_8$/LAS	25mM	50mM
0.75/0.25	0.12	0.13
0.5/0.5	0.17	0.18
0.25/0.75	0.19	0.19

Table 7.3: Variation in degree of ionisation, δ, with solution composition for $C_{12}E_8$/LAS, at 25°C, in D_2O containing $1x10^{-10}$ M NaOH.

All mixtures studied here have relatively low micelle surface charge, z, so the degree of ionisation is relatively low at all concentrations and compositions (typical values for ionic surfactants are of the order of 0.3[23]) showing that the mixed micelles are less strongly charged. However, as expected there is a modest increase in δ values as solutions become more anionic-rich.[3,11] Here this is due to the reduction in aggregation number in increasingly LAS-rich solutions, relative to the surface charge which does not change significantly. There is no significant change in δ with increasing concentration, where a decrease might be expected.[22] This was observed in the R1/R2 mixtures by Chen et al[19] where the degree of ionisation was lower at higher concentration, as the micelles grew in size towards an increasingly rod-like formation, and by Kuwamoto et al[20] due to growth of micelles of the gemini surfactant SPQ, where a more significant increase in aggregation number occurred than in micelle surface charge because of its large headgroup. It may be that here the increase in aggregation number, as the concentration increases, is not great enough, relative to the increase in micelle surface charge, for the degree of ionisation to be significantly reduced.

7.2.1.2 $C_{12}E_8$/SLES

Figure 7.3 shows typical SANS data for $C_{12}E_8$/SLES as a function of (a) solution concentration and (b) solution composition, with the associated model parameters given in Tables 7.4 and 7.5, respectively.

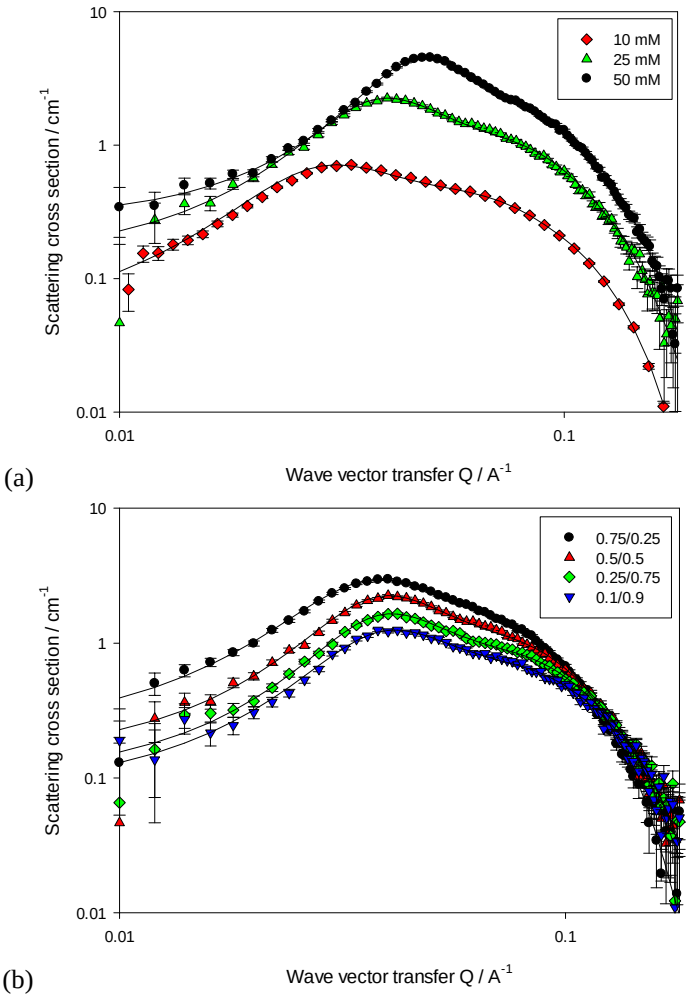

Figure 7.3: SANS data for (a) 0.5/0.5 $C_{12}E_8$/SLES at 25 and 50 mM, and (b) $C_{12}E_8$/SLES at compositions 0.75/0.25, 0.5/0.5, 0.25/0.75 and 0.1/0.9, at 25mM, both with the associated model fitting (solid lines), at 25°C, in D_2O containing $1x10^{-6}$ M NaOH.

Concentration / mM	Aggregation number, ν ± 5	Surface charge, z ± 1	R1 / ± 1 Å	R2 / ± 1 Å	ext / ± 0.05	ee / ± 0.02
10	82	16	18	23	1.11	1.24
25	96	19	18	24	1.10	1.21
50	100	22	18	24	1.10	1.26

Table 7.4: Core-Shell analysis parameters for 0.5/0.5 $C_{12}E_8$/SLES, at 25 and 50 mM, at 25°C, in D_2O containing $1x10^{-6}$ M NaOH.

Solution composition $C_{12}E_8$/SLES	Aggregation number, ν ± 5	Surface charge, z ± 1	R_1 / ±1 Å	R_2 / ±1 Å	ext / ± 0.05	ee / ± 0.02
0.75/0.25	109	15	18	25	1.10	1.31
0.5/0.5	96	19	18	24	1.10	1.21
0.25/0.75	92	19	18	23	1.10	1.16
0.1/0.9	93	17	18	25	1.10	1.12

Table 7.5: Core-Shell analysis parameters for $C_{12}E_8$/SLES mixture at solution compositions 0.75/0.25, 0.5/0.5, 0.25/0.75 and 0.1/0.9, at 25 mM, at 25°C, in D_2O containing $1x10^{-6}$M NaOH.

The scattering data for $C_{12}E_8$/SLES displayed in Figures 7.3 (a) and (b) are consistent with the presence of small globular interacting micelles up to 50 mM concentration and at all solution compositions, as found with $C_{12}E_8$/LAS and other similar anionic/nonionic systems.[3] A more pronounced peak at higher concentrations indicates stronger interactions between the micelles.

As reported for $C_{12}E_8$/SDS,[3] the interaction peak for $C_{12}E_8$/SLES micelles in Figure 7.3 (b) is shifted to slightly lower Q in solutions progressively richer in the nonionic component, signifying micellar growth. The suppression of scattering at low Q in SLES-rich solutions indicates strong micellar interactions. Nonionic-rich solutions also show slightly lower surface charge values, as well as significantly higher ellipticity values, attributed to the $C_{12}E_8$ inducing micellar growth. Figure 7.4 shows the variation in aggregation number with solution composition for $C_{12}E_8$/SLES at 10, 25 and 50 mM.

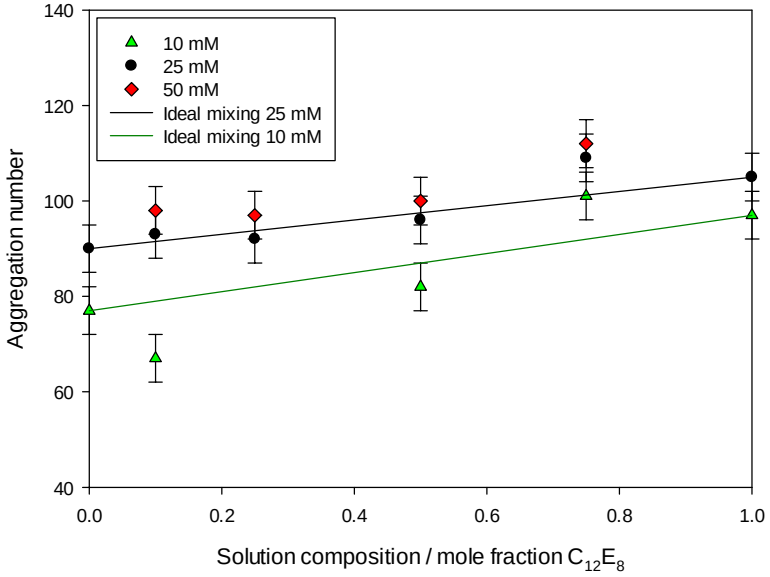

Figure 7.4: Micelle aggregation number for $C_{12}E_8$/SLES at 10, 25 and 50 mM concentration, at 25°C, in D_2O containing $1x10^{-6}$ M NaOH. Literature data for $C_{12}E_8$ at 15 mM[24] (closest measurements to 10 mM - aggregation numbers of $C_{12}E_8$ are comparable at all concentrations) and 25 mM,[11] and SLES at 10 mM[16] are included for comparison. Data are compared to ideal mixing lines at 10 mM and 25 mM.

An increase in the aggregation number is observed with an increasing mole fraction of $C_{12}E_8$ for $C_{12}E_8$/SLES, as seen for $C_{12}E_8$/LAS in Section 7.2.1.1. This is due to the $C_{12}E_8$ with no charge screening the headgroup charges on the anionic headgroups of SLES. Only very modest micellar growth is observed compared to mixtures of $C_{12}E_8$/LAS or $C_{12}E_8$/SDS[3] as the aggregation numbers of the pure $C_{12}E_8$ and SLES are relatively similar (105 at 25 mM[11] and ~90 at 20 mM,[16] respectively).

The aggregation numbers are also consistently higher at higher concentrations for all compositions studied. Light scattering measurements by Blankschtein et al[8] and SANS measurements by Penfold et al[5] and Tucker et al[25] showed nonionic-rich solutions to exhibit micellar growth, although in both data there existed a maximum in the aggregation number, due to a balance between the steric factors from the nonionic component and the electrostatic factors from the anionic component.

At the higher concentrations, the variation in aggregation number corresponds ideally to the variation in solution composition. However, at the lowest concentration measured (10 mM) values do not correlate so well with the ideal mixing line. This may be a result of the 10 mM concentration being sufficiently close to the mixed CMC, so that any non-ideal effects present in the system are visible, such as a different micelle composition to the bulk solution value, depending on the solution composition.[26,27]

Solution composition $C_{12}E_8$/SLES	10mM	25mM	50mM
0.75/0.25	0.12	0.14	0.14
0.5/0.5	0.20	0.20	0.22
0.25/0.75	*	0.21	0.24
0.1/0.9	0.18	0.18	0.24

Table 7.6: Variation in degree of ionisation with solution composition for $C_{12}E_8$/SLES, at 25°C, in D_2O containing $1x10^{-10}$ M NaOH. * indicates not measured.

Table 7.6 shows the variation in degree of ionisation as a function of solution concentration and composition. A modest increase in degree of ionisation is observed with increasing mole fraction of the anionic component. SLES was found to be only weakly charged due to strong binding of the Na^+ counterion.[14.15] As a result, these values are lower than those found in $C_{12}E_6$/SDS and $C_{12}E_8$/SDS mixtures,[3] in which at 25 mM the degree of ionisation, although very low in nonionic-rich mixtures, was almost that of pure SDS (0.25-0.3) in equimolar composition with SDS.[22,28]

7.2.1.3 LAS/SLES

Figure 7.5 shows typical SANS data for LAS/SLES as a function of (a) solution concentration and (b) solution composition, with the associated model parameters shown in Tables 7.7 and 7.8, respectively.

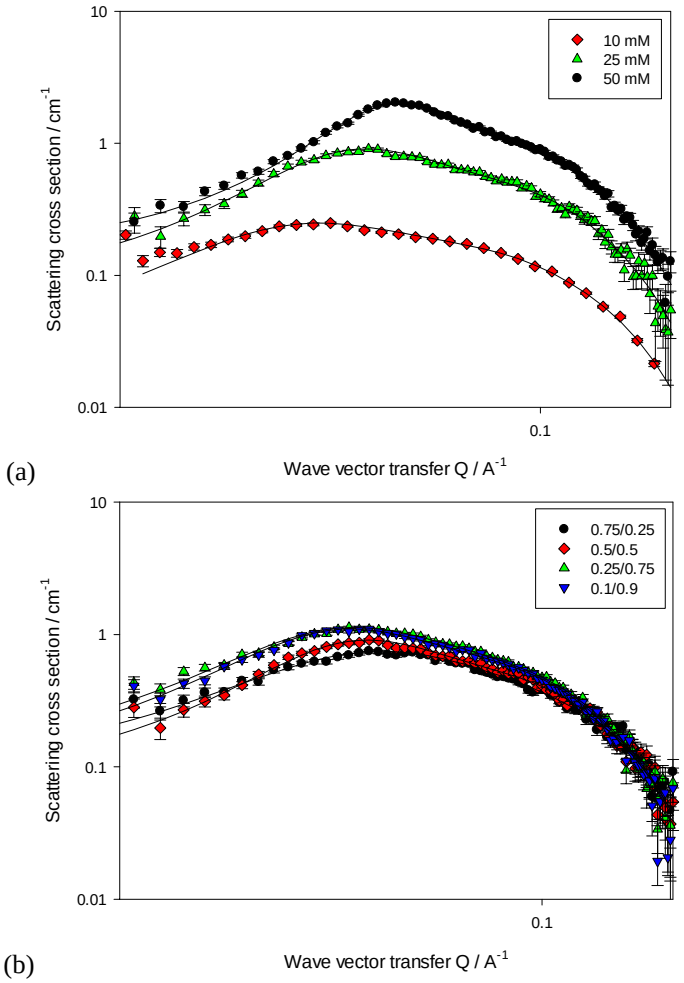

Figure 7.5: SANS data for (a) 0.5/0.5 LAS/SLES at 25 and 50 mM, and (b) LAS/SLES at compositions 0.75/0.25, 0.5/0.5, 0.25/0.75 and 0.1/0.9, at 25mM, both with the associated model fitting, at 25°C, in D_2O containing $1x10^{-6}$ M NaOH.

Concentration / mM	Aggregation number, ν ± 5	Surface charge, z / ± 1	R_1 / ± 1 Å	R_2 / ± 1 Å	ext / ± 0.05	ee / ± 0.02
10	52	8	15	18	1.00	1.79
25	70	13	16	21	1.10	1.50
50	80	17	20	23	1.35	1.00

Table 7.7: Core-Shell micelle analysis parameters for 0.5/0.5 LAS/SLES, at 25 and 50 mM, in D_2O containing $1x10^{-6}$ M NaOH.

Solution composition LAS/SLES	Aggregation number, ν ± 5	Surface charge, z / ± 1	R_1 / ± 1 Å	R_2 / ± 1 Å	ext / ± 0.05	ee / ± 0.02
0.75/0.25	60	9	15	18	1.10	1.69
0.5/0.5	70	13	16	21	1.10	1.50
0.25/0.75	87	11	17	23	1.10	1.43
0.1/0.9	92	12	18	25	1.10	1.29

Table 7.8: Core-Shell micelle analysis parameters for LAS/SLES mixture at solution compositions 0.75/0.25, 0.5/0.5, 0.25/0.75 and 0.1/0.9, at 25 mM, in D_2O containing $1x10^{-6}$ M NaOH.

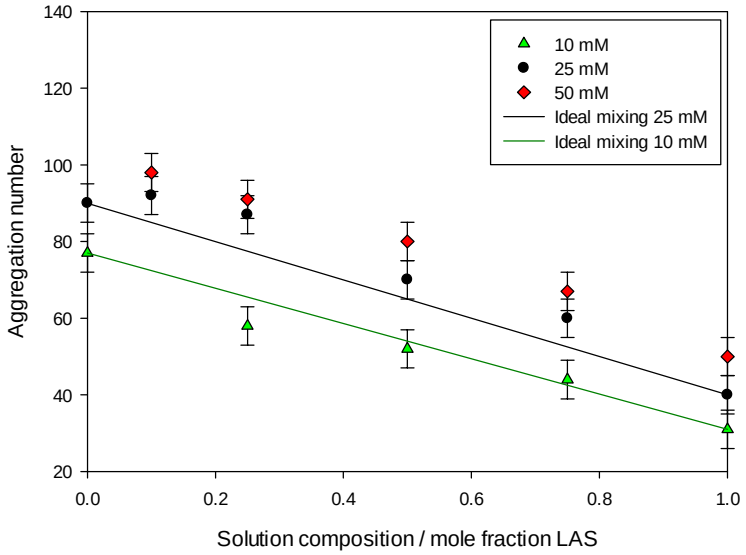

Figure 7.6: Variation in micelle aggregation number for LAS/SLES at 10, 25 and 50 mM concentration, at 25°C, in D_2O containing $1x10^{-6}$ M NaOH. Literature data for LAS at 10 and 25 mM[11] and SLES at 10 mM and 20 mM[16] are included for comparison. Data are compared to ideal mixing lines at 10 mM and 25 mM.

A more pronounced peak in the scattering for LAS/SLES is observed at higher solution concentrations (Figure 7.5 (a)), indicating stronger micellar interactions. However, only small globular interacting micelles are still observed up to 50 mM. There is an increase in surface charge with increasing solution concentration. Figure 7.5 (b) shows very similar scattering data at all solution compositions, as would be expected from an anionic/anionic surfactant mixture.

Figure 7.6 shows that the aggregation numbers of the mixed micelles decrease as the mole fraction of LAS increases. At 20 mM, pure SLES forms intermediate-sized globular micelles with an aggregation number of ~90 but LAS forms smaller micelles, with an aggregation number of only ~40, due to the di-chain nature of LAS-6. The aggregation number is systematically higher at higher solution concentrations. At all concentrations, the data correlate with the line of ideal mixing behaviour, within error, indicating similar solution compositions in the micelles and in the bulk solution.

Solution composition LAS/SLES	10 mM	25 mM	50 mM
0.75/0.25	0.17	0.15	0.22
0.5/0.5	0.14	0.19	0.21
0.25/0.75	0.16	0.13	0.21
0.1/0.9	*	0.13	0.24

Table 7.9: Variation in degree of ionisation with solution composition for $C_{12}E_8$/LAS, at 25°C, in D_2O containing $1x10^{-6}$ M NaOH. * indicates not measured.

As shown in Table 7.9, although no significant trends are evident for the variation in the degree of ionisation with solution composition, the degree of ionisation is systematically higher at 50 mM than 10 or 25 mM, which, as described in Section 7.2.1.1, is not consistent with the observations of others.[19,20]

The ellipticity values tend to increase as aggregation numbers rise and this is generally observed for $C_{12}E_8$/SLES, but for $C_{12}E_8$/LAS or LAS/SLES with varying solution composition the opposite occurs. The packing changes, variations in the mean extended alkyl chain length l_c and the ext value (ext = R_1 / l_c) for LAS and SLES compared to $C_{12}E_8$ must impact on the ultimate value of the elliptical ratio. For $C_{12}E_8$ and SLES, due to their same R1 values (~16.7 Å)^3 the expected increase in elliptical ratio occurs as the aggregation number increases (i.e. in increasingly $C_{12}E_8$-rich solutions).

7.2.2 Ternary surfactant mixtures

SANS measurements were made on the ternary mixture $C_{12}E_8$/LAS/SLES on the SANS2D diffractometer at the ISIS pulsed neutron source, UK. Figure 7.3 shows some typical SANS data, with the associated model fitting, for $C_{12}E_8$/LAS/SLES, (a) as a function of solution concentration, at a fixed solution composition of 0.33/0.33/0.33, and (b) as a function of $C_{12}E_8$ solution composition at 25 mM concentration. The associated model parameters are given in Tables 7.10 and 7.11.

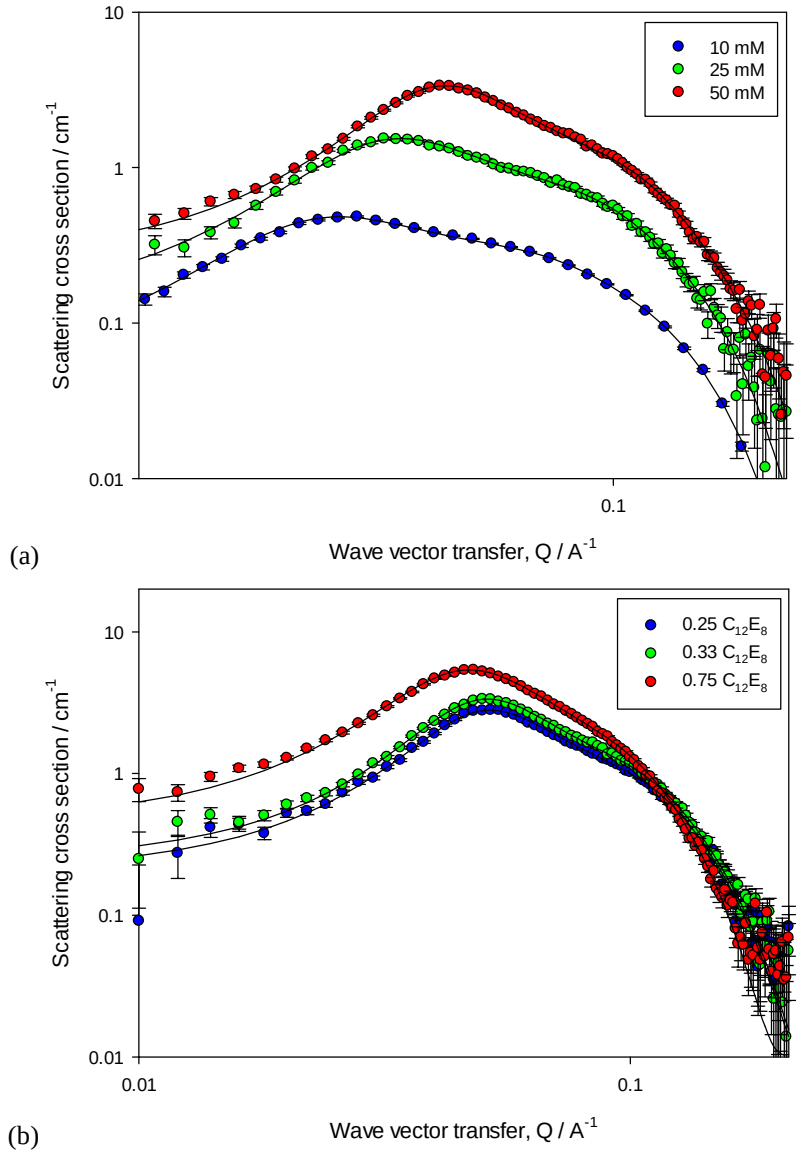

Figure 7.7: SANS raw data for (a) 0.33/0.33/0.33 $C_{12}E_8$/LAS/SLES at 10, 25 and 50 mM, and (b) $C_{12}E_8$/LAS/SLES at 0.25/0.375/0.375, 0.33/0.33/0.33 and 0.75/0.125/0.125 solution compositions, at 50 mM, both with associated model fits (solid lines), at 25°C, in D_2O containing 1x10^{-6}M NaOH.

Concentration / mM	Aggregation number, ν ± 5	Surface charge, z ± 1	R_1 / ± 1 Å	R_2 / ± 1 Å	ext / ± 0.05	ee / ± 0.01
10	65	14	17	21	1.12	1.44
25	83	16	18	25	1.20	1.17
50	88	18	18	23	1.17	1.31

Table 7.10: Core-Shell micelle data analysis for 0.33/0.33/0.33 $C_{12}E_8$/LAS/SLES at 10, 25 and 50 mM, at 25°C, in D_2O containing 1x10^{-6} M NaOH.

Solution composition / mole fraction $C_{12}E_8$	Aggregation number, ν ± 5	Surface charge, z ± 1	R_1 / ± 1 Å	R_2 / ± 1 Å	ext / ± 0.05	ee / ± 0.01
0.25	85	19	20	24	1.28	1.01
0.33	86	18	18	23	1.17	1.31
0.75	107	15	18	25	1.13	1.42

Table 7.11: Core-Shell micelle data analysis for $C_{12}E_8$/LAS/SLES at 0.25/0.375/0.375, 0.33/0.33/0.33 and 0.75/0.125/0.125 solution compositions, at 50 mM, at 25°C, in D_2O containing 1x10^{-6} M NaOH.

All data for solutions up to 50 mM concentration are consistent with small globular interacting micelles. The low Q values (less than 0.01 $Å^{-1}$) indicate micelle growth, which is seen at the higher concentrations. There is a modest decrease in ellipticity with increasing concentration, and this is due to different packing constraints within the core, defined as ext, which increases with increasing concentration. As expected, the aggregation number increases with increasing solution concentration, as larger micelles are formed at higher concentrations.

The influence of the $C_{12}E_8$ mole fraction on the scattering is shown in Figure 7.7 (b). The scattering cross section values are higher in increasingly $C_{12}E_8$-rich solutions. The increase in aggregation number, decrease in surface charge and increase in ellipticity ratio are all consistent with a surfactant mixture increasingly rich in a nonionic component. Figure 7.8 shows the variation in aggregation number for the ternary mixtures as a function of solution composition over the entire composition range investigated, at 10, 25 and 50 mM.

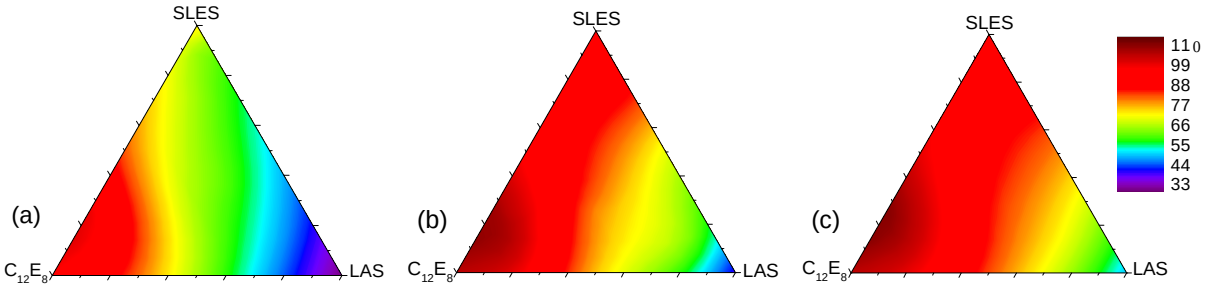

Figure 7.8: Variation in aggregation number with solution composition, at (a) 10 mM, (b) 25 mM and (c) 50 mM. The colour scale ranges from 30 (purple) to 115 (red).

There is a distinct systematic increase in aggregation number with increasing solution concentration. The aggregation number ranges from 44 to 101 and correlates with that of the aggregation numbers of the pure components, which for $C_{12}E_8$, LAS and SLES are 105 and ~40 at 25 mM[11] and ~90 at 20 mM,[16] respectively. This is to be expected in ideal mixing where the composition in the micelle reflects the solution composition. The variation in aggregation number with solution composition is related to the preferred micelle curvature of the three surfactants. The addition of nonionic surfactants promotes micellar growth, because of the reduction in the inter-headgroup electrostatic interaction between the anionic surfactant molecules. Aggregation numbers of the mixed micelles decrease with increasing solution composition of LAS, as LAS has the smallest pure aggregation number of the three

surfactants, due to its short di-chain nature. This variation of aggregation number with composition implies ideal mixing. However, this does not correspond to the surface behaviour, which shows highly non-ideal mixing behaviour at the air/water interface. Further discussion is postponed to Section 7.4.

Solution composition $C_{12}E_8$	10 mM	25 mM	50 mM
0.25	0.20	0.19	0.22
0.33	0.22	0.19	0.21
0.75	0.14	0.13	0.14

Table 7.12: Variation in degree of ionisation with $C_{12}E_8$ solution composition for $C_{12}E_8$/LAS/SLES, at 10, 25 and 50 mM, at 25°C, in D_2O containing $1x10^{-6}$ M NaOH.

Table 7.12 gives the variation in degree of micelle ionisation, δ, for the ternary mixture as a function of solution concentration and $C_{12}E_8$ solution composition. All ternary mixtures were shown to have a relatively low degree of ionisation, δ, between 0.1 and 0.2, lower than the usual value of 0.25-0.3 for purely ionic surfactants, such as SDS.[22] There is a significantly lower δ value in nonionic-rich solutions, which is consistent with the trends observed by others.[3,11] However, as described earlier for the binary mixtures, no significant change occurs with increasing surfactant concentration, as was observed in previous reports with binary R1/R2 mixtures[19] and with SPQ micelles.[20] It is possible that for $C_{12}E_8$/LAS/SLES micelles the aggregation number and the micelle charge are changing in the same relative amounts, so as to not have any effect on the degree of ionisation.

7.3 Multicomponent biosurfactant / conventional surfactant mixtures

The effect of the partial replacement of the ternary conventional surfactant system $C_{12}E_8$/LAS/SLES with the rhamnolipids R1 and R2 on the solution aggregation behaviour was studied using SANS. Measurements were made at 10, 25 and 50 mM, on the LOQ and SANS2D diffractometers at the ISIS pulsed neutron source and the D33 diffractometer at the ILL. The effect of the relative proportion of rhamnolipids was investigated, because increasing the proportion of rhamnolipids in the multicomponent mixtures had a profound effect on the surface adsorption behaviour of the mixtures (Chapter 6). Also, it is known that the relative size of the rhamnolipid headgroup impacts on both the surface and solution aggregate behaviour of surfactant mixtures,[19] so the effect of changing the R1:R2 ratio was also investigated. The five-component mixture R1/R2/$C_{12}E_8$/LAS/SLES was studied at an R/C ratio of 20/80 and 30/70 and an R1:R2 ratio of 1:1 and 2:1. Data are compared qualitatively to

literature data for R1/R2/LAS[17] although not quantitatively due to those results being made at pH 9 controlled by buffer.

Figure 7.9 shows typical SANS data for the conventional $C_{12}E_8$/LAS/SLES system at 25 mM and 50 mM, and their respective solutions containing a 30% replacement with rhamnolipids, at 1:1 R1:R2. The model fits from the micelle Core-Shell model for interacting globular micelles[22] are included for the micellar components.

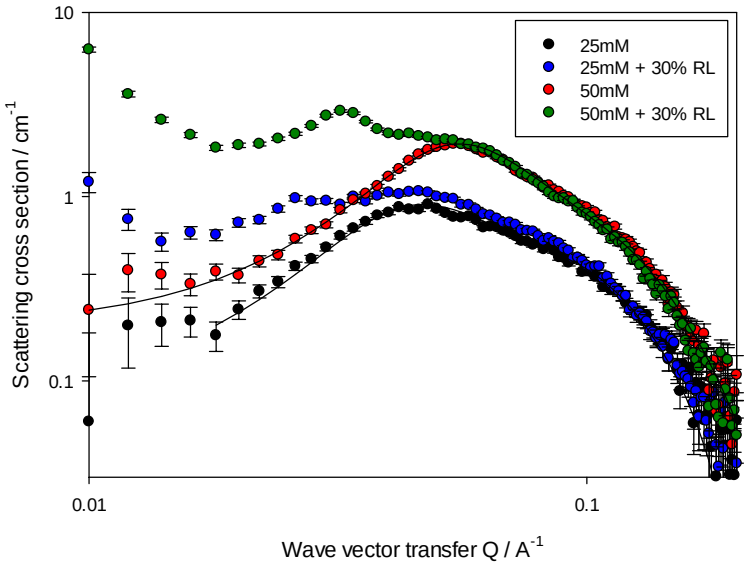

Figure 7.9: SANS data for 0.125/0.75/0.125 $C_{12}E_8$/LAS/SLES, in the absence and presence of 30% replacement with rhamnolipids in the ratio 1:1 R1:R2, at 25 and 50 mM, at 25°C, in D_2O containing $1x10^{-6}$ M NaOH.

It is clear that in the ternary conventional surfactant system, scattering is consistent with the presence of small globular interacting micelles even up to 50 mM, as shown by the scattering pattern at low Q values. In all conventional mixtures at these concentrations, and for each individual surfactant $C_{12}E_8$, LAS and SLES, only small globular micelles are present, as described in Section 7.2. On addition of the rhamnolipid biosurfactant to form the five-component mixture R1/R2/$C_{12}E_8$/LAS/SLES, significant micellar growth occurs, as shown by the upturn in the scattering at low Q. This is not observed in any conventional mixture or individual component at these concentrations and compositions. More importantly, on partial replacement with rhamnolipids, the scattering becomes consistent with the presence of both micelles (L_1) and lamellar (L_α) structures. The presence of mixed micellar L_1/lamellar L_α phase behaviour is divided qualitatively into phase behaviour which is richer in the micellar component (L_1/L_α) and richer in the lamellar component (L_α/L_1), the nature of which is

found to be dependent on four parameters: the solution concentration, LAS solution composition, relative proportion of rhammnolipid to conventional surfactant, and the relative proportion of R1 to R2. These results also correlate with some interesting changes in optical texture of the solutions in the presence of rhamnolipids; the opacity of the solution increases at a higher overall solution concentration, in progressively LAS-rich solutions, and at both higher R/C and R1:R2 ratios. The following sections discuss the effects of the solution composition of LAS, rhamnolipid and, more specifically, R1, in more detail.

7.3.1 Effect of LAS solution composition

Figure 7.10 shows the scattering data for the R1/R2/$C_{12}E_8$/LAS/SLES system as a function of LAS solution composition.

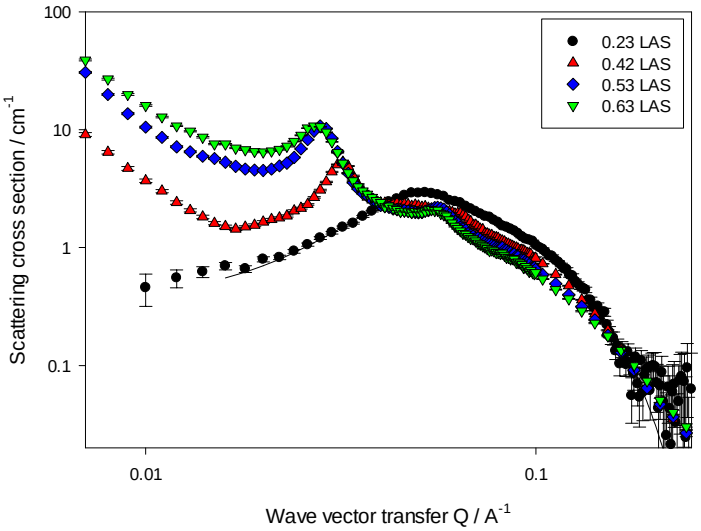

Figure 7.10: SANS data for 50 mM R1/R2/$C_{12}E_8$/LAS/SLES at 30/70 R/C and 1:1 R1:R2, as a function of LAS solution composition (equal $C_{12}E_8$ and SLES compositions), at 25°C, in D_2O containing $1x10^{-6}$ M NaOH.

For R1/R2/$C_{12}E_8$/LAS/SLES at the lowest LAS solution composition (0.23), small globular interacting micelles are present even at 50 mM. Between 0.4 and up to 0.63 mole fraction LAS this changes to mixed phase behaviour where the micellar component dominates (L_1/L_α), and at 0.63 mole fraction LAS and above the lamellar component dominates (L_α/L_1). At low Q there is a Q^{-2} dependence in the scattering data and the Bragg peaks are indicative of the presence of planar structures, which are more prominent in solutions richer in LAS. These data are consistent with those of R1/R2/LAS mixtures where L_1/L_α phase behaviour existed at 30/70 R/C and R1:R2 1:1.[17] The evolution of phase behaviour is attributed to the lower preferred curvature of LAS compared with the other two conventional

surfactants $C_{12}E_8$ and SLES; as a pure surfactant, LAS tends to form lamellar structures.[11] Mixed phase behaviour is even observed at 10 mM above a threshold LAS solution composition, which becomes successively lower at higher solution concentrations. However, no mixed phase behaviour is seen in the ternary conventional mixture in the absence of rhamnolipids, even at concentrations as high as 50 mM and in very LAS-rich solutions. These results imply a synergy in the packing of the rhamnolipid biosurfactant with the conventional surfactants, in the five-component mixture, that is not present in the ternary mixture alone.

For the mixtures where globular micelles are present, it has been possible to quantitatively analyse the micellar structure using the Core-Shell micelle model.[22] As shown in Table 7.13, the aggregation number increases with solution composition as expected, and also the LAS composition required to induce the transition to mixed phase behaviour decreases. The ternary phase diagrams in Figure 7.11 show these patterns visually, for 20/80 R/C at 2:1 R1:R2, at the equivalent ternary solution compostion (i.e. 0.125/0.75/0.125 $C_{12}E_8$/LAS/SLES for the five-component mixture 0.13/0.07/0.1/0.6/0.1 R1/R2/$C_{12}E_8$/LAS/SLES, at 20/80 R/C and 2:1 R1:R2.)

	Concentration / mM		
LAS solution composition	10	25	50
0.23	70	80	86
0.48	57	68	83
0.6	52	L_1/L_α	L_α/L_1
0.72	L_1/L_α	L_α/L_1	L_α/L_1

Table 7.13: Variation in aggregation number for micellar components of R1/R2/$C_{12}E_8$/LAS/SLES mixtures at R/C 20/80 and R1:R2 2:1, with varying concentration and LAS solution composition.

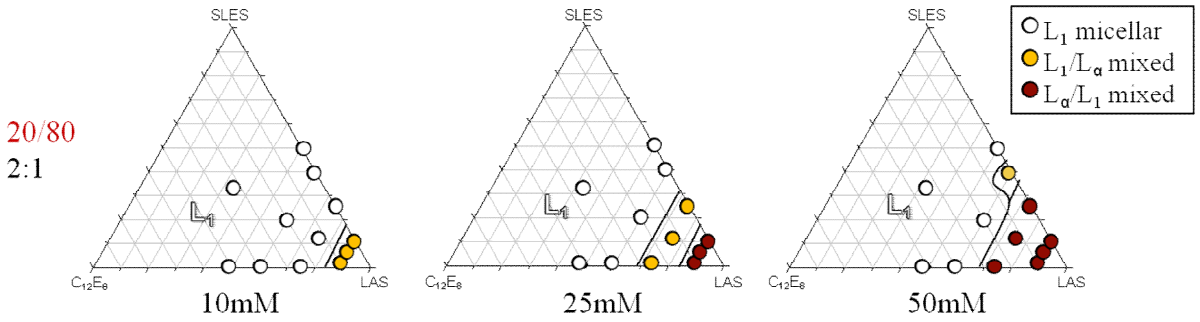

Figure 7.11: Variation in phase behaviour over the composition range for R1/R2/$C_{12}E_8$/LAS/SLES, at R/C 20/80 and R1:R2 2:1.

The effect of the ratio of the nonionic $C_{12}E_8$ to anionic SLES can be seen in Figure 7.12. The equivalent conventional ternary compositions of $C_{12}E_8$/LAS/SLES shown are 0.32/0.48/0, 0.16/0.48/0.16, 0/0.48/0.32, and 0.08/0.72/0, 0.04/0.72/0.04, 0/0.72/0.08, at 25 and 50 mM. Table 7.14 summarises the variation in aggregation number, for the former three solution compositions.

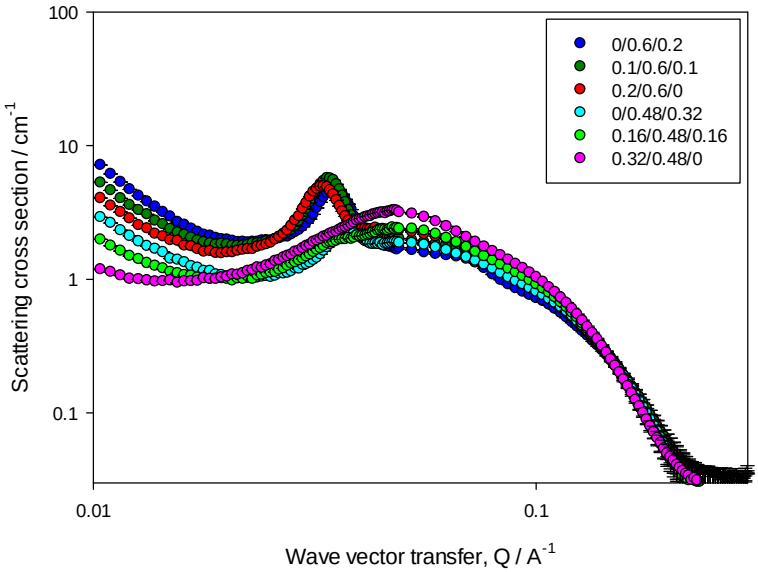

Figure 7.12: SANS data for R1/R2/$C_{12}E_8$/LAS/SLES at varying solution compositions, at 20/80 R/C and 2:1 R1:R2, at 50 mM, at 25°C, in D_2O containing $1x10^{-6}$ M NaOH.

	Solution composition $C_{12}E_8$/LAS/SLES		
Concentration / mM	0.32 / 0.48 / 0	0.16 / 0.48 / 0.16	0 / 0.48 / 0.32
10	67	61	58
25	72	68	64
50	90	83	L_1/L_α

Table 7.14: Variation in micelle aggregation number for R1/R2/$C_{12}E_8$/LAS/SLES mixtures, with varying solution composition, at 20/80 R/C and 2:1 R1:R2.

Figure 7.12 shows that with a higher proportion of nonionic surfactant, there is a more pronounced scattering peak and a higher aggregation number. The aggregation number of pure $C_{12}E_8$ is higher than pure SLES (105 at 25 mM[11] and ~90 at 20 mM[16]) and the nonionic nature of $C_{12}E_8$ induces micellar growth. Interestingly, as shown in Table 7.14, at the higher concentration of 50 mM and in the absence of $C_{12}E_8$, there is a transition from micellar to mixed micellar/lamellar, with a dominating L_α component: the presence of a Bragg peak is observed in Figure 7.12 for the $C_{12}E_8$/LAS/SLES solution composition 0/0.48/0.32, which is not observed at composition 0.32/0.48/0. This is attributed to the fact that the nonionic has a higher intrinsic curvature, so even though it induces the growth of micelles it will prevent transition to more planar structures. When the nonionic is not present, the lower preferred curvature of LAS will dominate and planar structures will more readily form.

7.3.2 Effect of R/C ratio

The solution behaviour of R1/R2/$C_{12}E_8$/LAS/SLES was studied at R/C ratios 20/80 and 30/70 for concentrations between 10 and 50 mM and at LAS compositions from 0.23 to 0.72. Figure 7.13 shows the variation in solution aggregate behaviour for R/C 20/80 and 30/70 with increasing solution composition, for 1:1 R1:R2, at a relative $C_{12}E_8$/LAS/SLES solution composition of 0.125/0.125/0.75 (i.e. an R1/R2/$C_{12}E_8$/LAS/SLES solution composition of 0.15/0.15/0.08/0.52/0.08 for 30/70 R/C, and 0.1/0.1/0.1/0.6/0.1 for 20/80 R/C.)

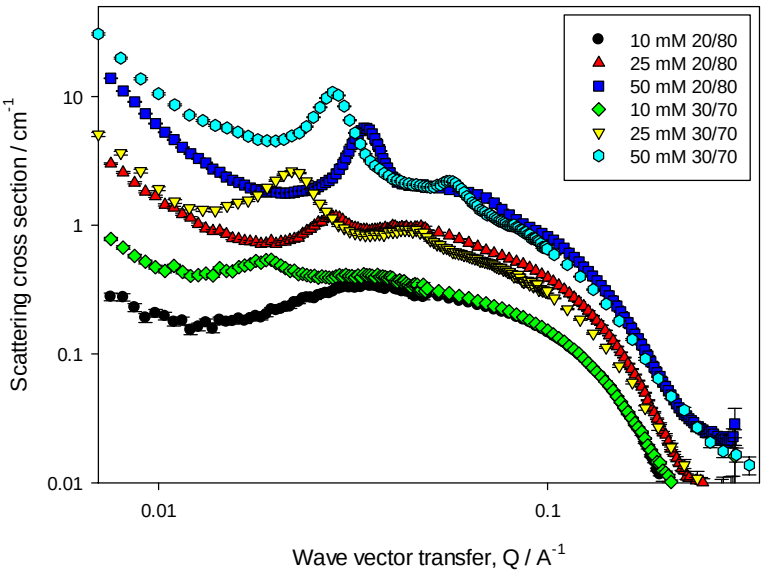

Figure 7.13: SANS data for R1/R2/$C_{12}E_8$/LAS/SLES at 20/80 and 30/70 R/C, at a fixed R1:R2 ratio of 2:1, at an equivalent $C_{12}E_8$/LAS/SLES solution composition of 0.125/0.75/0.125, at 10, 25 and 50 mM, at 25°C, in D_2O containing $1x10^{-6}$ M NaOH.

From the data in Figure 7.13, it is clear that a higher proportion of rhamnolipid to conventional surfactant results in more complex solution behaviour. At 10 mM at 20/80 R/C, only globular micelles form, with micelle growth, but at 30/70 R/C the micellar component at high Q, the Q^{-2} dependence at lower Q and the presence of Bragg peaks indicate mixed micellar/lamellar phase behaviour. The ternary phase diagrams in Figure 7.14 compare solutions at 20/80 and 30/70 R/C, for the concentrations 10, 25 and 50 mM over the whole solution composition range and at a fixed R1:R2 ratio of 1:1. In Figures 7.12 and 7.13, the upturn in the scattering at low Q for the predominantly globular structures is associated with the presence of a small fraction of more planar structures. Where such data has been modeled as globular micelles, a Q_{min} ~ 0.008 has been used, and the upturn ignored.

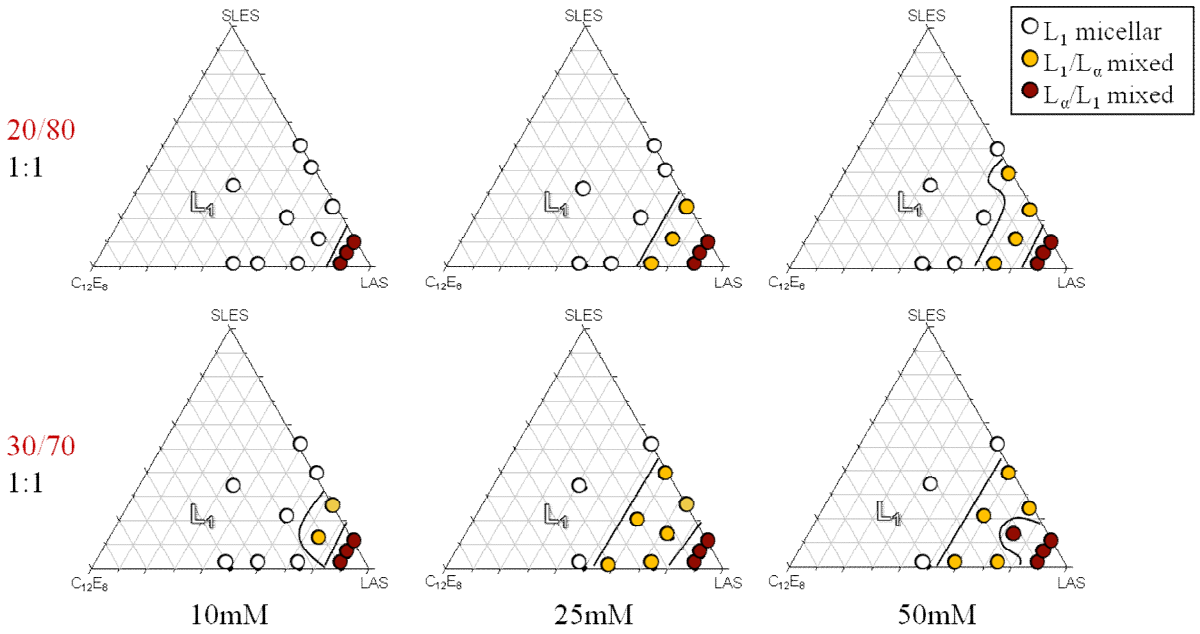

Figure 7.14: Variation in phase behaviour with R/C ratio from 20/80 to 30/70, at a fixed R1:R2 ratio of 1:1, at 10, 25 and 50 mM concentration.

The phase diagrams for 30/70 R/C show a larger coexistence region of micellar/lamellar behaviour than for 20/80 R/C. The phase behaviour changes from mostly L_1 and L_1/L_α, at 20/80 R/C to mostly L_1/L_α and L_α/L_1 at 30/70 R/C. A higher proportion of rhamnolipids in the multicomponent mixture also reduces the LAS composition required to induce the mixed L_1/L_α phase behaviour. For example, at 25 mM, for 20/80 R/C, L_1/L_α is observed above 0.6 mole fraction LAS, but for 30/70 R/C this occurs from 0.4 mole fraction LAS. On increasing concentration, the proportion of LAS required to induce this change in phase behaviour also decreases. Chen et al[17] found that in R1/R2/LAS ternary mixtures pure lamellar L_α was observed only above 40/60 R/C and at very high concentrations (100 mM and above).

The same trends with increasing R/C ratio are observed for 2:1 R1:R2, although the overall proportion of L_α/L_1 phase behaviour is larger, as will be explained in Section 7.3.3, showing the effects of varying the R1:R2 ratio.

7.3.3 Effect of R1:R2 ratio

The solution behaviour of R1/R2/$C_{12}E_8$/LAS/SLES was studied at R1:R2 ratios of 1:1 and 1:2. Figure 7.15 shows the variation in scattering data for R1/R2/LAS/SLES at 1:1 and 2:1 R1:R2 at a fixed R/C ratio of 30/70, at solution concentrations of 25 and 50 mM.

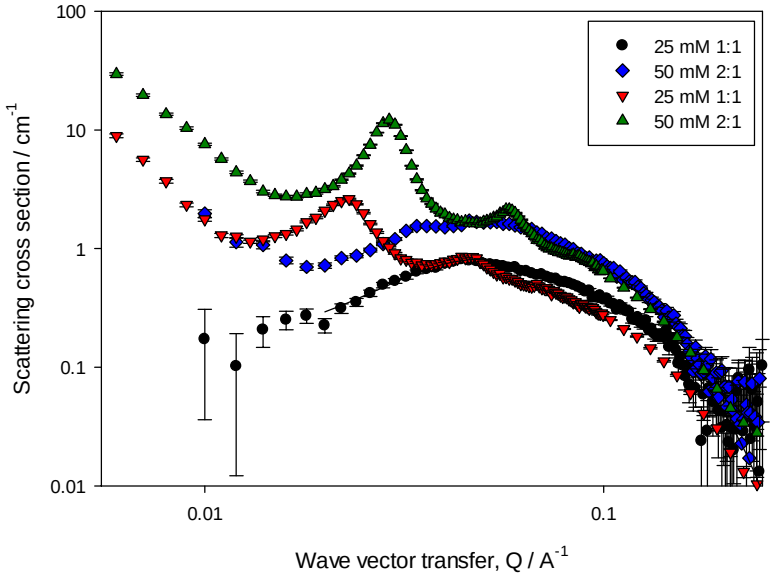

Figure 7.15: SANS data for R1/R2/LAS/SLES at 25 and 50 mM concentration, at an equivalent ternary composition of 0.75/0.25 LAS/SLES, at 1:1 and 2:1 R1:R2, at a fixed R/C ratio of 30/70, at 25°C, in D_2O containing $1x10^{-6}$ M NaOH.

Figure 7.15 clearly shows that a higher proportion of R1 to R2 results in a more complex phase behaviour. At both concentrations, small globular micelles are observed at 1:1 R1:R2, with micelle growth more significant at the higher solution concentration. At 2:1 R1:R2, however, there is a micellar component at high Q but the presence of Bragg peaks and the Q^{-2} dependence at low Q indicate more complex solution behaviour in the form of mixed micelles/lamellae. The ternary phase diagrams in Figure 7.16 show solutions at 1:1 and 2:1 R1:R2, for 10, 25 and 50 mM over the whole ternary solution composition range, at a fixed R/C ratio of 30/70.

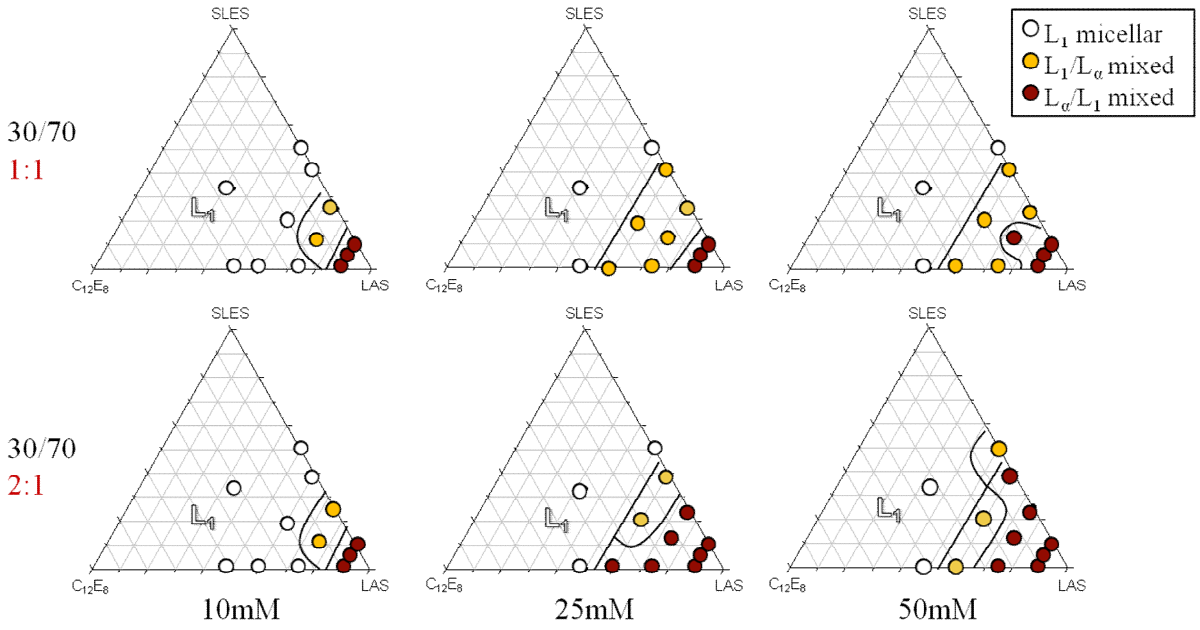

Figure 7.16: Variation in phase behaviour with R1:R2 ratio from 1:1 to 2:1, at a fixed R/C ratio of 30/70, at 10, 25 and 50 mM concentration.

Figure 7.16 shows the impact of the presence of a higher proportion of R1. On increasing R1:R2 ratio there is a pronounced increase in the L_α/L_1 coexistence region. The smaller headgroup of R1 means it has a lower intrinsic curvature, inducing the growth of more planar structures.[19] A similar variation in phase behaviour with R1:R2 composition is observed for R/C 20/80, although the smaller overall proportion of rhamnolipids results in the transition to L_1/L_α and L_α/L_1 occurring in solutions much richer in LAS.

In binary mixtures of R1 and R2,[19] the phase behaviour of the pure component dominated that of the mixture. For example, R2-rich solution compositions showed scattering data consistent with the presence of globular micelles, whereas in R1-rich solutions there was a transition to lamellar structures, with Q^{-2} dependence in the scattering data. Likewise, for binary R1/LAS mixtures, R1 dominated scattering and there was a L_α/L_1 coexistence to L_α with rigid lamellar structures in increasingly R1-rich solutions and at higher concentrations. For R2/LAS, small globular micelles were present with high aggregation numbers increasing in solutions progressively richer in LAS, due to the lower preferred micelle curvature of LAS than R2. Ternary R1/R2/LAS showed L_1/L_α coexistence, the dominance of the lamellar component varying with proportion of R1 present. Pure lamellar L_α behaviour was only observed when R1:R2 was 2:1 and only at 100 mM and above.

A similar pattern was observed when comparing the mixing behaviour of SDS/$C_{12}E_6$ with SDS/$C_{12}E_8$.[3] For both mixtures, aggregation numbers rose with increasing mole fraction of the nonionic surfactant, but micellar growth was more pronounced with increasing mole fraction of $C_{12}E_6$ due to its smaller headgroup area than in $C_{12}E_8$. Likewise, in mixtures of the di-chain cationic surfactant DHDAB with $C_{12}E_6$ and $C_{12}E_{12}$,[29] in nonionic-rich solutions, a more extensive region of L_α and multilamellar vesicles (MLV) existed in DHDAB/$C_{12}E_6$ mixtures due to the smaller intrinsic curvature associated with $C_{12}E_6$.

7.4 Discussion

In the $C_{12}E_8$/LAS/SLES conventional surfactant system, small interacting globular micelles are present at all concentrations, up to 50 mM, and at all solution compositions. The micelle aggregation number increases with increasing mole fraction of the nonionic surfactant, as expected.[3] The variation in aggregation number of the mixed micelles correlates with that of the pure components, and the aggregation numbers are not larger than for any of the individual component micelles, indicating ideal mixing. The composition of the micelles in general reflects the composition of the bulk solution. The observations in mixing behaviour correspond well to those reported for similar anionic/nonionic mixtures.[3,11,18]

For the five-component biosurfactant mixtures, where globular micelles exist, the variation in aggregation number with solution composition indicates mixing which is close to ideal, as in the ternary mixture. It was expected that introducing the rhamnolipid biosurfactant to the ternary conventional surfactant mixture would induce a phase behavioural change from micellar to more complex phase behaviour. In mixtures of rhamnolipids with LAS,[17] solutions containing a relatively high proportion of R1 induced lamellar phase behaviour at relatively low concentrations. In this work it was found that even at concentrations as low as 10 mM, the presence of rhamnolipids induces a phase transition to L_1/L_α. This transition is only seen above a certain threshold LAS solution composition, which varies depending on the R/C surfactant ratio, R1:R2 ratio and the overall solution concentration. There was a higher proportion of lamellae and a larger overall region of L_1/L_α and L_α/L_1

coexistence when the R/C ratio was changed from 20/80 to 30/70 and the R1:R2 ratio from 1:1 to 2:1. The degree of ionisation for mixtures containing rhamnolipid varies from predominantly 0.11 to 0.18, and is similar to values of pure rhamnolipids: Chen et al[19] found R1 and R2 both to be only weakly anionic, even at the highest pH investigated (pH 9) with degrees of ionisation for R1/R2 mixtures only up to 0.15, depending on the solution composition. The rhamnolipids affect the multicomponent mixtures by reducing electrostatic repulsions between the other anionic components in the mixture, inducing micellar growth and more planar phase behaviour.

The point at which the transition from L_1 to L_1/L_α occurs is dependent on the spontaneous curvatures of the individual components. The Israelachvili, Mitchell and Ninham critical packing parameter[30] (CPP) is an effective way of determining the evolution in aggregate structures of surfactants and their mixtures, and is defined in Equation 7.2:

$$CPP = \frac{V}{Al_c} \tag{7.2}$$

where V is the volume of the alkyl chain, A is the area per molecule and l_c is the extended alkyl chain length. For $C_{12}E_8$, CPP predicts ~0.32 on the border of spherical/elongated micelles.[3] This is correct for the measurements in this work in nonionic-rich $C_{12}E_8$/LAS/SLES mixtures. Using typical values for LAS, CPP is ~0.56, bordering between elongated micelles and planar structures.[12] However, in LAS-rich mixtures of $C_{12}E_8$/LAS/SLES, still only globular micelles were observed. This discrepancy is similar to that observed for R1 and R2,[19] where the CPP predicted lamellar structures and elongated micelles, respectively, due to the differences in the size of their hydrophilic headgroup. However, R2 was found to form small globular micelles, indicating that the rhamnolipids may adopt different conformations in the micelles to those at the air/water interface. This is similar to the different conformations of LAS isomers adopted at the interface and in solution reported by Goon et al.[31] Using partially deuterium-labelled surfactants for direct conformational analysis may give further valuable insight into the bulk aggregate structure.[2,4]

The variation in the solution behaviour does not correlate with trends in the surface adsorption behaviour acquired through surface tension and neutron reflectivity, which indicate highly non-ideal

mixing at the air/water interface between $C_{12}E_8$ and both LAS and SLES. This behaviour was not comparable to non-ideal mixing theories such as RST. A similar discrepancy between the surface adsorption and solution aggregate behaviour was also observed in the non-ideal mixing of DHDAB with $C_{12}E_6$.[32] Non-ideal mixing in solution can occur due to interactions between the micelles and also between micelles and the solvent.[33] However, at concentrations above the mixed CMC, which will be especially low for the rhamnolipid-containing multicomponent mixtures, most of the surfactant is present in the bulk aggregates and the concentration of monomers compared to that in micelle form will be negligible.[34] Therefore, although small angle scattering will not have particularly high sensitivity to changes in the bulk solution, any changes in the bulk can still have a large impact on the concentration and composition of the monomers in solution and hence at the interface.

The presence of $C_{12}E_8$ and SLES influences the ability of the mixed surfactants to form purely planar structures. Chapter 5 discussed the changes in optical texture observed in the presence of Ca^{2+} ions. The opacity of the solutions increases with increasing LAS mole fraction, to a greater extent with a higher relative proportion of SLES to $C_{12}E_8$. This is attributed to the low intrinsic curvature of LAS which promotes the formation of lamellar structures, but the competing force of the higher intrinsic curvature of $C_{12}E_8$ than SLES prevents the formation of more planar structures in solution. Additional SANS measurements in the presence of Na^+ and Ca^{2+} would be useful to complement the surface data.

Ma et al[12] found that for LAS-4, 5 and 6, there was a larger coexistence region of micelles and lamellar, which was more prominent in the lamellar component, over the whole solution composition range, due to their effectively short di-chain nature and lower intrinsic curvature than for LAS-1, 2 or 3. It is unlikely that the use of, for example, LAS-2 instead of LAS-6, would induce such phase behavioural changes as have been observed in this work. In commercial systems, LAS tends to be a combination of different isomers. Likewise, SLES and $C_{12}E_8$ are often a combination of different alkyl and EO chain lengths, and rhamnolipids have a natural abundance of over 60 possible congeners. Surfactant behaviour, and thus detergency, can be optimised by modifying the combination of isomers to form an optimum commercial formulation. Fewer EO groups on the nonionic surfactant would induce a lower preferred curvature, tuning the structure to a more planar geometry. For example, the

use of $C_{10}E_3$ induced the formation of lamellae in combination with LAS due to their similarly low curvatures.[18] Furthermore, the nonionic surfactant's alkyl chain length can be reduced to match that of LAS-6 to induce more planar aggregates. However, for SLES, increasing the number of EO groups was not shown to affect phase behaviour, with the micelle aggregation number remaining constant.[16,35] Instead, the micelle structure is thought to change from a compact structure to a looser one, as the polar OSO^{3-} and EO portions separate from each other to accommodate the longer headgroup, giving a larger volume of the polar layer at the air/water interface.[35]

References: Chapter 7

1. Thomas, H. G.; Lomakin, A.; Blankschtein, D.; Benedek, G. B., *Langmuir* **1997,** *13* (2), 209-218.
2. Penfold, J.; Staples, E.; Thompson, L.; Tucker, I.; Hines, J.; Thomas, R. K.; Lu, J. R., *Langmuir* **1995,** *11* (7), 2496-2503.
3. Penfold, J.; Tucker, I.; Thomas, R. K.; Staples, E.; Schuermann, R., *Journal of Physical Chemistry B* **2005,** *109* (21), 10760-10770.
4. Penfold, J.; Staples, E.; Thompson, L.; Tucker, I.; Hines, J.; Thomas, R. K.; Lu, J. R.; Warren, N., *Journal of Physical Chemistry B* **1999,** *103* (25), 5204-5211.
5. Penfold, J.; Staples, E.; Tucker, I., *Journal of Physical Chemistry B* **2002,** *106* (34), 8891-8897.
6. Penfold, J.; Staples, E.; Ugazio, S.; Tucker, I.; Soubiran, L.; Hubbard, J.; Noro, M.; O'Malley, B.; Ferrante, A.; Ford, G.; Buron, H., *Journal of Physical Chemistry B* **2005,** *109* (38), 18107-18116.
7. Abe, M.; Uchiyama, H.; Yamaguchi, T.; Suzuki, T.; Ogino, K.; Scamehorn, J. F.; Christian, S. D., *Langmuir* **1992,** *8* (9), 2147-2151.
8. Shiloach, A.; Blankschtein, D., *Langmuir* **1998,** *14* (25), 7166-7182.
9. Aoudia, M.; Al-Maamari, T.; Al-Salmi, F., *Colloids and Surfaces A: Physicochemical and Engineering Aspects* **2009,** *335*, 55-61.
10. Cerichelli, G.; Mancinit, G., *Current Opinion in Colloid and Interface Science* **1997,** *2* (6), 641-648.
11. Penfold, J.; Thomas, R. K.; Dong, C. C.; Tucker, I.; Metcalfe, K.; Golding, S.; Grillo, I., `*Langmuir* **2007,** *23* (20), 10140-10149.
12. Ma, J.-G.; Boyd, B. J.; Drummond, C. J., *Langmuir* **2006,** *22* (21), 8646-8654.
13. Caponetti, E.; Triolo, R.; Ho, P. C.; Johnson Jr, J. S.; Magid, L. J.; Butler, P.; Payne, K. A., *Journal of Colloid and Interface Science* **1987,** *116* (1), 200-210.
14. Xu, H.; Penfold, J.; Thomas, R. K.; Petkov, J. T.; Tucker, I., *Langmuir* **2013,** *29* (41), 12744-12753.
15. Xu, H.; Penfold, J.; Thomas, R. K.; Petkov, J. T.; Tucker, I.; Webster, J. P. R., *Langmuir* **2013,** *29* (37), 11656-11666.
16. Xu, H.; Penfold, J.; Thomas, R. K.; Petkov, J. T.; Tucker, I.; Grillo, I.; Terry, A., *Langmuir* **2013,** *29* (44), 13359-13366.
17. Chen, M.; Penfold, J.; Thomas, R. K.; Smyth, T. J. P.; Perfumo, A.; Marchant, R.; Banat, I. M.; Stevenson, P.; Parry, A.; Tucker, I.; Grillo, I., *Langmuir* **2010,** *26* (23), 17958-17968.
18. Tucker, I.; Penfold, J.; Thomas, R. K.; Dong, C. C.; Golding, S.; Gibson, C.; Grillo, I., *Langmuir* **2010,** *26* (13), 10614-10626.
19. Chen, M. L.; Penfold, J.; Thomas, R. K.; Smyth, T. J. P.; Perfumo, A.; Marchant, R.; Banat, I. M.; Stevenson, P.; Parry, A.; Tucker, I.; Grillo, I., *Langmuir* **2010,** *26* (23), 18281-92.
20. Kuwamoto, K.; Asakawa, T.; Ohta, A.; Miyagishi, S., *Langmuir* **2005,** *21* (17), 7691-7695.
21. Penfold, J.; Chen, M.; Thomas, R. K.; Dong, C.; Smyth, T. J. P.; Perfumo, A.; Marchant, R.; Banat, I. M.; Stevenson, P.; Parry, A.; Tucker, I.; Grillo, I., *Langmuir* **2011,** *27* (14), 8867-8877.
22. Hayter, J. B.; Penfold, J., *Colloid and Polymer Science* **1983,** *261* (12), 1022-1030.
23. Hayter, J. B., *Langmuir* **1992,** *8* (12), 2873-2876.
24. Zana, R.; Lévy, H.; Kwetkat, K., *Journal of Colloid and Interface Science* **1998,** *197* (2), 370-376.
25. Tucker, I.; Penfold, J.; Thomas, R. K.; Grillo, I.; Mildner, D. F. R.; Barker, J. G., *Langmuir* **2008,** *24* (18), 10089-10098.
26. Staples, E. J.; Thompson, L.; Tucker, I.; Penfold, J., *Langmuir* **1994,** *10* (11), 4136-4141.
27. Lu, J. R.; Thomas, R. K.; Penfold, J., *Advances in Colloid and Interface Science* **2000,** *84* (1-3), 143-304.

28. Griffiths, P. C.; Paul, A.; Heenan, R. K.; Penfold, J.; Ranganathan, R.; Bales, B. L., *Journal of Physical Chemistry B* **2004,** *108* (12), 3810-3816.
29. Tucker, I.; Penfold, J.; Thomas, R. K.; Tildesley, D. J., *Langmuir* **2009,** *25* (7), 3924-3931.
30. Israelachvili, J. N.; Mitchell, D. J.; Ninham, B. W., *Journal of the Chemical Society, Faraday Transactions 2: Molecular and Chemical Physics* **1976,** *72*, 1525-1568.
31. Goon, P.; Das, S.; Clemett, C. J.; Tiddy, G. J. T.; Kumar, V. V., *Langmuir* **1997,** *13* (21), 5577-5582.
32. Penfold, J.; Staples, E.; Tucker, I.; Thomas, R. K., *Langmuir* **2004,** *20* (4), 1269-1283.
33. Cebula, D. J.; Ottewill, R. H., *Colloid and Polymer Science* **1982,** *260* (12), 1118-1120.
34. Abe, M.; Uchiyama, H.; Yamaguchi, T.; Suzuki, T.; Ogino, K.; Scamehorn, J. F.; Christian, S. D., *Langmuir* **1992,** *8* (9), 2147-2151.
35. Aoudia, M.; Al-Haddabi, B.; Al-Harthi, Z.; Al-Rubkhi, A., *Journal of Surfactants and Detergents* **2010,** *13* (1), 103-111.

Chapter 8

Effects of low temperature on the surface adsorption behaviour of biosurfactant / conventional surfactant mixtures

The effect of temperature on the surface adsorption and solution aggregate behaviour of surfactants is very significant in terms of detergency performance. The awareness of energy conservation in commercial and domestic applications is growing and laundering at temperatures closer to ambient is one aspect which is attracting increasing interest, with many environmental and economic benefits. Unilever's Sustainable Living programme is a business strategy which involves the aim of reducing the environmental impact of their products by 2020. The concentration of laundry liquids and packaging, product reformulation and encouragement of the use of lower washing temperatures are three ways in which Unilever hope to reduce greenhouse gas emissions. This chapter discusses the impact of low temperature on the surface behaviour of the model conventional surfactant mixture $C_{12}E_8$/LAS/SLES and the multicomponent biosurfactant/conventional surfactant mixture R1/R2/$C_{12}E_8$/LAS/SLES, at the air/water interface, using surface tension and neutron reflectivity.

8.1 Literature review

The variation in surface tension of water with temperature is well known[1,2] with the Eötvös[3] equation showing a linear relationship of surface tension γ with temperature T. In general, the surface tension of a solution decreases with increasing temperature due to the increasing thermal motion in solution and the disruption of intermolecular forces, notably hydrogen bonds. The effects of temperature on the surface behaviour of surfactants are most important for the nonionic polyethylene glycol C_nE_m surfactants due to their Krafft temperature, below which micelles cannot form, and cloud temperature, above which phase separation of the solution occurs.[4] The Krafft temperature is also important for the performance of ionic surfactants.

A reduction in surface tension and an almost linear decrease in CMC with increasing temperature for nonionic C_nE_m surfactants has been extensively reported in the literature,[5] notably more recently by

Rosen et al[6] and Penfold et al.[7,8] However, the CMC has been reported to decrease to a minimum at a certain temperature, the value of which depends on the length of the ethylene oxide (EO) group, and above which the CMC increases again.[9] Similar minima in CMC have been found for a series of Tween surfactants studied over a wide temperature range using surface tension[10] and fluorescence intensity measurements.[11] Two competing forces occur as the temperature is raised; firstly, the EO chain becomes more dehydrated due to the disruption of hydrogen bonds between the water molecules in the solvent and the surfactant's hydrophilic headgroup. This increases the molecule's hydrophobicity and hence its surface activity. Conversely, the alkyl chain becomes more water-soluble due to the increased breakdown of hydrogen bonding surrounding the hydrophobic chain with higher temperatures. This makes the alkyl chain less hydrophobic and thus less surface active. For $C_{12}E_8$, the length of the EO chain means the former factor dominates as it is highly hydrated[9] and as a result an increase in temperature reduces its CMC and increases its surface adsorption.[6] Through detailed structural analysis of the adsorbed surfactant layers of $C_{12}E_8$, Lu and co-workers[12] observed this dehydration of the EO groups, as well as a thicker alkyl chain region, at higher temperatures.

For nonionic surfactant mixtures, for example $C_{12}E_3/C_{12}E_8$,[7,8] at higher temperatures the CMCs of the components become more comparable as the CMC of $C_{12}E_8$ decreases more rapidly than that of $C_{12}E_3$, and the composition of the mixed micelles that form above the CMC are closer to those of the solution composition, whilst at the air/water interface the surface composition becomes richer in the less surface-active component, i.e. $C_{12}E_8$. Below the CMC, the changes observed with varying temperature may be purely due to packing constraints associated with the temperature changes affecting the solubilities of the alkyl chain and hydrophilic headgroups, as described above.

For ionic surfactants, due to the changes in the hydrophobic and headgroup interactions with temperature, a minimum in CMC is found with increasing temperature where the CMC decreases and then increases again above a certain temperature, a well-established phenomenon in systems such as SDS,[5,13] dodecyltrimethylammonium bromide[14] and *N*-alkylpyridinium halides.[15] The initial decrease is due to the lower number of hydrogen bonds formed as the temperature increases, dehydrating the

polar headgroup and making the surfactant less hydrophilic. But the increase in temperature also increases the breakdown of hydrogen bonds surrounding the hydrophobic chain. This effect will dominate above a certain temperature and thus be observed as a rise in CMC after a minimum. For SDS this minimum exists at 25°C,[5] with SLES containing three EO groups or less showing similar temperature effects to SDS, but SLES with larger numbers of EO groups showing effects more similar to those for the nonionic dodecanol.

Although the behaviour of nonionic surfactants with temperature has been studied, little is published on the variation of anionic/nonionic surfactant mixtures with changing temperature. Golub and de Keizer[16] made calorimetric measurements of excess enthalpy values to study $C_{12}E_6$/SDS mixed micelle formation and a high affinity was found between the anionic and nonionic surfactants due to hydrogen bonding between the sulfate headgroup on SDS and the EO headgroups on $C_{12}E_6$. This affected the hydration of the EO groups, making them more hydrophobic. However, there are no detailed studies of the effect of temperature on the surface composition of individual surfactant components in surfactant mixtures at interfaces. C_{16}TAB/$C_{12}E_6$ mixture from 30°C to 50°C caused the surface adsorption of $C_{12}E_6$ to increase and that of C_{16}TAB to decrease, with an overall decrease in total coverage. At 0.25/0.75 C_{16}TAB/$C_{12}E_6$, dehydration of the EO group and thickening of the alkyl chain in $C_{12}E_6$ region resulted after increasing the temperature.

In this chapter, surface tension and neutron reflectivity have been used to study the impact of lower temperatures on the surface adsorption behaviour of each component in a model ternary anionic/nonionic surfactant mixture $C_{12}E_8$/LAS/SLES and a multicomponent biosurfactant/conventional surfactant mixture containing the biosurfactant rhamnolipid, R1/R2/$C_{12}E_8$/LAS/SLES. The data obtained at 25°C and 10°C are compared and the striking differences between the two mixtures are discussed.

8.2 Experimental

Surface tension measurements were made on a Krüss K10T maximum pull digital tensiometer, using a Pt/Ir du Nouy ring. Surface tension was measured for individual surfactants and their mixtures at 2 mM concentration, above the mixed CMC, all prepared in MilliQ ultrapure water containing $1x10^{-6}$ M NaOH. Measurements were carried out at 25°C and 10°C (± 0.1°C), with the temperature controlled using a Haake K15 water bath with a manual D30 circulator connected to the tensiometer. The tensiometer was first brought to the chosen temperature, 25°C or 10°C, and once at this temperature, 10 ml solution in a glass pot (dimensions 48 mm diameter by 30 mm depth) was placed in the tensiometer for at least 10 minutes for thermal equilibrium to be established. The surface tension measurement was taken, the temperature was then changed, thermal equilibrium was once again established and the surface tension at the second temperature was measured. An average of three measurements was taken at each temperature and values were always within ± 0.5 mN/m.

Neutron reflectivity measurements were carried out on the INTER reflectometer at the ISIS pulsed neutron source, UK. Solutions were held in specially-designed stainless steel troughs, with an inner network of tubing connected to a water/ethylene oxide bath to regulate the temperature. In between measurements, all troughs were cleaned *in situ* with IPA, ethanol and finally acetone, and then dried. Airtight steel lids were fitted during measurements to ensure minimal evaporation. The setup is shown in Figure 8.1.

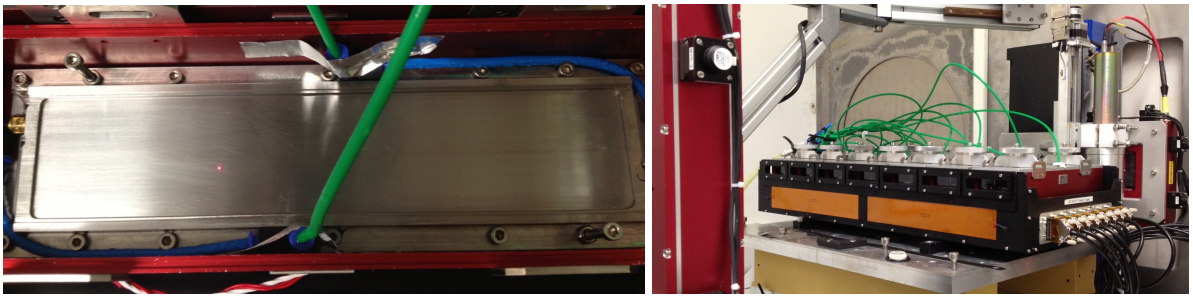

Figure 8.1: Images showing the set up of the stainless steel troughs for measurements at 25°C and 10°C, with 7 steel troughs in use simultaneously and each connected to a water/ethylene oxide bath to control temperature.

Instrumental set-up, background correction and data reduction were carried out as described in Chapter 2. All heights were aligned manually using a laser beam. For measurements at 25°C the temperature was set to 25.0°C and for low temperature measurements the temperature was set to 7.0°C

which allowed all troughs to reach 10.8°C. Reflectivity measurements were made on the ternary $C_{12}E_8$/LAS/SLES mixture at solution composition 0.375/0.375/0.25, just as was done with the surface tension. The multicomponent biosurfactant/conventional surfactant mixtures contained a 30% replacement of the ternary mixture with rhamnolipids in the ratio 1:1 R1:R2. All measurements were made at a total surfactant concentration of 2 mM, as for the surface tension described above and the previous work on surface adsorption behaviour (Chapters 4, 5 and 6).

8.3 Results

8.3.1 Surface tension

Surface tension measurements were made for the individual surfactants, the $C_{12}E_8$/LAS/SLES ternary mixture at composition 0.375/0.375/0.25, R1/R2/$C_{12}E_8$/LAS/SLES five-component mixture in which 30% of the ternary mixture was replaced by the rhamnolipids R1 and R2 in the ratio 1:1 R1:R2, and the mixtures R1/R2/$C_{12}E_8$, R1/R2/LAS, R1/R2/SLES, R1/R2/$C_{12}E_8$/LAS, R1/R2/$C_{12}E_8$/SLES and R1/R2/LAS/SLES, all at 30/70 R:C and 1:1 R1:R2. Surface tension data for the individual surfactants and their mixtures are summarised in Tables 8.1 and 8.2, respectively.

Surfactant	Surface tension, γ / mN/m		Δγ / %
	25°C	10°C	
$C_{12}E_8$	36.0	38.5	7.0
LAS	31.2	32.4	4.0
SLES	42.7	45.0	7.0
R1	27.2	28.1	3.0
R2	30.5	31.6	3.5

Table 8.1: Surface tension values for individual components, at 25°C and 10°C, at 2 mM concentration, prepared in MilliQ ultrapure water containing $1x10^{-6}$ M NaOH, and the percentage range in surface tension.

Surfactant	Surface tension, γ / mN/m		Δγ / %
	25°C	10°C	
0.375/0.375/0.25 $C_{12}E_8$/LAS/SLES	38.2	39.6	4.0
0.15/0.15/0.26/0.26/0.18 R1/R2/$C_{12}E_8$/LAS/SLES	29.5	30.1	2.0
0.15/0.15/0.7 R1/R2/$C_{12}E_8$	32.2	33.3	3.5
0.15/0.15/0.7 R1/R2/LAS	27.9	28.9	3.5
0.15/0.15/0.7 R1/R2/SLES	29.9	30.3	1.5
0.15/0.15/0.35/0.35 R1/R2/$C_{12}E_8$/LAS	29.3	30.0	2.5
0.15/0.15/0.35/0.35 R1/R2/$C_{12}E_8$/SLES	31.9	32.7	2.5
0.15/0.15/0.35/0.35 R1/R2/LAS/SLES	27.7	28.7	3.5

Table 8.2: Variation in surface tension for $C_{12}E_8$/LAS/SLES and the ternary, four- and five-component biosurfactant/conventional surfactant mixtures, at 25°C and 10°C, at a fixed concentration of 2 mM, prepared in MilliQ ultrapure water containing $1x10^{-6}$ M NaOH, and the percentage range in surface tension.

As anticipated, the surface tension for all individual surfactant solutions and mixtures increases as the temperature decreases from 25°C to 10°C. This is attributed to hydrogen bond formation between the molecules being more likely at lower temperatures, as discussed earlier. However, the relative increase (Δγ) with temperature between the individual conventional surfactants and their mixtures, and those with added rhamnolipids, show very striking differences. For the measurements of the individual components the largest increase in surface tension is observed for $C_{12}E_8$ and SLES. The surface tension for LAS also increases, although Δγ is lower, indicating a slightly higher tolerance to temperature. The relative increase in surface tension for the $C_{12}E_8$/LAS/SLES mixture is therefore also lower due to the presence of LAS. However the change in surface tension for R1 and R2 is even smaller, with only a 3% and 3.5% variation in surface tension between temperatures, respectively, and is even lower for the five-component R1/R2/$C_{12}E_8$/LAS/SLES mixture (2%). The variation in surface tension is relatively low for all the other ternary and four-component mixtures containing R1 and R2 so it is evident that the presence of rhamnolipids minimises any changes in surface tension as the temperature decreases. No further significant trends can be discerned, although it is interesting that the lowest Δγ is observed with R1/R2/SLES, signifying that the rhamnolipids have the largest temperature minimisation effects in mixtures with SLES. SLES is the least surface active of the conventional surfactants and was the most reluctant to adsorb to the air/water interface in the ternary

$C_{12}E_8$/LAS/SLES mixture, as described in Chapter 4. These important and significant initial surface tension measurements prompted further investigation into the variation in surface adsorption and composition with temperature for the multicomponent surfactant mixtures, using neutron reflectivity.

8.3.2 Neutron reflectivity

The ternary $C_{12}E_8$/LAS/SLES mixture at composition 0.375/0.375/0.25, and the 30% partial replacement of this with rhamnolipids at 1:1 R1:R2 to form the multicomponent mixture R1/R2/$C_{12}E_8$/LAS/SLES, were studied using neutron reflectivity. Tables 8.3 to 8.7 show the surface composition and total adsorption values for 0.375/0.375/0.25 $C_{12}E_8$/LAS/SLES, 0.15/0.15/0.26/0.26/0.18 R1/R2/$C_{12}E_8$/LAS/SLES, 0.15/0.15/0.70 R1/R2/LAS, 0.15/0.15/0.35/0.35 R1/R2/$C_{12}E_8$/LAS, and 0.15/0.15/0.35/0.35 R1/R2/LAS/SLES, respectively. The ternary R1/R2/LAS mixture and the four-component mixtures R1/R2/$C_{12}E_8$/LAS and R1/R2/LAS/SLES were studied to better understand the role of LAS in the surface behaviour of the multicomponent biosurfactant mixtures at lower temperatures.

		25°C			10°C		
Surfactant	Solution composition	Surface composition / ± 0.02	Adsorbed amount Γ / ± 0.02 x10^{-10} mol cm^{-2}	Total adsorption / ± 0.04 x10^{-10} mol cm^{-2}	Surface composition / ± 0.02	Adsorbed amount Γ / ± 0.02 x10^{-10} mol cm^{-2}	Total adsorption / ± 0.04 x10^{-10} mol cm^{-2}
$C_{12}E_8$	0.375	0.56	1.35	2.41	0.51	1.28	2.47
LAS	0.375	0.41	0.98		0.47	1.16	
SLES	0.25	0.03	0.08		0.01	0.03	

Table 8.3: Surface composition, adsorbed amounts and total adsorption for 2 mM $C_{12}E_8$/LAS/SLES at solution composition 0.375/0.375/0.25, in NRW containing 1x10^{-6} M NaOH.

		25°C			10°C		
Surfactant	Solution composition	Surface composition / ± 0.02	Adsorbed amount Γ / ± 0.02 x10^{-10} mol cm^{-2}	Total adsorption / ± 0.04 x10^{-10} mol cm^{-2}	Surface composition / ± 0.02	Adsorbed amount Γ / x10^{-10} mol cm^{-2}	Total adsorption / ± 0.04 x10^{-10} mol cm^{-2}
R1	0.15	0.34	0.94	2.75	0.36	1.02	2.87
R2	0.15	0.14	0.39		0.12	0.35	
$C_{12}E_8$	0.26	0.16	0.43		0.17	0.49	
LAS	0.26	0.25	0.70		0.25	0.72	
SLES	0.18	0.11	0.29		0.10	0.29	

Table 8.4: Surface composition, adsorbed amounts and total adsorption for 2 mM R1/R2/$C_{12}E_8$/LAS/SLES at solution composition 0.15/0.26/0.26/0.18, in NRW containing 1x10^{-6}M NaOH.

		25°C			10°C		
Surfactant	Solution composition	Surface composition / ± 0.02	Adsorbed amount Γ / ± 0.02 x10^{-10} mol cm^{-2}	Total adsorption Γ_{tot} / ± 0.04 x10^{-10} mol cm^{-2}	Surface composition / ± 0.02	Adsorbed amount Γ / ± 0.02 x10^{-10} mol cm^{-2}	Total adsorption / ± 0.04 x10^{-10} mol cm^{-2}
R1	0.15	0.34	1.10	3.19	0.34	1.10	3.23
R2	0.15	0.19	0.61		0.20	0.63	
LAS	0.70	0.47	1.48		0.46	1.50	

Table 8.5: Surface composition, adsorbed amounts and total adsorption for 2 mM R1/R2/LAS at solution composition 0.15/0.15/0.7, in NRW containing 1x10^{-6}M NaOH.

		25°C			10°C		
Surfactant	Solution composition	Surface composition / ± 0.02	Adsorbed amount Γ / ± 0.02 x10^{-10} mol cm^{-2}	Total adsorption / ± 0.04 x10^{-10} mol cm^{-2}	Surface composition / ± 0.02	Adsorbed amount Γ / ± 0.02 x10^{-10} mol cm^{-2}	Total adsorption / ± 0.04 x10^{-10} mol cm^{-2}
R1	0.15	0.43	1.36	3.15	0.45	1.46	3.23
R2	0.15	0.15	0.46		0.15	0.49	
$C_{12}E_8$	0.35	0.17	0.54		0.16	0.52	
LAS	0.35	0.25	0.79		0.24	0.76	

Table 8.6: Surface composition, adsorbed amounts and total adsorption for 2 mM R1/R2/$C_{12}E_8$/LAS at solution composition 0.15/0.15/0.35/0.35, in NRW containing 1x10^{-6}M NaOH.

		25°C			10°C		
Surfactant	Solution composition	Surface composition / ± 0.02	Adsorbed amount Γ / ± 0.02 x10^{-10} mol cm^{-2}	Total adsorption / ± 0.04 x10^{-10} mol cm^{-2}	Surface composition / ± 0.02	Adsorbed amount Γ / ± 0.02 x10^{-10} mol cm^{-2}	Total adsorption / ± 0.04 x10^{-10} mol cm^{-2}
R1	0.15	0.43	1.36	3.15	0.45	1.46	3.24
R2	0.15	0.15	0.46		0.15	0.48	
LAS	0.35	0.17	0.54		0.16	0.52	
SLES	0.35	0.25	0.79		0.24	0.78	

Table 8.7: Surface composition, adsorbed amounts and total adsorption for 2 mM R1/R2/LAS/SLES at solution composition 0.15/0.15/0.35/0.35, in NRW containing 1x10^{-6}M NaOH.

For the ternary $C_{12}E_8$/LAS/SLES mixture, the surface composition changes significantly with temperature, as seen in Table 8.3. On decreasing the temperature from 25°C to 10°C, the relative amount of $C_{12}E_8$ decreases and that of LAS increases. The relative amount of SLES remains approximately the same and is close to zero. This is not consistent with the results for $C_{12}E_3$/$C_{12}E_8$[7,8] where at a lower temperature the relative adsorption of the more surface active $C_{12}E_3$ was higher. However, as was observed previously both above and below the CMC,[7,8] there is a slight increase in total adsorption with decreasing temperature, as expected due to the exothermic nature of surface adsorption.

For all the ternary, four- and five-component mixtures that contain rhamnolipids (Tables 8.4 to 8.7), there is an increase in the total adsorption as the temperature decreases from 25°C to 10°C. The increase is generally associated with an increase in surface adsorption of R1, the most surface-active component, although a slight decrease in adsorption of the other components partially compensates for this increase.

The most striking finding is that the surface compositions for all solutions containing R1 and R2 are, within error, invariant with temperature, although there are very small changes in adsorbed amount. However, interestingly these changes in adsorbed amount are not reflected in the R1/R2/LAS mixture (Table 8.5), where no significant change occurs and no significant increase in total adsorption is observed. This signifies that the three surfactants in this solution are the most tolerant to temperature.

8.4 Discussion

The tolerance of surfactants and their mixtures to temperature changes has important implications for the ability of detergents to be as effective at lower temperatures as they are at higher temperatures, with positive environmental and economical impacts for industrial and domestic applications. It has been estimated that over 90% of the total energy required for washing clothes is in the heating of the washing water.[17] Having the ability to achieve the same detergency performance at a reduced washing temperature would be highly energy-saving and environmentally beneficial.

A 15°C decrease in temperature gives a significant increase in surface tension for the individual components $C_{12}E_8$ and SLES, although temperature appears to have a smaller effect on the surface tension of LAS and the ternary $C_{12}E_8$/LAS/SLES mixture. A change in the surface compositions of the components in the ternary conventional surfactant mixture exists, with a relative decrease and increase of $C_{12}E_8$ and LAS, respectively. However, partial replacement of the ternary mixture with the rhamnolipid biosurfactants R1 and R2 has a dramatic temperature-minimising effect on both surface tension and surface composition. The presence of rhamnolipids reduces any changes in adsorption for the three conventional surfactants to the point where the individual surface compositions are, within error, almost identical at both temperatures, indicating very similar surface properties at both temperatures. Although the systematic changes recorded are small and at the limit of the systematic errors in the measurements, the trends in the adsorption and the surface composition using neutron reflectivity are entirely consistent with those observed in surface tension.

The low temperature tolerance of the surfactants are in the order R1>LAS>R2>SLES>$C_{12}E_8$. This suggests that the incorporation of the rhamnolipids, especially R1, provide a degree of tolerance to low temperature detergency. A more systematic and extensive exploration of the effects of temperature is necessary to build on these initial measurements, which may include analysis over a wider temperature range and investigating the effects of varying the rhamnolipid/conventional surfactant ratio and R1:R2 ratio, as well as the investigation of bulk solution aggregate behaviour at both temperatures for comparison with the surface data.

References: Chapter 8

1. Gittens, G. J., *Journal of Colloid and Interface Science* **1969,** *30* (3), 406-412.
2. Vargaftik, N. B.; Volkov, B. N.; Voljak, L. D., *Journal of Physical and Chemical Reference Data* **1983,** *12* (3), 817-820.
3. Shereshefsky, J. L., *Journal of Physical Chemistry* **1931,** *35* (6), 1712-1720.
4. Mitchell, D. J.; Tiddy, G. J. T.; Waring, L.; Bostock, T.; McDonald, M. P., *Journal of the Chemical Society, Faraday Transactions 1: Physical Chemistry in Condensed Phases* **1983,** *79*, 975-1000.
5. Schick, M. J., *Journal of Physical Chemistry* **1963,** *67* (9), 1796-1799.
6. Rosen, M. J.; Cohen, A. W.; Dahanayake, M.; Hua, X., *Journal of Physical Chemistry* **1982,** *86* (4), 541-545.
7. Penfold, J.; Staples, E.; Thompson, L.; Tucker, I.; Thomas, R. K.; Lu, J. R., *Berichte der Bunsengesellschaft für physikalische Chemie* **1996,** *100* (3), 218-223.
8. Penfold, J.; Staples, E.; Tucker, I.; Thompson, L.; Thomas, R. K., *Journal of Colloid and Interface Science* **2002,** *247* (2), 404-411.
9. Chen, L.-J.; Lin, S.-Y.; Huang, C.-C.; Chen, E.-M., *Colloids and Surfaces A: Physicochemical and Engineering Aspects* **1998,** *135* (1-3), 175-181.
10. Mohajeri, E.; Noudeh, G. D., *Journal of Chemistry* **2012,** *9* (4), 2268-2274.
11. Mahmood, M. E.; Al-Koofee, D. A. F., *Global Journal of Science Frontier Research Chemistry* **2013,** *13* (4), 1-7.
12. Lu, J. R.; Li, X.; Thomas, R. K.; Staples, E. J.; Thompson, L.; Tucker, I.; Penfold, J., *Journal of Physical Chemistry* **1994,** *98* (26), 6559-6567.
13. Flockhart, B. D., *Journal of Colloid Science* **1961,** *16* (5), 484-492.
14. La Mesa, C., *Journal of Physical Chemistry* **1990,** *94* (1), 323-326.
15. Stead, J. A.; Taylor, H., *Journal of Colloid and Interface Science* **1969,** *30* (4), 482-488.
16. Golub, T. P.; de Keizer, A., *Langmuir* **2004,** *20* (22), 9506-9512.
17. Jokelainen, A.; Heino, H., *Journal of Consumer Studies and Home Economics* **1981,** *5* (4), 311-322.

Chapter 9

Conclusions

This thesis aimed to investigate in detail the surface adsorption and solution aggregate behaviour of a ternary conventional surfactant mixture, a model system representative of many current detergent formulations, and the effects of its partial replacement with the glycolipid biosurfactant rhamnolipid, a highly surface-active, natural biosurfactant which is of increasing commercial interest. The incorporation and ultimate replacement of the current synthetic chemical surfactants with biosurfactants, which are highly biodegradable and more environmentally compatible, is becoming increasingly appealing. In this work, a model ternary conventional surfactant mixture of the nonionic surfactant $C_{12}E_8$ with the anionic surfactants LAS and SLES, and a multicomponent biosurfactant/conventional surfactant mixture containing the rhamnolipids R1 and R2 was studied at the air/water interface, using surface tension and NR. The solution aggregate behaviour of the ternary and five-component mixtures was studied using SANS.

A pronounced departure from ideal mixing has been observed at the air/water interface. Surface tension measurements of the binary LAS/SLES mixture indicate ideal mixing, but a departure from ideality is observed for the $C_{12}E_8$/LAS and $C_{12}E_8$/SLES mixtures. NR reveals a dominance of $C_{12}E_8$ and LAS at the air/water interface, with a significant depletion of SLES at the interface. For example, at a solution composition of 0.9 SLES, only 42% of the surface is composed of this surfactant. The non-ideal regular solution theory fails to predict this pronounced departure from ideality, as observed with similar anionic/nonionic systems such as SDS/$C_{12}B$[1] and DHDAB/nonionic.[2] As described previously,[2] it is possible that this results from small changes in the bulk aggregates manifesting themselves as large effects at the interface.

SANS measurements have revealed the presence of small interacting globular micelles for the ternary surfactant mixture, at all solution compositions and up to a concentration of 50 mM. The aggregation numbers of the mixed micelles scale with those of the pure individual components, an indication of

ideal mixing behaviour, in which the composition of the mixed micelles is the same as in the bulk solution. Structural studies using partial deuteration of separate components in the mixed micelles, such as those done by Penfold et al,[3,4,5,6,7] may provide access to the exact composition of the mixed micelles, which can then be compared with the surfactant composition at the interface.

The precipitation of surfactants by hard water counterions often has negative consequences on detergency. Measurements were made on the ternary conventional surfactant mixture in the presence of monovalent Na^+ and divalent Ca^{2+} electrolyte counterions, in the form of NaCl and $CaCl_2$, to explore the effects of hard water ions and the effect of modifying the electrostatic interactions. Rather unexpected behaviour has been observed in the form of a pronounced change in surface composition towards that of the solution composition, which increases with increasing electrolyte concentration. The less surface-active SLES becomes more dominant at the interface whilst the $C_{12}E_8$ diminishes at the interface. The presence of electrolyte makes the CMC values and hence the surface behaviour of all components more comparable. A large synergy in the form of a 30% increase in total adsorption also occurs on addition of electrolyte. All these effects mentioned are more pronounced in the presence of the divalent Ca^{2+} than Na^+, with the concentration at which this occurs being at a much lower relative concentration than with Na^+, even allowing for the change in ionic strength.

It was thought that the presence of ethylene oxide groups on SLES may be a reason for the lack of surface activity of SLES when combined with the other two surfactants. However, on replacement of SLES with SDS, similar results were found in that the $C_{12}E_8$ and LAS dominates adsorption and SDS is depleted at the interface. On addition of Na^+, qualitatively similar results are observed in that the composition of $C_{12}E_8$ reduces and that of LAS and SDS increases. However, quantitatively there are some subtle differences. There is a more gradual change in surface composition on addition of electrolyte for SDS than for SLES. The effect of electrolyte on SDS is expected due to its highly anionic nature and the screening of the repulsive electrostatic charges between the anionic headgroups by the Na^+ counterion. However, these results are less expected for the more weakly anionic SLES, which has a low degree of ionisation compared to that of other pure anionic surfactants such as SDS[8] due to its strongly-bound counterion.[9]

Although the solution behaviour of the ternary mixture in the presence of electrolyte was not studied in this work, distinct visual changes in the solutions were observed for the $C_{12}E_8$/LAS/SLES system in the presence of Ca^{2+} when the LAS solution composition is above 0.6, indicating significant changes in the phase behaviour. LAS is effectively a di-chain anionic surfactant, with a low spontaneous micelle curvature, and it forms complex planar structures when pure.[10] It is known from previous work that it induces increased complexity of aggregate structures and changes in the pattern of adsorption from monolayers to multilayers.[11] Additional solution studies using SANS would be instructive in order to follow the solution behaviour of the conventional surfactants: it is expected that at higher solution concentrations, Ca^{2+} concentrations, and in very LAS-rich solutions, increasingly complex phase behaviour would occur.

On partial replacement of the ternary $C_{12}E_8$/LAS/SLES system with the rhamnolipid biosurfactant R1 and R2, to form the complex multicomponent mixture R1/R2/$C_{12}E_8$/LAS/SLES, fascinating changes occur both at the interface and in solution, which are not observed in the conventional surfactant mixtures at the same concentrations and compositions. The most important effect on the surface behaviour is the large increase in total adsorption and synergistic mixing between the five components, where the packing arrangements mitigate the unfavourable interactions between the headgroups at the air/water interface and lessen the packing constraints which are seen in the conventional surfactant mixtures. This is an important result which shows the positive impact which rhamnolipids have on packing in surfactant mixtures. The solution phase behaviour becomes increasingly complex, with a transition from micellar to mixed micellar/lamellar at higher overall surfactant concentration, and in increasingly LAS-rich, rhamnolipid-rich and R1-rich solutions. The change with R1:R2 ratio can be attributed to the smaller headgroup of R1 and its lower spontaneous curvature, which has previously been shown to induce the formation of more planar aggregate structures.[11,12]

The impact of lower temperatures on the surface behaviour of conventional and biosurfactant/conventional surfactant mixtures containing rhamnolipids has been studied, using surface tension and neutron reflectivity. This work is connected to Unilever's Sustainable Living

programme, which aims to significantly reduce the environmental impact of their products by 2020. Understanding the impact of lower temperatures on surface activity and detergency effectiveness is imperative, due to the increasing focus on environmentally-friendly, energy-saving consumer behaviour in the home and personal care industry. Some promising initial results have been found. All surface tension values for the individual surfactants increase as the temperature is reduced from 25°C to 10°C, as expected, but the difference in surface tension is much smaller for the rhamnolipids R1 and R2 and, surprisingly, LAS. Further exploration using NR found a significant change in relative surface adsorption with decreasing temperature for the conventional components and their mixtures, but almost no effect of temperature on the surface adsorption of the four-and five-component mixtures containing rhamnolipids. These important results suggest the incorporation of rhamnolipids, especially R1, provide a degree of tolerance to low temperature detergency. This has enormous implications for future temperature requirements and suggest a viable route to efficient low temperature detergency.

Two main barriers to the use of rhamnolipids and other biosurfactants in industrial applications are the cost of large-scale production and the difficulties in separation and purification of the components in the biosurfactant mixture. Manufacturing costs are much higher than that of their conventional alternatives, with the cost of raw materials adding up to 30% of the production cost.[13] However, the use of renewable hydrophobic and hydrophilic sources for raw materials is increasing.[14] The use of opportunistic pathogenic bacterial strains such as *P. aeruginosa* in large-scale production causes understandable safety concerns, but the recently investigated non-pathogenic *Pseudomonas* strains such as *P. chlororaphis*[15], with recent patents indicating viable yields,[16] are becoming increasingly possible substitutes for rhamnolipids produced in industry. In addition, the many positive attributes, such as their high biodegradability,[17] antimicrobial properties and exceptional surface activity,[18] mean rhamnolipids are becoming a serious alternative to the current chemical surfactants,[19] with uses already found in certain commercial products.[20] The results in this thesis serve to reinforce these trends and provide more detailed insight into the role of rhamnolipids in adsorption and self-assembly.

Much literature has studied the behaviour of surfactant mixtures at the solid/liquid interface and the oil/water interface. This has more industrial relevance in the fact that it can be used as a model for the

effectiveness of surfactants to adsorb at the interface of clothes and washing water. Ionic surfactants adsorb at the solid/liquid interface onto surfaces of opposite charge, although this can also occur on like-charged surfaces due to intermolecular forces such as hydrogen bonds. Surfactants at the solid surface affect the wettability of a liquid on that surface. Neutron reflectivity has been used to study the interfacial adsorption at the hydrophilic silicon surface of many nonionic,[21] anionic/nonionic mixtures[22] and cationic/nonionic[23] mixtures, in combination with D/H isotopic substitution. The effects of solution concentration, composition[23] and pH[24] have been investigated, with data compared to those obtained at the air/water interface. Studies of surfactant mixtures at the oil/water interface[25] have also been made. However, there has been little characterisation of biosurfactants at the solid/liquid interface, apart from some limited wetting studies, for example of rhamnolipids conducted by Ishigami et al[26] and Özdemir et al.[27] Thus, a detailed study of the surfactant behaviour in the ternary conventional $C_{12}E_8$/LAS/SLES and the multicomponent biosurfactant R1/R2/$C_{12}E_8$/LAS/SLES systems would be an important future addition to the present work at the solid/liquid and/or the oil/water interfaces, for comparison with the present work. The effect of temperature on these mixtures at solid and oil interfaces will be important additions to the significant and noteworthy changes which have been observed at lower temperatures at the air/water interface.

Until present, multicomponent surfactant mixtures as complex as this, exhibiting such highly non-ideal mixing behaviour, have not been explored in detail. The replacement of conventional chemical surfactants with “greener”, entirely biodegradable alternatives is becoming an increasingly important alternative. This thesis aimed to explore the surface adsorption and solution self-assembly behaviour of a model, “greener” alternative biosurfactant / conventional surfactant mixture. This work leads naturally to the further study of other biosurfactants, such as sophorolipids, of which detailed analysis with LAS has already been explored.[28,29]

References: Chapter 9

1. Hines, J. D.; Thomas, R. K.; Garrett, P. R.; Rennie, G. K.; Penfold, J., *Journal of Physical Chemistry B* **1998,** *102* (44), 8834-8846.
2. Tucker, I.; Penfold, J.; Thomas, R. K.; Tildesley, D. J., *Langmuir* **2009,** *25* (7), 3924-3931.
3. Lu, J. R.; Li, Z. X.; Thomas, R. K.; Staples, E. J.; Tucker, I.; Penfold, J., *Journal of Physical Chemistry* **1993,** *97* (30), 8012-8020.
4. Lu, J. R.; Li, Z. X.; Su, T. J.; Thomas, R. K.; Penfold, J., *Langmuir* **1993,** *9* (9), 2408-2416.
5. Lu, J. R.; Li, Z. X.; Smallwood, J.; Thomas, R. K.; Penfold, J., *Journal of Physical Chemistry* **1995,** *99* (20), 8233-8243.
6. Penfold, J.; Staples, E.; Tucker, I.; Thomas, R. K., *Journal of Colloid and Interface Science* **1998,** *201*, 223-232.
7. Penfold, J.; Staples, E.; Tucker, I.; Thomas, R. K.; Woodling, R.; Dong, C. C., *Journal of Colloid and Interface Science* **2003,** *262* (1), 235-242.
8. Hayter, J. B.; Penfold, J., *Colloid and Polymer Science* **1983,** *261* (12), 1022-1030.
9. Xu, H.; Penfold, J.; Thomas, R. K.; Petkov, J. T.; Tucker, I., *Langmuir* **2013,** *29* (41), 12744-12753.
10. Ma, J.-G.; Boyd, B. J.; Drummond, C. J., *Langmuir* **2006,** *22* (21), 8646-8654.
11. Chen, M.; Penfold, J.; Thomas, R. K.; Smyth, T. J. P.; Perfumo, A.; Marchant, R.; Banat, I. M.; Stevenson, P.; Parry, A.; Tucker, I.; Grillo, I., *Langmuir* **2010,** *26* (23), 17958-17968.
12. Chen, M. L.; Penfold, J.; Thomas, R. K.; Smyth, T. J. P.; Perfumo, A.; Marchant, R.; Banat, I. M.; Stevenson, P.; Parry, A.; Tucker, I.; Grillo, I., *Langmuir* **2010,** *26* (23), 18281-92.
13. Cameotra, S. S.; Makkar, R. S., *Applied Microbiology and Biotechnology* **1998,** *50* (5), 520-529.
14. Zhu, Y.; Gan, J.-J.; Zhang, G.-L.; Yao, B.; Zhu, W.-J.; Meng, Q., *Journal of Zhejiang University SCIENCE A* **2007,** *8* (9), 1514-1520.
15. Gunther IV, N. W.; Nuñez, A.; Fett, W.; Solaiman, D. K. Y., *Applied and Environmental Microbiology* **2005,** *71* (5), 2288-2293.
16. Gunther, N. W.; Solaiman, D. K. Y.; Fett, F. W. Processes for the production of rhamnolipids. 2007.
17. Zajic, J. E.; Guignard, H.; Gerson, D. F., *Biotecnology and Bioengineering* **1977,** *19* (9), 1303-1320.
18. Guerra-Santos, L.; Käppeli, O.; Fiechter, A., *Applied and Environmental Microbiology* **1984,** *48* (2), 301-305.
19. Banat, I. M.; Makkar, R. S.; Cameotra, S. S., *Applied Microbiology and Biotechnology* **2000,** *53* (5), 495-508.
20. Develter, D.; Jacobs, I.; Renkin, M. Detergent compositions. 2004.
21. Penfold, J.; Tucker, I.; Thomas, R. K., *Langmuir* **2005,** *21* (14), 6330-6336.
22. Penfold, J.; Staples, E.; Tucker, I.; Thomas, R. K., *Langmuir* **2002,** *18* (15), 5755-5760.
23. Penfold, J.; Staples, E. J.; Tucker, I.; Thomas, R. K., *Langmuir* **2000,** *16*, 8879-8883.
24. Penfold, J.; Staples, E. J.; Tucker, I.; Thompson, L. J.; Thomas, R. K., *International Journal of Thermophysics* **1999,** *20* (1), 19-34.
25. Staples, E.; Penfold, J.; Tucker, I., *Journal of Physical Chemistry B* **2000,** *104* (3), 606-614.
26. Ishigami, Y.; Gama, Y.; Ishii, F.; Choi, Y. K., *Langmuir* **1993,** *9* (7), 1634-1636.
27. Özdemir, G.; Malayoglu, U., *Colloids and Surfaces B: Biointerfaces* **2004,** *39* (1-2), 1-7.
28. Chen, M.; Dong, C. C.; Penfold, J.; Thomas, R. K.; Smyth, T., J. P.; Perfumo, A.; Marchant, R.; Banat, I. M.; Stevenson, P.; Parry, A.; Tucker, I.; Campbell, R. A., *Langmuir* **2011,** *27* (14), 8854-8866.
29. Penfold, J.; Chen, M.; Thomas, R. K.; Dong, C.; Smyth, T. J. P.; Perfumo, A.; Marchant, R.; Banat, I. M.; Stevenson, P.; Parry, A.; Tucker, I.; Grillo, I., *Langmuir* **2011,** *27* (14), 8867-8877.